



**HAL**  
open science

# Pesticides dissipation at the sediment-water interface : insight from compound-specific isotope analysis (CSIA)

Boris Droz-Dit-Busset

► **To cite this version:**

Boris Droz-Dit-Busset. Pesticides dissipation at the sediment-water interface : insight from compound-specific isotope analysis (CSIA). Earth Sciences. Université de Strasbourg, 2020. English. NNT : 2020STRAH015 . tel-03285775

**HAL Id: tel-03285775**

**<https://theses.hal.science/tel-03285775>**

Submitted on 13 Jul 2021

**HAL** is a multi-disciplinary open access archive for the deposit and dissemination of scientific research documents, whether they are published or not. The documents may come from teaching and research institutions in France or abroad, or from public or private research centers.

L'archive ouverte pluridisciplinaire **HAL**, est destinée au dépôt et à la diffusion de documents scientifiques de niveau recherche, publiés ou non, émanant des établissements d'enseignement et de recherche français ou étrangers, des laboratoires publics ou privés.

**ÉCOLE DOCTORALE des Sciences de la Terre et de l'Environnement (ED 413)**

**Laboratoire d'Hydrologie et de Géochimie de Strasbourg (LHyGeS)**

**UMR 7517 / ENGEES – CNRS**

**THÈSE** présentée par :

**Boris DROZ-DIT-BUSSET**

soutenue le : **14 Décembre 2020**

pour obtenir le grade de : **Docteur de l'université de Strasbourg**

Discipline/ Spécialité : Sciences de la Terre et de l'Univers/ Géochimie

**Pesticides dissipation at the sediment-water  
interface: insight from compound-specific  
isotope analysis (CSIA)**

**THÈSE dirigée par :**

**M. Payraudeau Sylvain**

**M. IMFELD Gwenaël**

Professeur, ENGEES, France

Directeur de recherche, CNRS, France

**RAPPORTEURS :**

**M. Höhener Patrick**

**M. Sebilo Mathieu**

Professeur, Université d'Aix-Marseille, France

Maître de conférences, Université de la Sorbonne, France

**AUTRES MEMBRES DU JURY :**

**Mme. Passeport Elodie**

**M. van Dijk Paul**

Professeure, Université de Toronto, Canada

Ph.D., Chambre d'Agriculture Grand Est, France

---

Ph.D. Thesis, University of Strasbourg  
© B. Droz-dit-Busset, 2020

This research has been funded by the Region Grand Est and the Rhine-Meuse Water Agency  
(AERM; Project PolISO No. 170293)



## **Acknowledgements**

This Ph.D. thesis was carried out at the Laboratory of Hydrology and Geochemistry of Strasbourg (LHyGeS), France, supported by the Région Grand Est and the Rhine-Meuse Water Agency (AERM; Project PolISO No. 170293). I want to thank all persons and institutions who have directly or indirectly contributed to this work.

I would like first to acknowledge my thesis director, Sylvain Payraudeau and my co-director Gwenaël Imfeld, who offered to me this motivate Ph.D. thesis subject, all resources needed to conduce properly my research and a nice environment to work at the LHyGeS.

I would like to thank the jury members for accepting to evaluate my Ph.D. work, Elodie Passeport, Paul van Dijk, Patrick Höhener and Mathieu Sebilo for the fruitfully discussions on research. I also thank to Boris van Breukelen and Mònica Rosell who advised and evaluated me during my mid-term Ph.D. evaluation.

I had to specially thank Guillaume Drouin, my office-mate, lab-mate, bike-mate, field-work-mate and co. I will never enough thank you for these three years where we had the opportunity to share the same project and work together. It was really a pleasure for me, and this collaboration was very fruitful in a scientific point of view as well as in a personal point of view. Thank you, buddy. I would like to specially acknowledge the two master students, who contributed to different sections of this work, Margaret Johnson and Jenna Lohmann. They worked hardly with Guillaume and me to gather data with always a good spirit in mind. It was a pleasure to work with them. They both contributed significatively to this work at all stages.

During this Ph.D., I had the chance to get a scholarship to go one month at the University of Toronto - UofT. I would thank Elodie Passeport to host me during that time, for the very fruitful discussion about data and advice during my Ph.D. I had the chance to learn in her laboratory some aspects of the radiolabel technique to track pesticide degradation in mesocosm. I would also thank my lab-mate during this time: Ka Yee (Shirley) Lam, Suchana Shamsunnahar, Kelsey Smyth, Zhu Hao (Eric) Yu and Shuyao Ta. We had a lot of fun in and outside of the lab. I would specially thank Leandra Rhodes-Dicker, who organized everything for my stay at UofT and by chance with whom I share the same hobbies: bike ride and beer. Thank you for the stunning rides to explore Toronto.

I am especially grateful to Loic Maurer, Dimitri Heintz and Claire Villette from the Plant Imaging and Mass Spectrometry (PIMS) at the University of Strasbourg. They opened me their laboratory and we had very nice scientific interactions. Their expertise added a tremendous data enrichment to my thesis.

## *Acknowledgements*

I would thank all persons at the different departments at the University of Strasbourg who helped me to set up my experiment, gather data, fix any issue in the laboratory, in the field and/or who supported me through open discussions and advised me for my career: Martine Trautmann, Sophie Gangloff, Benoit Guyot, Colin Fourtet, Eric Lascar, Amélie Aubert, Thierry Perrone, Eric Pernin, Sébastien Tetard, René Boutin, Agnès Herrmann, Carole Lutz, Paula Pérez, Jérémy Masbou, Charline Wiegert, Eric Pelt, Maurice Millet, Olivier Delhomme, Solenn Cotel, François Lehmann our Gyro Gearloose, Marwan Fahs, Didier Baumann, Benjamin Belfort, Gerhard Schaefer, François Chabaux, Joëlle Duplay, Hervé. Blumentritt, Youssef Zaiter, Stéphanie Lawniczak, Nolwenn Lesparre, Dimitri Rambourg, Sylvain Weill, Sylvain Benarioumlil, Damien Daval, Damien Lemarchand, Marie-Claire Pierret, Anne-Désirée Schmitt and Gilles Morvan. Thank you all of you for sharing your experiences and/or spending your time to work for my project.

I also thank Jeroen E. Sonke from the Laboratory for Environmental Geosciences of Toulouse for lending us a sunlight simulator, Thomas Cottineau from the Institute of Chemistry and Processes for Energy, Environment and Health from Strasbourg for his help in light spectrum characterization, Frank Leresche from University of Colorado Boulder for this contribution and help during the photolysis experiment and Laurent Mergnac from the Syndicat des Eaux et de l'Assainissement Alsace-Moselle (SDEA), who helped us during the entire Ph.D. through the paper work, authorizations and organization needed to accomplish our field work. I would thank the all persons who helped to gather additional data and to organize our field work: Guillaume Ryckelynck from the Région Grand Est, Blandine Fritsch from the Chambre d'Agriculture Alsace and Marie Manceau and Rémy Gentner from the Eurométropole Strasbourg, Quentin Morice from the Direction Régionale de l'Environnement, de l'Aménagement de du Logement (DREAL) and the city council of Mundolsheim.

I would also thank my lab and team-mates, other Ph. D. and post-doc in our department who provided my nice feedback and fruitful discussions to make progress in my project and of course with whom I had a lot of fun in and outside the laboratory: Maria (Lulú) De Lourdes Pietro Espinoza, Pablo Alvarez-Zaldivar, Fatima Meite, Tobias Junginger, Baptiste Baumlin, Tetyana Givleska, Rungroch Sungthong, Matthias Oursin, Flora Hochscheid, Arnaud Bouissonnie, Behshad Koohbor, Marianna Marinoni, Jean-Michel Brazier, Bastien Wild, Andreas Scharmüller Coralie Ranchoux, Benjamin Jeannot, Sara Tabrizinejadas, Aurélie Schulz, Ivan Toloni and Tchutchu.

At the end but maybe I should start by her, I thank my love Anna who supported me during these three years for the best and the worst. Thank you to motivate me and support me all the time in all conditions. Finally, I thank my friends David Ballarin, Francesco Marafatto and Laurie Boulard for the attentive reading and improvements at the very end stage of this thesis manuscript.

## **Résumé en Français**

Les pesticides représentent un des groupes de molécules de synthèse parmi les plus utilisés au monde, totalisant une utilisation de plus de  $2.6 \times 10^6$  tonnes par an.<sup>1</sup> Par leur épandage massif et direct dans l'environnement, les pesticides ont contaminé les eaux de surface à l'échelle de la planète,<sup>2, 3</sup> causant de sérieux problèmes en termes de qualité de l'approvisionnement en eau potable et pour l'être humain.<sup>4</sup> La demande accrue d'eau et la diminution en approvisionnement dues aux sécheresses prévues pour ces prochaines années,<sup>5</sup> associées à une probable augmentation d'utilisation de pesticides ;<sup>6</sup> vont probablement accentuer la problématique des pesticides et leurs impacts sur la biodiversité aquatique ces prochaines années.<sup>7</sup>

Le fonctionnement du compartiment aquatique en termes de transport et de dégradation des pesticides reste faiblement connu et requiert de sérieuses investigations.<sup>8</sup> En particulier, l'interface eau-sédiment (IES) a été identifiée comme zone majeure de la réactivité associée au compartiment aquatique, mais son fonctionnement demeure peu compris.<sup>9, 10</sup>

La globalité de ma thèse repose sur l'analyse isotopique composé-spécifique (CSIA) utilisée afin de prouver directement l'existence d'une dégradation sans l'aide de l'identification des produits de transformation ou d'un bilan de masse.<sup>11</sup> Le concept de la CSIA repose sur le fait que chaque cassure ou formation d'une liaison chimique dans une molécule est associée à un changement de composition isotopique. Ce changement s'explique par le fait que les isotopes légers, e.g.,  $^{12}\text{C}$  ou  $^{14}\text{N}$ , réagissent à une vitesse différente des isotopes lourds, e.g.,  $^{13}\text{C}$  ou  $^{15}\text{N}$ . Par conséquent, un enrichissement en isotopes lourds au cours de la réaction peut être observé, et celui-ci se nomme effet isotopique cinétique (KIE).<sup>12</sup> A l'opposé, les processus non dégradatifs tels que la sorption, la volatilisation, le transport, etc. sont généralement isotopiquement conservés.<sup>13</sup>

Le but général de cette thèse est d'augmenter la compréhension de la dégradation des pesticides ainsi que leur persistance dans le compartiment aquatique. Nous avons défini cinq objectifs spécifiques sur la base du manque de connaissances actuelles concernant l'IES :

1. Développer et valider une procédure optimale afin d'extraire des pesticides et de mesurer leur composition isotopique dans les sédiments.
2. Evaluer et interpréter les effets de la photodégradation des pesticides exposés à la lumière naturelle sur la composition isotopique.
3. Elucider les processus de dégradation et de transfert de phases dans un mélange eau-sédiment dans des conditions aérobiques et anaérobiques.
4. Comprendre l'influence de la vitesse de l'eau sur la dissipation des pesticides à l'interface eau-sédiment.
5. Evaluer et interpréter la contribution des processus destructifs et non-destructifs ainsi que le transport des pesticides en utilisant l'approche de la CSIA à l'échelle d'un bassin versant.

Nous avons concentré notre étude sur un mélange de pesticides sélectionnés sur la base de nos capacités restreintes pour analyser les composés en chromatographie gazeuse, représentant des composés mondialement utilisés,<sup>1, 14</sup> et figurant sur les listes des composés prioritaires de la Directive Cadre Européenne sur l'Eau (DCE)<sup>15</sup> ou/et sur la liste à surveiller.<sup>16</sup>

Dans le chapitre 2, nous présentons le développement analytique associé à un protocole modifié<sup>17</sup> d'extraction des pesticides, leur quantification par chromatographie gazeuse – spectrométrie de masse et leur analyse en isotope stable par chromatographie gazeuse – spectrométrie de masse à rapport isotopique pour le carbone et l'azote pour des sédiments et sols. Nous présentons les étapes qui ont conduit à accomplir une extraction quantitative (>70% de rendement d'extraction) pour le mélange de pesticides qui nous intéressait, i.e., atrazine, terbutryne, acétochlore, *S*-métolachlore et métalaxyl. Aucun enrichissement isotopique ( $|\Delta\delta^{13}C| < 0.7\text{‰}$ ) pour le carbone n'a été observé durant la procédure d'extraction.

Dans le chapitre 3, les changements de composition isotopique du carbone (C) et de l'azote (N) ont été mesurés durant la photodégradation directe et indirecte de l'atrazine et du *S*-métolachlore dans une eau synthétique reproduisant les conditions d'une rivière impactée par l'agriculture (nitrates = 20 mg L<sup>-1</sup> et matière organique dissoute (MOD) = 5.4 mg C L<sup>-1</sup>). L'atrazine et le *S*-métolachlore ont été rapidement photodégradés par voie directe et indirecte (demi-vie plus petite que 5 et 7 jours, respectivement). La MOD réduit la vitesse de dégradation tandis que les nitrates l'augmentent. Les produits de transformation analysés montrent que l'oxydation induite par les radicaux hydroxyles prédomine durant la photodégradation indirecte. Des expériences effectuées avec une lumière UV (254 nm) ont causé un changement de composition isotopique pour le C et N comme suivi  $\epsilon_C = 2.7 \pm 0.3$  et  $0.8 \pm 0.1\%$  et  $\epsilon_N = 2.4 \pm 0.3$  et  $-2.6 \pm 0.7\%$  pour l'atrazine et le *S*-métolachlore. En comparaison, la photodégradation effectuée avec un simulateur de lumière solaire a montré un changement de composition isotopique négligeable pour le C et très faible pour l'N. Cela corrobore les observations déjà faites sur le diclofénac<sup>18</sup> et le sulfaméthoxazole<sup>19</sup> préconisant que l'évaluation de la photodégradation pour l'étude environnementale soit systématiquement menée avec une lumière la plus proche de la lumière naturelle. Nous démontrons ici que, comme les tendances de changement de composition isotopique du carbone (C) et de l'azote (N) pour la photodégradation de l'atrazine et le *S*-métolachlore sont différentes de celles de la biodégradation et de l'hydrolyse, l'approche CSIA est capable de différencier la photodégradation des autres processus de dissipation dans les milieux aquatiques.

Dans le chapitre 4, la dégradation de l'acétochlore et du *S*-métolachlore est évaluée dans un système statique eau-sédiment au laboratoire. L'objectif spécifique était d'évaluer la contribution des processus dégradatifs et non dégradatifs en condition aérobie et anaérobie représentatifs de ce que l'on peut trouver à l'échelle d'une rivière. Nous avons émis l'hypothèse que ces deux conditions devaient présenter des voies et vitesses de dégradation contrastées.<sup>20</sup> <sup>21</sup> La CSIA a été utilisée conjointement avec l'identification des produits de transformation pour démontrer la dégradation et les voies réactionnelles possibles. Nous avons aussi utilisé un modèle de transfert de phase<sup>22</sup> pour calculer la dégradation à partir du changement de concentration, tenant compte également de la contribution de la sorption. La demi-vie de biodégradation pour l'acétochlore et le *S*-métolachlore dans la phase liquide a été plus lente dans le milieu anaérobie ( $DegT_{50,w} = 59 \pm 16$  et  $199 \pm 48$  jours) que dans la condition aérobie ( $DegT_{50,w} = 31 \pm 17$  et  $29 \pm 8$  jours). L'effet isotopique cinétique apparent pour le carbone (AKIE-C) étant entre  $1.018 \pm 0.001$  et  $1.075 \pm 0.008$ , la voie réactionnelle suggérée est une substitution nucléophile. La prédominance de l'acide oxalique comme produit de transformation suggère que la voie réactionnelle est identique dans les deux conditions, à savoir le glutathion *S*-transférase comme cela avait déjà été postulé pour les chloroacétanilides.<sup>23, 24</sup>



Dans le chapitre 5, nous avons recherché les effets de la vitesse d'écoulement de l'eau sur le transport et la réactivité de l'IES. Pour cela, nous avons construit un système expérimental de laboratoire reproduisant un tronçon de rivière. La caféine a été utilisée comme molécule modèle de l'activité anthropique comportant des propriétés proches d'un pesticide ( $\log P_{OW} < 10$ , très peu volatile et  $\log K_{OC}$  proche de deux). En parallèle, sur le même système expérimental, Drouin et al.<sup>25</sup> ont démontré numériquement que la vitesse d'écoulement de l'eau contrôle la vitesse d'incorporation de l'oxygène dans le sédiment. Sur la base de la littérature existante,<sup>8</sup> nous soumettons l'hypothèse que la dégradation se situe principalement au niveau de l'IES et que la couche aérobie du sédiment affecte la proportion dégradée. Nous avons artificiellement construit des expériences pour plusieurs vitesses d'écoulement (1.1, 3.2 and 4.8 cm s<sup>-1</sup>), avec peu de carbone organique dissout et particulaire afin de limiter le plus possible la dégradation dans la colonne d'eau. La contribution du transport et de la dégradation a été évaluée en couplant la CSIA et un modèle de transport réactif des flux (TRF). De plus, une série d'expériences statiques similaires au chapitre 4 a été effectuée dans des conditions aérobiques pour un rapport faible (0.2:5) et haut (1:5) entre le sédiment et l'eau et présentant des constantes de dégradation ( $k_{deg}$ ) pour la caféine entre  $0.658 \pm 0.065$  et  $1.616 \pm 0.248$  jour<sup>-1</sup>, respectivement. Ces valeurs sont en accord avec celles précédemment observées.<sup>26, 27</sup> Nos résultats sur le système expérimental suggère que 85% de la dégradation se situe dans la colonne d'eau, et pointent une contribution potentielle des microorganismes planctoniques et des enzymes extracellulaires provenant du sédiment. L'enrichissement isotopique,  $\epsilon_c = -0.59 \pm 0.10\%$ , suggère une voie de dégradation par *N*-déméthylation qui correspond avec la voie de dégradation principale identifiée dans la littérature.<sup>28</sup> De plus, la vitesse d'écoulement de l'eau ne corrèle pas à la vitesse de dégradation observée, ce qui suggère que l'échange des flux au sein de zone hyporhéique pour la gamme des débits testés ne contrôle pas la dégradation comme initialement suggéré.

Dans le chapitre 6, nous présentons les résultats d'une campagne d'échantillonnage et de mesures du *S*-métolachlore à l'échelle du bassin versant de la Souffel (Bas-Rhin, France; 120 km<sup>2</sup>) entre mars et septembre 2019. Nous avons combiné un bilan de masse et l'approche CSIA pour évaluer la dégradation et la persistance du *S*-métolachlore en tenant compte des différentes sources à l'échelle d'un bassin versant. Ce chapitre constitue une preuve par concept de l'utilisation des informations accumulées durant les chapitres et les études précédente par notre équipe<sup>29-34</sup> afin d'estimer in situ la dégradation en utilisant la CSIA. L'estimation de la persistance du *S*-métolachlore avec la CSIA correspond à celle établie sur la base du bilan de masse. Le bilan de masse démontre une dégradation du *S*-métolachlore de  $98.9 \pm 4.7\%$  ( $\bar{X} \pm SD$ ) au sein du bassin versant avec une dégradation faible pour la rivière étant estimée à  $12.7 \pm 3.1\%$ . La participation respective de la photodégradation et de la biodégradation étant de  $10 \pm 3$  et  $2.7 \pm 2.3\%$ . En comparaison, la CSIA du *S*-métolachlore à l'échelle du bassin versant indique que  $98 \pm 20\%$  était dégradé après quatre mois d'application sur les champs. Les stations d'épuration contribuent à  $52 \pm 18\%$  des apports de *S*-métolachlore dans la rivière, basés sur la moyenne journalière des volumes d'eau. En comparaison, la contribution des sources reste

difficile sur la base de la CSIA parce que la signature isotopique du *S*-métolachlore, provenant des parcelles ou des stations d'épuration, étaient très proches. En résumé, nos résultats démontrent que la CSIA pour les pesticides permet d'estimer la dégradation globale à l'échelle d'un bassin versant.

Nous terminons au chapitre 7 en soulignant les conclusions principales de ces travaux, associées aux chapitres 2 à 6. Au chapitre 8, nous dressons des pistes d'exploration future afin d'améliorer la connaissance sur la dégradation des pesticides en milieu aquatique.

## Références

1. Food and Agriculture Organization of the United Nations FAOSTAT. [www.fao.org/faostat/](http://www.fao.org/faostat/) (20<sup>th</sup> March 2019).
2. Stehle, S.; Schulz, R., Agricultural insecticides threaten surface waters at the global scale. *Proc. Natl. Acad. Sci. U.S.A.* **2015**, *112*, (18), 5750–5755.
3. de Souza, R. M.; Seibert, D.; Quesada, H. B.; de Jesus Bassetti, F.; Fagundes-Klen, M. R.; Bergamasco, R., Occurrence, impacts and general aspects of pesticides in surface water: A review. *Process Saf. Environ. Prot.* **2020**, *135*, 22–37.
4. Schwarzenbach, R. P.; Egli, T.; Hofstetter, T. B.; von Gunten, U.; Wehrli, B., Global water pollution and human health. *Annu. Rev. Env. Resour.* **2010**, *35*, 109–136.
5. Dieter, C. A.; Maupin, M. A.; Caldwell, R. R.; Harris, M. A.; Ivahnenko, T. I.; Lovelace, J. K.; Barber, N. L.; Linsey, K. S. *Estimated use of water in the United States in 2015*; 1441; USGS: Reston, VA, **2018**; p 76.
6. Maggi, F.; Tang, F. H. M.; la Cecilia, D.; McBratney, A., PEST-CHEMGRIDS, global gridded maps of the top 20 crop-specific pesticide application rates from 2015 to 2025. *Scientific Data* **2019**, *6*, 170.
7. Vörösmarty, C. J.; McIntyre, P. B.; Gessner, M. O.; Dudgeon, D.; Prusevich, A.; Green, P.; Glidden, S.; Bunn, S. E.; Sullivan, C. A.; Liermann, C. R.; Davies, P. M., Global threats to human water security and river biodiversity. *Nature* **2010**, *467*, 555–561.
8. Lewandowski, J.; Arnon, S.; Banks, E.; Batelaan, O.; Betterle, A.; Broecker, T.; Coll, C.; Drummond, J. D.; Gaona Garcia, J.; Galloway, J.; Gomez-Velez, J.; Grabowski, R. C.; Herzog, S. P.; Hinkelmann, R.; Höhne, A.; Hollender, J.; Horn, M. A.; Jaeger, A.; Krause, S.; Löchner Prats, A.; Magliozzi, C.; Meinikmann, K.; Mojarrad, B. B.; Mueller, B. M.; Peralta-Maraver, I.; Popp, A. L.; Posselt, M.; Putschew, A.; Radke, M.; Raza, M.; Riml, J.; Robertson, A.; Rutere, C.; Schaper, J. L.; Schirmer, M.; Schulz, H.; Shanafield, M.; Singh, T.; Ward, A. S.; Wolke, P.; Wörman, A.; Wu, L., Is the hyporheic zone relevant beyond the scientific community? *Water* **2019**, *11*, (11), 2230.

9. Schaper, J. L.; Posselt, M.; Bouchez, C.; Jaeger, A.; Nuetzmann, G.; Putschew, A.; Singer, G.; Lewandowski, J., Fate of trace organic compounds in the hyporheic zone: Influence of retardation, the benthic biolayer, and organic carbon. *Environ. Sci. Technol.* **2019**, *53*, (8), 4224–4234.
10. Schaper, J. L.; Posselt, M.; McCallum, J. L.; Banks, E. W.; Hoehne, A.; Meinikmann, K.; Shanafield, M. A.; Batelaan, O.; Lewandowski, J., Hyporheic exchange controls fate of trace organic compounds in an urban stream. *Environ. Sci. Technol.* **2018**, *52*, (21), 12285–12294.
11. Hunkeler, D.; Meckenstock, R. U.; Lollar, B. S.; Schmidt, T. C.; Wilson, J. T. *A guide for assessing biodegradation and source identification of organic ground water contaminants using compound specific isotope analysis (CSIA)*; Environmental Protection Agency (EPA), US: **2008**; p 68.
12. Elsner, M.; Zwank, L.; Hunkeler, D.; Schwarzenbach, R. P., A new concept linking observable stable isotope fractionation to transformation pathways of organic pollutants. *Environ. Sci. Technol.* **2005**, *39*, (18), 6896–6916.
13. Harrington, R. R.; Poulson, S. R.; Drever, J. I.; Colberg, P. J. S.; Kelly, E. F., Carbon isotope systematics of monoaromatic hydrocarbons: vaporization and adsorption experiments. *Org. Geochem.* **1999**, *30*, (8A), 765–775.
14. Atwood, D.; Paisley-Jones, C. *Pesticides industry sales and usage 2008-2012 market estimates*; U.S. Environmental Protection Agency: Washington (US), **2017**; p 24.
15. The European Parliament and the Council, Directive 2000/60/EC establishing a framework for community action in the field of water policy. *Off. J. Eur. Communities: Legis.* **2000**, *43*, (L327), 1–73.
16. Barbosa, M. O.; Moreira, N. F. F.; Ribeiro, A. R.; Pereira, M. F. R.; Silva, A. M. T., Occurrence and removal of organic micropollutants: An overview of the watch list of EU Decision 2015/495. *Water Res.* **2016**, *94*, 257–279.
17. Ivdra, N.; Herrero-Martin, S.; Fischer, A., Validation of user- and environmentally friendly extraction and clean-up methods for compound-specific stable carbon isotope analysis of organochlorine pesticides and their metabolites in soils. *J. Chromatogr. A* **2014**, *1355*, 36–45.
18. Maier, M. P.; Prasse, C.; Pati, S. G.; Nitsche, S.; Li, Z.; Radke, M.; Meyer, A.; Hofstetter, T. B.; Ternes, T. A.; Elsner, M., Exploring trends of C and N isotope fractionation to trace transformation reactions of diclofenac in natural and engineered systems. *Environ. Sci. Technol.* **2016**, *50*, (20), 10933–10942.
19. Willach, S.; Lutze, H. V.; Eckey, K.; Löppenberg, K.; Lüling, M.; Wolbert, J.-B.; Kujawinski, D. M.; Jochmann, M. A.; Karst, U.; Schmidt, T. C., Direct photolysis of sulfamethoxazole using various irradiation sources and wavelength ranges — insights from degradation product analysis and compound-specific stable isotope analysis. *Environ. Sci. Technol.* **2018**, *52*, (3), 1225–1233.

20. Shrestha, P.; Junker, T.; Fenner, K.; Hahn, S.; Honti, M.; Bakkour, R.; Diaz, C.; Hennecke, D., Simulation studies to explore biodegradation in water–sediment systems: From OECD 308 to OECD 309. *Environ. Sci. Technol.* **2016**, *50*, (13), 6856–6864.
21. Boye, K.; Noël, V.; Tfaily, M. M.; Bone, S. E.; Williams, K. H.; Bargar, John R.; Fendorf, S., Thermodynamically controlled preservation of organic carbon in floodplains. *Nat. Geosci.* **2017**, *10*, 415.
22. Honti, M.; Hahn, S.; Hennecke, D.; Junker, T.; Shrestha, P.; Fenner, K., Bridging across OECD 308 and 309 data in search of a robust biotransformation indicator. *Environ. Sci. Technol.* **2016**, *50*, (13), 6865–6872.
23. Feng, P. C. C., Soil transformation of acetochlor via glutathione conjugation. *Pestic. Biochem. Physiol.* **1991**, *40*, (2), 136–142.
24. Field, J. A.; Thurman, E. M., Glutathione conjugation and contaminant transformation. *Environ. Sci. Technol.* **1996**, *30*, (5), 1413–1418.
25. Drouin, G.; Fahs, M.; Droz, B.; Younes, A.; Imfeld, G.; Payraudeau, S., Pollutant dissipation at the sediment–water interface: a robust discrete continuum numerical model and recirculating laboratory experiments. *Water Resour. Res.* **2020**, *submitted*.
26. Bradley, P. M.; Barber, L. B.; Kolpin, D. W.; McMahon, P. B.; Chapelle, F. H., Biotransformation of caffeine, cotinine, and nicotine in stream sediments: Implications for use as wastewater indicators. *Environ. Toxicol. Chem.* **2007**, *26*, (6), 1116–1121.
27. Benotti, M. J.; Brownawell, B. J., Microbial degradation of pharmaceuticals in estuarine and coastal seawater. *Environ. Pollut.* **2009**, *157*, (3), 994–1002.
28. Mazzafera, P., Catabolism of caffeine in plants and microorganisms. *Front. Biosci.* **2004**, *9*, 1348–1359.
29. Alvarez-Zaldívar, P.; Payraudeau, S.; Meite, F.; Masbou, J.; Imfeld, G., Pesticide degradation and export losses at the catchment scale: Insights from compound-specific isotope analysis (CSIA). *Water Res.* **2018**, *139*, 198–207.
30. Meite, F.; Alvarez-Zaldívar, P.; Crochet, A.; Wiegert, C.; Payraudeau, S.; Imfeld, G., Impact of rainfall patterns and frequency on the export of pesticides and heavy-metals from agricultural soils. *Sci. Total Environ.* **2018**, *616–617*, 500–509.
31. Lefrancq, M.; Payraudeau, S.; Guyot, B.; Millet, M.; Imfeld, G., Degradation and transport of the chiral herbicide *S*-metolachlor at the catchment scale: Combining observation scales and analytical approaches. *Environ. Sci. Technol.* **2017**, *51*, (22), 13231–13240.
32. Elsayed, O. F.; Maillard, E.; Vuilleumier, S.; Nijenhuis, I.; Richnow, H. H.; Imfeld, G., Using compound-specific isotope analysis to assess the degradation of chloroacetanilide herbicides in lab-scale wetlands. *Chemosphere* **2014**, *99*, 89–95.

33. Lutz, S. R.; van der Velde, Y.; Elsayed, O. F.; Imfeld, G.; Lefrancq, M.; Payraudeau, S.; van Breukelen, B. M., Pesticide fate at catchment scale: conceptual modelling of stream CSIA data. *Hydrol. Earth Syst. Sci. Discuss.* **2017**, *2017*, 1–30.
34. Masbou, J.; Drouin, G.; Payraudeau, S.; Imfeld, G., Carbon and nitrogen stable isotope fractionation during abiotic hydrolysis of pesticides. *Chemosphere* **2018**, *213*, 368–376.

## Table of content

<b>Acknowledgements</b>	<b>1</b>
<b>Résumé en Français</b>	<b>3</b>
<b>Chapter 1.</b>	
<b>General introduction</b>	<b>23</b>
Context .....	23
Pesticide sources and surface water contaminants .....	23
Pesticide transport and interactions from diffuse sources to surface waters .....	24
Atrazine and <i>S</i> -metolachlor as examples of surface water contamination .....	26
Pesticide abiotic degradation pathways in the water column .....	28
The sediment–water interface as a reactive interface in the surface water.....	29
Pesticide exchange and degradation at the hyporheic zone (HZ) .....	30
Tracking pesticide degradation in rivers.....	32
Compound-Specific Isotope Analysis (CSIA) to track in situ degradation.....	33
Research priorities and implications .....	39
Thesis Goal and Objectives.....	41
Thesis Outline .....	42
References .....	46
<b>Chapter 2.</b>	
<b>Pesticide extraction from soil and sediments for compound-specific isotope analysis (CSIA)</b>	<b>63</b>
Abstract .....	63
Introduction .....	64
Materials and methods .....	66
Sampling location .....	66
Sediment collection and characterization .....	66
Selection of the extractant.....	67
Sample preparation for method validation.....	67
Optimized extraction procedure.....	68
Pesticide quantification and compound-specific isotope analysis (CSIA) .....	68

Results and discussion.....	69
Selection of the extractant.....	69
Extraction method validation.....	69
Further improvements.....	71
Environmental implications.....	71
References .....	72

### Chapter 3.

#### **Direct and indirect photodegradation of atrazine and S-metolachlor in agriculturally impacted surface water and associated C and N isotope fractionation** **79**

Abstract .....	79
Introduction .....	80
Materials and methods .....	82
Chemicals and preparation of solutions.....	82
Experimental section.....	82
Analytical section .....	84
Data Analysis.....	85
Results and discussion.....	86
Effects of the hydrochemistry on the photodegradation rates under simulated sunlight .....	86
Formation of phototransformation products .....	89
C and N isotope fractionation to trace atrazine and S-metolachlor photodegradation .....	91
Environmental Implications.....	93
References .....	94

### Chapter 4.

#### **Phase-transfer and biodegradation of acetochlor and S-metolachlor in water–sediment systems** **99**

Abstract .....	99
Introduction .....	100
Materials and methods .....	101
Sediment sampling and characteristics .....	101
Experimental set-up .....	102
Control experiments.....	103
Pesticide extraction and quantification .....	103
Compound-specific isotope analysis (CSIA).....	104
Suspect screenings of transformation products .....	105
Phase-transfer and biodegradation modelling.....	106

Results and discussion.....	106
Dissipation kinetics and isotope fractionation .....	106
Water–sediment phase-transfer and implications for interpreting degradation kinetics .....	110
Water–Sediment Phase-Transfer and Implications for Interpreting Isotope Signatures.....	112
Pesticide degradation pathways .....	113
Environmental implications for water–sediment studies.....	115
References .....	116

## Chapter 5.

### **Organic pollutant biodegradation at the sediment–water interface in a bench-scale river channel: insights of compound specific isotopes analysis (CSIA) 123**

Abstract .....	123
Introduction .....	125
Materials and methods .....	127
Sediment characterizations .....	127
Batch sorption and biodegradation experiments.....	127
Bench-scale river channel.....	128
Dynamic biodegradation experiment.....	129
Caffeine extraction and quantification.....	131
Compound-specific isotope analysis (CSIA).....	131
Flow reactive transport modelling .....	132
Results and discussion.....	134
Caffeine sorption and degradation batch experiments.....	134
Influence of water flow on the depth of the oxic layer in sediment .....	135
Influence of water flow on caffeine biodegradation at the SWI.....	137
Environmental implications and perspectives .....	139
References .....	141

## Chapter 6.

### **Persistence of S-metolachlor in rivers: Insights from compound-specific isotope analysis (CSIA) 149**

Abstract .....	149
Introduction .....	150
Materials and methods .....	151
Catchment description .....	151
S-metolachlor applications.....	151
Sampling locations.....	152



Continuous sampling .....	152
Grab sampling.....	153
<i>S</i> -metolachlor extraction and quantification .....	154
<i>S</i> -metolachlor loads and mass balance.....	154
<i>S</i> -metolachlor compound-specific isotope analysis (CSIA) .....	155
Results and discussion.....	157
Catchment hydrological response .....	157
Off-site transport of <i>S</i> -metolachlor .....	158
<i>S</i> -metolachlor dissipation along the river during the season .....	160
Point versus non-point sources apportionment.....	161
<i>S</i> -metolachlor isotope signature along the river .....	163
Degradation of <i>S</i> -metolachlor in the river reach.....	164
Potential of the CSIA approach .....	166
Environmental significance .....	167
References .....	168

## Chapter 7.

### **General conclusion** **175**

Introduction .....	175
A compartment system.....	176
Key findings for the sediment–water interface .....	178
Implications.....	180
References .....	182

## Chapter 8.

### **Perspectives and implications** **185**

General consideration.....	185
Towards future investigation of pesticide dissipation at the SWI.....	186
Compound-specific stable isotope analysis (CSIA) of organic micropollutants in the sediment-water interface (SWI): potential application, limits and implications.....	188
Toward the chlorine isotope measurement .....	190
Improving sample preparation, accuracy, reproducibility, and sensitivity for CSIA measurements.....	191
References .....	194

**Appendix.**

**Supporting information to chapter 3 201**

Supporting materials and methods .....	201
List of chemicals .....	201
Organic matter photobleaching.....	202
PNA/Pyr actinometer system.....	203
Light spectrum homogeneity within the light-proof box.....	204
Prediction of degradation rates and identification of dominant photodegradation pathways .....	206
Calculation of short-lived reactive intermediates steady state concentrations .....	207
Identification of main photosensitizers.....	207
Calculation of light absorption rates and screening factors.....	209
Supporting Results .....	209

**Supporting information to chapter 4 213**

Abbreviations .....	213
Supporting materials and methods .....	214
Chemicals reagents .....	214
Sediment sampling and properties .....	215
Hydrochemistry .....	216
Batch sorption isotherm .....	217
Water-sediment extraction and effect on stable isotope signature of pesticides ...	218
Pesticide quantification.....	219
Compound-specific isotope analysis (CSIA).....	219
Mass balance accounting for the phase-transfer model .....	221
Supporting results and discussion .....	226
Sediment characteristics .....	226
Hydrochemistry .....	227
Control experiment .....	229
Batch sorption experiment .....	229
Method validation and limits .....	230
Pesticides Dissipation .....	231
Transformation products analysis .....	232

**Supporting information to chapter 5 233**

Supporting materials and methods .....	233
Chemicals reagents .....	233
Synthetic water preparation and characterization .....	233
Sediment properties .....	234

Table of content

Caffeine biodegradation pathway .....	235
Relationship between the nephelometric turbidity units (NTU) and the total suspended solid (TSS) .....	235
Rayleigh plots .....	236
Prediction of carbonate dissolution using the conductivity .....	237
Flow reactive transport model parameters.....	238
<b>Supporting information to chapter 6</b>	<b>239</b>
Supporting material and methods.....	239
Likelihood of crop rotation and <i>S</i> -metolachlor application dose.....	239
Pesticide mass balance.....	241
Hydrochemistry .....	242
Data availability.....	242
Wetness index .....	243
Concentration change of <i>S</i> -metolachlor within topsoil.....	244
Estimation of the volatilization after application.....	246
Estimation of photodegradation at the Souffel river.....	248
<b>Additional supporting information</b>	<b>249</b>
X-ray diffraction (XRD) spectra .....	249
Importance of dissolved organic carbon during autoclaving .....	250
Isotopic bulk enrichment factor ( $\epsilon_{bulk,E}$ ) from previous studies .....	252
<b>Supporting references</b>	<b>253</b>

## List of Figures

Figure 1.1. River catchment impacted by (a) agricultural diffuse sources of pesticide and (b) urban point-sources. ....	25
Figure 1.2. Proposed chloroacetanilide degradation pathway by the glutathione- <i>S</i> -transferase.. ....	27
Figure 1.3. Reactive scheme of the water column and biogeochemical gradients driving the reactivity.....	28
Figure 1.4. Dissolved and particulate transport of pesticide (black dots) across the hyporheic zone (HZ) as a function of water discharge.. ....	31
Figure 1.5. Principle of compound-specific isotope analysis (CSIA) to track in situ pesticide degradation in a river. ....	34
Figure 1.6. Degradation pathways identification with dual-element CSIA.....	37
Figure 1.7. Overview of the thesis, highlighting the increase in the complexity of processes to approach the representativity of the complexity of the river.....	43
Figure 3.1. Observed and predicted half-lives of (a) atrazine and (b) <i>S</i> -metolachlor under simulated sunlight. ....	88
Figure 3.2. Transformation products for (a) atrazine and (b) <i>S</i> -metolachlor in photolysis experiment.....	89
Figure 4.1. Carbon isotope signature ( $\delta^{13}C$ ) as a function of the pesticide remaining fraction ( $P(t)/P_0$ ) of (a) acetochlor and (b) <i>S</i> -metolachlor in oxic and anoxic water–sediment systems.....	107
Figure 4.2. Conceptual models of pesticide phase-transfer and degradation in the water (w) and sediment (s) phase system. ....	111
Figure 4.3. <i>S</i> -metolachlor and acetochlor transformation products (TPs) under oxic and anoxic conditions. ....	114
Figure 5.1. Scheme of the bench-scale river channel. Water is recirculated by a centrifuge pump via a mixing beaker used to ensure complete mixing of the experimental solution. ....	129
Figure 5.2. Observed ( $O_2$ foil sensors) and simulated (whole domain mapping) oxygen gradients in the sediment bed under low (a) and high (b) flow. ....	136
Figure 5.3. Observed (points) and simulated (lines) caffeine concentrations ( $C(t)/C_0$ , black) and isotope signatures ( $\delta^{13}C$ , red) for the low, medium and high flow conditions.....	138
Figure 6.1. The Souffel catchment with the sampling locations (in green, red and white) and the associated land use. ....	153
Figure 6.2. Dissolved <i>S</i> -metolachlor concentrations and loads at the outlet of the Souffel catchment in 2019. ....	158

List of Figures

Figure 6.3. Contribution of river and WWTPs to the total reach discharge (a) and associated <i>S</i> -metolachlor loads (b) for monthly sampling.....	162
Figure 6.4. Upstream-downstream <i>S</i> -metolachlor (a) concentrations and (b) isotope signature ( $\delta^{13}\text{C}$ ) in April (label 4) and June (label 6). .....	164
Figure 6.5. <i>S</i> -metolachlor carbon isotope fractionation ( $\Delta\delta^{13}\text{C} = \delta^{13}\text{C}(t) - \delta^{13}\text{C}_0$ ) over the growing season compared to the predicted topsoil $\delta^{13}\text{C}$ .....	166
Figure 7.1. Overview of the developed approach from smaller to larger spatial scale, with corresponding increasing complexity and environmental representativeness. The dashed color boxes indicate the targeted SWI compartment and the corresponding scale of investigation in each chapter.....	176
Figure A1. Temporal changes of absorbance of the TOT solution caused by organic matter photobleaching.....	202
Figure A2. Spatial distribution of irradiation intensity within the light-proof box. ....	205
Figure A3. Absorption spectra of atrazine, <i>S</i> -metolachlor, nitrates and SRFA at experimental concentrations. ....	205
Figure A4. Absolute light intensity as a function of the wavelength for the Xenon Arc Lamp as measured in the quartz tube after the liquid light guide. ....	206
Figure A5. Observed degradation kinetics (A) and Rayleigh plots for carbon (B) and nitrogen (C) for atrazine.....	211
Figure A6. Observed. degradation kinetics (A) and Rayleigh plots for carbon (B) and nitrogen (C) for <i>S</i> -metolachlor. ....	211
Figure A7. Dual C and N isotope plot for atrazine reflecting contrasted enrichment patterns between biotic oxidative dealkylation by the bacterial strain <i>Rhodococcus</i> sp. NI86/21, abiotic alkaline hydrolysis at <i>pH</i> equal to 12 and photodegradation in agriculturally impacted surface waters. ....	212
Figure B1. Changes of hydrochemistry during biodegradation experiments. (a) <i>pH</i> , (b) magnesium-calcium ( $\text{Mg}^{2+} + \text{Ca}^{2+}$ ), (c) chloride ( $\text{Cl}^-$ ), (d) sulfate ( $\text{SO}_4^{2-}$ ) and (e) nitrate ( $\text{NO}_3^-$ ) concentration. ....	228
Figure B2. Half-life dissipation ( $\text{DT}_{50}$ ) for atrazine (atr), terbutryn (terb), acetochlor (acet), <i>S</i> -metolachlor ( <i>S</i> -meto) and metalaxyl (meta) under (a) oxic and (b) anoxic conditions in the water and the sediment phases.....	231
Figure C1. Oxic biodegradation pathway of caffeine.....	235
Figure C2. Relationship between the nephelometric turbidity units (NTU) record with a turbidity meter (HI 88713, HANNA) and the total suspended solids (TSS) measured by weighting. ....	235
Figure C3. Logarithmic Rayleigh plot for the caffeine batch biodegradation experiment. Solid and dash lines express the linear fit and the 95% confidence interval of the Rayleigh equation.....	236

*List of Figures*

Figure C4. Relationship between the measured and the predicted conductivity from the sum of the cation–anion molar content, multiplied by the molar conductivity. ....	237
Figure D1. Topographical wetness index (TWI) of the Souffel catchment.....	243
Figure D2. Upstream and downstream normalized flow, i.e., discharge divide by surface of the corresponding sub-catchment, for all grab sampling events.....	244
Figure D3. Comparison of measured and predicted <i>S</i> -metolachlor topsoil concentrations around G10 (purple) and G11 (green).....	246
Figure E1. X-ray diffraction (XRD) of the wetland sediment a) spectrum and b) residual between non-autoclaved and autoclaved sediment spectrum. ....	249
Figure E2. Dissolved organic carbon (DOC) in non-autoclaved and autoclaved biodegradation experiments under oxic condition. ....	251

## List of Tables

Table 1.1. Elements and analytical methods available for pesticide CSIA. ....	36
Table 2.1. Pesticides selection of present and legacy agricultural input from European regions. ....	65
Table 2.2. Location and characterization of the soils and sediment samples. ....	67
Table 2.3. Yield of the extraction pre-tests. ....	69
Table 2.4. Reproducibility of optimized extraction method. ....	70
Table 3.1. C and N isotope fractionation for atrazine and <i>S</i> -metolachlor ( $\Delta\delta^{13}C$ and $\Delta\delta^{15}N$ ). ....	92
Table 4.1. Dissipation half-life ( $DT_{50}$ ), degradation half-life ( $DegT_{50}$ ), carbon bulk isotopic enrichment factor ( $\epsilon_{bulk,C}$ ) and apparent kinetic isotope effect (AKIE) for the bulk, water (w) and sediment (s) phase under oxic and anoxic experiments ....	109
Table 5.1. Bench-scale river channel experimental conditions. ....	130
Table 5.2. Biodegradation batches' condition, dissipation and degradation kinetics and C-N isotope fractionation, and bulk enrichment factors at low (LSW) and high (HSW) sediment–water ratios. ....	135
Table 6.1. <i>S</i> -metolachlor concentrations and load dynamics at the outlet of the Souffel catchment for the main rainfall events (export of 91% of the seasonal load). ....	160
Table A1. Chemical composition of irradiation solutions ....	202
Table A2. Irradiation conditions with Xenon arc lamp and correction factors used to estimate photodegradation rates. ....	204
Table A3. Kinetic parameters for formation and consumption of short-lived reactive intermediates. ....	208
Table A4. Comparison of predicted and observed degradation rates and presentation of the predicted contribution of each short-lived reactive intermediate to the overall photodegradation. ....	210
Table B1. Sediment characteristics. ....	226
Table B2. Change from days 0 to 300 of the dissolved organic carbon content ( $\Delta DOC$ ), specific ultraviolet absorbance ( $SUVA_{254/280}$ ) and mean carbon oxidation state ( $Ox$ ) in biodegradation experiments. ....	227
Table B3. Change from days 0 to 300 of the pesticide remaining fraction ( $P(t)/P_0$ ) and carbon isotope signatures ( $\delta^{13}C$ ) in the control experiment. ....	229
Table B4. Pesticide sediment partitioning coefficients. ....	229
Table B5. Extraction efficiency, qualitative and quantitative limit of the analytical methods. ....	230

## List of Tables

Table B6. Suspect list of parent compound and transformation product identified from the literature and screened by liquid chromatography (LC) coupled to an Impact-II (Bruker, Germany) quadrupole time of flight (Q-TOF) to perform high resolution mass spectrometry (HR-MS/MS). .....	232
Table C1. Sediment properties.....	234
Table C2. Flow reactive transport model parameters. ....	238
Table D1. Main crops type and <i>S</i> -metolachlor application at the Souffel catchment.....	239
Table D2. Analytic methods description. ....	240
Table D3. Attempted mass balance at the catchment scale: agricultural field and river. ....	241
Table D4. Water composition during grab sampling at each location ( $\bar{X} \pm \text{SD}$ ; $n = 7$ per location). ....	242
Table D5. Isotope signature ( $\delta^{13}\text{C}$ ) of commercial products containing <i>S</i> -metolachlor.....	246
Table D6. Local parameters used for the volatilization estimation. ....	247
Table E1. Mineralogy semi-quantitative pattern assignment. ....	250
Table E2. Isotopic bulk enrichment factor ( $\epsilon_{\text{bulk},E}$ ) and apparent kinetic isotope effects for carbon, nitrogen and chlorine found in the literature. ....	252





# **Chapter 1**

## **General introduction**

### **Context**

#### **Pesticide sources and surface water contamination**

Out of the 140,000 chemicals globally produced by manufactures and used in large amounts, i.e., more than 1 ton per year,<sup>1</sup> 1,500 are used for farming purposes, to control pests, e.g., fungi, weed, insects.<sup>2</sup> Compared to any other chemicals, organic pesticide molecules, hereafter called pesticides, have two unique features. Firstly, they are one of the most used group of chemicals in the world, with up to  $2.6 \times 10^6$  tons per year.<sup>3</sup> Secondly, pesticides are intentionally applied on a large scale in the environment, with up to  $15.3 \times 10^6$  km<sup>2</sup> of croplands and gardens, corresponding to 10% of the global land surface.<sup>4</sup> As pesticides are found worldwide in surface waters, e.g., rivers, wetlands or ponds,<sup>5-7</sup> which often serve as drinking water resources, serious concerns arise for human health.<sup>8,9</sup>

Forecasts predict that water use, frequency, drought severity and water scarcity will increase over the next years,<sup>10,11</sup> thus globally increasing the pressure on human water security and river biodiversity.<sup>12,13</sup> In addition, the use of pesticides is also predicted to increase in the next decades,<sup>14</sup> thereby threatening surface water quality. In addition to pesticides, the number of newly produced chemicals has raised, between 2002 and 2019, from 20 million to 156 million, according to the Chemical Abstract Service (CAS) Registry.<sup>15</sup> This emphasizes the broad diversity of chemicals that may reach surface waters, and the need to improve our understanding of the degradation processes of organic compounds in general, including pesticides, to secure our drinking water resources.

Two types of pesticide sources can be distinguished: diffuse sources (Figure 1.1, a), e.g., from agricultural fields or gardens, and point-sources (Figure 1.1, b), e.g., from wastewater treatment plants (WWTPs) and storm sewers.<sup>16</sup> In the case of diffuse sources, the main road for off-site transports from the field are: spray drift during the application, surface runoff and leaching, with subsequent transport through drainage channels during rainfall events (Figure 1.1, i). Spray drift (Figure 1.1, ii) may account for up to 75% of the total mass of pesticides applied, depending on the meteorological conditions, application methods and pesticide physico-chemical properties.<sup>17</sup> Rainfall events export pesticides by runoff, with a rate depending on both the time between application and rain, and the persistence of the pesticides.<sup>18</sup> From these rainfall events, a fraction of water might not reach surface waters, and directly recharge groundwater by infiltration from the field, with the concomitant transport of dissolved pesticide (Figure 1.1, iv). Off-site export reaching the surface water is estimated to be from 1 to 10% of the total applied mass of pesticides.<sup>19-21</sup> Diffuse sources have received main attention and are considered as the major contributors of the presence of pesticides in surface waters.<sup>22</sup> As a result, a broad variety of mitigation strategies have been proposed to minimize pesticide diffuse sources in surface waters.<sup>23</sup>

In contrast to diffuse sources, WWTPs and storm sewers act as pesticides' point-sources (Figure 1.1, iii) by collecting pesticides applied on upstream gardens, roads or parks from constructed materials, or resulting from non-appropriate operations at the farmyard during the filling or washing of the pesticide spraying equipment.<sup>24, 25</sup> As the design of WWTPs generally does not allow efficient removal of pesticides from wastewater,<sup>26-29</sup> WWTPs might contribute from 20 up to 80% of the pesticides loaded into the river, and may also lead to the formation of transformation products (TPs).<sup>30</sup> Point-sources have received less attention so far compared to diffuse sources, which have been sometimes neglected or under-evaluated.<sup>16, 31</sup> Point sources are directly connected to the river, whereas diffuse sources undergo transport and reactive process, as described in the next sections, with a potentially higher contribution to surface water pollution. Hence, point-sources should be accounted for in ongoing and future research on pesticide degradation in surface waters.

### **Pesticide transport and interactions from diffuse sources to surface waters**

Currently used pesticides in agriculture are typically soluble organic compounds, slightly polar ( $\log P_{ow} < 10$ ), non-volatile and with a moderate sorption affinity ( $\log K_{OC}$  around two).<sup>32</sup> Following application, pesticides may be transported off-site and distributed among the environmental compartments, mainly: soil, sediment and water.<sup>33</sup> How many pesticides are transported and distributed among these compartments mainly depends on soil hydraulic properties (permeability, water flow patterns) as well as the environmental parameters, such as the topography of the catchment, and meteorological conditions which mainly drive the off-site transport from the source to the surface water.<sup>34</sup> Consequently, the off-site pattern of

pesticides during a growing season is dictated by the rainfall event and characteristics, which may transport pesticides in a soluble or particulate form.<sup>18, 35, 36</sup>

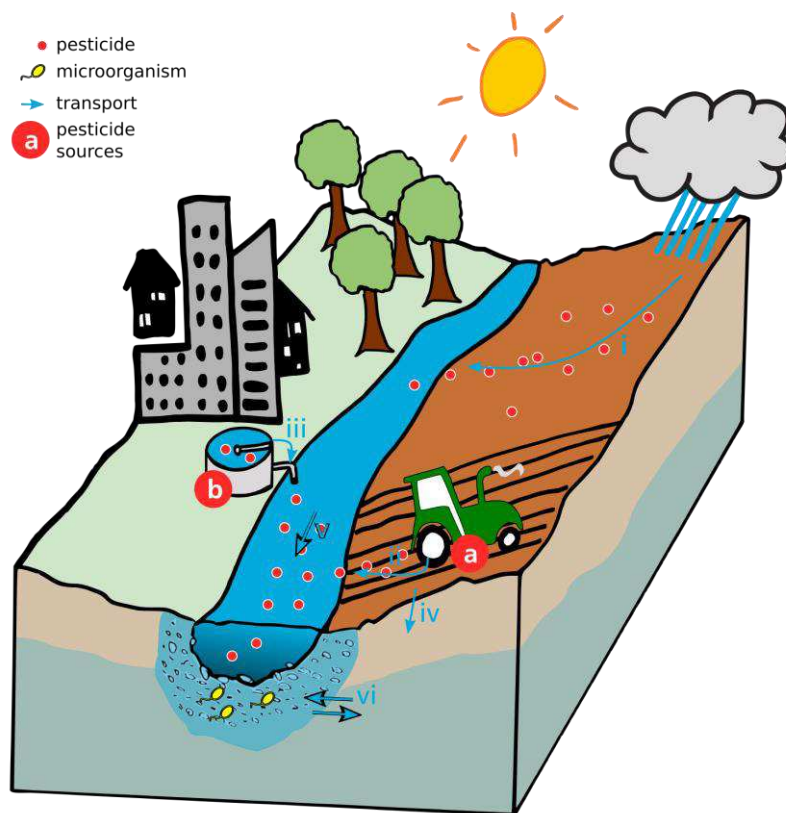


Figure 1.1. River catchment impacted by (a) agricultural diffuse sources of pesticide and (b) urban point-sources. Pesticide behavior is also governed by transport processes, including: (i) surface runoff through drainage channels during rainfall events; (ii) spray drift during application; (iii) wastewater discharge; (iv) groundwater recharge from the field; (v) river flow transport; and (vi) hyporheic exchange between the river and groundwater. Adapted from 16, 37, 38.

In contrast, physico-chemical properties of the pesticides, i.e.,  $P_{ow}$ ,  $K_{OC}$ , solubility of the pesticides have less impact on transport but explain differences between transport behaviors for different pesticides at the same location or at field scale.<sup>39, 40</sup> For instance, sorption properties ( $K_{OC}$ ) typically increase the pollutant residence time within the soil or sediment,<sup>41, 42</sup> thus decreasing availability for microbial degradation.<sup>43</sup> Along the road of the transport of pesticides from the source to the surface water, pesticides might be degraded by biotic and abiotic processes occurring in all compartments including soil, sediment, surface water and groundwater, which are described in the up-coming section. As this thesis focuses on surface waters, the following section describes the pesticide degradation processes in surface waters, including the water column and the sediment-water interface, although degradation occurs also in the soil.

## Atrazine and *S*-metolachlor as examples of surface water contaminants

One good example to witness the persistence and transport of pesticides from agricultural fields to surface waters is the atrazine. Atrazine was banned in Europe in 2004, and it remains one of the most-used herbicides in the U.S., Australia, Brazil, and India.<sup>2, 3, 44</sup> In Europe, atrazine and desethylatrazine (DEA), one of its main TPs, were detected in 68% and 48%, respectively, in the 122 European rivers investigated.<sup>45</sup> Occurrences of atrazine TPs prove atrazine degradation in the environment. Atrazine and DEA were detected in 56% and 55%, respectively on 164 groundwater bodies in a EU-survey with a concentration up to 253 ng L<sup>-1</sup> and 487 ng L<sup>-1</sup>, respectively.<sup>46</sup> Contamination is even higher in very intensive farming areas such as in Alsace, France, where atrazine and DEA were detected in more than 70% of the 274 wells.<sup>47</sup> In comparison, in the US, the National Water-Quality Assessment (NAWQA) by the United States Geological Survey (USGS), detected atrazine in 95% of 178 US rivers<sup>48</sup>, where about 45% were above 0.1 µg L<sup>-1</sup>. Atrazine was previously identified as degradable under oxic and anoxic conditions,<sup>49</sup> although biodegradation tends to slow down when atrazine concentrations are below 1 µg L<sup>-1</sup>.<sup>50</sup> At those concentrations, mass transfer across the membrane may become rate-limiting for degradation,<sup>51</sup> which may explain the persistence of atrazine in groundwater, and exemplifies the current challenge for the bioremediation at low concentrations.<sup>52</sup>

Another example of pesticide transport from the fields to the surface water is *S*-metolachlor, a chloroacetanilide herbicide, widely used all over the world (eighth rank of mass sold)<sup>3</sup> and frequently found in surface waters during the application period.<sup>53, 54</sup> *S*-metolachlor degradation in the field is faster than that of atrazine over the growing season (up to 93%).<sup>20</sup> Degradation of *S*-metolachlor could be proved by the presence of the TPs, which are usually detected in groundwater in higher concentrations than *S*-metolachlor.<sup>45, 55</sup> The two major TPs are the *S*-metolachlor oxalinic acid (MET-OXA) and the metolachlor ethanosulfonic acid (MET-ESA), which are more persistent but less toxic than their parent compounds.<sup>33</sup> The *S*-metolachlor degradation in SWI likely occurs through the glutathione-*S*-transferase (Figure 1.2) and seems to produce less MET-ESA than MET-OXA.<sup>56, 57</sup> Other chloroacetanilide pesticides, e.g., acetochlor, follow the same degradation pathway, i.e., the overall sequence of reactions from substrate to product(s), and fate in surface water.<sup>58</sup> Despite lower production, the MET-ESA is more soluble, i.e., mobile, and, as a consequence, can be found in the environment to a larger extent than any other *S*-metolachlor TPs.<sup>53</sup> However, the biochemical and environmental conditions leading to the dominant production of MET-OXA over the MET-ESA have not been elucidated, although it is a crucial to anticipate the TPs contamination in surface waters regarding to the larger mobility of MET-ESA.

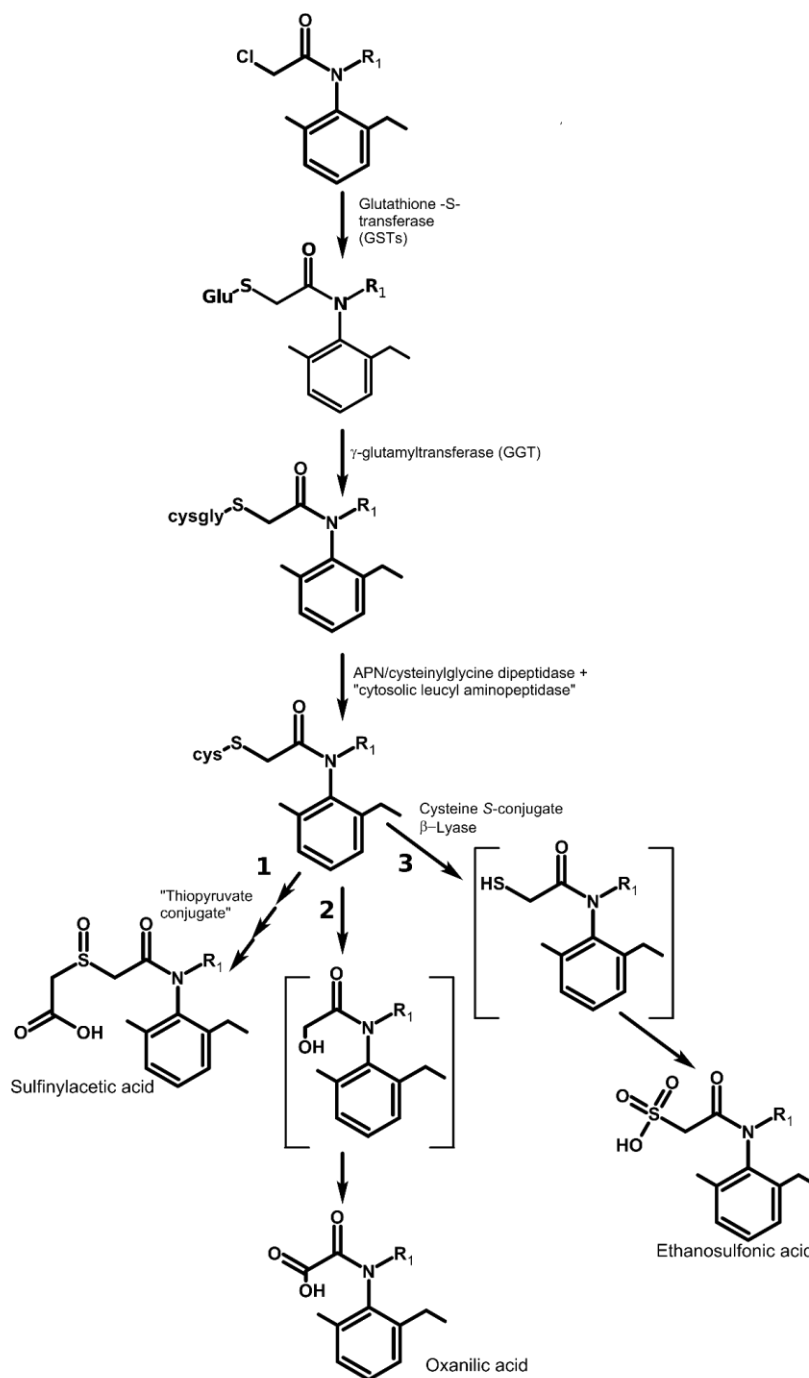


Figure 1.2. Proposed chloroacetanilide degradation pathway by the glutathione-S-transferase as described elsewhere.<sup>56, 57, 59</sup> The cysteine S-conjugate  $\beta$ -lyase is an intermediate with three reactions (1,2 & 3) ended to 1. the sulfinylacetic acid, 2. oxanilic and 3. ethanosulfonic acid TPs. Road 1 is considered as minor (<10%) compared to the pathways 2 & 3. In brackets, intermediate compounds have been suggested but never observed. Road leading to sulfinylacetic acid (1) is not elucidated.

## Pesticide abiotic degradation pathways in the water column

Abiotic degradation processes include hydrolysis and photolysis (Figure 1.3), which are occurring mostly in the water column, and to a lesser extent in other compartments, e.g., the soil. Hydrolysis occurs only in the presence of water, which limits the hydrolysis in dry soil. However, hydrolysis depends on *pH* and mainly concerns ionizable pesticides in the environment.<sup>60</sup> In contrast, photolysis mainly occurs in the water column due to a large penetration of the solar spectrum into water, from one to several meters deep, depending on the amount of turbidity of the water,<sup>61,62</sup> whereas photolysis typically acts in less than one mm in soil.<sup>63</sup> Photolysis occurs under direct photolysis and indirect photolysis (Figure 1.3a).<sup>64</sup>

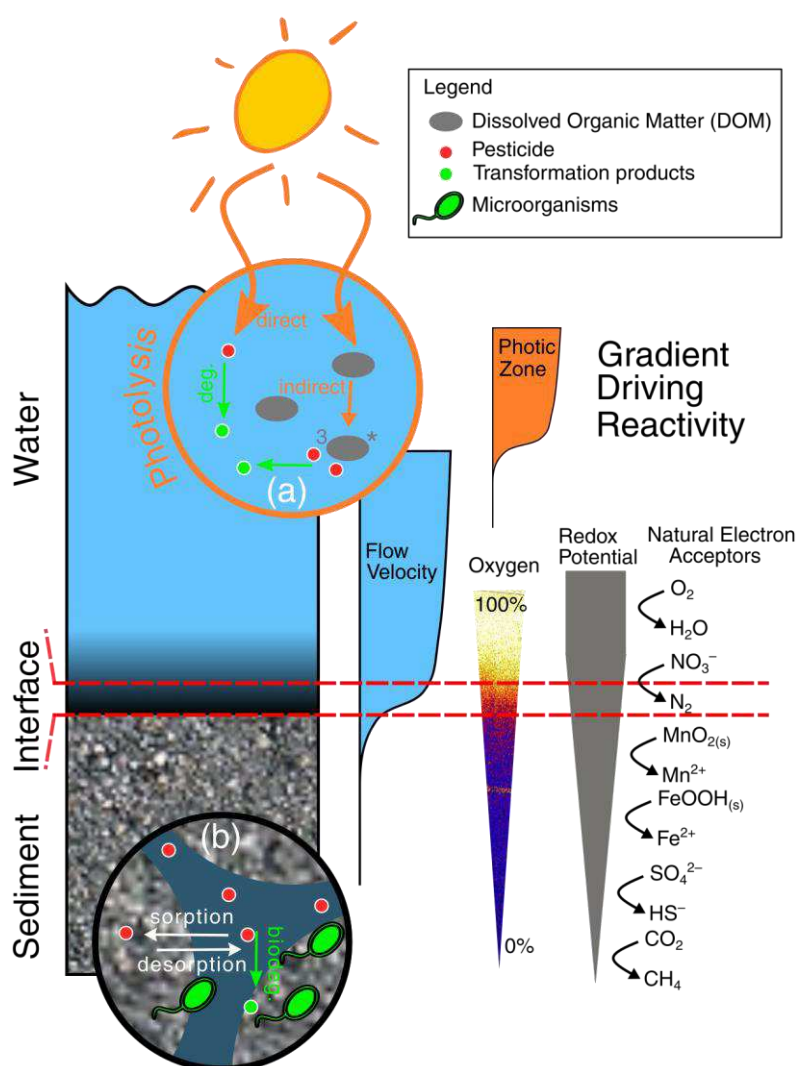


Figure 1.3. Reactive scheme of the water column and biogeochemical gradients driving the reactivity. Main processes are: (a) photodegradation and (b) phase-transfer and biodegradation.

Direct photolysis is relevant for a few pesticides, absorbing the natural light spectrum and can be predicted from their molecular structure.<sup>64, 65</sup> In contrast, indirect photolysis involves short-life reactive intermediates (RIs), such as singlet oxygen ( $^1\text{O}_2$ ), hydroxyl radical ( $\text{HO}\bullet$ ) or dissolved organic matter (DOM) excited triplet states ( $^3\text{DOM}^*$ ), depending on the water chemistry rather than the physico-chemical properties of the organic compound.<sup>62, 66</sup> The RIs production and their relative contribution to the degradation of specific pesticides could be estimated based on the photon flux, i.e., the number of photon per second per unit area, and the composition of dissolved species in water.<sup>67-69</sup> RIs can be produced by dissolved oxygen, DOM and nitrate. DOM is composed of a myriad of compounds, including photoreactive structure, such as aromatic ketones and aldehydes, quinones and phenolic compounds.<sup>70-72</sup> In opposite to RIs production, phenolic compounds that constitute DOM tend to inhibit the formation of  $^3\text{DOM}^*$  and by consequence the indirect photolysis.<sup>73, 74</sup> Altogether, knowledge of the origin of RIs-DOM and predictions from the optical properties, i.e., absorbance and fluorescence remains limited. Moreover, direct and indirect photolysis are conjointly occurring at surface waters with biodegradation process. Despite these limitations, the photodegradation should be evaluated, considered and predicted for a given pesticide and water composition as it might constitute an important degradation pathway in surface waters.<sup>66, 75, 76</sup>

### **The sediment–water interface as a reactive interface in the surface water**

In surface waters, the sediment–water interface (SWI) is identified as the reactive interface where sediments provide a large surface supporting microbial development (Figure 1.3b)<sup>77</sup> and where nutrients settling provide favorable conditions for microbial activities.<sup>43</sup> This interface occurs between two compartments in surface waters: the water column, including total suspended solid (TSS), and the sediment bed, with the pore water. Due to the low abundance of freely microorganisms in water phase and the low activity of free-enzyme, the sediment bed is considered as a main compartment for biodegradation.<sup>78, 79</sup>

The reactive zone of the river, where surface water and groundwater meet, is the hyporheic zone (HZ; Figure 1.1, vi).<sup>80</sup> The HZ plays a critical role in self-purification of rivers, as the interplay of complex physical, chemical and biological processes, creating ideal conditions for organic matter decomposition, oxygen transfer and biodegradation of contaminants,<sup>81, 82</sup> which could contribute to various biotic and abiotic degradation pathways across gradients of redox conditions.<sup>83</sup> At the HZ, common degradative enzymatic pathways involving the superoxide production<sup>84</sup> or the glutathione<sup>85</sup> seem ubiquitous in microorganisms' world, which attest the capabilities of several microbial taxa to efficiency degrade pesticides. In addition, microorganisms can produce new nonspecific enzymes capable to degrade newly introduced organic compounds and facilitate their degradation.<sup>86</sup>



In contrast to processes in the water column, abiotic pesticide degradation in the SWI remains limited. Abiotic oxidative/reductive degradation processes at the SWI (Figure 1.3b) constitute the boundary between abiotic and biotic degradation because they are often microorganism mediated processes.<sup>87, 88</sup> For instance with the production of iron or manganese oxide by some bacteria which could rapidly degrade pesticides.<sup>89, 90</sup> Finally, few complete abiotic reductive degradation pathways are reported in literature.<sup>37</sup> The nucleophile substitution by bisulfide ( $\text{HS}^-$ ) and polysulfides ( $\text{S}_n^{2-}$ ) seems to be the most reported pathways, although suitable conditions for this degradation pathway seems to be only present in hypoxic marine waters<sup>91-93</sup> or rich sulfidic peat bog environment.<sup>94</sup>

Current methodologies to evaluate the dissipation efficiency at SWI are generally assessed in laboratory systems called water–sediment systems, where observed dissipation processes include biodegradation and phase-transfer (i.e., adsorption–desorption).<sup>95</sup> However, the combination of both processes is rarely estimated, which constitutes a current gap of knowledge for predicting pesticide behavior at the SWI.<sup>96</sup>

### **Pesticide exchange and degradation at the hyporheic zone (HZ)**

Pesticide dissipation along a river from upstream to downstream depends on the contribution of degradative and non-degradative processes described in the previous sections. The water discharge driving dissolved and particulate pesticides transport (Figure 1.1, v) from upstream to downstream and across the HZ.<sup>97, 98</sup> The mass exchanges of dissolved organic compounds and oxygen across the HZ, called hyporheic exchange flows (HEFs), strongly depend on water discharge, sediment morphology and texture, i.e., sand, silt and clay composition, leading to significant variations of organic compounds over sediment depth.<sup>80, 99-101</sup> Hence, the relative contribution of degradation and transport processes depends on the hydraulic forcing, and drastically varies from quasi-static, e.g., base flow, to turbulent regimes, e.g., floods.<sup>100</sup>

Under low discharge (Figure 1.4a), dissolved organic compound and oxygen transport is solely driven by the molecular diffusion coefficient whereas transport for dispersive and turbulent regimes is controlled both by diffusion and advection (Figure 1.4b & c). Under dynamic conditions, dissolved organic compounds and oxygen exchanges across the HZ are both molecular diffusion and advection depending on water flow regime.<sup>97</sup> Relationships describing the normalized effective diffusivity of a dissolved organic compound and oxygen through the SWI in the function of the water flow regime have been reported.<sup>97, 102-107</sup> However, despite identifying the role of sediment in the degradation of organic compounds<sup>108-111</sup> and the degradation pathway occurring at the oxic HZ,<sup>81, 82, 112-115</sup> to our knowledge, the relationship between water discharge and the HZ biodegradation activity have not been addressed for pesticides yet.

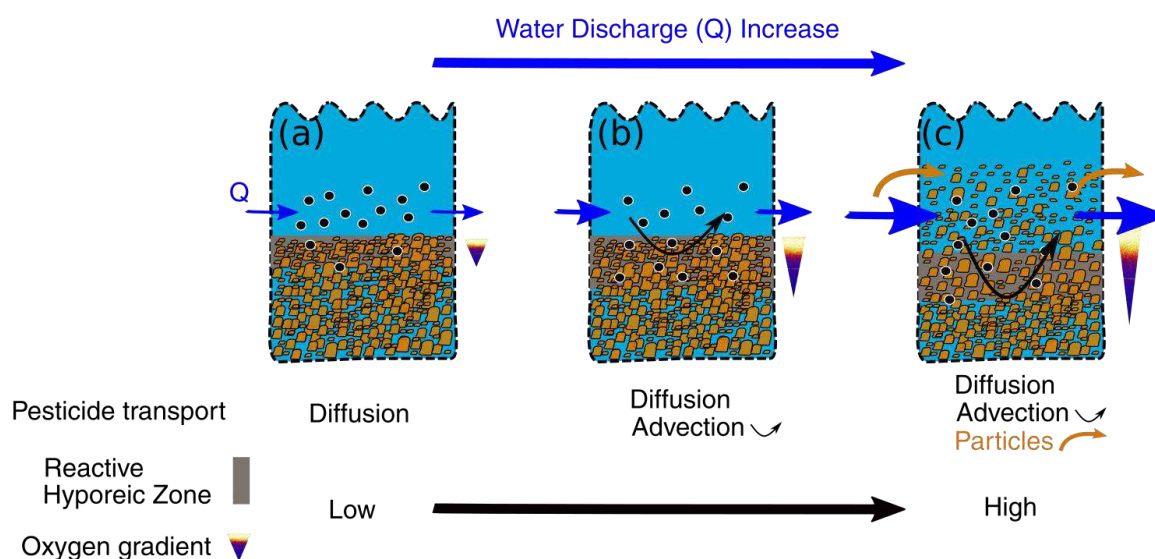


Figure 1.4. Dissolved and particulate transport of pesticide (black dots) across the hyporheic zone (HZ) as a function of water discharge. Scheme (a), (b) and (c) represent the hypothetical relationship between pesticide transport, sediment mobilization, flow regimes and the increase of the oxygen gradients for low-, medium- and high-water discharges (Q).

In addition to dissolved species, suspended particles may transport a significant amount of hydrophobic, solid-bound organic compounds during flood events (similar as shown in Figure 1.3b). The particulate transport includes off-site from the field by erosion<sup>20, 116</sup> and remobilization from the riverbed sediment in the water column.<sup>117-119</sup> Transport of dissolved and solid-bound organic compound is controlled by sorption–desorption processes occurring in soil and sediment. The partitioning coefficient ( $K_d$ ) is used to predict the extent of these partitioning processes along the transport in the river.<sup>40, 120</sup> Reversible sorption processes within the riverbed sediment of dissolved pesticides on organic matter could decrease pesticide degradation along with the HZ and acting as a source of organic compound leading to an overestimation of the in situ reactivity.<sup>121-123</sup>

Despite the importance of the HZ in biodegradation, the interest has been focused to understand the transport of organic compound rather than the association between transport and reactivity. As a consequence, the hypothesis that water discharge controls the reactivity of the HZ through the incorporation of dissolved oxygen and pesticides and HEFs has been broadly raised but never addressed experimentally.

## **Tracking pesticide degradation in rivers**

Although large pesticide contamination on surface waters has been widely reported over decades of environmental monitoring,<sup>124</sup> knowledge about the fate and transport of pesticide and TPs in surface waters and the SWI remains poorly understood.<sup>125</sup> One major difficulty is to track the occurrence of degradation and predict the time, i.e., “hot-moment”, and the location, i.e., “hotspot”, of pesticide degradation or persistence within a river stretch.<sup>96,</sup>  
126

Studies about pesticide dissipation in rivers mainly rely on concentrations of parent pesticides and their TPs, to estimate impacts on ecosystems and on the drinkability of surface waters. Indeed, ecotoxicological impacts and drinkability are assessed, based on concentration threshold. However, concentration measurement alone cannot differentiate degradative and non-degradative processes and can hardly provide estimates for the extent of degradation along a river stretch. In addition, traditional methods use in laboratory to directly identify pesticide degradation with mass balance might required significant monitoring efforts to quantify both discharge and associated pesticide concentrations with continuous or flow proportional sampling.<sup>127</sup> Discharge monitoring and concentration sampling strategies may produce large uncertainties on the calculated masses flow,<sup>128</sup> larger than the extent of degradation along a river. As a consequence, in most of the cases, traditional mass balance approaches are only applicable for significant pesticide degradation extents, i.e., for pesticides with low persistence and/or concerning a sufficiently long river section.

On the other hand, the identification of TPs, used to prove the evidence of a degradation, only do so assuming that the TPs are known, which is not always the case. Moreover, TPs quantification to estimate the extent of degradation faces two major problems. Firstly, only a proportion – between 10 to 70% – of the total number of TPs can generally be identified.<sup>124, 129</sup> Secondly, only a few detected TPs have available standards to allow quantification. Recent development in liquid chromatography coupled with high-resolution mass spectrometry (HR-MS/MS) has partially addressed these two limitations. While most TPs can now be predicted from a parent pesticide structure,<sup>15</sup> machine learning helps in estimating the concentration without available standards for a calibration.<sup>130</sup> However, prediction of TPs structures and the use of machine learning are built on knowledge from analogue pesticides, thereby limiting the development for new classes of pesticides.

Finally, twenty-five percent of pesticides are chiral,<sup>131</sup> i.e., pesticides presenting one or more carbon bonds with four different substituents, resulting in a number of enantiomers equaling twice the number of chiral carbon.<sup>62</sup> Enantiomers are molecules non-superimposable mirror images of each other, they may react at different rates depending on the environment.<sup>132</sup> Thus, some degradation pathways can be enantio-selective, i.e., degrading selectively or quicker one enantiomer compared to the others. As a consequence, an enantiomeric enrichment can be observed and used to derive degradation extents.<sup>116, 133, 134</sup> Following the same approach, the change of stable isotope ratios of pesticide can be used as an alternative to mass balance approaches along a river.

### **Compound-Specific Isotope Analysis (CSIA) to track in situ degradation**

To improve interpretation of pesticide degradation in river systems, compound-specific isotope analysis (CSIA) has the advantage to provide evidence of the in-situ degradation without knowledge about TPs and without complete mass balance. CSIA has already proved the long-time scale monitoring studies on degradation of organic contaminant in groundwater and the ability to track source apportionment.<sup>135</sup> For each element, different stable isotopes exist with different natural isotope abundance, e.g., the ratio of  $^{13}\text{C}/^{12}\text{C}$  and  $^{15}\text{N}/^{14}\text{N}$  are equal to 1.123 and 0.366%, respectively (Table 1.1). The concept of CSIA relies on isotope fractionation, i.e., the isotope ratio change, caused by the cleavage or formation of a chemical bond of an organic compound. Light, e.g.,  $^{12}\text{C}$  or  $^{14}\text{N}$  and heavy, e.g.,  $^{13}\text{C}$  or  $^{15}\text{N}$  isotopes are degraded at slightly different rates and enrichment in the heavier isotopes of the non-degraded organic compound fraction in environmental samples may be observed.<sup>136</sup> This effect, called kinetic isotope effect (KIE), reflects the rate-limiting step of the involved mechanism. In contrast to degradation, non-degradative processes, such as phase transfer (e.g., sorption, volatilization), dilution by water or transport processes (diffusion) are generally conservative in terms of isotope ratios.<sup>137</sup>

In the context of pesticide polluted rivers, change of stable isotope ratios of a pesticide along a river (Figure 1.5) can provide information of ongoing pesticide degradation. With some laboratory experiments about the hypothesis and calculation described below, CSIA may allow quantifying degradation extent along a river.

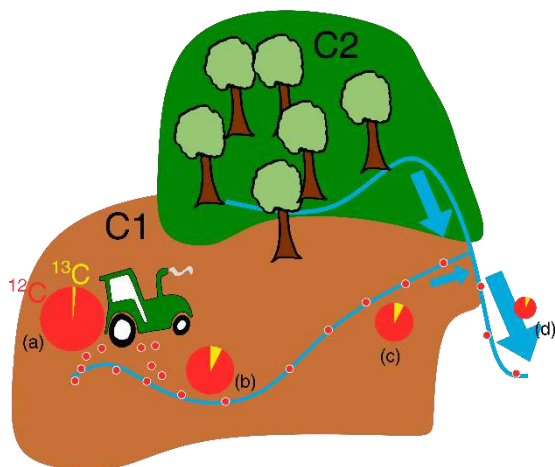


Figure 1.5. Principle of compound-specific isotope analysis (CSIA) to track in situ pesticide degradation in a river: C1 (brown) impacted catchment by pesticide (red dots) and C2 (green) catchment without pesticide sources. The diameter of the pie chart is proportional to the pesticide concentration along the river (in blue, the arrow sizes are proportional to discharge). The yellow to red ratio on the pie chart corresponds to the isotope ratio  $^{13}\text{C}/^{12}\text{C}$  of the targeted pesticide. (a) Pesticide source, i.e., the sprayer tank or top-soil concentration after application: isotope signatures of pesticides

differ if they are manufactured from different raw materials or by different synthesis processes, (b) Case 1: Lower pesticide concentrations and corresponding enrichment in  $^{13}\text{C}$  of the pesticide molecule close to the area of pesticide application indicates the occurrence of degradation in the river, (c) Case 2: Lower pesticide concentrations without change of isotope ratios along the river indicates non-degradative processes, e.g., dilution and/or sorption, (d) Case 3: Lower pesticide concentration due to dilution (pristine water coming from C2 catchment) without degradation is characterized by similar isotope ratios.

Isotope ratio measurements are reported as delta notation per element ( $\delta^h E$ ), in parts per thousand (‰) relative to a standard measurement specific for the element (Table 1.1),

$$\delta^h E = \frac{R(^h E/^l E)_{\text{sample}}}{R(^h E/^l E)_{\text{standard}}} - 1 \quad (1.1)$$

where  $\delta^h E$  is the isotope signature of the respective element ( $E$ ) and  $R(^h E/^l E)$  is the isotope ratio of heavy ( $h$ ) to light ( $l$ ) isotopes in a sample and standard ((Table 1.1). In laboratory, under closed system and pseudo first-order kinetics, bulk isotopic enrichment factor ( $\epsilon_{\text{bulk}, E}$ ), i.e., a change in overall  $^{13}\text{C}/^{12}\text{C}$  or  $^{15}\text{N}/^{14}\text{N}$ , associated with a specific degradation pathway, generally follows the Rayleigh equation:<sup>138</sup>

$$\ln\left(\frac{\delta^h E(t) + 1}{\delta^h E_0 + 1}\right) = \varepsilon_{bulk,E} \times \ln\left(\frac{P(t)}{P_0}\right) \quad (1.2)$$

where  $\delta^h E_0$  and  $\delta^h E(t)$  represent the isotope signatures of an element  $E$  at time zero and  $t$  of the degradation respectively, while  $P(t)/P_0$  is the fraction of the remaining pesticide at time  $t$ .

Once a specific  $\varepsilon_{bulk,E}$  has been obtained under specific conditions from laboratory experiment, it can be used on the environment to evaluate the extent of degradation ( $B$ ) without any information on TPs and concentration,

$$B = \left(\frac{\delta^h E(t) + 1}{\delta^h E_0 + 1}\right)^{1/\varepsilon_{bulk,E}} \quad (1.3)$$

However, CSIA is a relatively new tool used in surface waters and research on pesticide degradation, which currently faces some challenges.<sup>126</sup> A major challenge is the low concentration of pesticides present in the surface water in comparison with the typical current sensitivity of the GC-IRMS (Table 1.1). Second, the analytical uncertainty associated with the observed fractionation limits our capability to detect a biodegradation extent when the  $\varepsilon_{bulk}$  is small. For instance, for the  $\delta^{13}C$ , with a typical uncertainty of  $\pm 0.5\%$  and considering a methyl group oxidation ( $\varepsilon_C = -3.0\%$ ) or a ring oxidation ( $\varepsilon_C = -0.4\%$ ) on toluene, the biodegradation extent could be precisely estimated only if 15% and 70% have been degraded respectively.<sup>139</sup> Third, accurate GC-IRMS measurement is very sensitive to the background signal measurement effect caused by the sample matrix, e.g., natural organic matter compounds containing carbon and nitrogen, which are generally abundant in environmental samples, compared to experimental samples. This limit accurate measurements of pesticides' isotope ratio in samples with a large amount of elementary carbon or nitrogen. Finally, highly polar pesticides cannot be detected directly on GC-IRMS without derivatization prior to GC separation.<sup>140, 141</sup> However, derivatization induces an additional isotope signal accounted for the derivation product, which should be corrected. Hence, preparation methods to reduce sample matrix and to analyze more polar compounds are some current challenges that need to be tackled to develop pesticide CSIA in surface waters.

Table 1.1. Elements and analytical methods available for pesticide CSIA.

isotope ratio	separation - interface system - detection	abundance in standard (%)	reference material <sup>a</sup>	analyte gas	typical uncertainty (%) <sup>b</sup>	typical sensitivity (nmol) <sup>b</sup>
<sup>2</sup> H/ <sup>1</sup> H	GC-Pyr-IRMS <sup>c</sup>	0.01558	water (VSMOW)	H <sub>2</sub>	2–5	10–50
<sup>13</sup> C/ <sup>12</sup> C	GC-Comb-IRMS	1.123	carbonate (VPDB)	CO <sub>2</sub>	0.1–0.5	0.1–5
<sup>15</sup> N/ <sup>14</sup> N	GC-Comb/Red-IRMS	0.366	air (air)	N <sub>2</sub>	0.3–1.0	1–10
<sup>18</sup> O/ <sup>16</sup> O	GC-Pyr-IRMS	0.201	water (VSMOW)	CO	0.3–0.6	4–14
<sup>34</sup> S/ <sup>32</sup> S	Comb-IRMS <sup>d</sup>	4.416	Barium Sulfate (IAEA-SO-5)	SO <sub>2</sub>	n.r.	n.r.
	GC-ICP-HRMS <sup>e</sup>		Vienna-Canyon Diablo Troilite (VCDT)	S	<0.3	n.r.
	GC-Comb-IRMS <sup>f</sup>			HCl	<0.3	<0.015
<sup>35</sup> Cl/ <sup>37</sup> Cl	GC-ICP-HRMS <sup>g</sup>	31.96	water (SMOC)	Cl	0.12	0.2
	GC-qMS <sup>h</sup>			frag.	0.5–1	<0.1
<sup>81</sup> Br/ <sup>79</sup> Br	GC-ICP-HRMS <sup>i</sup>	97.27	water (SMOB)	Br	0.3	0.3
	GC-qMS <sup>j</sup>			frag.	0.2–0.3	n.r.

Adapted from<sup>139, 142</sup> Ref. <sup>a</sup> 143, 144, <sup>b</sup> 145, <sup>c</sup> note that CSIA measurement for compound with heteroatoms (i.e., N, Cl, S, I, Br) has been affected by the formation of compounds of HCN, HCl, H<sub>2</sub>S, HBr or HI who hamper the measurement. Strategy using Chromium-Based High-Temperature Conversion (Cr/HTC) instead of classic HTC has been used for those compounds.<sup>146</sup> <sup>d</sup>No CSIA application exist yet but the comb-IRMS system allow the measurements.<sup>147, e</sup> 148, <sup>f</sup> 149, <sup>g</sup> 150, 151, <sup>h</sup> 152, <sup>i</sup> 153, <sup>j</sup> 154. GC: gaz chromatography, Comb: combustion, Comb/red: combustion followed by reduction, Pyr: pyrolysis, IRMS: isotope ratio mass spectrometer, HRMS: high-resolution mass spectrometer, qMS: quadrupole mass spectrometer, ICP: inductively coupled plasma, n.r. not reported. frag: mass fragment, for instance for the analysis of the pentachlorophenol the MS mass fragment 264 and 266 are produced use to calculate the isotope ratio.<sup>155</sup>

Currently used pesticides are organic compounds, very often containing heteroatoms, i.e., other than carbon or hydrogen, which may express higher isotope fractionation than C during degradation<sup>126</sup>, and as a consequence provide a very sensitive indicator of degradation.<sup>156</sup> However, commercially available gas chromatography–isotope ratio mass spectrometry (GC-IRMS) allows precise and accurate measurement of major isotope ratios, e.g., <sup>2</sup>H/<sup>1</sup>H, <sup>13</sup>C/<sup>12</sup>C, <sup>15</sup>N/<sup>14</sup>N and <sup>18</sup>O/<sup>16</sup>O (Table 1.1). Current analytical methods and approaches to expand measurements to promising heteroatom isotope ratio, e.g., <sup>34</sup>S/<sup>32</sup>S, <sup>35</sup>Cl/<sup>37</sup>Cl and <sup>81</sup>Br/<sup>79</sup>Br, are summarized in Table 1.1. However, all methods currently face unresolved drawbacks from both instrumental and methodological aspects: i) commercial devices exist, but are not currently available in most laboratories, ii) suitable sustainable reference material with inter-laboratory validations are still lacking, and iii) specific methods should be developed for accurate measurements. As demonstrated below and in chapter 4 & 6 of this thesis, dual isotopes element studies became necessary to retrieve a degradation pathway and increase the accuracy of estimates of the degradation's extent in the surface water. By consequence, the future of the micropollutant CSIA also depends on future progresses to address the analytical challenges posed by heteroatoms' measurement.

The  $\varepsilon_{bulk,E}$  value is often specific to one degradation pathway and can be evaluated for each degradation pathway under closed systems.<sup>136</sup> However, in surface waters, a targeted pesticide might be degraded by different degradation pathways, e.g., elimination, substitution, dealkylation, and depends on different processes, e.g., biodegradation and photolysis. As a consequence, the  $\varepsilon_{bulk,E}$  observed may reflect distinct degradation pathways. When multiple pathways exist, the degradation pathway might be elucidated by multi-element isotope signature, e.g., carbon and nitrogen and degradation pathway identification by plot representing  $\delta^{15}N$  against  $\delta^{13}C$  values using dual element isotope plots (Figure 1.6). Slope of the dual element isotope ( $\Lambda$ ) are good approximation of the ratios of  $\varepsilon$  values, e.g.,  $\varepsilon_N/\varepsilon_C$  which indicate the isotopic enrichment factor for the corresponding degradation pathway. Thus, degradation pathway could be elucidated from  $\varepsilon_N/\varepsilon_C$  obtained under laboratory conditions and found in literature.

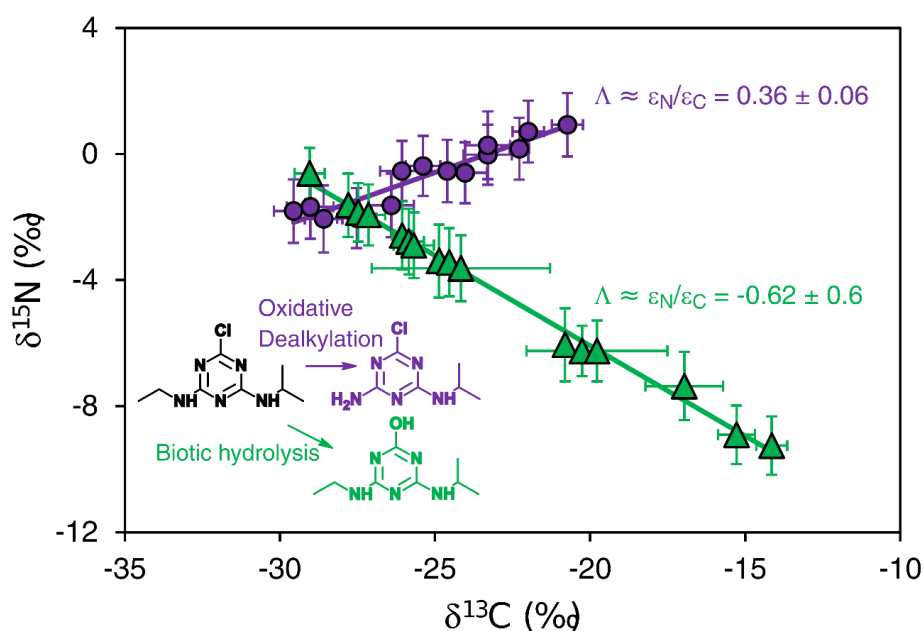


Figure 1.6. Degradation pathways identification with dual-element CSIA. Example of biodegradation of atrazine by *Rhodococcus* sp. strain NI86/21 for the oxidative dealkylation and by *Arthrobacter aurescens* TC1 for the biotic hydrolysis. Adapted from Meyer et al.<sup>157, 158</sup>

Another advantage of dual or multiple element CSIA is the potential to combine quantification of source apportionment and degradation of organic pollutants.<sup>159, 160</sup> The concept of source apportionment is relatively simple and relies on mixing different contaminant pools for which the mixture is conservative, i.e., the isotope signature of the mixture is intermediate between the compositions of the endmembers.<sup>161</sup> However, this estimation is only possible when the source exhibits a larger isotope signature difference than the analytical



uncertainties associated with the measurements. To our knowledge, the mathematical framework to use combined source apportionment and degradation quantification of organic pollutants has been established and validated with a simulation scenario<sup>159, 162</sup> but never used in the environment. A remaining challenge that must be addressed to fill the gap between model validation and environmental application is to simultaneously manage the follow-up of multiple degradation processes and high analytical uncertainties from soil, sediment or surface water sample.

Previous sections of this introduction have underline the difficulties to interpret pesticide degradation in the water–sediment system such as rivers using CSIA, and accounting for low pollutant concentrations ( $\text{ng L}^{-1}$  to  $\mu\text{g L}^{-1}$ ) and matrix effects. Despite recent efforts to apply CSIA on pesticides in low concentration from an analytical point of view<sup>163</sup> and in the environment, for surface waters<sup>20, 141, 164</sup> and soils,<sup>165-167</sup> the feasibility of pesticide CSIA, as a complementary line of evidence for understanding and quantifying pesticide degradation in rivers, should be demonstrated.

## **Research priorities and implications**

As demonstrated in the previous sections, pesticides may threaten drinking water supplies and river biodiversity.<sup>12, 13</sup> Despite decades of research, we are still limited in our capacities to understand, demonstrate and predict the conditions leading to pesticide degradation from the bench-scale up to the environmental scales, e.g., catchment scale. The challenge is thus to correctly measure pesticide degradation, while only few methods have the potential to identify and estimate the extent of pesticide degradation from in situ measurements. Compound-specific isotope analysis (CSIA) is one of these methods, that may provide evidence of in situ pesticide degradation, without prior knowledge of TPs, and allow quantification of degradation without cumbersome mass balance methods.<sup>126</sup> CSIA can also provide information on source apportionment.<sup>160</sup> However, research questions still need to be addressed with respect to priority bench-scale and in situ experiments to develop future applications of pesticide CSIA in rivers.

Four research gaps and associated questions are identified in this thesis to develop and apply CSIA as a tool to improve the evaluation of degradation and persistence of pesticides in rivers:

### **1 - Evaluating the potential of CSIA to resolve direct and indirect photodegradation pathways in surface water**

Photodegradation may significantly contribute to pesticide degradation in the water column through direct or indirect photolysis.<sup>168</sup> Consequently, the presence of different electronic states (singlet, triplet), as well as non-radiative transition and a large number of RIs with a different energy from one excitation might lead to many possible photodegradation pathways and KIE.<sup>169</sup> Despite our ability to predict photodegradation rates,<sup>69, 170</sup> it remains difficult to predict photodegradation pathways and their contribution from the organic compound structures. Hence, a complementary strategy is necessary to estimate in situ photodegradation in the environment. Despite a growing number of organic compound photodegradation studies using CSIA,<sup>169, 171-176</sup> few have focused on sunlight degradation.<sup>177, 178</sup> The ability of CSIA to evaluate the contribution of pesticide photodegradation among other degradation pathways under sunlight conditions is currently lacking.

A remaining question is: **How can isotope signatures reflect ongoing direct and indirect photolysis processes?**

## **2 - Understanding the interplay between degradative and non-degradative processes associated with pesticide dissipation in the water–sediment systems**

The water–sediment system was identified as a hotspot of pesticide biodegradation in surface waters. It involves non-degradative phase-transfer between the sediment and the water phase with biodegradation. In addition, the water–sediment system includes contrasted environmental conditions, i.e., oxic-anoxic, which may lead to different pesticide biodegradation pathways. However, pesticide dissipation accounting for degradative and non-degradative processes has not been well elucidated in model systems yet. This constitutes a critical gap to interpret the combination of dissipation processes in environmental relevant systems, including the effect of photolysis and reactive transport across the SWI reactivity. In this context, the use of CSIA can provide an additional line of evidence for in situ degradation in water–sediment system to decipher the degradative from the non-degradative process. Several analytical challenges currently limit the use of pesticide CSIA in water–sediment systems by consequence isotopic enrichment factors have yet to be evaluated from elementary degradation experiments in the laboratory.

A remaining question is: **What is the extent of biodegradation in the water–sediment system?**

## **3 - Interpreting the relationship between water flow velocity and biodegradation at the hyporheic zone (HZ)**

The HZ has been hypothesized to control biodegradation at river scale by enhancing pollutant mixing and biogeochemical activity in the sediment bed.<sup>80</sup> Despite decades of intense research on HZ, the dynamics of HZ interplaying hydraulic forcing, pollutant partitioning and the efficiency of the biodegradation has not been established, which limits our understanding of the fate of organic pollutants in surface waters.<sup>38</sup> This remaining gap should necessarily be filled in, to identify the dominant factors controlling interactions between pollutants and river sediment beds at river scale.

A remaining question is: **How does water flow velocity influence pesticide dissipation and the contribution of non-degradative and degradative processes in the water column and in the hyporheic zone (HZ)?**

#### **4 - Evaluating pesticide degradation at catchment scale and hydrologically connected rivers**

To our knowledge, the evaluation and the quantitative contribution of degradative versus non-degradative processes and transport via multiple sources at catchment scale has not been resolved. If it is well accepted that HZ constitutes the hotspot of the degradation process because contact between pesticides and microorganisms potentially involved in the degradation pathways is facilitated in surface waters,<sup>82, 112-115</sup> conditions of preferential degradation (hot-spot and hot-moment) or persistence remain elusive. CSIA framework has been recently developed to evaluate the degradation extent at the scale of a headwater catchment<sup>20</sup> and numerical case study with a subsurface-surface reactive transport model (HydroGeoSphere) has validated the potential of CSIA to evaluate pesticide degradation from hillslope to river stretch scales<sup>179</sup> although the concept has never been demonstrated in surface waters.

A remaining question is: **What are the potential and limits of CSIA to evaluate pesticide degradation and persistence in rivers under environmental conditions during a growing season?**

### **Thesis Goal and Objectives**

The overall goal of this Ph.D. is to improve the interpretation of pesticides' degradation and persistence in surface waters, including knowledge of their kinetics and pathways. Based on the identified gaps in current knowledge, and the four abovementioned research questions, five specific objectives are addressed in this thesis:

1. Developing and validating a sensitive and accurate procedure for pesticides' extraction, concentration, quantification and CSIA for soils and sediments without isotope (C and N) fractionation.
2. Evaluating and interpreting the effect of sunlight photodegradation on pesticide isotope fractionation.
3. Elucidating the degradation pathways accounting for non-degradative processes in a two water-sediment phases system, under oxic and anoxic conditions.
4. Interpreting the impact of water flow velocity on pesticide dissipation at the sediment-water interface in bench-scale channel experiments.
5. Evaluating and interpreting the contribution of degradative versus non-degradative processes and transport via multiple sources using CSIA in an agricultural catchment-river system (Souffel river, Bas-Rhin, France, 120 km<sup>2</sup>).

## **Thesis Outline**

The thesis is structured with an introduction (Chap. 1), describing the context of the study, highlighting the main gaps in current knowledge and presenting the research questions, goals and objectives. Followed by a methodological section (Chap. 2), describing the development of the extraction of pesticides from water, soil and sediments. Then, a result section (Chap. 3 to 6) presents designs and results of experiments associated to the specific objectives 2 to 5, respectively. Finally, a general discussion and implication section (Chap. 7 and 8) provides the overall conclusion of the project, the main implications of the research for surface waters, and future perspectives for using CSIA to investigate pesticide degradation in rivers, and more broadly in water–sediment systems. The Figure 1.7 provides an overview of the approach and how chapters interact to answer the five objectives in this thesis.

To achieve the above-described objectives, a pesticides' mixture was selected (atrazine, terbutryn, acetochlor, *S*-metolachlor and metalaxyl) as being representative of the currently used pesticides, following the next criteria: high worldwide applications,<sup>2, 3</sup> being on the priority list of the European (EU) water framework directive<sup>180</sup> and/or being on the EU watch list.<sup>181</sup>

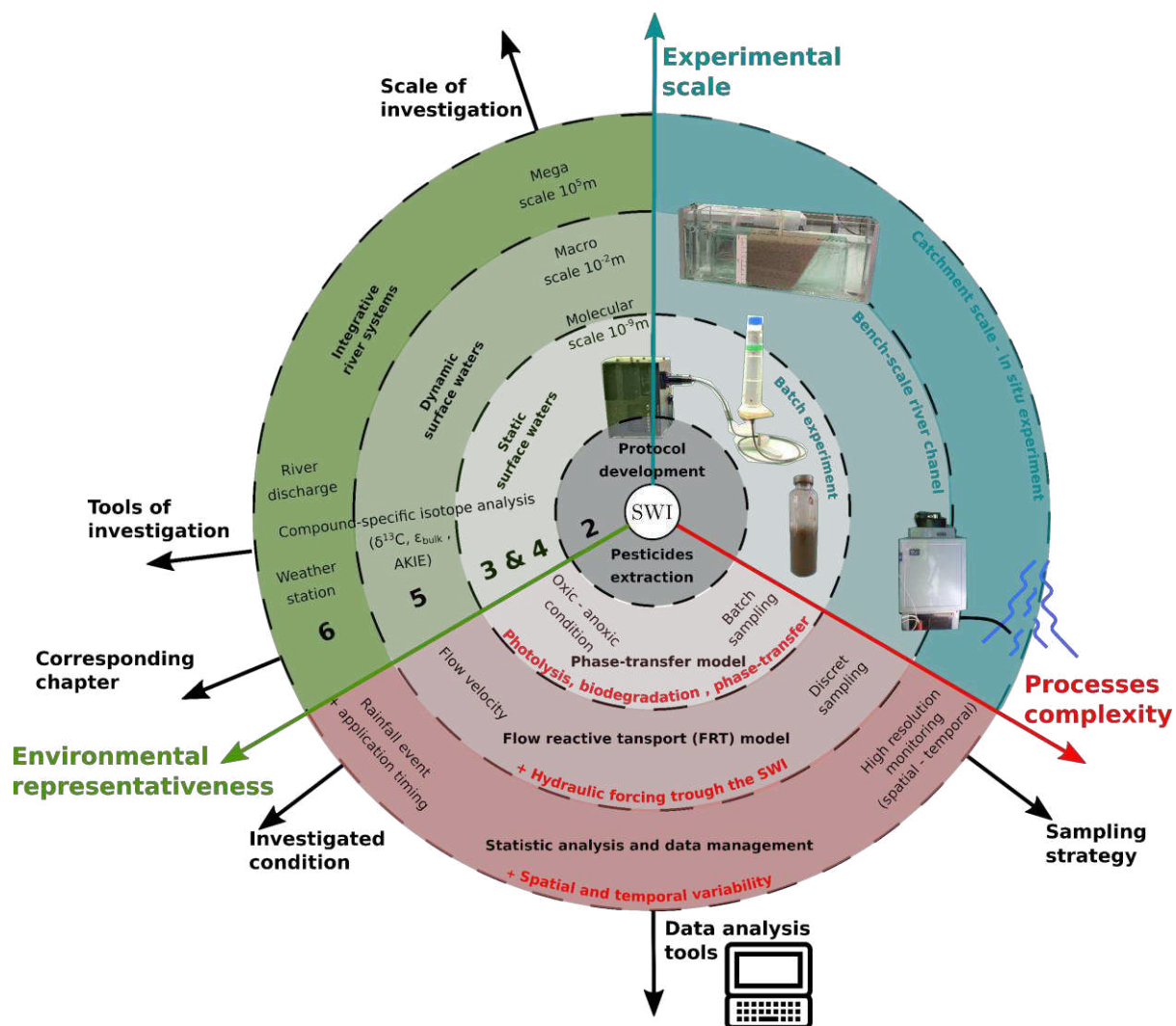


Figure 1.7. Overview of the thesis, highlighting the increase in the complexity of processes to approach the representativity of the complexity of the river.

Chapter 2 presents the development and validation of a protocol for pesticide extraction, quantification by gas chromatography–mass spectrometry (GC-MS) and stable isotope analysis of carbon (C) and nitrogen (N) by gas chromatography–isotope ratio mass spectrometry (GC-IRMS) from sediments and agricultural soils. My specific objective was to quantitatively extract a mixture of pesticides (atrazine, terbutryn, acetochlor, *S*-metolachlor and metalaxyl) without any isotope fractionation ( $\delta^{13}\text{C}$  and  $\delta^{15}\text{N}$ ) from different sediments and soils' matrix. The methods developed in this chapter constitute an essential basis for further experiments developed in this thesis. The work conducted in Chap. 2 addresses objective (1).

Chapter 3 investigates sunlight photodegradation of atrazine and *S*-metolachlor and associated effects on stable isotope fractionation. In this chapter, I focused on atrazine and *S*-metolachlor as the main used of two families of pesticides: triazine and chloroacetanilides. These two pesticides were irradiated with a simulated sunlight under hydro-chemical compositions, representative of agriculturally impacted surface waters, i.e., containing nitrate and DOM. The main objective of this study was to evaluate the capability of CSIA to follow-up pesticide photodegradation in surface waters. For that, C and N enrichment factors were derived for direct and indirect photodegradation with the presence of nitrates and/or DOM. In addition, complementary experiments were conducted with ultraviolet (UV) light at 254 nm to evaluate the effect of light spectrum on C and N isotope fractionation during pesticide photodegradation. The work presented in chapter 3 addresses part of the objective (2).

Chapter 4 presents a microcosm study on a water–sediment system to simulate the dissipation of pesticides in the surface water. In this chapter, I focused on acetochlor and *S*-metolachlor which are the most used chloroacetanilide pesticides sold on the market, rank 3 and 7 of the total worldwide pesticides sold. They were selected because they had degraded in a reasonable time scale (half-life <300 days), inducing a significant isotope fractionation allowing us to apply the CSIA. The objective of this study was to evaluate the contribution of degradation and phase-transfer, responsible for acetochlor and *S*-metolachlor dissipation for two contrasted oxic and anoxic conditions. Those two conditions are realistic of environmental conditions in the river SWI. The oxic conditions predominate in a water column with sediment particulate content in re-suspension. In contrast, anoxic conditions predominate in the riverbed sediment with pore water nearby the sediment phase. I hypothesized that biodegradation pathways and kinetics may differ between those two conditions. CSIA was used to provide, based on change of stable isotope signature, an evidence of pesticide degradation. In addition, HR-MS/MS was used to elucidate the degradation pathway of pesticides in the water–sediment system. Phase specific degradation rates constant and bulk isotopic enrichment factors, which could be used in models to improve prediction of biodegradation and assessing the extent of biodegradation in the environment, are discussed. To this end, I used a two-phase conceptual model validated for laboratory conditions,<sup>95</sup> and evaluated the current limitations of this approach for further laboratory-based experiments using CSIA. The work conducted in chapter 4 addresses the objective (3).

Chapter 5 investigates the effect of water flow velocity on pesticides' transport and degradation at the sediment–water interface. A recirculated bench scale laboratory flume (15 cm long) was constructed to mimic the behavior of a small river. Caffeine was used as an anthropogenic surrogate compound with physico-chemical properties close to current agriculturally used pesticides ( $\log P_{OW} < 10$ , not volatile and  $\log K_{OC}$  around two). In a parallel study on the same flume, Drouin et al.<sup>182</sup> numerically demonstrated that water flow velocity controls the incorporation rate of dissolved oxygen and pesticides within the sediment–water interface. I hypothesized that caffeine degradation mostly occurs at the sediment–water interface and in the oxic layer of the sediment whose thickness may be affected by water flow velocity. To test my hypothesis, experiments with three representative water flow regimes of a small river were conducted (1.1, 3.2 and 4.8 cm s<sup>-1</sup>). The objective was to evaluate whether the isotope signature of caffeine ( $\delta^{13}C$  and  $\delta^{15}N$ ) measured in water can be related to a specific extent of degradation for each of the three water flow velocity conditions. The contribution of pesticides' transport and degradation to the overall pesticide dissipation was evaluated with a methodology coupling pesticide concentration measurements, compound-specific isotopes analysis (CSIA) and flow-reactive-transport (FRT) modelling developed in the PhD project of G. Drouin. The work presented in chapter 5 addresses the objective (4).

Chapter 6 presents the results of a sampling campaign conducted from March to September 2019 in the Souffel catchment (Bas-Rhin, France; 120 km<sup>2</sup>). My objective was to demonstrate the feasibility and limits of CSIA to evaluate degradation and/or multiple sources of pesticides at the river and catchment scale. More specifically, this campaign was designed to identify hotspots and hot-moments affecting the degradation of the herbicide *S*-metolachlor. I focused on the *S*-metolachlor which is currently widely applied in the Souffel catchment. This chapter constitutes a proof of the concept for using laboratory-based knowledge from the previous chapter 3–5 and previous studies in the research group<sup>20, 35, 116, 164, 179, 183</sup> to estimate in situ degradation in surface waters using CSIA. The work presented in this chapter addresses the objective (5).

Chapter 7 presents the main conclusions from chapter 2–6 including the general approach of (i) sample preparation and (ii) the necessity of laboratory scale experiment to support field scale pesticide CSIA.

Chapter 8 identifies and demonstrates the actual remaining steps to continue improving the accuracy and sensitivity of CSIA for in situ degradation measurement in surface waters. Additionally, I provide ideas for future research, to improve the interpretation of pesticide degradation in surface waters.



## References

1. *REACH in brief*; European Commission: **2007**; p 19.
2. Atwood, D.; Paisley-Jones, C. *Pesticides industry sales and usage 2008-2012 market estimates*; U.S. Environmental Protection Agency: Washington (US), **2017**; p 24.
3. Food and Agriculture Organization of the United Nations FAOSTAT. [www.fao.org/faostat/](http://www.fao.org/faostat/) (20<sup>th</sup> March **2019**).
4. Foley, J. A.; DeFries, R.; Asner, G. P.; Barford, C.; Bonan, G.; Carpenter, S. R.; Chapin, F. S.; Coe, M. T.; Daily, G. C.; Gibbs, H. K.; Helkowski, J. H.; Holloway, T.; Howard, E. A.; Kucharik, C. J.; Monfreda, C.; Patz, J. A.; Prentice, I. C.; Ramankutty, N.; Snyder, P. K., Global consequences of land use. *Science* **2005**, *309*, (5734), 570–574.
5. Stehle, S.; Schulz, R., Agricultural insecticides threaten surface waters at the global scale. *Proc. Natl. Acad. Sci. U.S.A.* **2015**, *112*, (18), 5750–5755.
6. de Souza, R. M.; Seibert, D.; Quesada, H. B.; de Jesus Bassetti, F.; Fagundes-Klen, M. R.; Bergamasco, R., Occurrence, impacts and general aspects of pesticides in surface water: A review. *Process Saf. Environ. Prot.* **2020**, *135*, 22–37.
7. Whalley, C.; Völker, J.; Mohaupt, V.; Šubelj, G.; Kirst, I.; Küster, E.; Semeradova, S.; Kühnel, D.; Altenburge, R. *Technical report on pesticides in surface waters and groundwater in Europe*; European Environment Agency (EEA): **2020**; p.81.
8. Rosario-Ortiz, F.; Rose, J.; Speight, V.; von Gunten, U.; Schnoor, J., How do you like your tap water? *Science* **2016**, *351*, (6276), 912–914.
9. Schwarzenbach, R. P.; Egli, T.; Hofstetter, T. B.; von Gunten, U.; Wehrli, B., Global water pollution and human health. *Annu. Rev. Env. Resour.* **2010**, *35*, 109–136.
10. Collins, R.; Thyssen, N.; Kristensen, P. *Water resources across Europe: Confronting water scarcity and drought*; European Environment Agency: Copenhagen, Denmark, **2009**; p 55.
11. Dieter, C. A.; Maupin, M. A.; Caldwell, R. R.; Harris, M. A.; Ivahnenko, T. I.; Lovelace, J. K.; Barber, N. L.; Linsey, K. S. *Estimated use of water in the United States in 2015*; U.S. Geological Survey Circular 1441: Reston, VA, US, **2018**; p 76.
12. Vörösmarty, C. J.; McIntyre, P. B.; Gessner, M. O.; Dudgeon, D.; Prusevich, A.; Green, P.; Glidden, S.; Bunn, S. E.; Sullivan, C. A.; Liermann, C. R.; Davies, P. M., Global threats to human water security and river biodiversity. *Nature* **2010**, *467*, 555–561.
13. Spycher, S.; Mangold, S.; Doppler, T.; Junghans, M.; Wittmer, I.; Stamm, C.; Singer, H., Pesticide risks in small streams—How to get as close as possible to the stress imposed on aquatic organisms. *Environ. Sci. Technol.* **2018**, *52*, (8), 4526–4535.

14. Maggi, F.; Tang, F. H. M.; la Cecilia, D.; McBratney, A., PEST-CHEMGRIDS, global gridded maps of the top 20 crop-specific pesticide application rates from 2015 to 2025. *Scientific Data* **2019**, *6*, 170.
15. Escher, B. I.; Stapleton, H. M.; Schymanski, E. L., Tracking complex mixtures of chemicals in our changing environment. *Science* **2020**, *367*, (6476), 388–392.
16. Gerecke, A. C.; Schärer, M.; Singer, H. P.; Müller, S. R.; Schwarzenbach, R. P.; Sägesser, M.; Ochsenein, U.; Popow, G., Sources of pesticides in surface waters in Switzerland: pesticide load through waste water treatment plants—current situation and reduction potential. *Chemosphere* **2002**, *48*, (3), 307–315.
17. Barbash, J. E., The geochemistry of pesticides. In *Treatise on geochemistry*, second ed.; Holland, H. D.; Turekian, K. K., Eds. Elsevier: Oxford, **2014**; pp 535–572.
18. Imfeld, G.; Meite, F.; Wiegert, C.; Guyot, B.; Masbou, J.; Payraudeau, S., Do rainfall characteristics affect the export of copper, zinc and synthetic pesticides in surface runoff from headwater catchments? *Sci. Total Environ.* **2020**, *741*, 140437.
19. Schulz, R., Field studies on exposure, effects, and risk mitigation of aquatic nonpoint-source insecticide pollution: A review. *J. Environ. Qual.* **2004**, *33*, (2), 419–448.
20. Alvarez-Zaldívar, P.; Payraudeau, S.; Meite, F.; Masbou, J.; Imfeld, G., Pesticide degradation and export losses at the catchment scale: Insights from compound-specific isotope analysis (CSIA). *Water Res.* **2018**, *139*, 198–207.
21. Lefrancq, M.; Payraudeau, S.; García Verdú, A. J.; Maillard, E.; Millet, M.; Imfeld, G., Fungicides transport in runoff from vineyard plot and catchment: contribution of non-target areas. *Environ. Sci. Pollut. Res.* **2014**, *21*, (7), 4871–4882.
22. Leu, C.; Singer, H.; Stamm, C.; Müller, S. R.; Schwarzenbach, R. P., Simultaneous assessment of sources, processes, and factors influencing herbicide losses to surface waters in a small agricultural catchment. *Environ. Sci. Technol.* **2004**, *38*, (14), 3827–3834.
23. Reichenberger, S.; Bach, M.; Skitschak, A.; Frede, H.-G., Mitigation strategies to reduce pesticide inputs into ground- and surface water and their effectiveness; A review. *Sci. Total Environ.* **2007**, *384*, (1), 1–35.
24. Spahr, S.; Teixidó, M.; Sedlak, D. L.; Luthy, R. G., Hydrophilic trace organic contaminants in urban stormwater: occurrence, toxicological relevance, and the need to enhance green stormwater infrastructure. *Environ. Sci.: Water Res. Technol.* **2020**, *6*, 15–44.
25. Burri, N. M.; Weatherl, R.; Moeck, C.; Schirmer, M., A review of threats to groundwater quality in the anthropocene. *Sci. Total Environ.* **2019**, *684*, 136–154.
26. Melvin, S. D.; Leusch, F. D. L., Removal of trace organic contaminants from domestic wastewater: A meta-analysis comparison of sewage treatment technologies. *Environ. Int.* **2016**, *92-93*, 183–188.

27. Schaidler, L. A.; Rodgers, K. M.; Rudel, R. A., Review of organic wastewater compound concentrations and removal in onsite wastewater treatment systems. *Environ. Sci. Technol.* **2017**, *51*, (13), 7304–7317.
28. Gogoi, A.; Mazumder, P.; Tyagi, V. K.; Tushara Chaminda, G. G.; An, A. K.; Kumar, M., Occurrence and fate of emerging contaminants in water environment: A review. *Groundwater for Sustainable Development* **2018**, *6*, 169–180.
29. Glassmeyer, S. T.; Furlong, E. T.; Kolpin, D. W.; Batt, A. L.; Benson, R.; Boone, J. S.; Conerly, O.; Donohue, M. J.; King, D. N.; Kostich, M. S.; Mash, H. E.; Pfaller, S. L.; Schenck, K. M.; Simmons, J. E.; Varughese, E. A.; Vesper, S. J.; Villegas, E. N.; Wilson, V. S., Nationwide reconnaissance of contaminants of emerging concern in source and treated drinking waters of the United States. *Sci. Total Environ.* **2017**, *581-582*, 909–922.
30. Sutton, R.; Xie, Y.; Moran, K. D.; Teerlink, J., Occurrence and sources of pesticides to urban wastewater and the environment. In *Pesticides in Surface Water: Monitoring, Modeling, Risk Assessment, and Management*, American Chemical Society: **2019**; Vol. 1308, pp 63–88.
31. Fairbairn, D. J.; Arnold, W. A.; Barber, B. L.; Kaufenberg, E. F.; Koskinen, W. C.; Novak, P. J.; Rice, P. J.; Swackhamer, D. L., Contaminants of emerging concern: Mass balance and comparison of wastewater effluent and upstream sources in a mixed-use watershed. *Environ. Sci. Technol.* **2016**, *50*, (1), 36–45.
32. Latino, D. A. R. S.; Wicker, J.; Gütlein, M.; Schmid, E.; Kramer, S.; Fenner, K., Eawag–Soil in enviPath: A new resource for exploring regulatory pesticide soil biodegradation pathways and half-life data. *Environ. Sci. Process. Impacts* **2017**, *19*, (3), 449–464.
33. Boxall, A. B. A.; Sinclair, C. J.; Fenner, K.; Kolpin, D.; Maud, S. J., When synthetic chemicals degrade in the environment. *Environ. Sci. Technol.* **2004**, *38*, (19), 368A–375A.
34. Leu, C.; Singer, H.; Stamm, C.; Müller, S. R.; Schwarzenbach, R. P., Variability of herbicide losses from 13 fields to surface water within a small catchment after a controlled herbicide application. *Environ. Sci. Technol.* **2004**, *38*, (14), 3835–3841.
35. Meite, F.; Alvarez-Zaldívar, P.; Crochet, A.; Wiegert, C.; Payraudeau, S.; Imfeld, G., Impact of rainfall patterns and frequency on the export of pesticides and heavy-metals from agricultural soils. *Sci. Total Environ.* **2018**, *616-617*, 500–509.
36. Gramlich, A.; Stoll, S.; Stamm, C.; Walter, T.; Prasuhn, V., Effects of artificial land drainage on hydrology, nutrient and pesticide fluxes from agricultural fields – A review. *Agric., Ecosyst. Environ.* **2018**, *266*, 84–99.
37. Fenner, K.; Canonica, S.; Wackett, L. P.; Elsner, M., Evaluating pesticide degradation in the environment: Blind spots and emerging opportunities. *Science* **2013**, *341*, (6147), 752–758.

38. Krause, S.; Lewandowski, J.; Grimm, N. B.; Hannah, D. M.; Pinay, G.; McDonald, K.; Martí, E.; Argerich, A.; Pfister, L.; Klaus, J.; Battin, T.; Larned, S. T.; Schelker, J.; Fleckenstein, J.; Schmidt, C.; Rivett, M. O.; Watts, G.; Sabater, F.; Sorolla, A.; Turk, V., Ecohydrological interfaces as hot spots of ecosystem processes. *Water Resour. Res.* **2017**, *53*, (8), 6359–6376.
39. Gassmann, M.; Olsson, O.; Stamm, C.; Weiler, M.; Kummerer, K., Physico-chemical characteristics affect the spatial distribution of pesticide and transformation product loss to an agricultural brook. *Sci. Total Environ.* **2015**, *532*, 733–743.
40. Arias-Estévez, M.; López-Periago, E.; Martínez-Carballo, E.; Simal-Gándara, J.; Mejuto, J.-C.; García-Río, L., The mobility and degradation of pesticides in soils and the pollution of groundwater resources. *Agric., Ecosyst. Environ.* **2008**, *123*, 247–260.
41. Ren, J. H.; Packman, A. I., Stream-subsurface exchange of zinc in the presence of silica and kaolinite colloids. *Environ. Sci. Technol.* **2004**, *38*, (24), 6571–6581.
42. Ren, J.; Packman, A. I., Modeling of simultaneous exchange of colloids and sorbing contaminants between streams and streambeds. *Environ. Sci. Technol.* **2004**, *38*, (10), 2901–2911.
43. Menz, J.; Müller, J.; Olsson, O.; Kummerer, K., Bioavailability of antibiotics at soil–water interfaces: A comparison of measured activities and equilibrium partitioning estimates. *Environ. Sci. Technol.* **2018**, *52*, (11), 6555–6564.
44. Singh, S.; Kumar, V.; Chauhan, A.; Datta, S.; Wani, A. B.; Singh, N.; Singh, J., Toxicity, degradation and analysis of the herbicide atrazine. *Environ. Chem. Lett.* **2018**, *16*, (1), 211–237.
45. Loos, R.; Gawlik, B. M.; Locoro, G.; Rimaviciute, E.; Contini, S.; Bidoglio, G., EU-wide survey of polar organic persistent pollutants in European river waters. *Environ. Pollut.* **2009**, *157*, (2), 561–568.
46. Loos, R.; Locoro, G.; Comero, S.; Contini, S.; Schwesig, D.; Werres, F., Pan-European survey on the occurrence of selected polar organic persistent pollutants in ground water. *Water Res.* **2010**, *44*, 4115–4126.
47. Aprona *État de la nappe phréatique d’Alsace et des aquifères du Sundgau: Premiers résultats sur les nitrates et les pesticides*; Aprona: Colmar, Strasbourg, France, **2016**; p 24.
48. Gilliom, R. J., Pesticides in U.S. streams and groundwater. *Environ. Sci. Technol.* **2007**, *41*, (10), 3408–3414.
49. Wang, Y.; Lai, A.; Latino, D.; Fenner, K.; Helbling, D. E., Evaluating the environmental parameters that determine aerobic biodegradation half-lives of pesticides in soil with a multivariable approach. *Chemosphere* **2018**, *209*, 430–438.
50. Egli, T., How to live at very low substrate concentration. *Water Res.* **2010**, *44*, (17), 4826–4837.

51. Ehrl, B. N.; Kundu, K.; Gharasoo, M.; Marozava, S.; Elsner, M., Rate-limiting mass transfer in micropollutant degradation revealed by isotope fractionation in chemostat. *Environ. Sci. Technol.* **2018**, *53*, (3), 1197–1205.
52. Helbling, D. E., Bioremediation of pesticide-contaminated water resources: the challenge of low concentrations. *Curr. Opin. Biotechnol.* **2015**, *33*, 142–148.
53. Huntscha, S.; Singer, H.; Canonica, S.; Schwarzenbach, R. P.; Fenner, K., Input dynamics and fate in surface water of the herbicide metolachlor and of its highly mobile transformation product metolachlor ESA. *Environ. Sci. Technol.* **2008**, *42*, (15), 5507–5513.
54. Casado, J.; Brigden, K.; Santillo, D.; Johnston, P., Screening of pesticides and veterinary drugs in small streams in the European Union by liquid chromatography high resolution mass spectrometry. *Sci. Total Environ.* **2019**, *670*, 1204–1225.
55. Kolpin, D. W.; Schnoebelen, D. J.; Thurman, E. M., Degradates provide insight to spatial and temporal trends of herbicides in ground water. *Groundwater* **2004**, *42*, (4), 601–608.
56. Graham, W. H.; Graham, D. W.; deNoyelles, F.; Smith, V. H.; Larive, C. K.; Thurman, E. M., Metolachlor and alachlor breakdown product formation patterns in aquatic field mesocosms. *Environ. Sci. Technol.* **1999**, *33*, (24), 4471–4476.
57. Feng, P. C. C., Soil transformation of acetochlor via glutathione conjugation. *Pestic. Biochem. Physiol.* **1991**, *40*, (2), 136–142.
58. Thurman, E. M.; Goolsby, D. A.; Aga, D. S.; Pomes, M. L.; Meyer, M. T., Occurrence of alachlor and its sulfonated metabolite in rivers and reservoirs of the midwestern United States: The importance of sulfonation in the transport of chloroacetanilide herbicides. *Environ. Sci. Technol.* **1996**, *30*, (2), 569–574.
59. Cooper, A.; Hanigan, M. H., Metabolism of glutathione S-conjugates – multiple pathways. In *Comprehensive Toxicology*, McQueen, C. A., Ed. Elsevier: Oxford, **2015**; Vol. 4, pp 323–366.
60. Katagi, T., Abiotic hydrolysis of pesticides in the aquatic environment. In *Reviews of Environmental Contamination and Toxicology*, Vol 175, Ware, G. W., Ed. **2002**; Vol. 175, pp 79–261.
61. Fono, L. J.; Kolodziej, E. P.; Sedlak, D. L., Attenuation of wastewater-derived contaminants in an effluent-dominated river. *Environ. Sci. Technol.* **2006**, *40*, (23), 7257–7262.
62. Schwarzenbach, R. P.; Gschwend, P. M.; Imboden, D. M., *Environmental organic chemistry*. third ed.; John Wiley & Sons: **2016**, p. 1024.
63. Ciani, A.; Goss, K.-U.; Schwarzenbach, R. P., Light penetration in soil and particulate minerals. *Eur. J. Soil Sci.* **2005**, *56*, (5), 561–574.

64. Katagi, T., Direct photolysis mechanism of pesticides in water. *J. Pestic. Sci.* **2018**, *43*, (1-2), 57–72.
65. Yuan, C.; Tebes-Stevens, C.; Weber, E. J., A reaction library to predict direct photochemical transformation products of environmental organic contaminants in sunlit aquatic systems. *Environ. Sci. Technol.* **2020**, *54*, (12), 7271–7279.
66. Remucal, C. K., The role of indirect photochemical degradation in the environmental fate of pesticides: A review. *Environ. Sci. Process. Impacts* **2014**, *16*, (4), 628–653.
67. Bodrato, M.; Vione, D., APEX (Aqueous Photochemistry of Environmentally occurring Xenobiotics): a free software tool to predict the kinetics of photochemical processes in surface waters. *Environ. Sci. Process. Impacts* **2014**, *16*, (4), 732–740.
68. Vione, D.; Maurino, V.; Minero, C.; Carlotti, M. E.; Chiron, S.; Barbati, S., Modelling the occurrence and reactivity of the carbonate radical in surface freshwater. *Comptes Rendus Chimie* **2009**, *12*, (8), 865–871.
69. Janssen, E. M. L.; Erickson, P. R.; McNeill, K., Dual roles of dissolved organic matter as sensitizer and quencher in the photooxidation of tryptophan. *Environ. Sci. Technol.* **2014**, *48*, (9), 4916–4924.
70. Wenk, J.; Aeschbacher, M.; Salhi, E.; Canonica, S.; von Gunten, U.; Sander, M., Chemical oxidation of dissolved organic matter by chlorine dioxide, chlorine, and ozone: Effects on Its optical and antioxidant properties. *Environ. Sci. Technol.* **2013**, *47*, (19), 11147–11156.
71. Ma, J.; Del Vecchio, R.; Golanoski, K. S.; Boyle, E. S.; Blough, N. V., Optical properties of humic substances and CDOM: Effects of borohydride reduction. *Environ. Sci. Technol.* **2010**, *44*, (14), 5395–5402.
72. Del Vecchio, R.; Blough, N. V., On the origin of the optical properties of humic substances. *Environ. Sci. Technol.* **2004**, *38*, (14), 3885–3891.
73. Wenk, J.; Canonica, S., Phenolic antioxidants inhibit the triplet-induced transformation of anilines and sulfonamide antibiotics in aqueous solution. *Environ. Sci. Technol.* **2012**, *46*, (10), 5455–5462.
74. Leresche, F.; von Gunten, U.; Canonica, S., Probing the photosensitizing and inhibitory effects of dissolved organic matter by using *N,N*-dimethyl-4-cyanoaniline (DMABN). *Environ. Sci. Technol.* **2016**, *50*, (20), 10997–11007.
75. Zeng, T.; Arnold, W. A., Pesticide photolysis in prairie potholes: Probing photosensitized processes. *Environ. Sci. Technol.* **2013**, *47*, (13), 6735–6745.
76. Burrows, H. D.; Canle, M.; Santaballa, J. A.; Steenken, S., Reaction pathways and mechanisms of photodegradation of pesticides. *J. Photoch. Photobio. B.* **2002**, *67*, (2), 71–108.

77. Battin, T. J.; Besemer, K.; Bengtsson, M. M.; Romani, A. M.; Packmann, A. I., The ecology and biogeochemistry of stream biofilms. *Nat. Rev. Microbiol.* **2016**, *14*, (4), 251–263.
78. Kunkel, U.; Radke, M., Biodegradation of acidic pharmaceuticals in bed sediments: Insight from a laboratory experiment. *Environ. Sci. Technol.* **2008**, *42*, (19), 7273–7279.
79. Zumstein, M. T.; Helbling, D. E., Biotransformation of antibiotics: Exploring the activity of extracellular and intracellular enzymes derived from wastewater microbial communities. *Water Res.* **2019**, *155*, 115–123.
80. Boano, F.; Harvey, J. W.; Marion, A.; Packman, A. I.; Revelli, R.; Ridolfi, L.; Wörman, A., Hyporheic flow and transport processes: Mechanisms, models, and biogeochemical implications. *Rev. Geophys.* **2014**, *52*, (4), 603–679.
81. Schaper, J. L.; Posselt, M.; Bouchez, C.; Jaeger, A.; Nuetzmann, G.; Putschew, A.; Singer, G.; Lewandowski, J., Fate of trace organic compounds in the hyporheic zone: Influence of retardation, the benthic biolayer, and organic carbon. *Environ. Sci. Technol.* **2019**, *53*, (8), 4224–4234.
82. Schaper, J. L.; Posselt, M.; McCallum, J. L.; Banks, E. W.; Hoehne, A.; Meinikmann, K.; Shanafield, M. A.; Batelaan, O.; Lewandowski, J., Hyporheic exchange controls fate of trace organic compounds in an urban stream. *Environ. Sci. Technol.* **2018**, *52*, (21), 12285–12294.
83. Lewandowski, J.; Arnon, S.; Banks, E.; Batelaan, O.; Betterle, A.; Broecker, T.; Coll, C.; Drummond, J. D.; Gaona Garcia, J.; Galloway, J.; Gomez-Velez, J.; Grabowski, R. C.; Herzog, S. P.; Hinkelmann, R.; Höhne, A.; Hollender, J.; Horn, M. A.; Jaeger, A.; Krause, S.; Löchner Prats, A.; Magliozzi, C.; Meinikmann, K.; Mojarrad, B. B.; Mueller, B. M.; Peralta-Maraver, I.; Popp, A. L.; Posselt, M.; Putschew, A.; Radke, M.; Raza, M.; Riml, J.; Robertson, A.; Rutere, C.; Schaper, J. L.; Schirmer, M.; Schulz, H.; Shanafield, M.; Singh, T.; Ward, A. S.; Wolke, P.; Wörman, A.; Wu, L., Is the hyporheic zone relevant beyond the scientific community? *Water* **2019**, *11*, (11), 2230.
84. Diaz, J. M.; Hansel, C. M.; Voelker, B. M.; Mendes, C. M.; Andeer, P. F.; Zhang, T., Widespread production of extracellular superoxide by heterotrophic bacteria. *Science* **2013**, *340*, (6137), 1223–1226.
85. Allocati, N.; Federici, L.; Masulli, M.; Di Ilio, C., Glutathione transferases in bacteria. *FEBS J.* **2009**, *276*, (1), 58–75.
86. Copley, S. D., Evolution of efficient pathways for degradation of anthropogenic chemicals. *Nat. Chem. Biol.* **2009**, *5*, (8), 559–566.
87. Hennebel, T.; De Gussemé, B.; Boon, N.; Verstraete, W., Biogenic metals in advanced water treatment. *Trends Biotechnol.* **2009**, *27*, (2), 90–98.
88. Borch, T.; Kretzschmar, R.; Kappler, A.; Cappellen, P. V.; Ginder-Vogel, M.; Voegelin, A.; Campbell, K., Biogeochemical redox processes and their impact on contaminant dynamics. *Environ. Sci. Technol.* **2010**, *44*, (1), 15–23.

89. Xu, J. C.; Stucki, J. W.; Wu, J.; Kostka, J. E.; Sims, G. K., Fate of atrazine and alachlor in redox-treated ferruginous smectite. *Environ. Toxicol. Chem.* **2001**, *20*, (12), 2717–2724.
90. Remucal, C. K.; Ginder-Vogel, M., A critical review of the reactivity of manganese oxides with organic contaminants. *Environ. Sci. Process. Impacts* **2014**, *16*, (6), 1247–1266.
91. Loch, A. R.; Lippa, K. A.; Carlson, D. L.; Chin, Y. P.; Traina, S. J.; Roberts, A. L., Nucleophilic aliphatic substitution reactions of propachlor, alachlor, and metolachlor with bisulfide ( $\text{HS}^-$ ) and polysulfides ( $\text{S}_n^{2-}$ ). *Environ. Sci. Technol.* **2002**, *36*, (19), 4065–4073.
92. Lippa, K. A.; Roberts, A. L., Nucleophilic aromatic substitution reactions of chloroazines with bisulfide ( $\text{HS}^-$ ) and polysulfides ( $\text{S}_n^{2-}$ ). *Environ. Sci. Technol.* **2002**, *36*, (9), 2008–2018.
93. Gong, W. W.; Liu, X. H.; Xia, S. H.; Liang, B. C.; Zhang, W., Abiotic reduction of trifluralin and pendimethalin by sulfides in black-carbon-amended coastal sediments. *J. Hazard. Mater.* **2016**, *310*, 125–134.
94. Zeng, T.; Chin, Y. P.; Arnold, W. A., Potential for abiotic reduction of pesticides in prairie pothole porewaters. *Environ. Sci. Technol.* **2012**, *46*, (6), 3177–3187.
95. Honti, M.; Hahn, S.; Hennecke, D.; Junker, T.; Shrestha, P.; Fenner, K., Bridging across OECD 308 and 309 data in search of a robust biotransformation indicator. *Environ. Sci. Technol.* **2016**, *50*, (13), 6865–6872.
96. Moser, A.; Wemyss, D.; Scheidegger, R.; Fenicia, F.; Honti, M.; Stamm, C., Modelling biocide and herbicide concentrations in catchments of the Rhine basin. *Hydrol. Earth Syst. Sci.* **2018**, *22*, (8), 4229–4249.
97. Voermans, J. J.; Ghisalberti, M.; Ivey, G. N., A model for mass transport across the sediment-water Interface. *Water Resour. Res.* **2018**, *54*, (4), 2799–2812.
98. Grant, S. B.; Marusic, I., Crossing turbulent boundaries: Interfacial flux in environmental flows. *Environ. Sci. Technol.* **2011**, *45*, (17), 7107–7113.
99. Hester, E. T.; Young, K. I.; Widdowson, M. A., Mixing of surface and groundwater induced by riverbed dunes: Implications for hyporheic zone definitions and pollutant reactions. *Water Resour. Res.* **2013**, *49*, (9), 5221–5237.
100. Kaufman, M. H.; Cardenas, M. B.; Buttles, J.; Kessler, A. J.; Cook, P. L. M., Hyporheic hot moments: Dissolved oxygen dynamics in the hyporheic zone in response to surface flow perturbations. *Water Resour. Res.* **2017**, *53*, (8), 6642–6662.
101. Ren, X. W.; Santamarina, J. C., The hydraulic conductivity of sediments: A pore size perspective. *Eng. Geol.* **2018**, *233*, 48–54.



102. Richardson, C. P.; Parr, A. D., Modified Fickian model for solute uptake by runoff. *J. Environ. Eng.-Asce* **1988**, *114*, (4), 792–809.
103. Marion, A.; Bellinello, M.; Guymer, I.; Packman, A., Effect of bed form geometry on the penetration of nonreactive solutes into a streambed. *Water Resour. Res.* **2002**, *38*, (10), 1209.
104. Rehg, K. J.; Packman, A. I.; Ren, J. H., Effects of suspended sediment characteristics and bed sediment transport on streambed clogging. *Hydrol. Process.* **2005**, *19*, (2), 413–427.
105. Nagaoka, H.; Ohgaki, S., Mass transfer mechanism in a porous riverbed. *Water Res.* **1990**, *24*, (4), 417–425.
106. Lai, J. L.; Lo, S. L.; Lin, C. F., Effects of hydraulic and medium characteristics on solute transfer to surface runoff. *Water Sci. Technol.* **1994**, *30*, (7), 145–155.
107. Chandler, I. D.; Guymer, I.; Pearson, J. M.; van Egmond, R., Vertical variation of mixing within porous sediment beds below turbulent flows. *Water Resour. Res.* **2016**, *52*, (5), 3493–3509.
108. Löffler, D.; Römbke, J.; Meller, M.; Ternes, T. A., Environmental fate of pharmaceuticals in water/sediment systems. *Environ. Sci. Technol.* **2005**, *39*, (14), 5209–5218.
109. Honti, M.; Bischoff, F.; Moser, A.; Stamm, C.; Baranya, S.; Fenner, K., Relating degradation of pharmaceutical active ingredients in a stream network to degradation in water-sediment simulation tests. *Water Resour. Res.* **2018**, *54*, (11), 9207–9223.
110. Radke, M.; Maier, M. P., Lessons learned from water/sediment-testing of pharmaceuticals. *Water Res.* **2014**, *55*, 63–73.
111. Li, Z.; Maier, M. P.; Radke, M., Screening for pharmaceutical transformation products formed in river sediment by combining ultrahigh performance liquid chromatography/high resolution mass spectrometry with a rapid data-processing method. *Anal. Chim. Acta* **2014**, *810*, 61–70.
112. Posselt, M.; Jaeger, A.; Schaper, J. L.; Radke, M.; Benskin, J. P., Determination of polar organic micropollutants in surface and pore water by high-resolution sampling-direct injection-ultra high performance liquid chromatography-tandem mass spectrometry. *Environ. Sci. Process. Impacts* **2018**, *20*, (12), 1716–1727.
113. Schaper, J. L.; Seher, W.; Nützmann, G.; Putschew, A.; Jekel, M.; Lewandowski, J., The fate of polar trace organic compounds in the hyporheic zone. *Water Res.* **2018**, *140*, 158–166.
114. Lewandowski, J.; Putschew, A.; Schwesig, D.; Neumann, C.; Radke, M., Fate of organic micropollutants in the hyporheic zone of a eutrophic lowland stream: Results of a preliminary field study. *Sci. Total Environ.* **2011**, *409*, (10), 1824–1835.

115. Jaeger, A.; Coll, C.; Posselt, M.; Mechelke, J.; Rutere, C.; Betterle, A.; Raza, M.; Mehrstens, A.; Meinikmann, K.; Portmann, A.; Singh, T.; Blaen, P. J.; Krause, S.; Horn, M. A.; Hollender, J.; Benskin, J. P.; Sobek, A.; Lewandowski, J., Using recirculating flumes and a response surface model to investigate the role of hyporheic exchange and bacterial diversity on micropollutant half-lives. *Environ. Sci. Process. Impacts* **2019**, *21*, (12), 2093–2108.
116. Lefrancq, M.; Payraudeau, S.; Guyot, B.; Millet, M.; Imfeld, G., Degradation and transport of the chiral herbicide *S*-metolachlor at the catchment scale: Combining observation scales and analytical approaches. *Environ. Sci. Technol.* **2017**, *51*, (22), 13231–13240.
117. Boithias, L.; Sauvage, S.; Merlina, G.; Jean, S.; Probst, J.-L.; Sánchez Pérez, J. M., New insight into pesticide partition coefficient  $K_d$  for modelling pesticide fluvial transport: Application to an agricultural catchment in south-western France. *Chemosphere* **2014**, *99*, 134–142.
118. Warren, N.; Allan, I. J.; Carter, J. E.; House, W. A.; Parker, A., Pesticides and other micro-organic contaminants in freshwater sedimentary environments - a review. *Appl. Geochem.* **2003**, *18*, (2), 159–194.
119. Massei, R.; Busch, W.; Wolschke, H.; Schinkel, L.; Bitsch, M.; Schulze, T.; Krauss, M.; Brack, W., Screening of pesticide and biocide patterns as risk drivers in sediments of major european river mouths: Ubiquitous or river basin-specific contamination? *Environ. Sci. Technol.* **2018**, *52*, (4), 2251–2260.
120. Wauchope, R. D.; Yeh, S.; Linders, J. B. H. J.; Kloskowski, R.; Tanaka, K.; Rubin, B.; Katayama, A.; Kordel, W.; Gerstl, Z.; Lane, M.; Unsworth, J. B., Pesticide soil sorption parameters: theory, measurement, uses, limitations and reliability. *Pest Manage. Sci.* **2002**, *58*, (5), 419–445.
121. MacKay, A. A.; Vasudevan, D., Polyfunctional ionogenic compound sorption: Challenges and new approaches to advance predictive models. *Environ. Sci. Technol.* **2012**, *46*, (17), 9209–9223.
122. Schaffer, M.; Börnick, H.; Nödler, K.; Licha, T.; Worch, E., Role of cation exchange processes on the sorption influenced transport of cationic  $\beta$ -blockers in aquifer sediments. *Water Res.* **2012**, *46*, 5472–5482.
123. Writer, J. H.; Antweiler, R. C.; Ferrer, I.; Ryan, J. N.; Thurman, E. M., In-stream attenuation of neuro-active pharmaceuticals and their metabolites. *Environ. Sci. Technol.* **2013**, *47*, (17), 9781–9790.
124. Moschet, C.; Wittmer, I.; Simovic, J.; Junghans, M.; Piazzoli, A.; Singer, H.; Stamm, C.; Leu, C.; Hollender, J., How a complete pesticide screening changes the assessment of surface water quality. *Environ. Sci. Technol.* **2014**, *48*, (10), 5423–5432.

125. Wang, R.; Chen, H.; Luo, Y.; Yen, H.; Arnold, J. G.; Bubenheim, D.; Moran, P.; Zhang, M., Modeling pesticide fate and transport at watershed scale using the soil & water assessment tool: General applications and mitigation strategies. In *Pesticides in Surface Water: Monitoring, Modeling, Risk Assessment, and Management*, American Chemical Society: **2019**; Vol. 1308, pp 391–419.
126. Elsner, M.; Imfeld, G., Compound-specific isotope analysis (CSIA) of micropollutants in the environment — current developments and future challenges. *Curr. Opin. Biotechnol.* **2016**, *41*, 60–72.
127. Carpenter, C. M. G.; Wong, L. Y. J.; Johnson, C. A.; Helbling, D. E., Fall creek monitoring station: Highly resolved temporal sampling to prioritize the identification of nontarget micropollutants in a small stream. *Environ. Sci. Technol.* **2019**, *53*, (1), 77–87.
128. Moatar, F.; Meybeck, M.; Raymond, S.; Birgand, F.; Curie, F., River flux uncertainties predicted by hydrological variability and riverine material behaviour. *Hydrol. Process.* **2013**, *27*, (25), 3535–3546.
129. Hollender, J.; Rothardt, J.; Radny, D.; Loos, M.; Epting, J.; Huggenberger, P.; Borer, P.; Singer, H., Comprehensive micropollutant screening using LC-HRMS/MS at three riverbank filtration sites to assess natural attenuation and potential implications for human health. *Water Research X* **2018**, *1*, 100007.
130. Liigand, J.; Wang, T.; Kellogg, J.; Smedsgaard, J.; Cech, N.; Krueve, A., Quantification for non-targeted LC/MS screening without standard substances. *Sci. Rep.* **2020**, *10*, (1), 5808.
131. Can-güven, E.; Bolat, D.; Gedik, K.; Kurt-karakuş, P. B., Chiral pollutants and their significance in the environment. *Pamukkale Univ Muh Bilim Derg* **2016**, *22*, (6), 486–496.
132. Ramezani, M. K.; Oliver, D. P.; Kookana, R. S.; Lao, W. J.; Gill, G.; Preston, C., Faster degradation of herbicidally-active enantiomer of imidazolinones in soils. *Chemosphere* **2010**, *79*, (11), 1040–1045.
133. Petrie, B.; Camacho Muñoz, M. D.; Martín, J., Stereoselective LC–MS/MS methodologies for environmental analysis of chiral pesticides. *TrAC, Trends Anal. Chem.* **2019**, *110*, 249–258.
134. Buser, H.-R.; Müller, M. D., Occurrence and transformation reactions of chiral and achiral phenoxyalkanoic acid herbicides in lakes and rivers in Switzerland. *Environ. Sci. Technol.* **1998**, *32*, (5), 626–633.
135. Hunkeler, D.; Meckenstock, R. U.; Lollar, B. S.; Schmidt, T. C.; Wilson, J. T. *A guide for assessing biodegradation and source identification of organic ground water contaminants using compound specific isotope analysis (CSIA)*; Environmental Protection Agency (EPA), US: Washington, DC, US, **2008**, p.68.

136. Elsner, M.; Zwank, L.; Hunkeler, D.; Schwarzenbach, R. P., A new concept linking observable stable isotope fractionation to transformation pathways of organic pollutants. *Environ. Sci. Technol.* **2005**, *39*, (18), 6896–6916.
137. Harrington, R. R.; Poulson, S. R.; Drever, J. I.; Colberg, P. J. S.; Kelly, E. F., Carbon isotope systematics of monoaromatic hydrocarbons: vaporization and adsorption experiments. *Org. Geochem.* **1999**, *30*, (8A), 765–775.
138. Rayleigh, L., Theoretical considerations respecting the separation of gases by diffusion and similar processes. *The London, Edinburgh, and Dublin Philosophical Magazine and Journal of Science* **1896**, *42*, (259), 493–498.
139. Hofstetter, T. B.; Berg, M., Assessing transformation processes of organic contaminants by compound-specific stable isotope analysis. *TrAC, Trends Anal. Chem.* **2011**, *30*, (4), 618–627.
140. Maier, M. P.; De Corte, S.; Nitsche, S.; Spaett, T.; Boon, N.; Elsner, M., C & N isotope analysis of diclofenac to distinguish oxidative and reductive transformation and to track commercial products. *Environ. Sci. Technol.* **2014**, *48*, (4), 2312–2320.
141. Schürner, H. K. V.; Maier, M. P.; Eckert, D.; Brejcha, R.; Neumann, C.-C.; Stumpp, C.; Cirpka, O. A.; Elsner, M., Compound-specific stable isotope fractionation of pesticides and pharmaceuticals in a mesoscale aquifer model. *Environ. Sci. Technol.* **2016**, *50*, (11), 5729–5739.
142. Hofstetter, T. B.; Schwarzenbach, R. P.; Bernasconi, S. M., Assessing transformation processes of organic compounds using stable isotope fractionation. *Environ. Sci. Technol.* **2008**, *42*, (21), 7737–7743.
143. Gröning, M., Chapter 40 - International stable isotope reference materials. In *Handbook of Stable Isotope Analytical Techniques*, de Groot, P. A., Ed. Elsevier: Amsterdam, **2004**; pp 874–906.
144. de Laeter, J. R.; Böhlke, J. K.; De Bièvre, P.; Hidaka, H.; Peiser, H. S.; Rosman, K. J. R.; Taylor, P. D. P., Atomic weights of the elements. Review 2000 (IUPAC Technical Report). *Pure Appl. Chem.* **2003**, *75*, (6), 683–800.
145. Sessions, A. L., Isotope-ratio detection for gas chromatography. *J. Sep. Sci.* **2006**, *29*, (12), 1946–1961.
146. Renpenning, J.; Kümmel, S.; Hitzfeld, K. L.; Schimmelmann, A.; Gehre, M., Compound-specific hydrogen isotope analysis of heteroatom-bearing compounds via gas chromatography–chromium-based high-temperature conversion (Cr/HTC)–isotope ratio mass spectrometry. *Anal. Chem.* **2015**, *87*, (18), 9443–9450.
147. Eriksen, J., Measuring natural abundance of stable s isotopes in soil by isotope ratio mass spectrometry. *Commun. Soil Sci. Plant Anal.* **1996**, *27*, (5-8), 1251–1264.

148. Amrani, A.; Sessions, A. L.; Adkins, J. F., Compound-Specific  $\delta^{34}\text{S}$  Analysis of Volatile Organics by Coupled GC/Multicollector-ICPMS. *Anal. Chem.* **2009**, *81*, (21), 9027–9034.
149. Renpenning, J.; Hitzfeld, K. L.; Gilevska, T.; Nijenhuis, I.; Gehre, M.; Richnow, H.-H., Development and validation of an universal interface for compound-specific stable isotope analysis of chlorine ( $^{37}\text{Cl}/^{35}\text{Cl}$ ) by GC-high-temperature conversion (HTC)-MS/IRMS. *Anal. Chem.* **2015**, *87*, (5), 2832–2839.
150. Van Acker, M. R. M. D.; Shahar, A.; Young, E. D.; Coleman, M. L., GC/multiple collector-ICPMS method for chlorine stable isotope analysis of chlorinated aliphatic hydrocarbons. *Anal. Chem.* **2006**, *78*, (13), 4663–4667.
151. Lihl, C.; Renpenning, J.; Kümmel, S.; Gelman, F.; Schürner, H. K. V.; Daubmeier, M.; Heckel, B.; Melsbach, A.; Bernstein, A.; Shouakar-Stash, O.; Gehre, M.; Elsner, M., Toward improved accuracy in chlorine isotope analysis: synthesis routes for in-house standards and characterization via complementary mass spectrometry methods. *Anal. Chem.* **2019**, *91*, (19), 12290–12297.
152. Ponsin, V.; Torrentó, C.; Lihl, C.; Elsner, M.; Hunkeler, D., Compound-specific chlorine isotope analysis of the herbicides atrazine, acetochlor and metolachlor. *Anal. Chem.* **2019**, *91*, (22), 14290–14298.
153. Sylva, S. P.; Ball, L.; Nelson, R. K.; Reddy, C. M., Compound-specific  $^{81}\text{Br}/^{79}\text{Br}$  analysis by capillary gas chromatography/multicollector inductively coupled plasma mass spectrometry. *Rapid Commun. Mass Spectrom.* **2007**, *21*, (20), 3301–3305.
154. Zakon, Y.; Halicz, L.; Gelman, F., Bromine and carbon isotope effects during photolysis of brominated phenols. *Environ. Sci. Technol.* **2013**, *47*, (24), 14147–14153.
155. Aeppli, C.; Holmstrand, H.; Andersson, P.; Gustafsson, O., Direct compound-specific stable chlorine isotope analysis of organic compounds with quadrupole GC/MS using standard isotope bracketing. *Anal. Chem.* **2010**, *82*, (1), 420–426.
156. Zimmermann, J.; Halloran, L. J. S.; Hunkeler, D., Tracking chlorinated contaminants in the subsurface using compound-specific chlorine isotope analysis: A review of principles, current challenges and applications. *Chemosphere* **2020**, *244*, 125476.
157. Meyer, A. H.; Penning, H.; Elsner, M., C and N isotope fractionation suggests similar mechanisms of microbial atrazine transformation despite involvement of different enzymes (AtzA and TrzN). *Environ. Sci. Technol.* **2009**, *43*, (21), 8079–8085.
158. Meyer, A. H.; Dybala-Defratyka, A.; Alaimo, P. J.; Geronimo, I.; Sanchez, A. D.; Cramer, C. J.; Elsner, M., Cytochrome P450-catalyzed dealkylation of atrazine by *Rhodococcus* sp. strain N186/21 involves hydrogen atom transfer rather than single electron transfer. *Dalton Trans.* **2014**, *43*, (32), 12175–12186.
159. Lutz, S. R.; Van Breukelen, B. M., Combined source apportionment and degradation quantification of organic pollutants with CSIA: 2. Model validation and application. *Environ. Sci. Technol.* **2014**, *48*, (11), 6229–6236.

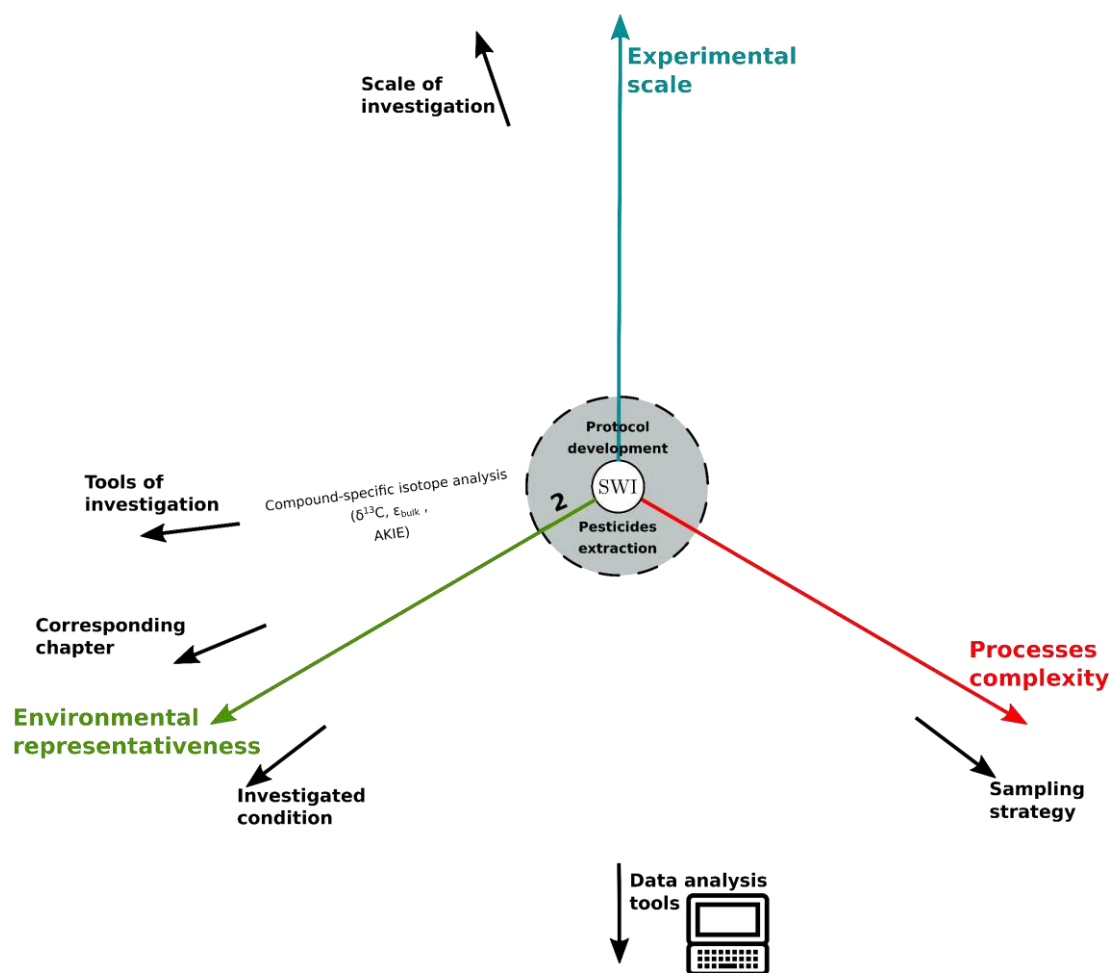
160. Kuntze, K.; Eisenmann, H.; Richnow, H.-H.; Fischer, A., Compound-specific stable isotope analysis (CSIA) for evaluating degradation of organic pollutants: An overview of field case studies. In *Anaerobic Utilization of Hydrocarbons, Oils, and Lipids*, Boll, M., Ed. Springer International Publishing: Cham, **2020**; pp 323–360.
161. Kendall, C.; Caldwell, A. E., Fundamental of isotope geochemistry. In *Isotope tracers in catchment hydrology*, Kendall, C.; McDonnell, J. J., Eds. Elsevier: **1998**; pp 51–86.
162. Lutz, S. R.; Van Breukelen, B. M., Combined source apportionment and degradation quantification of organic pollutants with CSIA: 1. Model derivation. *Environ. Sci. Technol.* **2014**, *48*, (11), 6220–6228.
163. Schreglmann, K.; Hoeche, M.; Steinbeiss, S.; Reinnicke, S.; Elsner, M., Carbon and nitrogen isotope analysis of atrazine and desethylatrazine at sub-microgram per liter concentrations in groundwater. *Anal. Bioanal. Chem.* **2013**, *405*, (9), 2857–2867.
164. Elsayed, O. F.; Maillard, E.; Vuilleumier, S.; Nijenhuis, I.; Richnow, H. H.; Imfeld, G., Using compound-specific isotope analysis to assess the degradation of chloroacetanilide herbicides in lab-scale wetlands. *Chemosphere* **2014**, *99*, 89–95.
165. Torabi, E.; Wiegert, C.; Guyot, B.; Vuilleumier, S.; Imfeld, G., Dissipation of S-metolachlor and butachlor in agricultural soils and responses of bacterial communities: Insights from compound-specific isotope and biomolecular analyses. *J. Environ. Sci.* **2020**, *92*, 163–175.
166. Ivdra, N.; Herrero-Martin, S.; Fischer, A., Validation of user- and environmentally friendly extraction and clean-up methods for compound-specific stable carbon isotope analysis of organochlorine pesticides and their metabolites in soils. *J. Chromatogr. A* **2014**, *1355*, 36–45.
167. Wijker, R. S.; Bolotin, J.; Nishino, S. F.; Spain, J. C.; Hofstetter, T. B., Using compound-specific isotope analysis to assess biodegradation of nitroaromatic explosives in the subsurface. *Environ. Sci. Technol.* **2013**, *47*, (13), 6872–6883.
168. Michl, J., Photophysics of organic molecules in solution In *Handbook of Photochemistry* Montalti, M.; Credi, A.; Prodi, L.; Gandolfi, M. T., Eds. CRC Press **2006**; p 664.
169. Ratti, M.; Canonica, S.; McNeill, K.; Erickson, P. R.; Bolotin, J.; Hofstetter, T. B., Isotope fractionation associated with the direct photolysis of 4-chloroaniline. *Environ. Sci. Technol.* **2015**, *49*, (7), 4263–4273.
170. Apell, Jennifer N.; McNeill, K., Updated and validated solar irradiance reference spectra for estimating environmental photodegradation rates. *Environ. Sci. Process. Impacts* **2019**, *21*, (3), 427–437.
171. Birkigt, J.; Gilevska, T.; Ricken, B.; Richnow, H.-H.; Vione, D.; Corvini, P. F. X.; Nijenhuis, I.; Cichocka, D., Carbon stable isotope fractionation of sulfamethoxazole during biodegradation by *Microbacterium* sp. strain BR1 and upon direct photolysis. *Environ. Sci. Technol.* **2015**, *49*, (10), 6029–6036.

172. Passeport, E.; Zhang, N.; Wu, L.; Herrmann, H.; Sherwood Lollar, B.; Richnow, H.-H., Aqueous photodegradation of substituted chlorobenzenes: Kinetics, carbon isotope fractionation, and reaction mechanisms. *Water Res.* **2018**, *135*, 95–103.
173. Ratti, M.; Canonica, S.; McNeill, K.; Bolotin, J.; Hofstetter, T. B., Isotope fractionation associated with the photochemical dechlorination of chloroanilines. *Environ. Sci. Technol.* **2015**, *49*, (16), 9797–9806.
174. Ratti, M.; Canonica, S.; McNeill, K.; Bolotin, J.; Hofstetter, T. B., Isotope fractionation associated with the indirect photolysis of substituted anilines in aqueous solution. *Environ. Sci. Technol.* **2015**, *49*, (21), 12766–12773.
175. Wu, L.; Yao, J.; Trebse, P.; Zhang, N.; Richnow, H. H., Compound specific isotope analysis of organophosphorus pesticides. *Chemosphere* **2014**, *111*, 458–463.
176. Hartenbach, A. E.; Hofstetter, T. B.; Tentscher, P. R.; Canonica, S.; Berg, M.; Schwarzenbach, R. P., Carbon, hydrogen, and nitrogen isotope fractionation during light-induced transformations of atrazine. *Environ. Sci. Technol.* **2008**, *42*, (21), 7751–7756.
177. Willach, S.; Lutze, H. V.; Eckey, K.; Löppenberg, K.; Lüling, M.; Wolbert, J.-B.; Kujawinski, D. M.; Jochmann, M. A.; Karst, U.; Schmidt, T. C., Direct photolysis of sulfamethoxazole using various irradiation sources and wavelength ranges — insights from degradation product analysis and compound-specific stable isotope analysis. *Environ. Sci. Technol.* **2018**, *52*, (3), 1225–1233.
178. Maier, M. P.; Prasse, C.; Pati, S. G.; Nitsche, S.; Li, Z.; Radke, M.; Meyer, A.; Hofstetter, T. B.; Ternes, T. A.; Elsner, M., Exploring trends of C and N isotope fractionation to trace transformation reactions of diclofenac in natural and engineered systems. *Environ. Sci. Technol.* **2016**, *50*, (20), 10933–10942.
179. Lutz, S. R.; Velde, Y. V. D.; Elsayed, O. F.; Imfeld, G.; Lefrancq, M.; Payraudeau, S.; van Breukelen, B. M., Pesticide fate on catchment scale: conceptual modelling of stream CSIA data. *Hydrol. Earth Syst. Sci.* **2017**, *21*, (10), 5243–5261.
180. The European Parliament and the Council, Directive 2000/60/EC establishing a framework for community action in the field of water policy. *Off. J. Eur. Communities: Legis.* **2000**, *43*, (L327), 1–73.
181. Barbosa, M. O.; Moreira, N. F. F.; Ribeiro, A. R.; Pereira, M. F. R.; Silva, A. M. T., Occurrence and removal of organic micropollutants: An overview of the watch list of EU Decision 2015/495. *Water Res.* **2016**, *94*, 257–279.
182. Drouin, G.; Fahs, M.; Droz, B.; Younes, A.; Imfeld, G.; Payraudeau, S., Pollutant dissipation at the sediment–water interface: a robust discrete continuum numerical model and recirculating laboratory experiments. *Water Resour. Res.* **2020**, *in prep.*
183. Masbou, J.; Drouin, G.; Payraudeau, S.; Imfeld, G., Carbon and nitrogen stable isotope fractionation during abiotic hydrolysis of pesticides. *Chemosphere* **2018**, *213*, 368–376.

## Preface to Chapter 2

The following chapter describes the development and validation of carbon-based compound-specific isotope analysis (CSIA) for a panel of pesticides in water sediments and agricultural soils. The chapter details the adaptation of existing protocols from the literature<sup>1</sup> for pesticide extraction, quantification by gas chromatography–mass spectrometry (GC-MS) and stable isotope analysis of carbon (C) and nitrogen (N) by gas chromatography–isotope ratio mass spectrometry (GC-IRMS) from water, sediments and agricultural soils.

This methodological development was a key preliminary step to reliably measure C and N isotope signatures of pesticide along this Ph.D. project and was used in chapter 3 to 6.



1. Ivdra, N.; Herrero-Martin, S.; Fischer, A., Validation of user- and environmentally friendly extraction and clean-up methods for compound-specific stable carbon isotope analysis of organochlorine pesticides and their metabolites in soils. *J. Chromatogr. A* **2014**, *1355*, 36–45.



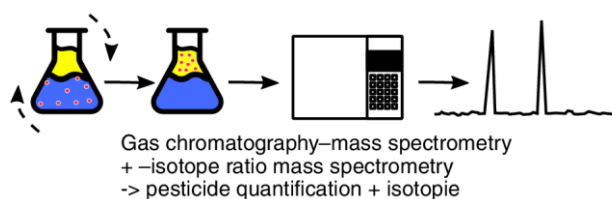


## Chapter 2

# Pesticide extraction from soil and sediments for compound-specific isotope analysis (CSIA)

### Abstract

Due to the limitation in sensitivity of gas chromatography used in combination with isotope-ratio mass spectrometry (GC-IRMS), applications of compound-specific isotope analysis (CSIA) need to extract and concentrate pesticides accurately for their determination. One challenge was to



- ✓ extraction yield >70%
- ✓ no isotope fractionation  $|\Delta\delta^{13}\text{C}| < 0.7\text{‰}$

extract and concentrate the pesticides without the spurious effect of organic matter from the sample matrix, which could compromise the GC-IRMS measurement. Here, we adapted and validated a protocol to increase the sensitivity of pesticide quantification by gas chromatography – mass spectrometry (GC-MS), and stable isotope analysis of Carbon by gas chromatography – isotope ratio mass spectrometry (GC-IRMS), from soils and sediments. The method was simple, robust, quick, and inexpensive, while achieving an extraction yield larger than 70% for sediment with all pesticides of interest, i.e., atrazine, terbutryn, acetochlor, S-metolachlor and metalaxyl. However, with yield of extraction lower than 60%, the method seemed to be not applicable for soil samples, likely due to a more complex matrix. Finally, the extraction method caused no significant isotope fractionation for C ( $|\Delta\delta^{13}\text{C}_{ext}| < 0.7\text{‰}$ ) for natural sediment samples.

---

This chapter gathers the contributions of an unpublished study by Charline Wiegert, and method developments and validations by Paula Perez, Benoît Guyot and Boris Droz for their respective experiments.

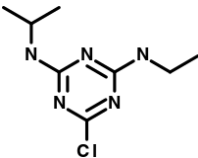
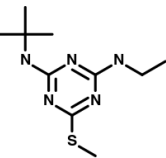
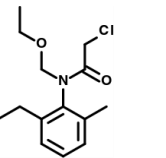
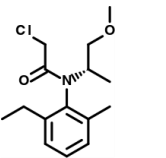
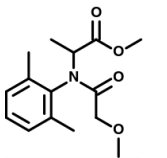
## **Introduction**

Compound-specific isotope analysis (CSIA) has become a widely used method to identify the source of organic pollution and identify their degradation pathways.<sup>1</sup> However, due to the limitation in sensitivity of gas chromatography used in combination with isotope-ratio mass spectrometry (GC-IRMS),<sup>2</sup> applications of CSIA were originally restricted to pollutants found in aqueous concentrations in the  $\mu\text{g L}^{-1}$  to  $\text{mg L}^{-1}$  range, which could be easily extracted from environmental matrices. Applications were originally dedicated to legacy contaminants, such as chlorinated solvents, BTEX and MTBE found in groundwater, for which pre-concentration and purification could be performed easily due to their high volatility.<sup>3, 4</sup> Recently, method developments were made on less hydrophobic, more soluble compounds like pesticides<sup>5-7</sup> with the common objective to use CSIA of trace concentrations ( $\text{ng L}^{-1}$  to  $\mu\text{g L}^{-1}$  range) in surface water systems. However, efficient extraction protocols for solid matrices, such as soil and sediment, that could be combined with CSIA, were only available for a limited number of compounds including: hexachlorocyclohexanes (HCHs), *p,p*-dichlorodiphenyltrichloroethane (DDT) and their environmental metabolites (chlorinated benzenes, dichlorodipenyldichloroethylene (DDE) and dichlorodipenyldichloroethane (DDD)),<sup>8, 9</sup> for polycyclic aromatic hydrocarbons (PAH),<sup>10</sup> for the fatty acid (FA),<sup>11</sup> for the alpha-cypermethrin,<sup>12</sup> and for nitroaromatic compounds such as 2,4,6-trinitrotoluene (TNT) and two dinitrotoluene isomers (2,4-DNT and 2,6-DNT).<sup>13</sup>

We herein adapted an efficient solid-liquid extraction method developed by Ivdra et al.<sup>8</sup> for HCH, DDT and DDD to investigate a pesticide mixture in sediment and soil samples. This protocol was selected because HCH, DDT and DDD physicochemical properties ( $\log P_{ow}$  between 2.4 to 6.5 and  $\log K_{oc}$  between 1.7 and 5.2) were in the same range as our pesticides of interest (Table 2.1). Our goal was thus to validate a protocol for sensitive pesticide quantification by gas chromatography coupled to mass spectrometry (GC-MS) and stable isotope analysis of C and N by GC-IRMS from sediments and agricultural soils. The method (i) should be able to extract pesticides in low concentrations ( $< \mu\text{g g}^{-1}$ ) with a decent yield of extraction ( $>70\%$ ), (ii) be reproducible on diverse soils and sediments types, (iii) generate no isotope fractionation (C and N), and (iv) result in low matrix effects, e.g., generating low soil C matrix extraction, for accurate GC-IRMS measurement.

The method developed in this chapter constitutes an essential basis for further experiments developed in this thesis. We also tested the protocol on some sterile samples, which could be further used as experimental abiotic control. A pesticide mixture (atrazine, terbutryn, acetochlor, *S*-metolachlor and metalaxyl; Table 2.1) were selected due to their suitability for gas chromatography to ensure accurate GC-IRMS measurement, and the following criteria: high worldwide applications,<sup>14</sup> be on the priority list of the European (EU) water framework directive<sup>15</sup> and/or be on the EU watch list.<sup>16</sup>

Table 2.1. Pesticides selection of present and legacy agricultural input from European regions.

compound	atrazine	terbutryn	acetochlor	S-metolachlor	metalaxyl
general description of use <sup>a</sup>					
usage		herbicide			fungicide
rank in used global (US) <sup>b</sup>	10 (2)	-	12 (7)	8 (3)	-
expiration of approval in Eu <sup>c</sup>	banned (2004)	banned (2002)	banned (2013)	approved (2021)	approved (2023)
priority concern		Yes			No
chemical structure and major transformation products (TPs) <sup>d</sup>					
family	triazine		chloroacetamide		phenylamide
structure					
formula	C <sub>8</sub> H <sub>14</sub> ClN <sub>5</sub>	C <sub>10</sub> H <sub>19</sub> N <sub>5</sub> S	C <sub>14</sub> H <sub>20</sub> ClNO <sub>2</sub>	C <sub>15</sub> H <sub>22</sub> ClNO <sub>2</sub>	C <sub>15</sub> H <sub>21</sub> NO <sub>4</sub>
major TPs	desethylatrazine (DEA), desisopropyl-atrazine (DIA), hydroxyatrazine (HA)	terbutylazine-2-hydroxy, Terbutryn sulfoxide, desethylhydroxy-terbutryne	acetochlor oxanilic acid (AOXA), acetochlor ethanesulfonic acid (AESAs), 2-hydroxy-acetochlor	metolachlor oxanilic acid (MOXA), metolachlor ethane sulfonic acid (MESA)	carboxylic acid metalaxyl, demethyl-metalaxyl, hydroxy-metalaxyl, didemethyl-metalaxyl
physico-chemical properties <sup>e</sup>					
pKa	1.6	4.3	-	-	-
half-life wat.-sed. (days)	80	60	20	47	32
solubility (mg L <sup>-1</sup> ) <sup>f</sup>	35	25	280	480	8400
octanol/water coef. (Log(P <sub>ow</sub> ))	2.7	3.7	4.1	3	1.8
sorption (K <sub>oc</sub> ; mg g C <sup>-1</sup> )	100	2432	156	185	162

<sup>a</sup> Ref.<sup>17</sup>, <sup>b</sup> ref.<sup>14</sup> & [www.fao.org/faostat/](http://www.fao.org/faostat/) (20th March 2019), <sup>c</sup> revision date in parenthesis from <https://ec.europa.eu/food/plant/pesticides/eu-pesticides-database/>, <sup>d</sup> ref.<sup>18-21</sup>, <sup>e</sup> ref.<sup>17,22</sup>, <sup>f</sup> at 20°C pH= 7 in water.

## **Materials and methods**

All chemicals were of analytical grade purity (>99%) (detailed in Appendix B). All aqueous solutions were prepared with ultrapure water (>18 M $\Omega$  cm). A pesticide mixture (atrazine, terbutryn, acetochlor, *S*-metolachlor and metalaxyl) in a stock solution (5g L<sup>-1</sup> per pesticide in acetonitrile, ACN) was prepared and stored at -20°C prior to experiment.

### **Sampling location**

Five sampling locations (Table 2.2) were selected to have very contrasted soil or sediment physico-chemical properties, i.e., low and neutral *pH*, low to high organic carbon content and carbonates to generalize as much as possible our methodological development. The locations correspond to different study sites with intensives ongoing projects. The Rouffach catchment (43 ha), the Alteckendorf catchment (47 ha), and the Strengbach catchment (80 ha) are located in Alsace, France. The Rouffach is a vineyard catchment where 68% of the land is farmed with conventional and organic farming as part of the agricultural and viticultural college of Rouffach.<sup>23</sup> The prevalent soil type of the catchment is calcareous clay loam with medium permeability capacity. The catchment is equipped at the outlet with a 1,500 m<sup>3</sup> stormwater wetland.<sup>24, 25</sup> Alteckendorf is an agricultural catchment, mainly sugar beet (70%) and corn (18%; 2016 landuse).<sup>7, 26</sup> The main soil type of the catchment is Cambisol. Sediment samples were collected in a small stream at the outlet of the catchment. The Strengbach catchment is covered at 85% with forest and is one of the French critical zone observatories (<https://www.ozcar-ri.org>).<sup>27</sup> The bedrock is a Ca-poor (less than 1%) Hercynian leucogranite. The soil types were sandy and stony and vary from entic Podzol to Cambisol.<sup>28</sup> The bioretention cell is located at the Kortright center for conservation in Vaughan, Ontario, Canada. It is an engineered structure dedicated to treat the water coming from a small parking lot. The bioretention cell is covered with 7.5 cm of hardwood mulch followed by a mix of sand and some soil rich in organic matter content.<sup>29</sup>

### **Sediment collection and characterization**

Soils and sediments were collected at five different locations (Table 2.2) from the top ten cm. A total of five to ten randomly selected sub-samples, each between 2 and 10 kg per location were collected with a shovel, successively cleaned with distilled water, acetone and dried with a towel. The sub-samples were pooled together, and thoroughly mixed. Samples were wet-sieved at 2 mm and stored at 4°C prior to further manipulation. Characterizations were made by in-house or NF/ISO methods (detailed in Appendix B). Soil and sediment samples dried at 40°C were used to validate our tests.

Table 2.2. Location and characterization of the soils and sediment samples.

	wetland sediment Rouffach, FR 47°57'43"N, 7°17'26"E	river sediment Alteckendorf, FR 48°47'17"N, 7°35'25"E	vigneyard soil Rouffach, FR 47°57'44"N, 7°17'27"E	forest soil Strengbach, FR 48°12'58"N, 7°11'53"E	bioretention cell Vaughan, CA 43°49'50"N, 79°35'24"W
residual humidity (%)	37 ± 3	39 ± 3	18 ± 3	47 ± 13	27 ± 1
bulk density (g cm <sup>-3</sup> )	1.7 ± 0.1	n.m.	1.5 ± 0.2	1.0 ± 0.1	0.57 ± 0.2 <sup>a</sup>
<i>pH</i> <sub>H<sub>2</sub>O</sub>	7.5 ± 0.5	7.0 ± 0.2	8.0 ± 0.2	3.4 ± 0.2	6.1 ± 0.6
<i>CEC</i> (cmol kg <sup>-1</sup> )	14.3 ± 2.8	14.7 ± 1.5	18.0 ± 0.1	14.3 ± 0.1	34.8 ± 1.0
clay (< 2 μm; %)	21.2 ± 2.5	14.4	24.4	6.8	4.5
silt (2 - 50 μm; %)	67.4 ± 2.5	73.1	61.1	31.6	17.4
sand (50 - 2000 μm; %)	11.4 ± 4.3	12.5	14.5	61.6	78.2
<i>f</i> <sub>OC</sub> (%)	2.3 ± 2.1	2.0	1.1	4.5	11.7
<i>C/N</i>	7.2 ± 1.5	10.7	4.2	26.8	14.3
<i>C</i> <sub>min</sub>	3.9 ± 0.5	2.0	2.9	0 <sup>b</sup>	0.44

n.m.: not measured, *CEC*: cation exchange capacity, *f*<sub>OC</sub>: fraction of organic carbon and *C*<sub>min</sub>: mineral carbon, respectively. <sup>a</sup>measured posteriori in the laboratory. <sup>b</sup>assumed to be zero from the *pH* measurement.

### Selection of the extractant

The extractant was constituted by a solvent or solvent mixture with the requirement that extraction of the targeted pesticides with a decent extraction yield (>70%) could be obtained, be compatible with gas chromatography and exhibit a matrix effect allowing CSIA. We tested several solvent mixtures with a polarity close to the range of the targeted pesticides, including: i) ethyl acetate alone, ii) & iii) pentane:ethyl acetate 1:1 & 3:1 (v:v), and iv) & v) pentane:dichloromethane (DCM) 3:1 & 3:2 (v:v), respectively. For all preliminary tests, the extraction procedure was carried out as described below after spiking with a 50 mg g<sup>-1</sup> pesticide mixture. The selection of the extractant was based on the extraction yield and used in a following step for CSIA.

### Sample preparation for method validation

Five grams of dried soil or sediment were added to 15 mL centrifuge tubes and either adjusted at the original residual humidity (*RH*; Table 2.2) or to 50% *RH* with ultrapure water, respectively. A series of soil or sediment samples was spiked with the pesticide mixture from a diluted stock solution (1g L<sup>-1</sup> in acetonitrile) at 0, 0.5, 5, 10, 20, 30, 40, 50 75, 100, 125 and 150 μg g<sup>-1</sup>. An additional sample was prepared with a 3 μg g<sup>-1</sup> concentration and tested for the soil series. The tubes were manually shaken, then vortexed for 30 min to ensure homogenization. Each series of samples were performed in duplicate.

Additionally, blank controls without soil or sediment were processed in parallel to test whether pesticide sorption occurred during the extraction procedure. Sterile controls with soil and sediment autoclaved two times within a 24 h interval at 125 °C and 103 kPa for 20 min were conducted to quantify potential abiotic degradation. The sample series, blanks and sterile controls were stored for 7 days in the dark at 4°C prior to extraction to ensure equilibrium between the solid and liquid phase.

### **Optimized extraction procedure**

Pesticides from soil or sediment (5 g dry mass) previously transferred into a centrifuge tube were extracted with 3 mL of solvent added directly to the centrifuge tube. The highest extraction yield was obtained with pentane:DCM (3:1, v:v). The centrifuge tube was then vortexed for 5 s, placed for 5 min into an ultrasonic bath (Branson 5510, 40 kHz), vortexed again for 1 min, and centrifuged at 2400 RCF for 20 min. this amount of centrifugation was found to be the optimum to ensure the settling of fine clay particles. The supernatant was then transferred into an amber glass vial. The whole extraction procedure was repeated an additional two times. The three supernatants were then pooled together, dried under gentle nitrogen stream at room temperature, re-suspended into ACN up to 1 mL, and vortexed to collect residues on the glassware. The clean-up phase and elimination of residual water were performed by adding in each vial about 75 mg of anhydrous MgSO<sub>4</sub> and 13 mg of Primary-secondary amine (PSA).<sup>30</sup> The vial was then vortexed for 30 s, centrifuged at 2400 RCF 5 min and the supernatant was eventually transferred into a clean amber glass vials for further pesticide quantification and CSIA.

### **Pesticide quantification and compound-specific isotope analysis (CSIA)**

Pesticides were quantified using an established procedure for GC-MS (detailed in Appendix B) in the quantification range between 40 to 800 µg L<sup>-1</sup>. C and N CSIA were conducted using established procedure for GC-IRMS (detailed in Appendix B).<sup>5</sup>

## Results and discussion

### Selection of the extractant

From pre-tests of different extractants, only the two mixtures with pentane:DCM resulted in fair extraction yields (>70%; Table 2.3). The less polar mixture with 3:1 pentane:DCM was thus selected for further soil and sediment extraction because the average extraction yield of the 3:1 pentane:DCM ( $\bar{X} \pm SD = 92.7 \pm 5.3\%$ ) was higher than that of the 3:2 mixture ( $76.7 \pm 9.5\%$ ).

*Table 2.3. Yield of the extraction pre-tests.*

extractant	ratio (v:v)	extraction yield (%)				
		atrazine	terbutryn	acetochlor	S-metolachlor	metalaxyl
ethyl acetate	100% <sup>a</sup>	n.m	n.m.	31	34	71
pentane:ethyl acetate	1:1 <sup>a</sup>	n.m	n.m.	15	15	30
	3:1	55	62	72	45	52
pentane:dichloromethane	3:1	98	89	99	92	87
	3:2	77	86	88	78	64

<sup>a</sup> preliminary data from Charline Wiegert, n.m.: not measured.

### Extraction method validation

#### *Extraction yield*

An extraction yield of  $98 \pm 20\%$  from blank samples indicated no sorption on the polyethylene centrifuge tube or any material used in our experiment. This suggests no measurement bias for extraction from spiked soil and sediment. Quantitative extraction yields (>70%; Table 2.4) were obtained from the wetland and river sediments and the bioretention cell, for both non-autoclaved and autoclaved conditions. This indicates that autoclaved sediments could be used as sterile controls in further experiments. Like previous studies,<sup>8, 13</sup> the type of sediment and autoclaving did not significantly influence the extraction yield (Tukey test,  $p < 0.01$ ). Nevertheless, the extraction yield was generally higher for non-autoclaved (average extraction yield: 87 to 102%) than for autoclaved samples (average extraction yield: 67 to 89%). Extraction yields for soil sample were lower than those for sediments. While larger amounts of organic carbon content in soil may partly explain this result, the soil matrix may have a larger affinity (i.e., stronger bounds) for pesticides than sediment. Some parallels could be made with the non-extractable residues, i.e., “bound residues representing compounds in soil which persist in the matrix in the form of the parent substance or its metabolites after extraction”.<sup>31</sup> For instances, higher atrazine non-extractable residues were observed when fresh amendment of compost material or humified material were added to the soil.<sup>32</sup> An alternative hypothesis might be that the inorganic material also participates to the sorption process, since



soils offer more micropores, i.e., pore smaller than 50 nm, than sediments. Slow kinetics of sorption–desorption were due to diffusion into and out of the micropores.<sup>33</sup> Additionally, since the activation energy of the sorption equilibrium depends strongly on pore sizes,<sup>34</sup> the smaller the pore size, the stronger the sorption to the mineral phase.

*Table 2.4. Reproducibility of optimized extraction method.*

	atrazine	terbutryn	acetochlor	S-metolachlor	metalaxyl
i) extraction recovery (%) for the solid-liquid					
wetland sediment ( <i>n</i> = 22)	88.7 ± 18.0	86.9 ± 18.8	91.6 ± 22.4	88.1 ± 20.3	76.0 ± 18.8
river sediment ( <i>n</i> = 21)	97.0 ± 21.6	97.4 ± 24.4	102.3 ± 24.2	102.8 ± 25.4	100.4 ± 20.8
vineyard soil ( <i>n</i> = 26)	54.4 ± 1.9	41.6 ± 1.1	41.0 ± 1.4	49.2 ± 1.3	36.3 ± 1.4
forest soil ( <i>n</i> = 26)	44.5 ± 2.2	17.5 ± 2.2	40.0 ± 2.5	43.3 ± 2.3	43.4 ± 2.8
bioretention cell ( <i>n</i> = 12)	119.3 ± 23.5				
ii) extraction recovery (%) for the solid-liquid (autoclaved)					
wetland sediment ( <i>n</i> = 22)	85.1 ± 27.7	76.6 ± 31.4	86.5 ± 29.6	81.2 ± 29.5	75.5 ± 26.3
river sediment ( <i>n</i> = 21)	88.5 ± 18.1	66.7 ± 18.7	82.2 ± 18.1	76.5 ± 17.8	79.4 ± 14.6
vineyard soil ( <i>n</i> = 26)	79.7 ± 2.6	57.8 ± 1.9	59.5 ± 2.2	63.9 ± 1.9	67.8 ± 2.6
forest soil ( <i>n</i> = 26)	44.3 ± 2.2	20.1 ± 1.5	49.8 ± 3.5	49.2 ± 2.9	57.8 ± 2.9
iii) deviation of carbon isotope signatures ( $\Delta\delta^{13}\text{C}$ (‰))					
wetland sediment ( <i>n</i> = 12)	-0.28 ± 0.49	0.06 ± 1.87	-0.17 ± 0.22	-0.55 ± 1.00	0.61 ± 0.94
river sediment ( <i>n</i> = 9)	0.36 ± 2.02	0.15 ± 1.93	-0.23 ± 0.24	-0.45 ± 1.41	0.29 ± 0.49
vineyard soil ( <i>n</i> = 11)	-1.90 ± 0.70	1.90 ± 0.40	-0.10 ± 0.00	-0.70 ± 0.10	0.10 ± 0.20
forest soil ( <i>n</i> = 11)	-1.60 ± 1.00	9.30 ± 1.60	0.00 ± 0.10	-0.50 ± 0.00	-0.20 ± 0.20
iv) deviation of carbon isotope signatures ( $\Delta\delta^{13}\text{C}$ (‰); autoclaved)					
wetland sediment ( <i>n</i> = 12)	-0.83 ± 0.37	1.40 ± 0.79	-0.84 ± 0.30	-1.23 ± 0.32	2.38 ± 0.36
river sediment ( <i>n</i> = 8)	-0.11 ± 1.04	0.64 ± 1.79	-0.20 ± 0.18	-0.90 ± 1.06	0.33 ± 0.54
vineyard soil ( <i>n</i> = 11)	-1.30 ± 0.30	-0.10 ± 0.10	-0.20 ± 0.00	-0.90 ± 0.30	-0.50 ± 0.10
forest soil ( <i>n</i> = 11)	-2.40 ± 0.40	3.40 ± 1.70	-1.20 ± 0.40	-0.50 ± 0.10	-0.80 ± 0.10
v) deviation of nitrogen isotope signatures ( $\Delta\delta^{15}\text{N}$ (‰))					
wetland sediment ( <i>n</i> = 5)	-0.10 ± 1.08	0.69 ± 0.91	1.20 ± 0.40	1.58 ± 0.60	1.86 ± 0.43

### *Effect on the stable isotope signature*

Pesticide extraction from non-autoclaved sediments did not cause any carbon isotope fractionation ( $|\Delta\delta^{13}\text{C}_{ext}| < 0.7\text{‰}$ ). However, a small isotope fractionation ( $|\Delta\delta^{13}\text{C}_{ext}| < 2.4\text{‰}$ ) was observed for non-autoclaved soil and autoclaved soil or sediment samples, suggesting a background effect on carbon isotope fractionation. Dissolved organic carbon generated by autoclaving (10 mg L<sup>-1</sup> in non-autoclaved samples vs between 50 and 100 ppm in autoclaved samples) might be the source of such an interference. The isotope signature of pesticides did not significantly change between the two types sediments (Rouffach and Alteckendorf) and the

autoclaved/no-autoclaved conditions (Tukey test,  $p < 0.5$ ). Co-elution between matrix and atrazine was frequently observed<sup>35</sup> and has tendency to reduce the accuracy of measurement. No measurements were possible from the bioretention cell samples because the extract was associated with a large amount of organic matter resulting in a large GC-IRMS background signal, which overlapped the peak of targeted pesticides. Nitrogen isotope fractionation ( $|\Delta\delta^{15}N_{ext}| > 1\text{‰}$ ) was observed and considered as unacceptable in all series. From a back envelope calculation, we could estimate that the lowest measurable C isotope signature corresponding to a pesticide to DOC ratio of 5 and a C/N ratio of 7, may generate with our extraction method a N signal background, corresponding at 100 to 200mV, enough to generate a matrix effect and alter the measurements.

### **Further improvements**

The method adapted here did not seem to be universal for sediment and soil matrices, even for the five targeted pesticides. Further improvements could be made to increase the extraction yield or decrease the background effect for accurate CSIA determination of pesticides in soils/sediments. Adding salts, such as NaCl or CaCl<sub>2</sub>, into the liquid phase is a generally accepted approach to increase the yield of extraction.<sup>30, 36</sup> This is because organic matter in soils and sediments is negatively charged, and thus has more affinity to sorb cations than organic compounds. As a result, cations just replace organic compounds by affinity. Second, we recommend to adopt the florisil® cleaning step<sup>8, 37</sup> to reduce the matrix effect in the case of highly organic matrix, such as those from the bioretention cell.<sup>29, 38, 39</sup> Third, to extract selectively the compound of interest molecularly imprinted polymers (MIPs) could be synthesized and used as a secondary separation step after the regular SPE extraction.<sup>40</sup> MIPs has become commercially available for triazine pesticides by Sigma-Aldrich (SupelMIP).<sup>41</sup> Finally, the extraction procedure carried out at room temperature and the repeated centrifugation generate elevated heat within the sample, which could degrade sensitive compounds, such as chloropyrifos. Care must be therefore taken to reduce the extraction and centrifugation temperature for such compounds.

### **Environmental implications**

The procedure did not cause any C isotope fractionation ( $|\Delta\delta^{13}C_{ext}| < 0.7\text{‰}$ ) for pesticides from sediment samples, whereas N isotope signature of pesticide was significantly affected. The extraction capacity of the solid-liquid extraction method was about 0.5  $\mu\text{g g}^{-1}$  of soil which corresponds to a 0.5  $\text{mg L}^{-1}$  extract at the end of the extraction. By consequence, the isotopic ratio measurement will be limited by the sensitivity of the GC-IRMS (between 16 to 200  $\text{mg L}^{-1}$ ; Appendix B, Table B5) rather than the extraction method. N-CSIA results for

pesticides may depend on the type of matrix and further improvements should focus on N-CSIA of pesticide from sediment and soil samples. The extraction method was suitable for C-CSIA of pesticides under low DOC content (<20 mg L<sup>-1</sup>), and may be suited for a range of compounds with chemical properties similar as those of pesticides targeted in this study:  $K_{OC}$  ranging from 100 to 2500 mg pest g C<sup>-1</sup> and log  $P_{OW}$  from 1 to 4.

## References

1. Elsner, M.; Imfeld, G., Compound-specific isotope analysis (CSIA) of micropollutants in the environment — current developments and future challenges. *Curr. Opin. Biotechnol.* **2016**, *41*, 60–72.
2. Hofstetter, T. B.; Schwarzenbach, R. P.; Bernasconi, S. M., Assessing transformation processes of organic compounds using stable isotope fractionation. *Environ. Sci. Technol.* **2008**, *42*, (21), 7737–7743.
3. Zwank, L.; Berg, M.; Schmidt, T. C.; Haderlein, S. B., Compound-specific carbon isotope analysis of volatile organic compounds in the low-microgram per liter range. *Anal. Chem.* **2003**, *75*, (20), 5575–5583.
4. Schmidt, T. C.; Zwank, L.; Elsner, M.; Berg, M.; Meckenstock, R. U.; Haderlein, S. B., Compound-specific stable isotope analysis of organic contaminants in natural environments: a critical review of the state of the art, prospects, and future challenges. *Anal. Bioanal. Chem.* **2004**, *378*, (2), 283–300.
5. Masbou, J.; Drouin, G.; Payraudeau, S.; Imfeld, G., Carbon and nitrogen stable isotope fractionation during abiotic hydrolysis of pesticides. *Chemosphere* **2018**, *213*, 368–376.
6. Torrentó, C.; Bakkour, R.; Glauser, G.; Melsbach, A.; Ponsin, V.; Hofstetter, T.; Elsner, M.; Hunkeler, D., Solid-phase extraction method for stable isotope analysis of pesticides from large volume environmental water samples. *Analyst* **2019**, *144*, 2898–2908
7. Alvarez-Zaldívar, P.; Payraudeau, S.; Meite, F.; Masbou, J.; Imfeld, G., Pesticide degradation and export losses at the catchment scale: Insights from compound-specific isotope analysis (CSIA). *Water Res.* **2018**, *139*, 198–207.
8. Ivdra, N.; Herrero-Martin, S.; Fischer, A., Validation of user- and environmentally friendly extraction and clean-up methods for compound-specific stable carbon isotope analysis of organochlorine pesticides and their metabolites in soils. *J. Chromatogr. A* **2014**, *1355*, 36–45.
9. Wu, L.; Moses, S.; Liu, Y.; Renpenning, J.; Richnow, H. H., A concept for studying the transformation reaction of hexachlorocyclohexanes in food webs using multi-element compound-specific isotope analysis. *Anal. Chim. Acta* **2019**, *1064*, 56–64.

10. Buczyńska, A. J.; Geypens, B.; Van Grieken, R.; De Wael, K., Stable carbon isotopic ratio measurement of polycyclic aromatic hydrocarbons as a tool for source identification and apportionment—A review of analytical methodologies. *Talanta* **2013**, *105*, 435–450.
11. Reiffarth, D. G.; Petticrew, E. L.; Owens, P. N.; Lobb, D. A., Sources of variability in fatty acid (FA) biomarkers in the application of compound-specific stable isotopes (CSSIs) to soil and sediment fingerprinting and tracing: A review. *Sci. Total Environ.* **2016**, *565*, 8–27.
12. Xu, Z.; Shen, X.; Zhang, X.-C.; Liu, W.; Yang, F., Microbial degradation of alpha-cypermethrin in soil by compound-specific stable isotope analysis. *J. Hazard. Mater.* **2015**, *295*, 37–42.
13. Wijker, R. S.; Bolotin, J.; Nishino, S. F.; Spain, J. C.; Hofstetter, T. B., Using compound-specific isotope analysis to assess biodegradation of nitroaromatic explosives in the subsurface. *Environ. Sci. Technol.* **2013**, *47*, (13), 6872–6883.
14. Atwood, D.; Paisley-Jones, C. *Pesticides industry sales and usage 2008-2012 market estimates*; U.S. Environmental Protection Agency: Washington, DC, US, **2017**; p 24.
15. The European Parliament and the Council, Directive 2000/60/EC establishing a framework for community action in the field of water policy. *OJEC* **2000**, *43*, (L327), 1–73.
16. Barbosa, M. O.; Moreira, N. F. F.; Ribeiro, A. R.; Pereira, M. F. R.; Silva, A. M. T., Occurrence and removal of organic micropollutants: An overview of the watch list of EU Decision 2015/495. *Water Res.* **2016**, *94*, 257–279.
17. Lewis, K. A.; Tzilivakis, J.; Warner, D. J.; Green, A., An international database for pesticide risk assessments and management. *Hum. Ecol. Risk Assess.* **2016**, *22*, (4), 1050–1064.
18. Fenner, K.; Canonica, S.; Wackett, L. P.; Elsner, M., Evaluating pesticide degradation in the environment: Blind spots and emerging opportunities. *Science* **2013**, *341*, (6147), 752–758.
19. Berg, M.; Muller, S. R.; Schwarzenbach, R. P., Simultaneous determination of triazines including atrazine and their major metabolites hydroxyatrazine, desethylatrazine and deisopropylatrazine in natural waters. *Anal. Chem.* **1995**, *67*, (11), 1860–1865.
20. Luft, A.; Wagner, M.; Ternes, T. A., Transformation of biocides irgarol and terbutryn in the biological wastewater treatment. *Environ. Sci. Technol.* **2014**, *48*, (1), 244–254.
21. Wang, X. R.; Qiu, J.; Xu, P.; Zhang, P.; Wang, Y.; Zhou, Z. G.; Zhu, W. T., Rapid metabolite discovery, identification, and accurate comparison of the stereoselective metabolism of metalaxyl in rat hepatic microsomes. *J. Agric. Food. Chem.* **2015**, *63*, (3), 754–760.
22. Kegley, S. E.; Hill, B. R.; Orme, S.; Choi, A. H. PAN pesticide database, pesticide action network, North America <http://www.pesticideinfo.org> (18<sup>th</sup> January **2019**).

23. Gregoire, C.; Payraudeau, S.; Domange, N., Use and fate of 17 pesticides applied on a vineyard catchment. *Int. J. Environ. Anal. Chem.* **2010**, *90*, (3-6), 406–420.
24. Maillard, E.; Imfeld, G., Pesticide mass budget in a stormwater wetland. *Environ. Sci. Technol.* **2014**, *48*, (15), 8603–8611.
25. Maillard, E.; Payraudeau, S.; Faivre, E.; Grégoire, C.; Gangloff, S.; Imfeld, G., Removal of pesticide mixtures in a stormwater wetland collecting runoff from a vineyard catchment. *Sci. Total Environ.* **2011**, *409*, (11), 2317–2324.
26. Lefrancq, M.; Payraudeau, S.; Guyot, B.; Millet, M.; Imfeld, G., Degradation and transport of the chiral herbicide *S*-metolachlor at the catchment scale: Combining observation scales and analytical approaches. *Environ. Sci. Technol.* **2017**, *51*, (22), 13231–13240.
27. Pierret, M.-C.; Cotel, S.; Ackerer, P.; Beaulieu, E.; Benarioumlil, S.; Boucher, M.; Boutin, R.; Chabaux, F.; Delay, F.; Fourtet, C.; Friedmann, P.; Fritz, B.; Gangloff, S.; Girard, J.-F.; Legtchenko, A.; Viville, D.; Weill, S.; Probst, A., The Strengbach Catchment: A Multidisciplinary Environmental Sentry for 30 Years. *Vadose Zone Journal* **2018**, *17*, (1), 1–17.
28. Fichter, J.; Turpault, M.-P.; Dambrine, E.; Ranger, J., Mineral evolution of acid forest soils in the Strengbach catchment (Vosges mountains, N-E France). *Geoderma* **1998**, *82*, (4), 315–340.
29. Rhodes-Dicker, L.; Passeport, E., Effects of cold-climate environmental factors temperature and salinity on benzotriazole adsorption and desorption in bioretention cells. *Ecol. Eng.* **2019**, *127*, 58–65.
30. Anastassiades, M.; Lehotay, S. J.; Stajnbaher, D.; Schenck, F. J., Fast and easy multiresidue method employing acetonitrile extraction/partitioning and "dispersive solid-phase extraction" for the determination of pesticide residues in produce. *J. AOAC Int.* **2003**, *86*, (2), 412–431.
31. Barriuso, E.; Benoit, P.; Dubus, I. G., Formation of pesticide nonextractable (bound) residues in soil: Magnitude, controlling factors and reversibility. *Environ. Sci. Technol.* **2008**, *42*, (6), 1845–1854.
32. Barriuso, E.; Houot, S.; Serra-Wittling, C., Influence of compost addition to soil on the behaviour of herbicides. *Pestic. Sci.* **1997**, *49*, (1), 65–75.
33. Werth, C. J.; Reinhard, M., Effects of temperature on trichloroethylene desorption from silica gel and natural sediments. 2. Kinetics. *Environ. Sci. Technol.* **1997**, *31*, (3), 697–703.
34. Chantong, A.; Massoth, F. E., Restrictive diffusion in aluminas. *AlChE J.* **1983**, *29*, (5), 725–731.

35. Stahnke, H.; Kittlaus, S.; Kempe, G.; Alder, L., Reduction of matrix effects in liquid chromatography–electrospray ionization–mass spectrometry by dilution of the sample extracts: How much dilution is needed? *Anal. Chem.* **2012**, *84*, (3), 1474–1482.
36. Perry, R. H.; W., G. D., *Perry's chemical engineers' handbook*. McGraw Hill: **1999**; p 50–54.
37. US EPA *Method 3620C - florisol cleanup, test methods for evaluating solid waste, physical/chemical methods*; United States Environmental Protection Agency: **2007**; p 27.
38. Ding, B.; Rezanezhad, F.; Gharedaghloo, B.; Van Cappellen, P.; Passeport, E., Bioretention cells under cold climate conditions: Effects of freezing and thawing on water infiltration, soil structure, and nutrient removal. *Sci. Total Environ.* **2019**, *649*, 749–759.
39. Ulrich, B. A.; Vignola, M.; Edgehouse, K.; Werner, D.; Higgins, C. P., Organic carbon amendments for enhanced biological attenuation of trace organic contaminants in biochar-amended stormwater biofilters. *Environ. Sci. Technol.* **2017**, *51*, (16), 9184–9193.
40. Bakkour, R.; Bolotin, J.; Sellergren, B.; Hofstetter, T. B., Molecularly imprinted polymers for compound-specific isotope analysis of polar organic micropollutants in aquatic environments. *Anal. Chem.* **2018**, *90*, (12), 7292–7301.
41. Widstrand, C.; Björk, H.; Yilmaz, E., Analysis of analytes: The use of MIPs in solid-phase extraction increases efficiency and improves detection limits. *Laboratory news* **2006**, *June*, 14–15.

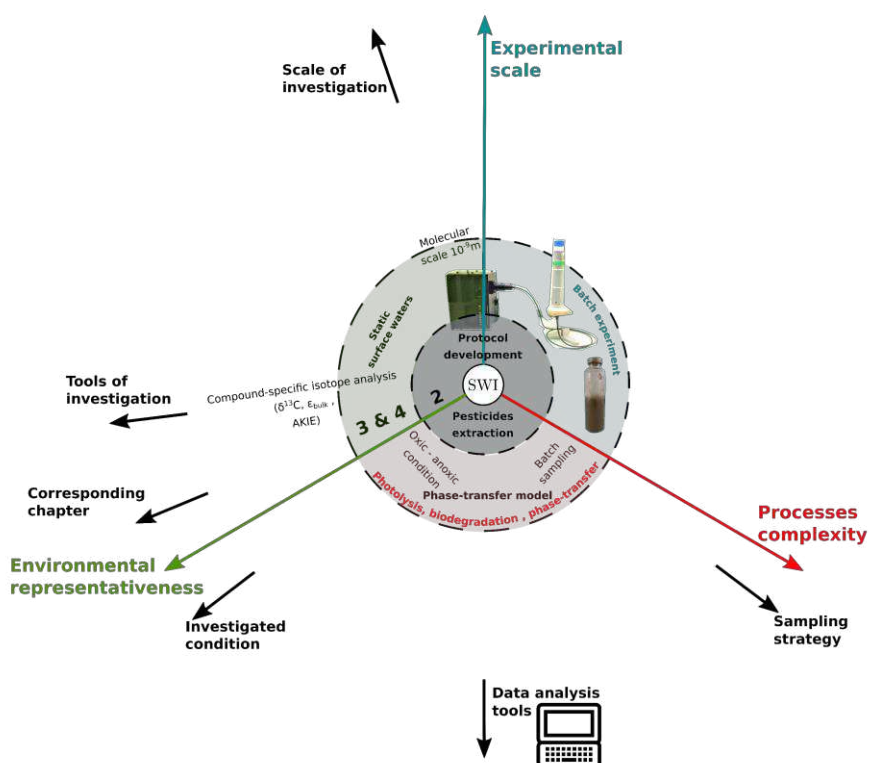


## Preface to Chapter 3 & 4

Elementary batch photolysis (Chap. 3) and biodegradation (Chap. 4) experiments were conducted to derive degradation rates and associated C and N isotopic enrichment factors associated to each process. This elementary experiment step constitutes a prerequisite to support degradation interpretation of bench-scale river channel experiment (Chap. 5) and at the catchment scale (Chap. 6).

Chapter 3 investigates direct and indirect photodegradation under UV light and simulated sunlight in synthetic water mimicking agriculturally impacted surface waters with nitrates and dissolved organic matter. Photodegradation was hypothesized as the main degradation pathways in the photic layer (several meter) of the surface waters.

Chapter 4 presents a microcosm study on a water–sediment system to simulate the dissipation of pesticides in the surface water. The contribution of degradation and phase-transfer is addressed together. Biodegradation is hypothesized as the main degradation pathways at the water-sediment interface.





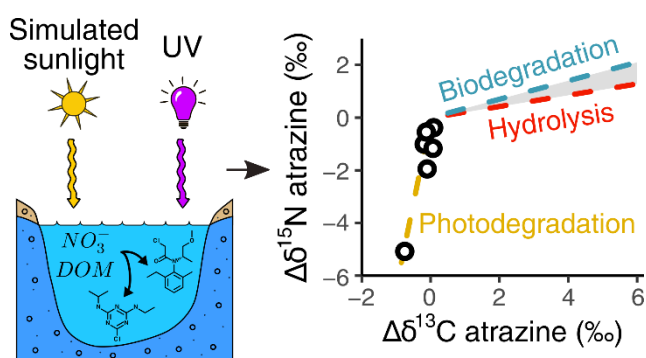


## Chapter 3

# Direct and indirect photodegradation of atrazine and *S*-metolachlor in agriculturally impacted surface water and associated C and N isotope fractionation

### Abstract

Limited knowledge of photodegradation-induced isotope fractionation hampers the application of compound-specific isotope analysis (CSIA) to trace pesticide degradation in surface waters. Here, we investigated



carbon and nitrogen isotope fractionation during direct and indirect photodegradation of the herbicides atrazine and *S*-metolachlor in synthetic water mimicking agriculturally impacted surface waters containing nitrates ( $20 \text{ mg L}^{-1}$ ) and dissolved organic matter (DOM,  $5.4 \text{ mg C L}^{-1}$ ). Atrazine and *S*-metolachlor were quickly photodegraded by direct and indirect pathways (half-lives  $<5$  and  $<7$  days, respectively). DOM slowed down photodegradation while nitrates increased degradation rates. Transformation products analysis showed that oxidation mediated by hydroxyl radicals ( $\text{HO}\cdot$ ) predominate during indirect photodegradation. UV light (254 nm) caused significant C and N isotope fractionation, yielding enrichment factors  $\epsilon_{\text{C}} = 2.7 \pm 0.3$  and  $0.8 \pm 0.1\text{‰}$  and  $\epsilon_{\text{N}} = 2.4 \pm 0.3$  and  $-2.6 \pm 0.7\text{‰}$  for atrazine and *S*-metolachlor respectively. In contrast, photodegradation under simulated sunlight led to negligible C and slight N isotope fractionation. As the radiation wavelength influenced the direct photodegradation-induced isotope fractionation, the use of simulated sunlight is recommended to evaluate photodegradation pathways in the environment. Since C and N isotope fractionation patterns for atrazine and *S*-metolachlor photodegradation differed from those reported for biodegradation and hydrolysis, CSIA offers new opportunities to distinguish between photodegradation and other dissipation pathways in surface waters.

---

This chapter is an edited version of: Drouin, G., Droz, B., Leresche F., Payraudeau, S., Masbou, J. & Imfeld, G. Direct and indirect photodegradation of atrazine and *S*-metolachlor in agriculturally impacted surface water and associated C and N isotope fractionation submitted in *Env. Sci. & Tech.*

G. D & B.D. contribute at all stages of this chapter.

## **Introduction**

The ever-increasing use of pesticides, mainly for agricultural purposes, has led to ubiquitous contamination of surface waters,<sup>1</sup> which may affect environmental biodiversity and human health.<sup>2</sup> Understanding pesticide transformation in surface waters is thus crucial for predicting their persistence, the formation of transformation products (TPs) and mitigating detrimental effects of further pollution. While biodegradation is an important process of pesticide degradation in the environment, photodegradation also plays a prominent role in surface waters.<sup>3</sup> Pesticide photodegradation is compound- and condition-specific, which often limits the interpretation of photodegradation kinetics and pathways in various types of surface water.<sup>4,5</sup> In particular, the influence of the hydrochemical composition, the nature of dissolved organic matter (DOM) as well as the light spectrum on pesticide photodegradation remains poorly understood.<sup>6</sup>

Pesticides undergo photodegradation by direct and indirect pathways. During direct photodegradation, pesticide molecules absorb light resulting in bond cleavage. Indirect photodegradation involves reactions with short-lived reactive intermediates, such as hydroxyl radical (HO•) or DOM excited triplet states (<sup>3</sup>DOM\*<sup>7</sup>). Nitrate photolysis produces HO• that can react with pesticides in surface waters, even at nitrate concentrations as low as 0.02 mg L<sup>-1</sup>.<sup>5</sup> DOM has both inhibitory and/or photosensitizing effects, depending on its concentration and composition.<sup>8</sup> On the one hand, DOM absorbs light, reducing direct photodegradation of pesticides and HO• generation from nitrate photolysis. On the other hand, upon absorbing light, DOM generates <sup>3</sup>DOM\* that is the precursor of <sup>1</sup>O<sub>2</sub> in surface waters. Both <sup>3</sup>DOM\* and <sup>1</sup>O<sub>2</sub> can react with pesticides. DOM is also a major sink of HO• in surface waters, reducing HO• reactions with pesticides. DOM can also reduce pesticide oxidation intermediates back to the parent compounds, and limit pesticide photodegradation.<sup>9</sup> The effects of DOM on pesticide photodegradation are, however, compound-specific and involve mostly unknown mechanisms.<sup>10</sup> While the combined effect of nitrates and DOM on pesticide photodegradation is relevant for surface waters in agricultural areas, few studies on the subject have been carried out to date.<sup>4,11</sup>

The ability of compound-specific isotope analysis (CSIA) to specifically evaluate micropollutant degradation, including pesticides and pharmaceuticals, has already been exploited in diverse environmental compartments.<sup>12</sup> Pollutant molecules displaying different ratios of light over heavy isotopes are degraded at slightly different rates, resulting in a kinetic isotope effect (KIE) quantifiable by CSIA.<sup>13</sup> However, dilution processes, such as transport or sorption, generally do not alter stable isotope ratios (e.g., <sup>2</sup>H/<sup>1</sup>H, <sup>13</sup>C/<sup>12</sup>C, and <sup>15</sup>N/<sup>14</sup>N) within pollutant molecules.<sup>14</sup> As the KIE reflects the rate-limiting step of the involved pathway, each degradation pathway displays a specific isotope fractionation patterns, which may allow to differentiate co-occurring degradation processes in the environment. For example, CSIA was used to distinguish the contribution of direct photodegradation from other processes, including

biodegradation, abiotic oxidation and dilution, affecting the dissipation of the pharmaceutical diclofenac in riverine systems.<sup>15</sup> Although CSIA has been recently applied to characterize pesticide degradation in the environment,<sup>16</sup> little is known about stable isotope fractionation of pesticides during direct and indirect photodegradation in surface waters.

To the best of our knowledge, only Hartenbach et al.<sup>17</sup> have evaluated isotope fractionation for direct and indirect photodegradation of atrazine under specific conditions of irradiation and water chemistry. However, isotope fractionation may depend on the irradiation source and the DOM nature. Negligible fractionation in <sup>13</sup>C of the antibiotic sulfamethoxazole was observed in experiments with UV-C light, while significant isotopic enrichment factor ( $\epsilon_C = -4.8 \pm 0.1\%$ ) was observed when UV-B and UV-A prevailed.<sup>18</sup> Slight C isotopic enrichment factor ( $\epsilon_C = -0.7 \pm 0.2\%$ ) has also been observed during direct photodegradation of diclofenac under sunlight.<sup>15</sup> Differences in <sup>13</sup>C vs <sup>15</sup>N fractionation trends suggest distinct pathways associated with photodegradation of the nitrile herbicide bromoxynil when irradiated either with a UV lamp or exposed to sunlight under environmental conditions.<sup>19</sup> Isotopic enrichment factor may also depend on the nature of DOM and its propensity to favor HO• and <sup>3</sup>DOM\* short-lived reactive intermediates oxidation, as observed for methyl *tert*-butyl ether and ethyl *tert*-butyl ether.<sup>20</sup> Although these results emphasize the potential of CSIA to evaluate photodegradation in laboratory and in natural systems, isotopic enrichment factor to characterize pesticide photodegradation in agriculturally impacted surface waters are currently missing.

In this context, the purpose of this study was to examine typical patterns of photodegradation and associated isotopic enrichment factor for atrazine and *S*-metolachlor in agriculturally impacted surface waters. We irradiated atrazine and *S*-metolachlor with a simulated sunlight ( $\lambda$  from 270 to 720 nm) under hydrochemical conditions representative of agriculturally impacted surface waters (DOM = 5.4 mg C L<sup>-1</sup>; NO<sub>3</sub><sup>-</sup> = 20 mg L<sup>-1</sup>). We hypothesized that the hydrochemical composition of surface waters differently affect pesticide photodegradation and associated isotopic fractionation through direct and indirect pathways. In particular irradiation of nitrates and DOM may lead to the formation of short-lived reactive intermediates controlling underlying photodegradation pathways. Direct and indirect photodegradation of pesticides were thus tested, separately and concomitantly, in the presence of nitrates and DOM. C and N isotopic enrichment factor were derived for direct and indirect photodegradation of atrazine and *S*-metolachlor. Complementary experiments were conducted with an ultraviolet (UV) light ( $\lambda = 254$  nm) to evaluate the influence of irradiation wavelength on C and N isotopic fractionation during pesticide photodegradation.

## **Materials and methods**

### **Chemicals and preparation of solutions**

All chemicals were at least HPLC grade (>97%) (detailed in Appendix A (AA)). Atrazine and *S*-metolachlor (Pestanal, >99.9%) stock solutions were individually prepared at 5 g L<sup>-1</sup> in dichloromethane (DCM) and aliquots were stored at -20°C in brown glass vials. Before irradiation, pesticide stock solutions were spiked and stirred for one hour, until complete DCM volatilization. Suwannee River Fulvic Acid (SRFA - 2S101F) was obtained from the International Humic Substances Society (IHSS) and selected as a source of DOM representative of headwater rivers.<sup>20</sup> Stock solutions of SRFA were prepared at a concentration of 50 mg L<sup>-1</sup> by dissolving 10 mg of SRFA in 100 mL of ultrapure water (UW; Resistivity >15MΩ, dissolved organic matter (DOM; <0.2 mg C L<sup>-1</sup>), followed by 15 min sonication (Branson 5510, 40 kHz). The solutions were filtered through sterile 0.22 μm pore diameter cellulose acetate membranes and stored at 4°C in brown glass vials. The synthetic surface water was prepared to target the ionic composition of typical soft surface waters.<sup>21</sup>

### **Experimental section**

Atrazine and *S*-metolachlor were selected as representatives of widely used and ubiquitously detected triazine and chloroacetanilide pesticides,<sup>1</sup> and based on existing degradation rates (Table 2.1). Direct photolysis experiments were carried out independently for atrazine and *S*-metolachlor in UW with a 50 mM phosphate buffer (KH<sub>2</sub>PO<sub>4</sub>/Na<sub>2</sub>HPO<sub>4</sub>) at *pH* = 7.9 ± 0.2, as it has no significant effects on photodegradation rates and isotope fractionation.<sup>22</sup> The effect of nitrates on pesticide photodegradation was investigated in buffered synthetic water by adding 331 ± 2 μM of sodium nitrate salts (NO<sub>3</sub><sup>-</sup> = 20 mg L<sup>-1</sup>), considered as representative of agriculturally impacted surface waters in Europe.<sup>23</sup> The effect of DOM was studied by adding 5.4 ± 0.2 mg C L<sup>-1</sup> of SRFA considered as a representative concentration of rivers worldwide.<sup>24</sup> The concomitant effect of nitrates and DOM was investigated in synthetic water, spiked with sodium nitrates, SRFA and atrazine(5 μM) or *S*-metolachlor (3 μM) (AA, Table A1). DIR254 refers to direct photodegradation experiments conducted with a low-pressure mercury lamp (LP Hg; Philips, TUV 6W G6T5 – λ = 254 nm). DIR, NIT, SRFA, and TOT stand for irradiation conditions under simulated sunlight to test direct photodegradation (DIR), the effect of nitrates (NIT), dissolved organic matter (SRFA), and the combined effect of nitrates and dissolved organic matter (TOT), respectively.

Experiments were conducted in a 500 mL quartz tube (5 cm diam.) beyond 90% degradation of atrazine and S-metolachlor, with an irradiation duration from 7 to 600 hours. Aliquots from 15 to 200 mL were sequentially collected during the experiments. No significant degradation (<5%) in sterile and dark controls for all experimental conditions indicated insignificant hydrolysis and biodegradation during the photodegradation experiments. Photo-bleaching of DOM by HO• only slightly decreased the initial DOM content (<18%) after more than 310 h of irradiation (AA, Figure A1). Irradiation conditions in experiments with DOM were thus assumed constant.

Direct and indirect irradiations were carried out under simulated sunlight with a stand-alone lighting system (Sutter Instrument® - Lambda LS) fitted with a 300 W xenon (Xe) arc lamp (Cermax® - PE300BUV). A liquid optic fibre transmitted the light to a quartz tube covered with an aluminium foil, with a cut-off of ultra-violet (UV) radiations below  $\lambda = 270\text{nm}$ . The light spectrum obtained through the quartz tube, characterized with a calibrated spectroradiometer ILT 900C (International Light®), was in the range 270 to 720 nm. The mean photon fluence rate was estimated to be  $7 \mu\text{E m}^{-2} \text{s}^{-1}$  in the 290 to 400 nm range using a *p*-nitroanisole (PNA; 30  $\mu\text{M}$ )/pyridine (10 mM) actinometer system prepared as previously described.<sup>25</sup> Up to date values of quantum yields independent from wavelength for PNA,  $\theta_{PNA} = 3.19 \times 10^{-3} \text{ mol E}^{-1}$  were used (detailed in AA).<sup>26</sup> Due to long irradiation times, fluctuations of light intensity were monitored for the ranges UVA ( $320 < \lambda < 400 \text{ nm}$ ), UVB ( $280 < \lambda < 320 \text{ nm}$ ) and visible light (VIS,  $360 < \lambda < 830 \text{ nm}$ ) using a calibrated SOLAR® light PMA2200 radiometer. Xe arc lamps were systematically replaced when the total light intensity dropped or whenever shift in the UVA/UVB/VIS ratios exceeded 5% of the original value (AA, Table A2).

The effect of the irradiation wavelength on direct photodegradation of pesticides was examined using a light-proof box with black material equipped with the LP Hg lamp providing a monochromatic light source ( $\lambda = 254 \text{ nm}$ ). Open beakers in borosilicate type 3.3 were filled with 50 mL of buffered solution and spiked either with atrazine (90  $\mu\text{M}$ ) or S-metolachlor (70  $\mu\text{M}$ ). Beakers were placed into the light-proof box, irradiated on the top, and sequentially removed to determine pesticide degradation rates. Light intensity within the box was homogeneous ( $83 < I_{\text{average}} < 121\%$ ; AA, Figure A2). Control experiments without pesticides showed no cross-contamination. In this case photon fluence rate was not determined since these experiments were solely designed to evaluate the effect of the irradiation wavelength on atrazine and S-metolachlor isotope fractionation induced by photodegradation and not to derive degradation rates.

## **Analytical section**

**Pesticide extraction.** Solid phase extraction (SPE) of pesticides was carried out using SolEx C18 cartridges (1 g, Dionex®, CA, USA) and an AutoTrace 280 SPE system (Dionex®, CA, USA) as described elsewhere.<sup>27</sup> This procedure led to quantitative extraction ( $\eta \approx 100\%$ ) and did not result in significant C and N stable isotope fractionation for atrazine and S-metolachlor ( $|\Delta\delta^{13}\text{C}| = |\delta^{13}\text{C}_{EA-IRMS} - \delta^{13}\text{C}_{GC-IRMS}| = 0.6 \pm 0.2\text{‰}$  and  $|\Delta\delta^{15}\text{N}| = 0.3 \pm 0.2\text{‰}$ ).<sup>27</sup>

**Chemical analysis and pesticide quantification.** The ionic composition of irradiated solutions was determined by ion-chromatography (Dionex ICS-51000) for main anions and cations and by TOC analyzer (Shimadzu TOC-V CPH) for the carbon content in DOM. *pH* was measured using a 350i WTW *pH*-meter and a SenTix® electrode. Absorption spectra of pesticides, NIT and DOM solutions were measured using a UV-VIS Shimadzu UV 1700 spectrophotometer over the range 200 to 500 nm with a 1 nm resolution or taken from the literature whenever available (AA, Figure A3).

Atrazine and S-metolachlor were quantified in selected-ion-monitoring (SIM) mode by gas-chromatography (GC, Trace 1300, Thermo Fisher Scientific) coupled with a mass-spectrometer (MS, ISQ™, Thermo Fisher Scientific), as previously described elsewhere<sup>27</sup> and detailed in Appendix B. Atrazine and S-metolachlor TPs were identified by target screening using a liquid-chromatography coupled with a quadrupole time of flight high resolution mass spectrometer (LC/Q-TOF) following the methodology described elsewhere.<sup>28</sup> A suspected list of molecules used for screening of TPs was generated using a pathway prediction system and by reviewing the literature (AB, Table B6). When available, suspected molecules were confirmed by matching residence times using analytical standards. Otherwise, tentative candidates were assigned using a mass deviation criteria ( $\Delta m/z$ ) of 3 ppm.

**Analysis of C and N stable isotope composition of pesticides.** C and N stable isotope ratios ( $\delta^{13}\text{C}$  and  $\delta^{15}\text{N}$ ) of atrazine and S-metolachlor were measured using a GC-C-IRMS system consisting of a gas chromatograph (TRACE™ Ultra, ThermoFisher Scientific, Germany) coupled via a GC IsoLink/Conflow IV interface with an isotope ratio mass spectrometer (DeltaV Plus, ThermoFisher Scientific, Germany), and configured as described elsewhere and detailed in the AB.<sup>27</sup>

$\delta^{13}\text{C}$  and  $\delta^{15}\text{N}$  values were normalized by the Vienna Pee Dee Belemnite (VPDB) standard for carbon and by air for nitrogen as follows:

$$\delta^h X = 1000 \times \left( \frac{R_{\text{sample}}}{R_{\text{standard}}} - 1 \right) \quad (3.1)$$

where  $\delta^h X$  is expressed in per thousand (‰) and  $R$  refers to the ratio of heavy ( $h$ ) to light ( $l$ ) isotopes of the element  $X$  ( $\frac{h_X}{l_X}$ ) in the analyzed samples and the international standards. Samples were injected in triplicate and  $\delta^{13}C$  and  $\delta^{15}N$  values are reported as the associated arithmetic mean. Each measurement was checked to remain within the linearity ranges for C and N. A set of in-house BTEX (for C), caffeine (AIEA 600, for N) and pesticide (for C and N) standards with known isotopic composition (determined by EA-IRMS) was measured at least every ten injections to control the measurement quality. Reference  $\delta^{13}C$  and  $\delta^{15}N$  compositions of BTEX and pesticide standards were determined at our isotope facility using an elemental analyzer-isotopic ratio mass spectrometer (Flash EA IsoLink™ CN IRMS, Thermo Fisher Scientific, Bremen, Germany). An analytical uncertainty of  $1\sigma_{\delta^{13}C} \leq 0.5\text{‰}$  ( $n = 43$ ) and  $1\sigma_{\delta^{15}N} < 0.6\text{‰}$  ( $n = 72$ ) was attributed to each measurement, corresponding to the long term accuracy and reproducibility of pesticide standards measured across the analytical sessions.

## Data Analysis

Pesticide degradation followed the linearized pseudo-first order equation ( $R^2 > 0.82$ ,  $p < 0.05$ ,  $n > 5$ ). Degradation rates ( $k_{deg}$ ) were normalized by the mean irradiation intensity (AA, Table A2) according to eq. 3.2, allowing comparison among experiments. Degradation rates presented below refer to the normalized value,  $k_{eff}$ :

$$k_{eff} = \frac{I_{exp}}{I_{max}} \times k_{deg} \quad (3.2)$$

where  $I_{exp}$  and  $I_{max}$  stand for the light intensities measured during each experiment and the maximal inter-experiment value used as the reference for normalization.

The Rayleigh equation eq. 3.3 was used to relate pesticide degradation to changes in stable isotope ratios of the non-degraded fraction of atrazine and *S*-metolachlor. Bulk isotopic enrichment factors ( $\epsilon_{bulk}$ ) for C and N ( $\epsilon_C$  and  $\epsilon_N$ ) were derived from the linearized Rayleigh equation and was not forced through the origin.<sup>29</sup> Isotopic enrichment factors were only reported when the regression with the linearized Rayleigh equation was significant ( $p < 0.05$ ).

$$\frac{\delta^h X_t + 1000}{\delta^h X_0 + 1000} = \frac{X_t^{\epsilon_{bulk}}}{X_0} \quad (3.3)$$

$\delta^h X_0$  and  $\delta^h X_t$  are expressed in ‰ and refer to the initial and current isotope composition of atrazine or *S*-metolachlor (eq. 3.2), and  $\frac{X_t}{X_0}$  to the non-degraded fraction.



Correction of  $\varepsilon_{bulk}$  values accounting for repetitive sampling in batch experiments was deemed irrelevant here as it systematically fell within the regression confidence interval.<sup>30</sup>

In addition to  $\varepsilon_{bulk}$  values, dual element isotope plots of  $\delta^{15}N$  against  $\delta^{13}C$  values ( $A_{N/C}$ , eq. 3.4) were established to relate possible specific transformation pathways in the laboratory to photodegradation pathways in the environment.<sup>12, 31</sup>

$$A_{N/C} = \frac{\ln\left(\frac{\delta^{15}N + 1}{\delta^{15}N_0 + 1}\right)}{\ln\left(\frac{\delta^{13}C + 1}{\delta^{13}C_0 + 1}\right)} \approx \frac{\varepsilon_N}{\varepsilon_C} \quad (3.4)$$

All statistical analysis and regressions were performed in R version 3.6.3.<sup>32</sup> Data from linear regression (i.e.,  $k_{eff}$ ,  $\varepsilon_C$  and  $\varepsilon_N$ ) are reported with their confidence interval at level 95%

## Results and discussion

### Effects of the hydrochemistry on the photodegradation rates under simulated sunlight

Nitrates and DOM under simulated sunlight affected atrazine and S-metolachlor photodegradation rates. Direct observed photodegradation in UW (DIR) exhibited the quickest degradation rates for both pesticides with  $k_{ATZ, DIR} = (6.6 \pm 0.4) \times 10^{-6} \text{ s}^{-1}$  ( $DT_{50} = 29.0 \pm 1.7$  h) and  $k_{SMET, DIR} = (3.3 \pm 0.2) \times 10^{-6} \text{ s}^{-1}$  ( $DT_{50} = 58.8 \pm 3.2$  h). Although atrazine was slightly more sensitive to direct photodegradation than S-metolachlor, degradation rates were in the same order of magnitude as those previously reported.<sup>5, 11</sup> The strong light absorption of atrazine and S-metolachlor in the near UV range overlaps the Xe lamp radiation spectrum (<320 nm; AA, Figure A3) and explains their high reactivity. The simulated sunlight spectrum is provided in the AA, Figure A4.

In contrast, the addition of 5.4 mg C L<sup>-1</sup> of DOM, with or without 20 mg L<sup>-1</sup> of nitrates, decreased by 4.1 and 3.0 times the photodegradation rates of atrazine and S-metolachlor, respectively, compared to the UW experiments. This supports the idea that SRFA decreases atrazine and S-metolachlor photodegradation in surface waters with typical DOM contents. However, photodegradation rates in experiments with nitrates only were similar to rates in direct photodegradation experiments ( $\frac{k_{ATZ, NIT}}{k_{ATZ, DIR}} = 0.8$  and  $\frac{k_{SMET, NIT}}{k_{SMET, DIR}} = 1.0$ ). Addition of nitrates to the SRFA solution enhanced the reaction rates ( $\frac{k_{ATZ, TOT}}{k_{ATZ, SRFA}} = 2.1$  and  $\frac{k_{SMET, TOT}}{k_{SMET, SRFA}} = 1.2$ ), highlighting oxidation of atrazine and S-metolachlor with HO• originating from nitrate irradiation. DOM and nitrates in surface waters thus display similar photosensitizing or inhibitory effects on atrazine and S-metolachlor photodegradation. Similar effects can be

explained by absorption spectra of atrazine and *S*-metolachlor in the near UV range, and similar one-electron oxidation potentials ( $E1_{S\text{-metolachlor}} = -2.40$  V vs NHE and  $E1_{\text{atrazine}} = -2.41$  V vs NHE). One-electron oxidation potentials are often used as a reliable indicator of the potential of organic contaminants to react with  ${}^3\text{DOM}^*$  and  $\text{HO}\cdot$ .<sup>8, 10, 33</sup>

The contributions of direct and indirect pathways to photodegradation were inferred from photochemical predictions using eq. 3.5 (Figure 3.1). This equation decomposes observed degradation rates as the sum of contributions of direct and indirect photodegradation pathways (i.e.,  $\text{HO}\cdot$  and  ${}^3\text{DOM}^*$  mediated).<sup>5, 34, 35</sup> Carbonate radicals ( $\text{CO}_3\cdot^-$ ) were not included as potential relevant photosensitizers because oxidation of atrazine and anilines with  $\text{CO}_3\cdot^-$  under simulated sunlight remains limited, even in carbonate-rich surface waters ( $[\text{HCO}_3^-]$  and  $[\text{CO}_3^{2-}] \approx 10$  times higher than in our conditions).<sup>36</sup> Carbonates were, however, considered as potential quenchers of  $\text{HO}\cdot$ .<sup>5</sup> The calculation procedure and required parameters from the literature are summarized in AA, Table A3:

$$\begin{aligned} \frac{dC}{dt} &= -k_{obs} \times C \\ &= -\left(k_{dir} + k_{\text{HO}\cdot} \times [\text{HO}\cdot]_{ss} + k_{{}^3\text{DOM}^*} \times [{}^3\text{DOM}^*]_{ss} + k_{{}^1\text{O}_2} \times [{}^1\text{O}_2] \right) \times C \end{aligned} \quad (3.5)$$

$C$  stands for pesticide concentration, and  $k_{obs}$  the observed degradation rate ( $\text{s}^{-1}$ ), which can be expressed as the sum of direct ( $k_{dir}$ ) and selected indirect processes ( $k_{\text{HO}\cdot}$ ,  $k_{{}^3\text{DOM}^*}$  and  $k_{{}^1\text{O}_2}$ ). The latter degradation rates are second order and depend on the steady state concentrations of the short-lived reactive intermediates ( $[\text{HO}\cdot]_{ss}$ ,  $[{}^1\text{O}_2]_{ss}$  and  $[{}^3\text{DOM}^*]_{ss}$ ).

Observed and predicted degradation rates were consistent, suggesting that dominant photodegradation pathways could be identified in all experiments (Figure 3.1; Table A4). Nitrate-mediated photodegradation contributed to 60% of atrazine and 90% of *S*-metolachlor photodegradation in TOT conditions and is thus expected to dominate in agriculturally impacted surface waters. Although competing for UV light and limiting direct photodegradation, SRFA favored indirect photodegradation with  ${}^3\text{DOM}^*$  and  $\text{HO}\cdot$ . Accordingly, atrazine was slightly more sensitive than *S*-metolachlor to oxidation by  ${}^3\text{DOM}^*$ , whereas  $\text{HO}\cdot$  mostly affected *S*-metolachlor. Nitrate mediated photodegradation was, however, partly hampered in the TOT experiment as compared with the NIT experiment. Indeed, DOM at  $5.4 \text{ mg C L}^{-1}$  not only competes for light irradiance with nitrates but also quenches  $\text{HO}\cdot$ , reducing the photosensitizing effect of nitrates as observed in the NIT condition.<sup>8, 37</sup> Direct photodegradation contributed less in SRFA than in DIR experiments because UV light absorption by DOM limited direct photodegradation. Consequently, direct photodegradation rates were 10 to 30 times slower in SRFA than in DIR experiments for atrazine and *S*-metolachlor. Finally,  ${}^1\text{O}_2$  stemming from reactions between dissolved oxygen and  ${}^3\text{DOM}^*$  contributed to less than 2% for atrazine and 4% for *S*-metolachlor of observed degradation

rates. In aqueous solution, water immediately scavenges most of the produced  $^1\text{O}_2$ , limiting its reaction with pesticides.<sup>35</sup>

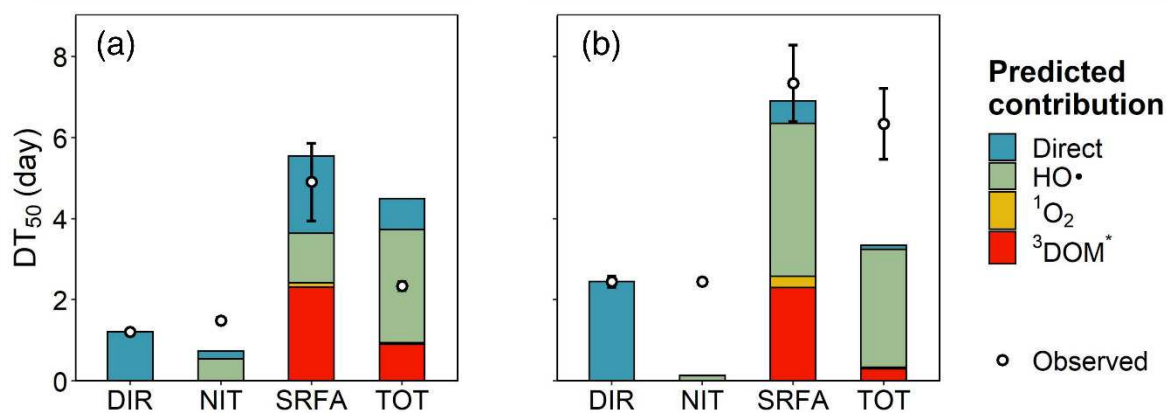


Figure 3.1. Observed and predicted half-lives of (a) atrazine and (b) S-metolachlor under simulated sunlight. Predicted contributions of direct and indirect pathways ( $\text{HO}\cdot$ ,  $^1\text{O}_2$  and  $^3\text{DOM}^*$ ) to the total pesticide photodegradation is displayed within the stacked bars. Photolysis condition: DIR: direct photodegradation, NIT: effect of nitrates, SRFA: effect of DOM and TOT: combined effects of nitrates and DOM. Half-life values were calculated from degradation rates according to  $DT_{50} = \frac{\ln(2)}{k}$ . Error bars correspond to the 95% confidence interval.

While direct and nitrate mediated photodegradation have strong potentials to transform atrazine and S-metolachlor in agriculturally impacted surface waters, DOM greatly reduces their potential by competing for UV light with pesticides and nitrates. By consequence, pesticides with the strongest light absorption spectrum in the near UV, such as atrazine, are less impacted. However, nitrates with concentrations about  $20 \text{ mg L}^{-1}$  would partly compensate for UV light competition caused by DOM by promoting  $\text{HO}\cdot$  oxidation. As discussed below, specific patterns of TPs formation and stable isotope fractionation further confirmed the predominance of nitrate- and DOM-mediated indirect pathways in NIT, SRFA and TOT experiments.

### Formation of phototransformation products

Ts were analyzed in samples displaying similar extent of degradation ( $\approx 80\%$ ). Atrazine irradiation led to desethylatrazine (DEA) and desisopropylatrazine (DIA) in all experiments, whereas 2-hydroxyatrazine (A-OH) was specific to direct photodegradation (Figure 1.3a)<sup>38</sup> or produced by biotic hydrolysis.<sup>39</sup> Indirect photolysis may proceed through atrazine oxidation at the *N*-ethyl and *N*-isopropyl group by  $^3\text{DOM}^*$  and  $\text{HO}\cdot$ .<sup>38</sup> Non-selective attacks of  $\text{HO}\cdot$  on the *N*-ethyl and *N*-isopropyl groups might thermodynamically favor the formation of DEA since weaker N–C bond dissociation energy is associated to the *N*-ethyl group.<sup>40</sup> A steric effect is also expected to favor the formation of DEA as the isopropyl group is less reactive than the ethyl group.<sup>41</sup> On the other hand, the intermediate formed during the hydrogen abstraction by  $\text{HO}\cdot$  would electronically favor DIA formation due to the weaker C–H bond, and weaker intermediate stabilization by the isopropyl group than by the ethyl group.<sup>42</sup>

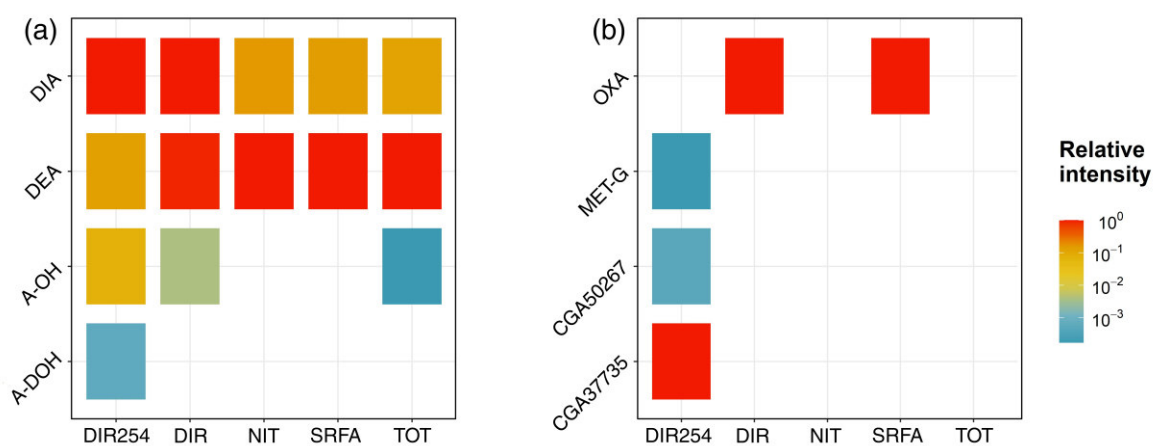


Figure 3.2. Transformation products for (a) atrazine and (b) S-metolachlor in photolysis experiment. Relative intensity refers to the peak amplitude of transformation product normalized by the intensity of the dominant transformation product peak for each sample. Photolysis condition are: DIR254: direct photodegradation at 254 nm, DIR: direct photodegradation under simulated sunlight, NIT: effect of nitrates, SRFA: the effect of DOM, and TOT: concomitant effects of nitrates and DOM together. TPs are: DIA: desisopropyl atrazine, DEA: desethyl atrazine, A-OH: hydroxyl atrazine and A-DOH: desethyl 2 hydroxy atrazine, OXA: metolachlor oxalinic acid, MET-G: 1-(1-methoxypropan-2-yl)-5,9-dimethyl-1,5-dihydro-4,1-benzoxazepin-2(3H)-one found by Lui *et al.*,<sup>43</sup> CGA37735: metolachlor CGA 37735 and CGA50267: metolachlor CGA 50267.

Four TPs of *S*-metolachlor were identified (Figure 3.2b). Hydroxymetolachlor was observed in neither DIR254 nor DIR, although it was reported in previous studies<sup>11, 44, 45</sup> as the major TP formed during direct photodegradation of (*S*-)metolachlor. We postulate that after 80% degradation of *S*-metolachlor, hydroxymetolachlor was further degraded into secondary TPs. In the SRFA and DIR experiments, only metolachlor oxalinic acid (OXA) was observed, whereas in NIT and TOT experiments, no TPs were detected. This suggests that *S*-metolachlor was easily oxidized by <sup>3</sup>DOM\* and HO• into *S*-metolachlor OXA, its acidic form. In the presence of nitrates, the large and constant generation of nonselective HO• may favor fast *S*-metolachlor OXA degradation,<sup>11</sup> explaining the absence of detected TPs in NIT and TOT experiments. The absence of TPs in the NIT and TOT experiments also supports the idea that nitrates mainly contribute to *S*-metolachlor photodegradation, even with 5.4 mg C L<sup>-1</sup> of DOM.

It is also worth noting that the number of detected TPs was maximum for both compounds during irradiations at  $\lambda = 254$  nm in DIR254 experiments (Figure 3.2b). In the case of *S*-metolachlor, metolachlor CGA 37735, metolachlor CGA 50267 and MET-G<sup>43</sup> were specific suspected TPs in DIR254 experiments, although only Metolachlor CGA 37735 could be confirmed with analytical standards (Appendix B, Table B6). This suggests that the spectrum of degradation pathways associated with monochromatic UV light is wider than that with simulated sunlight, and/or that the specific TPs result from further degradation of the first generation of TPs.

Altogether, patterns of TPs formation slightly differed between direct and indirect photodegradation. While the dechlorinated compound A-OH feature direct photodegradation for atrazine, oxidized compounds (e.g., atrazine DEA and DIA and *S*-metolachlor OXA) are likely to predominate in agriculturally impacted surface waters. TPs are likely transient and rapidly degraded into secondary and unidentified TPs, as shown during *S*-metolachlor photodegradation. Nonetheless, TPs patterns were identical for atrazine in NIT and SRFA experiments, although <sup>3</sup>DOM\* oxidation was predicted to prevail over HO•. Similarly, indirect photodegradation of *S*-metolachlor did not generate specific patterns of TPs. Interestingly, *S*-metolachlor ESA was not detected. Since *S*-metolachlor ESA is frequently measured in the environment and is neither a transformation product associated with hydrolysis<sup>27</sup> nor photodegradation, its detection might indicate *S*-metolachlor biodegradation.

### **C and N isotope fractionation to trace atrazine and S-metolachlor photodegradation**

Direct photolysis of atrazine in the DIR254 experiment with a low-pressure mercury lamp caused inverse isotope fractionation for both C and N ( $\Delta_{N/C} = 0.9 \pm 0.1$ ; Table 3.1), in agreement with previous results from Hartenbach et al.<sup>17</sup> ( $\Delta_{N/C} = 1.05 \pm 0.14$ ). In contrast, S-metolachlor featured a less pronounced and inverse C fractionation and stronger N fractionation ( $\Delta_{N/C} = -3.2 \pm 1.0$ ).

An inverse C fractionation in the DIR254 with atrazine was explained by the generation of a singlet state radical stabilized by the ring delocalization. Then the singlet undergo through singlet to triplet state and hydrolyze to form the A-OH. As the likelihood to recombine back to their original state is higher for the light carbon isotope in the C–Cl bond, inverse C fractionation is observed.<sup>17, 19</sup> The observation of the inverse N isotope fractionation has been suggested to follow the same mechanism. However, for S-metolachlor the reactive site is too far from the ring and is a priori inconsistent with a nucleophilic substitution of the chlorine atom by a hydroxyl group at the C–Cl bond expected for the formation of the TPs MET-OH. In contrast, the inverse C fractionation cannot be explained by the cleavage of the C–N bond at the N-ethyl or N-isopropyl group. Indeed, a cleavage at the N-ethyl or N-isopropyl group leading to DEA and DIA should reflect a normal primary isotopic effect.<sup>13</sup> In addition, two non-exclusive hypotheses may explain the isotopic patterns obtained in DIR254 experiments. First, successive steps of intersystem crossing before atrazine dechlorination can lead to inverse fractionation during direct photolysis of atrazine.<sup>17</sup> Second, a magnetic mass-independent isotope effect (MIE) involving spin carrying nuclei and unpaired electrons may cause an inverse isotope fractionation.<sup>22, 46</sup>

In contrast, direct photodegradation under simulated sunlight (DIR experiment) was characterized by non-significant C and N isotope fractionation for both pesticides (Table 3.1). Together with preliminary evidence from diclofenac photolysis,<sup>15</sup> our results suggest that C isotope fractionation associated with direct photodegradation under simulated sunlight of organic micropollutants remains limited.

Most importantly, our results indicate that photo-induced C and N isotope fractionation depends on the irradiation wavelength. Similar results have been reported by Willach et al.<sup>18</sup> for the antibiotic sulfamethoxazole under broad and cut off light spectrums. Instead of generating a single-band UV light as with the Hg lamp ( $\lambda = 254$  nm), the Xe lamp emits light over a broad and continuous range of wavelengths and energies from the near UV ( $\lambda > 270$  nm) to the near infrared ( $\lambda < 600$  nm). Xe lamp emission may thus generate a miscellaneous population of excited triplet states, which affected photolytic dechlorination of 4-Cl-aniline and led to varying C and N isotope fractionation caused by a spin selective isotope effect.<sup>47</sup> Hence, the average isotope value of the residual fraction of atrazine and S-metolachlor may

indicate multiple and co-occurring underlying photodegradation reactions under simulated sunlight.

*Table 3.1. C and N isotope fractionation for atrazine and S-metolachlor ( $\Delta\delta^{13}\text{C}$  and  $\Delta\delta^{15}\text{N}$ ).*

pesticide	experiment (degradation extent in %)	$\Delta\delta^{13}\text{C}$ (‰)	$\Delta\delta^{15}\text{N}$ (‰)	$\epsilon_{\text{C}}$ (‰)	$\epsilon_{\text{N}}$ (‰)
atrazine	DIR 254 (99)	8.9	11.0	$+2.7 \pm 0.3$	$+2.4 \pm 0.3$
	DIR (90)	1.2	1.4	n.s.	n.s.
	NIT (99)	1.7	2.0	n.s.	$+0.7 \pm 0.3$
	SRFA (97)	0.6	2.1	n.c.	$+0.6 \pm 0.2$
	TOT (98)	1.0	4.8	$+0.1 \pm 0.1$	$+0.9 \pm 0.6$
S- metolachlor	DIR 254 (99)	2.6	-8.4	$+0.8 \pm 0.1$	$-2.6 \pm 0.7$
	DIR (80)	-2.0	-1.0	n.s.	n.s.
	NIT (98)	1.2	-3.4	n.s.	$-0.8 \pm 0.1$
	SRFA (94)	0.6	-2.3	n.c.	$-0.7 \pm 0.4$
	TOT (94)	0.7	-1.9	n.c.	$-0.7 \pm 0.1$

$\Delta\delta$  values stand for the difference between initial and final stable isotope ratios. Isotopic enrichment factors ( $\epsilon$ ) are reported with their uncertainties corresponding to the 95% confidence interval from the regression analysis. n.s.: not significant ( $p>0.05$ ). n.c.: not computed. Rayleigh plots are presented in AA, Figure A5 & Figure A6.

In the case of indirect photodegradation with simulated sunlight, insignificant C and significant N isotope fractionations for both pesticides were systematically observed in NIT and TOT experiments with nitrates. Inverse and normal N fractionations were observed for atrazine and S-metolachlor, respectively ( $\frac{\epsilon_{\text{N}}^{\text{TOT}}}{\epsilon_{\text{N}}^{\text{NIT}}} = 1.3 \pm 0.5$  for atrazine and  $\frac{\epsilon_{\text{N}}^{\text{TOT}}}{\epsilon_{\text{N}}^{\text{NIT}}} = 0.9 \pm 0.2$  for S-metolachlor). Similar N isotope fractionation in NIT and TOT experiments further confirms the predominance of nitrate-mediated photodegradation in agriculturally impacted surface waters, even in the presence of  $5.4 \text{ mg C L}^{-1}$  of DOM. Accordingly,  $\epsilon_{\text{N}}$  values for atrazine and S-metolachlor in the NIT experiments represent reference values, specific for HO• oxidation in the presence of nitrates.

In the SRFA experiments, where  $^3\text{DOM}^*$  oxidation presumably drove indirect photodegradation along with HO•, only N isotope fractionation was observed for both pesticides ( $\epsilon_{\text{N}} = 0.6 \pm 0.2\text{‰}$  for atrazine and  $\epsilon_{\text{N}} = -0.7 \pm 0.4\text{‰}$  for S-metolachlor). Low N fractionation through  $^3\text{DOM}^*$  oxidation is consistent with the absence of C–N bond cleavage during S-metolachlor dechlorination leading to OXA. In addition, similar N fractionation in NIT and SRFA experiments ( $\frac{\epsilon_{\text{N}}^{\text{SRFA}}}{\epsilon_{\text{N}}^{\text{NIT}}} = 0.9 \pm 0.5$ ) confirms the predicted significant contribution of HO• generated by DOM irradiation (HO• = 54% and  $^3\text{DOM}^* = 33\%$ ). A similar conclusion

can be drawn for atrazine as  $\frac{\epsilon_N^{SRFA}}{\epsilon_N^{NIT}} = 0.9 \pm 0.5$ . The inverse N fractionation observed also agrees with oxidation by  $^3\text{DOM}^*$  at the *N*-ethyl or *N*-isopropyl side chain leading to either DEA or DIA proceeding through single electron transfer.<sup>20, 48</sup> Accordingly, inverse C fractionation should also have been observed, which was not the case. The large collection of chromophores occurring in natural DOM (i.e., SRFA) can be promoted to their singlet or triplet states under simulated sunlight, thereby providing a wide range of excited state reduction potentials, enabling oxidation at bonds involving irrespectively heavy and light isotopes.<sup>9</sup> This could be confirmed experimentally using  $\text{Cs}^+$  as a quencher of excited singlet states to enhance the contribution of excited triplet states and by evaluating the corresponding decrease of  $\epsilon_C$  and  $\epsilon_N$  values, as previously shown for 2-Cl-anilines.<sup>47</sup>

## **Environmental Implications**

Depending on hydrochemistry and the targeted pesticides, photodegradation can contribute to pesticide degradation to a similar or greater extent than biodegradation<sup>3</sup> in static surface waters (e.g., ponds, lakes, etc.) and rivers with long transit time.<sup>49</sup> Direct photodegradation of atrazine and *S*-metolachlor was particularly fast, and was slowed down due to UV light absorption caused by DOM. However, nitrate concentrations higher than 20 mg L<sup>-1</sup> can significantly enhance oxidation with HO• and level off the photodegradation inhibition caused by DOM in surface waters. Under simulated sunlight and environmentally-relevant hydrochemistry (*pH* = 8; 20 mg L<sup>-1</sup> of nitrates and 5.4 mg C L<sup>-1</sup> of DOM), half-lives of atrazine and *S*-metolachlor were as short as a few days ( $1 < DT_{50} < 10$  days). However, strong variations of solar irradiance in the UV region due to gaseous light absorption by ozone, altitude or geographic location or rapid absorption of UV lights in water, restrict our findings to shallow surface waters (i.e., <50 cm deep).<sup>50</sup> Altogether, this advocates for a more systematic account of local irradiation spectrum and hydrochemistry to estimate the contribution and half-lives of pesticide photodegradation.<sup>51</sup>

While CSIA offers a new opportunity to evaluate pesticide degradation in surface waters, identifying photodegradation pathways of micropollutants in the field remains challenging, as also confirmed by recent studies.<sup>15, 18</sup> Under simulated sunlight irradiation, C isotope composition of atrazine and *S*-metolachlor are likely not affected by photodegradation, although photodegradation can significantly contribute to the pesticide degradation. Accordingly, changes in C stable isotope ratios may almost exclusively reflect atrazine or *S*-metolachlor biodegradation. Indeed, biodegradation is typically characterized by significant isotope fractionation (e.g., biotic oxidative dealkylation of atrazine,  $\Delta_{N/C} = 0.35$ )<sup>52</sup> in contaminated surface waters with high nitrate and DOM concentrations, as illustrated by the N/C dual plot comparing isotopic enrichment factors determined in this study with others from



the literature (AA, Figure A7). However, an opposite and similar absolute  $\epsilon_N$  value for atrazine photodegradation and biodegradation would hamper a specific evaluation of photodegradation relying solely on changes of N isotope ratios. Since photodegradation pathways of atrazine and S-metolachlor mostly involve C–H and C–Cl bonds,<sup>15, 17</sup> multi-element isotope analysis (e.g., H, C, N and Cl) of pesticides by CSIA from environmental samples may help in the future to tease apart photodegradation pathways and evaluate their contribution among degradative processes. In contrast, abiotic hydrolysis is a slow process at *pH* of most surface waters (e.g., half-life value for alkaline abiotic hydrolysis of atrazine at *pH* = 9 and 20°C higher than 200 days),<sup>27</sup> and is thus unlikely to significantly contribute to pesticide degradation in surface waters.

Most importantly, the irradiation source strongly influences C and N fractionation patterns. Our results advocate for a more systematic use of simulated sunlight when characterizing photodegradation pathways using CSIA in laboratory experiments. In addition, the nature of DOM under different environmental contexts can affect the production of HO•, and thus alter changes of the stable isotope composition of pesticides.<sup>20, 45</sup> Although SRFA serves as a model DOM representative of headwater rivers,<sup>8</sup> site-specific studies should be deployed to address the specific role of DOM during pesticide photodegradation. Altogether, this study highlights the relevance of pesticide photodegradation in agriculturally impacted surface waters with nitrates and DOM.

## References

1. de Souza, R. M.; Seibert, D.; Quesada, H. B.; de Jesus Bassetti, F.; Fagundes-Klen, M. R.; Bergamasco, R., Occurrence, impacts and general aspects of pesticides in surface water: A review. *Process Saf. Environ. Prot.* **2020**, *135*, 22–37.
2. Stehle, S.; Schulz, R., Agricultural insecticides threaten surface waters at the global scale. *Proc. Natl. Acad. Sci. U.S.A.* **2015**, *112*, (18), 5750–5755.
3. Fenner, K.; Canonica, S.; Wackett, L. P.; Elsner, M., Evaluating pesticide degradation in the environment: Blind spots and emerging opportunities. *Science* **2013**, *341*, (6147), 752–758.
4. Remucal, C. K., The role of indirect photochemical degradation in the environmental fate of pesticides: A review. *Environ. Sci. Process. Impacts* **2014**, *16*, (4), 628–653.
5. Zeng, T.; Arnold, W. A., Pesticide photolysis in prairie potholes: Probing photosensitized processes. *Environ. Sci. Technol.* **2013**, *47*, (13), 6735–6745.

6. Celeiro, M.; Facorro, R.; Dagnac, T.; Vilar, V. J. P.; Llompert, M., Photodegradation of multiclass fungicides in the aquatic environment and determination by liquid chromatography-tandem mass spectrometry. *Environ. Sci. Pollut. Res.* **2017**, *24*, (23), 19181–19193.
7. Vione, D.; Minella, M.; Maurino, V.; Minero, C., Indirect photochemistry in sunlit surface waters: Photoinduced production of reactive transient species. *Chem. Eur. J.* **2014**, *20*, (34), 10590-10606.
8. Leresche, F.; von Gunten, U.; Canonica, S., Probing the photosensitizing and inhibitory effects of dissolved organic matter by using *N,N*-dimethyl-4-cyanoaniline (DMABN). *Environ. Sci. Technol.* **2016**, *50*, (20), 10997–11007.
9. Rosario-Ortiz, F. L.; Canonica, S., Probe compounds to assess the photochemical activity of dissolved organic matter. *Environ. Sci. Technol.* **2016**, *50*, (23), 12532–12547.
10. Karpuzcu, M. E.; McCabe, A. J.; Arnold, W. A., Phototransformation of pesticides in prairie potholes: Effect of dissolved organic matter in triplet-induced oxidation. *Environ. Sci. Process. Impacts* **2016**, *18*, (2), 237–245.
11. Dimou, A. D.; Sakkas, V. A.; Albanis, T. A., Metolachlor photodegradation study in aqueous media under natural and simulated solar irradiation. *J. Agric. Food. Chem.* **2005**, *53*, (3), 694–701.
12. Elsner, M.; Imfeld, G., Compound-specific isotope analysis (CSIA) of micropollutants in the environment — current developments and future challenges. *Curr. Opin. Biotechnol.* **2016**, *41*, 60–72.
13. Elsner, M.; Zwank, L.; Hunkeler, D.; Schwarzenbach, R. P., A new concept linking observable stable isotope fractionation to transformation pathways of organic pollutants. *Environ. Sci. Technol.* **2005**, *39*, (18), 6896–6916.
14. Thullner, M.; Centler, F.; Richnow, H. H.; Fischer, A., Quantification of organic pollutant degradation in contaminated aquifers using compound specific stable isotope analysis - Review of recent developments. *Org. Geochem.* **2012**, *42*, (12), 1440–1460.
15. Maier, M. P.; Prasse, C.; Pati, S. G.; Nitsche, S.; Li, Z.; Radke, M.; Meyer, A.; Hofstetter, T. B.; Ternes, T. A.; Elsner, M., Exploring trends of C and N isotope fractionation to trace transformation reactions of diclofenac in natural and engineered systems. *Environ. Sci. Technol.* **2016**, *50*, (20), 10933–10942.
16. Torabi, E.; Wiegert, C.; Guyot, B.; Vuilleumier, S.; Imfeld, G., Dissipation of S-metolachlor and butachlor in agricultural soils and responses of bacterial communities: Insights from compound-specific isotope and biomolecular analyses. *J. Environ. Sci.* **2020**, *92*, 163–175.
17. Hartenbach, A. E.; Hofstetter, T. B.; Tentscher, P. R.; Canonica, S.; Berg, M.; Schwarzenbach, R. P., Carbon, hydrogen, and nitrogen isotope fractionation during light-induced transformations of atrazine. *Environ. Sci. Technol.* **2008**, *42*, (21), 7751–7756.

18. Willach, S.; Lutze, H. V.; Eckey, K.; Löppenber, K.; Lüling, M.; Wolbert, J.-B.; Kujawinski, D. M.; Jochmann, M. A.; Karst, U.; Schmidt, T. C., Direct photolysis of sulfamethoxazole using various irradiation sources and wavelength ranges — insights from degradation product analysis and compound-specific stable isotope analysis. *Environ. Sci. Technol.* **2018**, *52*, (3), 1225–1233.
19. Knossow, N.; Siebner, H.; Bernstein, A., Isotope analysis method for the herbicide bromoxynil and its application to study photo-degradation processes. *J. Hazard. Mater.* **2020**, *388*, 122036.
20. Zhang, N.; Schindelka, J.; Herrmann, H.; George, C.; Rosell, M.; Herrero-Martín, S.; Klán, P.; Richnow, H. H., Investigation of humic substance photosensitized reactions via carbon and hydrogen isotope fractionation. *Environ. Sci. Technol.* **2015**, *49*, (1), 233–242.
21. Smith, E. J.; Davison, W.; Hamilton-Taylor, J., Methods for preparing synthetic freshwaters. *Water Res.* **2002**, *36*, (5), 1286–1296.
22. Ratti, M.; Canonica, S.; McNeill, K.; Erickson, P. R.; Bolotin, J.; Hofstetter, T. B., Isotope fractionation associated with the direct photolysis of 4-chloroaniline. *Environ. Sci. Technol.* **2015**, *49*, (7), 4263–4273.
23. European Environment Agency (EEA) *The European environment – state and outlook 2020 : Knowledge for transition to a sustainable Europe*; Copenhagen, DK, **2019**; p 499.
24. Raymond, P. A.; Spencer, R. G. M., Chapter 11 - Riverine DOM. In *Biogeochemistry of marine dissolved organic matter (Second edition)*, Hansell, D. A.; Carlson, C. A., Eds. Academic Press: Boston, US, **2015**; pp 509–533.
25. Dulin, D.; Mill, T., Development and evaluation of sunlight actinometers. *Environ. Sci. Technol.* **1982**, *16*, (11), 815–820.
26. Laszakovits, J. R.; Berg, S. M.; Anderson, B. G.; O'Brien, J. E.; Wammer, K. H.; Sharpless, C. M., *p*-nitroanisole/pyridine and *p*-nitroacetophenone/pyridine actinometers revisited: Quantum yield in comparison to ferrioxalate. *Environ. Sci. Technol. Lett.* **2017**, *4*, (1), 11–14.
27. Masbou, J.; Drouin, G.; Payraudeau, S.; Imfeld, G., Carbon and nitrogen stable isotope fractionation during abiotic hydrolysis of pesticides. *Chemosphere* **2018**, *213*, 368–376.
28. Villette, C.; Maurer, L.; Wanko, A.; Heintz, D., Xenobiotics metabolization in *Salix alba* leaves uncovered by mass spectrometry imaging. *Metabolomics* **2019**, *15*, (9), 122.
29. Scott, K. M.; Lu, X.; Cavanaugh, C. M.; Liu, J. S., Optimal methods for estimating kinetic isotope effects from different forms of the Rayleigh distillation equation. *Geochim. Cosmochim. Acta* **2004**, *68*, (3), 433–442.
30. Buchner, D.; Jin, B.; Ebert, K.; Rolle, M.; Elsner, M.; Haderlein, S. B., Experimental determination of isotope enrichment factors - bias from mass removal by repetitive sampling. *Environ. Sci. Technol.* **2017**, *51*, (3), 1527–1536.

31. Wijker, R. S.; Adamczyk, P.; Bolotin, J.; Paneth, P.; Hofstetter, T. B., Isotopic analysis of oxidative pollutant degradation pathways exhibiting large H isotope fractionation. *Environ. Sci. Technol.* **2013**, *47*, (23), 13459–13468.
32. R Core Team R: A language and environment for statistical computing. <http://www.R-project.org> (2018).
33. Arnold, W. A., One electron oxidation potential as a predictor of rate constants of N-containing compounds with carbonate radical and triplet excited state organic matter. *Environ. Sci. Process. Impacts* **2014**, *16*, (4), 832–838.
34. Bodrato, M.; Vione, D., APEX (Aqueous Photochemistry of Environmentally occurring Xenobiotics): a free software tool to predict the kinetics of photochemical processes in surface waters. *Environ. Sci. Process. Impacts* **2014**, *16*, (4), 732–740.
35. Janssen, E. M. L.; Erickson, P. R.; McNeill, K., Dual roles of dissolved organic matter as sensitizer and quencher in the photooxidation of tryptophan. *Environ. Sci. Technol.* **2014**, *48*, (9), 4916–4924.
36. Vione, D.; Maurino, V.; Minero, C.; Carlotti, M. E.; Chiron, S.; Barbati, S., Modelling the occurrence and reactivity of the carbonate radical in surface freshwater. *Comptes Rendus Chimie* **2009**, *12*, (8), 865–871.
37. Garbin, J. R.; Milori, D. M. B. P.; Simões, M. L.; da Silva, W. T. L.; Neto, L. M., Influence of humic substances on the photolysis of aqueous pesticide residues. *Chemosphere* **2007**, *66*, (9), 1692–1698.
38. Torrents, A.; Anderson, B. G.; Bilbouljian, S.; Johnson, W. E.; Hapeman, C. J., Atrazine photolysis: Mechanistic investigations of direct and nitrate mediated hydroxy radical processes and the influence of dissolved organic carbon from the Chesapeake Bay. *Environ. Sci. Technol.* **1997**, *31*, (5), 1476–1482.
39. Meyer, A. H.; Penning, H.; Elsner, M., C and N isotope fractionation suggests similar mechanisms of microbial atrazine transformation despite involvement of different enzymes (AtzA and TrzN). *Environ. Sci. Technol.* **2009**, *43*, (21), 8079–8085.
40. Vollhardt, K. P. C.; Schore, N. E., *Organic chemistry: Structure and function*. Freemann, W.H.: **1999**.
41. Smith, M. B.; March, J., *March's advanced organic chemistry: Reactions, mechanisms, and structure*. Sixth Edition. ed.; John Wiley & Sons: **2006**; p 2357.
42. Hapeman, C. J.; Karns, J. S.; Shelton, D. R., Total mineralization of aqueous atrazine in the presence of ammonium nitrate using ozone and *Klebsiella terrigena* (strain drs-i): mechanistic considerations for pilot scale disposal. *J. Agric. Food. Chem.* **1995**, *43*, (5), 1383–1391.
43. Liu, S. Y.; Freyer, A. J.; Bollag, J. M., Microbial dechlorination of the herbicide metolachlor. *J. Agric. Food. Chem.* **1991**, *39*, (3), 631–636.

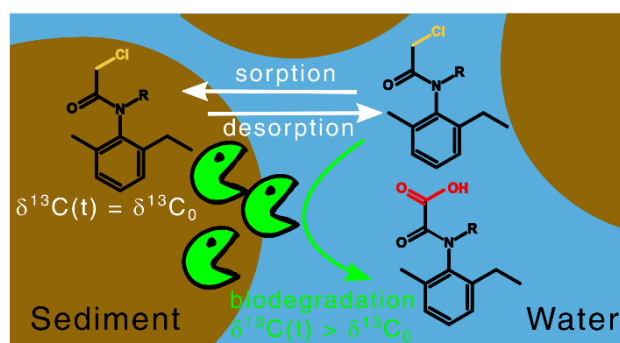
44. Gutowski, L.; Baginska, E.; Olsson, O.; Leder, C.; Kummerer, K., Assessing the environmental fate of S-metolachlor, its commercial product Mercantor Gold<sup>®</sup> and their photoproducts using a water-sediment test and in silico methods. *Chemosphere* **2015**, *138*, 847–855.
45. Gutowski, L.; Olsson, O.; Leder, C.; Kümmerer, K., A comparative assessment of the transformation products of S-metolachlor and its commercial product Mercantor Gold<sup>®</sup> and their fate in the aquatic environment by employing a combination of experimental and in silico methods. *Sci. Total Environ.* **2015**, *506-507*, 369–379.
46. Buchachenko, A. L., Mass-independent isotope effects. *J. Phys. Chem. B* **2013**, *117*, (8), 2231–2238.
47. Ratti, M.; Canonica, S.; McNeill, K.; Bolotin, J.; Hofstetter, T. B., Isotope fractionation associated with the photochemical dechlorination of chloroanilines. *Environ. Sci. Technol.* **2015**, *49*, (16), 9797–9806.
48. Meyer, A. H.; Dybala-Defratyka, A.; Alaimo, P. J.; Geronimo, I.; Sanchez, A. D.; Cramer, C. J.; Elsner, M., Cytochrome P450-catalyzed dealkylation of atrazine by *Rhodococcus* sp. strain N186/21 involves hydrogen atom transfer rather than single electron transfer. *Dalton Trans.* **2014**, *43*, (32), 12175–12186.
49. Fono, L. J.; Kolodziej, E. P.; Sedlak, D. L., Attenuation of wastewater-derived contaminants in an effluent-dominated river. *Environ. Sci. Technol.* **2006**, *40*, (23), 7257–7262.
50. Schwarzenbach, R. P.; Gschwend, P. M.; Imboden, D. M., *Environmental organic chemistry*. third ed.; John Wiley & Sons: **2016**, p.1024.
51. Apell, Jennifer N.; McNeill, K., Updated and validated solar irradiance reference spectra for estimating environmental photodegradation rates. *Environ. Sci. Process. Impacts* **2019**, *21*, (3), 427–437.
52. Meyer, A. H.; Elsner, M., <sup>13</sup>C/<sup>12</sup>C and <sup>15</sup>N/<sup>14</sup>N isotope analysis to characterize degradation of atrazine: Evidence from parent and daughter compound values. *Environ. Sci. Technol.* **2013**, *47*, (13), 6884–6891.

## Chapter 4

# Phase-transfer and biodegradation of acetochlor and S-metolachlor in water–sediment systems

### Abstract

Current approaches are limited in their ability to evaluate the contribution of pesticide dissipation processes in water–sediment systems since both degradation and phase-transfer, i.e., sorption-desorption, contribute to apparent decrease of pesticide concentration. Here the dissipation of widely used herbicides acetochlor and S-metolachlor was examined in laboratory water–sediment batch experiments under oxic and anoxic conditions. Degradation pathways were elucidated with compound-specific isotope analysis (CSIA), a phase-transfer model to evaluate biodegradation, and high-resolution tandem mass spectrometry (HR-MS/MS) to identify transformation products. Biodegradation half-life of acetochlor and S-metolachlor in water were slower under anoxic ( $DegT_{50,w} = 59 \pm 16$  and  $199 \pm 48$  days, respectively) than under oxic conditions ( $DegT_{50,w} = 31 \pm 17$  and  $29 \pm 8$  days). Carbon apparent kinetic isotope effects (AKIE<sub>c</sub>) ranged from  $1.018 \pm 0.001$  to  $1.075 \pm 0.008$ , suggesting degradation via nucleophilic substitution. Together with the predominance of the oxalinic acids transformation product, this suggests that the glutathione transferase pathway prevailed under both anoxic and oxic conditions in the water–sediment batch experiments. CSIA coupled with transformation product identification and an adapted phase-transfer model is a promising approach to interpret pesticide in water–sediment systems.



---

This chapter is an edited version of: Droz, B., Drouin, G., Maurer, L., Villette, C., Payraudeau, S. & Imfeld, G. Phase-transfer and biodegradation of acetochlor and S-metolachlor in water–sediment systems submitted in Env. Sci. & Tech.

## **Introduction**

Up to  $2.6 \times 10^6$  tons of pesticides are applied yearly on about 10% of the global land surface.<sup>1</sup> Off-site export of pesticides from agricultural or urbanized areas and potential persistence in surface waters are frequently observed.<sup>2</sup> Pesticides raise considerable toxicological concerns as they may impact surface waters and reduce the quality of drinking water supply.<sup>3, 4</sup> Pesticide biodegradation in surface waters is a prevailing degradative dissipation process at the water–sediment system.<sup>5</sup> Pesticide biodegradation in surface water occurs in the oxic water column and the anoxic sediment bed. Contrasted biogeochemical conditions in these two environments may favor distinct biodegradation pathways and kinetics.<sup>6, 7</sup> Pesticide biodegradation studies have focused mainly on oxic conditions and associated pathways,<sup>8</sup> whereas only few studies have examined biodegradation pathways under anoxic conditions in the water–sediment system.<sup>9</sup>

Pesticide dissipation processes in water–sediment systems include biodegradation, phase-transfer (i.e., adsorption–desorption) and transport (i.e., diffusion, advection). Pesticide biodegradation rates derived from laboratory experiments usually serve to predict the pesticide behavior in the environment.<sup>10</sup> However, concerns have been recently raised about the representativeness of study conditions, claiming that derived pesticide biodegradation rates may be biased when co-occurring dissipation processes are not considered.<sup>11, 12</sup> Recently, conceptual model to evaluate processes contributing to pesticide dissipation has been validated for a broad spectrum of compounds and study conditions.<sup>7, 13</sup> The model considers phase-transfer between the water phase with freely dissolved species, and the sediment phase including species sorbed on particles or dissolved organic carbon (DOC). However, knowledge of the contribution of pesticide biodegradation and phase-transfer to the overall pesticide dissipation in surface waters remains scarce, although this information is crucial for both sediment and water management.

As a direct evidence of degradation, high resolution tandem mass spectrometry (HR-MS/MS) allows identifying known and unknown transformation product (TPs) in water–sediment system to elucidate degradation pathways.<sup>14</sup> Complementarily, compound-specific isotope analysis (CSIA) may help teasing apart pesticide biodegradation from other dissipation processes and identifying degradation pathways. The degradation rate of pesticide molecules with light isotopes is slightly faster than that of pesticides with heavy isotopes at the reactive site, resulting in a kinetic isotope effect (KIE).<sup>15</sup> Within KIE, primary isotope effect results in larger isotope fractionation as it corresponds to degradative processes involving bond cleavage atoms. In addition, pesticide biodegradation pathway generally modifies their stable isotope signature in a systematic way, while the extent of isotope fractionation may indicate the underlying biodegradation pathway. In contrast, pesticide sorption is likely associated with minor isotope fractionation, even after successive sorption-desorption steps in water–sediment

systems.<sup>16</sup> The applicability of CSIA to evaluate pesticide dissipation in water–sediment systems, accounting for phase-transfer and biodegradation, still needs to be demonstrated.

Here, we examined pesticide dissipation in surface waters using laboratory water–sediment batch experiments. The widely used chloroacetanilide herbicides acetochlor and S-metolachlor, ranking twelve and eight among the top twenty worldwide sold pesticides,<sup>17</sup> were selected as representative pesticides in surface waters.<sup>18</sup> The purpose of this study was to examine degradation of acetochlor and S-metolachlor and associated pathways under contrasted oxic and anoxic conditions in relation to phase-transfer in water–sediment systems. CSIA, transformation product identification, and a simplified version of a phase-transfer model<sup>19</sup> were combined to improve interpretation of pesticide degradation in water–sediment systems.

## **Materials and methods**

The list of chemicals including suppliers and purities is provided in the Appendix B (AB). Five widely used or legacy pesticides (acetochlor, S-metolachlor, atrazine, terbutryn, and metalaxyl) were initially selected for the study (details on the mixture in AB). Results and discussion were, however, restricted to acetochlor and S-metolachlor since low concentrations or limited degradation in the water phase hampered CSIA measurements of atrazine, terbutryn, and metalaxyl. The pesticide mixture was prepared in a 5 g L<sup>-1</sup> stock solution in acetonitrile (ACN) and stored at –20°C. Experiments were carried out using a soft (<10 mg L<sup>-1</sup> of inorganic carbon) synthetic water<sup>20</sup> corresponding to an average surface waters content of DOC = 1.6 ± 0.2 mg L<sup>-1</sup>.<sup>21</sup> Synthetic water preparation and hydrochemical characteristics are provided in AB.

### **Sediment sampling and characteristics**

Sediment was collected (detailed in AB) in an experimental stormwater wetland located at the outlet of a vineyard catchment (Rouffach, France, 47°57'43" N, 7°17'26" E),<sup>22</sup> wet-sieved at 2 mm and stored wet at 4°C before the experiment and analysis. The sediment physico-chemical parameters were measured following standard analytical procedure (NF/ISO; detailed in AB). The sediment characteristics were as follows:  $pH_{H_2O} = 7.5 \pm 0.5$  ( $\bar{X} \pm SD$ ;  $n = 3$ ), cation exchange capacities ( $CEC$ )  $14.3 \pm 2.8$  cmol kg<sup>-1</sup>, residual humidity ( $RH$ , w/w)  $37 \pm 3\%$ , clay (<2 μm)  $21.2 \pm 2.5\%$ , silt (2 to 50 μm)  $67.4 \pm 2.5\%$ , sand (50 to 2000 μm)  $11.4 \pm 4.3\%$ , organic carbon ( $f_{oc}$ )  $2.3 \pm 2.1\%$  and mineral carbon ( $C_{min}$ )  $3.9 \pm 0.5\%$ . Sediment partitioning coefficients ( $K_d$ ) were determined under batch sorption experiments:<sup>23</sup>  $K_{d,acetochlor} = 5.8 \pm 2.3$



$\text{L kg}^{-1}$  and  $K_{d,S\text{-metolachlor}} = 6.6 \pm 1.7 \text{ L kg}^{-1}$ . Abiotic degradation associated with reactive solid phases<sup>24</sup> and/or with bisulfide<sup>25</sup> was assumed insignificant, since redox-reactive elements remained low in the sediment and the synthetic water (i.e., iron and manganese remained below  $1 \text{ mg g}^{-1}$  in both the water and the sediment phase; AB, Table B1).

## **Experimental set-up**

Two series of biodegradation batch experiments were set-up in duplicate under oxic and anoxic conditions to evaluate pesticide dissipation in the water–sediment system. The biodegradation experiment preparation followed the original<sup>26</sup> and the modified OECD 309 test<sup>7</sup> to ensure homogeneous redox conditions and an optimal balance between pesticide degradation and phase partitioning ( $K_d < 2000 \text{ L kg}^{-1}$ ). The sediment-water ratio was representing conditions in settled ponds or river bed systems.<sup>13</sup> Shaking was preferred over stirring to limit the impact of grain size change over time (AB, Table B1).<sup>7</sup>

Biodegradation batch experiments were prepared with 5 g equivalent dried mass of wet sediment in a 50 mL head-space glass vials. A filter-sterilized ( $0.2 \mu\text{m}$  cellulose acetate, CA) synthetic water was spiked with the pesticide mixture ( $5 \text{ g L}^{-1}$ ) stock solution in ACN to reach a final concentration of  $25 \text{ mg L}^{-1}$  of each pesticide. The solution was undersaturated with respect to the pesticide mixture, as calculated on phreeqc-v3.0 (USGS)<sup>27</sup> with stability constants from the MINQEL+ v4.6<sup>28</sup> thermodynamic database and solubility correction of each pesticide for ionic strength. The solution was stirred until complete ACN evaporation. The sediment was then mixed with the pesticide solution to reach a sediment-water ratio (w/w) of 1:6. All batch experiments were crimped with butyl/PTFE caps. Under oxic conditions, i.e., dissolved oxygen concentration between 6 to  $9 \text{ mg L}^{-1} \text{ O}_2$ , a  $0.2 \mu\text{m}$  PTFE syringe filter was mounted on a needle inserted through the vial cap to allow gas exchange in the vials while limiting water loss and avoiding microbial contamination.<sup>29</sup> Anoxic batch experiments were flushed with  $\text{N}_2$  (5.0) and vortexed three times to maintain a dissolved oxygen concentration below  $0.02 \text{ mg L}^{-1} \text{ O}_2$ .

The oxic and anoxic batch experiments were incubated in the dark at  $20 \pm 5 \text{ }^\circ\text{C}$  on an overhead shaker (80 rpm; reax-2, Heidolph). Kinetics of the degradation was investigated under a pseudo first-order kinetic condition. Batch experiments were sacrificed on days 2, 5, 15, 50, 80, 100, 150, 200, 250 and 300. At each sampling time, dissolved oxygen was measured with a fiber optic oxygen meter (SP-PSt3-YAU with a Fibox3, PreSens). *pH* was recorded with an electrode (*pH/cond* multi 350i, WTW) and remained constant across the experiments ( $7.6 \pm 0.4$ ). Cation-anion concentrations were analyzed from a water aliquot (detailed in AB). Water and sediment phases were collected for pesticide analysis.

Parallel duplicate batch experiments were sacrificed on days 0, 150 and 300 to measure dissolved organic/inorganic carbon (DOC/DIC), chemical oxygen demand (COD) and UV-Visible light absorbance (AB, Table B2). These experiments were prepared as the biodegradation batch experiments, but the water was filtered through a 0.45  $\mu\text{m}$  CA syringe filter only prior to the analysis.

### **Control experiments**

Abiotic controls were prepared and incubated as the biodegradation batch experiments but using sediment previously autoclaved twice at 24 h intervals (steam under 103 kPa at 125 °C for 20 min) to evaluate abiotic pesticide degradation during the experiment. Hydrolysis experiments were conducted in autoclaved synthetic water amended with a 50 mM phosphate buffer ( $\text{KH}_2\text{PO}_4/\text{Na}_2\text{HPO}_4$ ) at *pH* equal to 8. Blank experiments without pesticide spiking allowed to evaluate the initial background concentration of pesticides. Control and blank experiments were sacrificed on days 15, 50, 200 and 300. Abiotic controls confirmed insignificant pesticide dissipation at the end of the experiment (<10%; AB, Table B3). Insignificant pesticide dissipation in abiotic controls was associated with insignificant carbon isotope fractionation in water ( $|\Delta\delta^{13}\text{C}_{obs,w}| < |\Delta\delta^{13}\text{C}_{min,w}|$ , with  $|\Delta\delta^{13}\text{C}_{min,w}|$  the minimal change of isotope signature in water above which isotope fractionation can be attributed degradation (see below and AB, Table B5). The initial background concentration of pesticides in the sediment phase in blank controls was below the limit of detection (<0.1  $\mu\text{g L}^{-1}$ ). Biodegradation and sorption batch experiments for individual pesticides confirmed the absence of inhibitory or synergistic effects on pesticide degradation rate constants and partitioning coefficients (AB, Table B4).<sup>30</sup>

### **Pesticide extraction and quantification**

Water and sediment phases were separated by centrifugation at 2400 RCF during 20 min. Water samples were successively filtered through 0.45  $\mu\text{m}$  and 0.2  $\mu\text{m}$  CA syringe filter to limit clogging during solid phase extraction (SPE). Pesticides were extracted from water using SPE with SolEx C18 cartridges (1 g phase, Dionex-Thermo Fischer) following an in-house method previously described.<sup>31</sup> Pesticides in sediment were extracted using a modified solid–liquid extraction protocol.<sup>32</sup> Details on both extraction methods are provided in AB. Methods used for extraction from water and sediment samples yielded extraction recoveries higher than 81%. Pesticides were quantified using established procedure for gas chromatography–mass spectrometry (GC-MS method detailed in AB).<sup>33</sup> Instrumental quantification limits were 33 and 30  $\mu\text{g L}^{-1}$  for acetochlor and S-metolachlor, respectively.

Instrumental detection limits, instrumental reproducibility and uncertainties are provided in AB, Table B5.

### **Compound-specific isotope analysis (CSIA)**

Carbon and nitrogen compound-specific isotope analyses (CSIA) of acetochlor and S-metolachlor in water and sediment samples were carried out following established procedures for gas chromatography–isotope ratio mass spectrometry (GC-IRMS method detailed in AB).<sup>33</sup> Briefly,  $^{13}\text{C}/^{12}\text{C}$  and  $^{15}\text{N}/^{14}\text{N}$  isotope ratios values were measured in triplicate for each batch experiment with a typical uncertainty of  $\pm 0.5\%$  and  $\pm 1.0\%$  for C and N, respectively. Average triplicate values were reported in delta notation per element ( $\delta^h E$ ) with the uncertainty corresponding to the 95% confidence interval, in parts per thousand (‰) relative to Vienna PeeDee Belemnite (V-PDB) and air standards, respectively:

$$\delta^h E = \frac{R(^h E/^l E)_{\text{sample}}}{R(^h E/^l E)_{\text{standard}}} - 1 \quad (4.1)$$

where  $\delta^h E$  is the isotope signature of the respective element ( $E$ ) and  $R(^h E/^l E)$  are the isotope ratios of heavy ( $h$ ) divided by light ( $l$ ) isotopes in the sample or the standard.

The  $\delta^h E$  linearity range of the measurement was defined as the range of injected mass of C and N to which the  $\delta^{13}\text{C}$  and  $\delta^{15}\text{N}$  values of the pesticide stay within a  $\pm 0.5\%$  and  $\pm 1\%$  interval, respectively.<sup>34</sup> The  $\delta^h E$  linearity ranges of the measurement were established as 6 to 300 ng and 40 to 300 ng, for C and N, respectively. Extraction procedures from water and sediment samples did not cause significant carbon isotope fractionation (water:  $|\Delta\delta^{13}\text{C}_{\text{ext},w}| < 0.5\%$ , sediment:  $|\Delta\delta^{13}\text{C}_{\text{ext},s}| < 0.6\%$ ; AB, Table B5). Although extraction procedures from water samples did not cause significant nitrogen isotope fractionation ( $|\Delta\delta^{15}\text{N}_{\text{ext},w}| < 0.9\%$ ), extraction from sediment samples was associated with significant nitrogen isotope fractionation ( $|\Delta\delta^{15}\text{N}_{\text{ext},s}| < 1.6\%$ ; AB, Table B5). Therefore,  $\delta^{15}\text{N}$  data were interpreted with caution.

The minimal change of isotope signature ( $\Delta\delta^h E_{\text{min}}$ ) above which isotope fractionation was attributed to degradation was determined as the propagation of uncertainty associated with sample preparation and measurements (eq. B7).<sup>29</sup>  $\Delta\delta^{13}\text{C}_{\text{min}}$  for water ( $w$ ) and sediment ( $s$ ) were, respectively, 0.94 and 0.91‰ for acetochlor, and 0.95‰ and 1.77‰ for S-metolachlor (AB, Table B5).  $\Delta\delta^{15}\text{N}_{\text{min},w}$  was 1.70‰ and 1.99‰ for acetochlor and S-metolachlor, respectively.

Bulk isotopic enrichment factors ( $\varepsilon_{bulk,E}$ ), that relate a change in  $^{13}\text{C}/^{12}\text{C}$  or  $^{15}\text{N}/^{14}\text{N}$  isotope ratios to the extent of degradation, were determined under representative conditions in the closed batch experiments and derived from the Rayleigh equation, eq. 4.2, without forcing the regression through the origin:<sup>35</sup>

$$\ln\left(\frac{\delta^h E(t) + 1}{\delta^h E_0 + 1}\right) = \varepsilon_{bulk,E} \times \ln\left(\frac{P(t)}{P_0}\right) \quad (4.2)$$

where  $\delta^h E_0$  and  $\delta^h E(t)$  represented the isotope signatures of an element  $E$  at time zero and  $t$  of the degradation respectively, while  $P(t)/P_0$  is the fraction of remaining pesticides at time  $t$ .

To interpret and compare  $\varepsilon_{bulk,E}$  values in terms of underlying degradation pathways, apparent kinetic isotope effects ( $AKIE_E$ ) were calculated for each element to correct  $\varepsilon_{bulk,E}$  for isotope dilution, number of reactive sites and intramolecular isotopic competition in eq. 4.3:

$$AKIE_E \approx \frac{1}{1 + z \times \left(\frac{n}{x}\right) \times \frac{\varepsilon_{bulk,E}}{1000}} \quad (4.3)$$

where  $n$  is the total number of atoms of the element,  $x$  the number of atoms in reactive positions and  $z$  the number of atoms which are in intramolecular isotopic competition.<sup>36</sup>

### **Suspect screenings of transformation products**

Selected water and sediment samples on days 50, 150, 200 and 250 were screened for TPs identification from oxic and anoxic experiments, and blank samples on days 0 and 200 to evaluate background of pesticides and TPs. The method and mass spectra analysis followed Villette et al.<sup>37</sup> Levels (L) of identification confidence were assigned according to Schymanski et al.<sup>38</sup> Briefly, samples were analyzed using a Dionex Ultimate 3000 (Thermo-Fischer Scientific, USA) liquid chromatography (LC) coupled to an Impact-II (Bruker, Germany) quadrupole time of flight (Q-TOF) to perform high resolution mass spectrometry (HR-MS/MS). Mass spectra of each sample were acquired in positive and negative ion modes on a mass range from 30 to 1,000 Da at a resolution of 54,000 at  $m/z$  400. In parallel, a list of suspected TPs and corresponding pathways were generated from the aerobic microbial metabolites pathway prediction system (UM-PPS),<sup>39</sup> Metabolite Predict 2.0 (Bruker, Germany), META Ultra 1.2, Meta PC 1.8.1 (MultiCASE, Beachwood, OH, US), and extracted from selected literature (AB, Table B6). The list of suspected TPs was converted in an exact mass list used as an analyte list for annotation in Metaboscape 4.0. All adduct forms containing the exact  $m/z$  (L5) were pooled in a bucket using an intensity MS signal threshold of 1,000.

Tentative candidate annotations were assigned using a criteria of mass deviation ( $\Delta m/z$ ) below 3 ppm and mSigma value below 30 (L3). The confirmed pesticide structures and some TPs were eventually assigned by matching exact masses and retention times ( $RT < 0.2$  min; L1).

### **Phase-transfer and biodegradation modelling**

Pesticide concentrations and associated isotope fractionation were interpreted using an adapted version of the phase-transfer model developed previously.<sup>19</sup> The model concepts and assumptions are detailed in AB. Data treatment and model-assisted interpretation including CSIA data are discussed below.

## **Results and discussion**

Partitioning coefficients and hydrochemistry indicated steady-state conditions over time in the batch experiments. Partitioning coefficients of pesticides between the sediment phase ( $P_s$ ) and the water phase ( $P_w$ ) during the experiments were similar as sediment partitioning coefficients (average  $\log |P_s/P_w - K_d| = 0.5 \pm 0.2$ ; AB, Table B4).  $P_s/P_w$  ratios indicated that phase partitioning equilibrium was reached within two days and maintained over time. Hydrochemistry ( $\text{Ca}^{2+}$ ,  $\text{Mg}^{2+}$ ,  $\text{NO}_3^-$ ,  $\text{SO}_4^{2-}$ ,  $\text{Cl}^-$ ,  $pH$ ) (AB, Figure B1) did not vary much in all experiments, indicating constant conditions for biodegradation over time, although sulfate concentrations slightly increased over time under oxic conditions ( $\Delta \text{SO}_4^{2-}{}_{t=0 \text{ to } 300 \text{ days}} = 0.20 \pm 0.05 \text{ mmol L}^{-1}$ ). Under anoxic conditions, depletion of  $\text{NO}_3^-$  and  $\text{SO}_4^{2-}$  in the aqueous phase within two days indicated reducing conditions. DOC content and properties, i.e., ultraviolet absorbance and oxidation state, did not change over time (AB, Table B2).

### **Dissipation kinetics and isotope fractionation**

Pesticide dissipation followed pseudo first-order kinetics in both oxic and anoxic batch experiments. Dissipation half-lives in water and sediment for acetochlor and *S*-metolachlor under oxic and anoxic conditions ( $DT_{50}$ ; Table 4.1) were in the range reported in the literature.<sup>40, 41</sup> Worthy of note,  $DT_{50}$  values in water were higher under anoxic than under oxic conditions. Higher  $DT_{50}$  values under anoxic conditions supports the assumption that oxic degradation of pesticides is more energetically favorable than anoxic degradation using weaker electron acceptors, e.g., Mn,  $\text{NO}_3^-$ , Fe,  $\text{SO}_4^{2-}$ , than oxygen.<sup>8</sup> Acetochlor dissipation was faster than *S*-metolachlor dissipation, which is consistent with previous studies.<sup>41</sup> The comparatively

large *S*-metolachlor headgroup may sterically reduce the enzyme access to the C–Cl bond, thereby reducing *S*-metolachlor degradation rates.<sup>40</sup>

Isotope fractionation for acetochlor and *S*-metolachlor in the water phase confirmed that biodegradation contributed to dissipation (Figure 4.1a & b).  $\epsilon_{bulk,C}$  under oxic and anoxic conditions ranged, respectively, from  $-4.97 \pm 1.62\text{‰}$  and  $-3.62 \pm 0.70\text{‰}$  for acetochlor to  $-1.20 \pm 0.35\text{‰}$  and  $-1.87 \pm 0.58\text{‰}$  for *S*-metolachlor (Table 4.1).

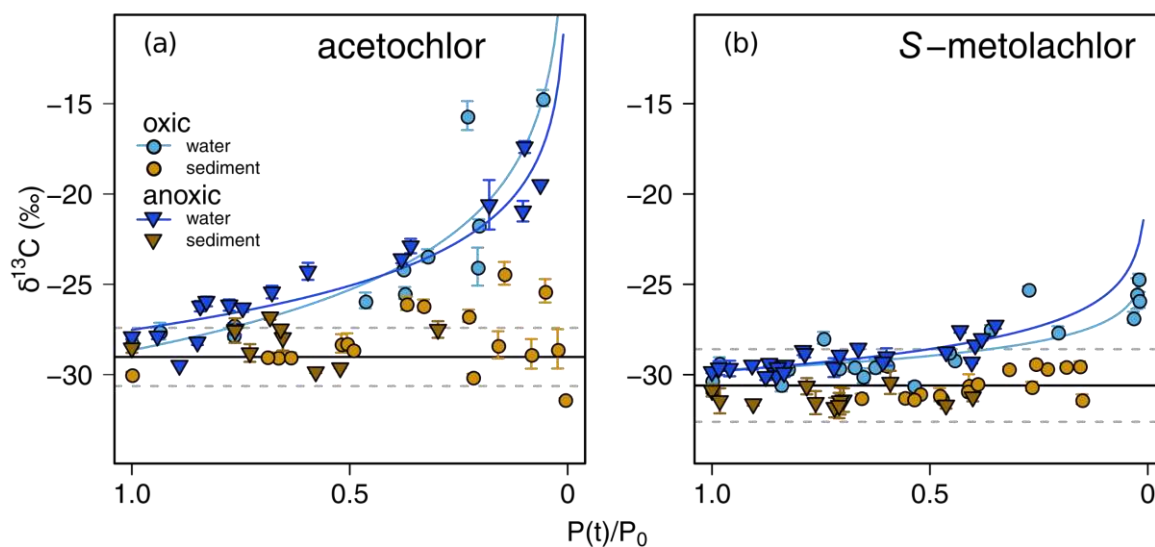


Figure 4.1. Carbon isotope signature ( $\delta^{13}C$ ) as a function of the pesticide remaining fraction ( $P(t)/P_0$ ) of (a) acetochlor and (b) *S*-metolachlor in oxic and anoxic water–sediment systems. Error bars indicate the 95% confidence intervals of  $\delta^{13}C$  values. Black lines indicate the reference carbon isotope signatures of standards measured with an elemental analyzer–isotope ratio mass spectrometry (EA-IRMS). Grey dotted lines represent the  $\Delta\delta^{13}C_{min,w}$ . Colored curves are fitting to isotope data using the logarithmic expression of the Rayleigh equation (eq. 4.2).

Similar  $DT_{50}$  values ( $t$ -test;  $p < 0.05$ ) for acetochlor and *S*-metolachlor in the water and the sediment phases suggest similar degradation rates in both phases (Table 4.1; AB, Figure B2). However, insignificant isotope fractionation was observed in the sediment ( $0.9\text{‰} < |\Delta\delta^{13}C_{min,s}|$ , Figure 4.1; AB, Table B5). Hence, CSIA data indicated prevailing degradation in water and low or insignificant degradation in sediment since CSIA is limited in our case to detect low extent of biodegradation (eq. B9). Assuming a similar degradation pathway, it is estimated that at least 16% of acetochlor and 40% of *S*-metolachlor should be degraded to detect with CSIA biodegradation in sediment. We thus hypothesized that pesticides did not degrade significantly in sediment, but rather desorbed from the sediment to the water to fulfill the phase-transfer equilibrium during pesticide degradation in water. As the result, pesticide dissipation rate constants in the sediment phase were close to the dissipation rate constants in the water phase ( $k_{obs,w}$ ) reflected both pesticide dissipation during biodegradation and phase-transfer from sediment to water. Overall, our results emphasize that phase-transfer should be accounted for when quantifying pesticide degradation rate constants ( $k_{deg}$ ) in water–sediment systems.

Table 4.1. Dissipation half-life ( $DT_{50}$ ), degradation half-life ( $DegT_{50}$ ), carbon bulk isotopic enrichment factor ( $\varepsilon_{bulk,C}$ ) and apparent kinetic isotope effect (AKIE) for the bulk, water (*w*) and sediment (*s*) phase under oxic and anoxic experiments

	$DT_{50,w}$ (days) <sup>a</sup>		$DT_{50,s}$ (days) <sup>a</sup>		$DegT_{50,w}$ (days) <sup>a</sup>		$\varepsilon_{bulk,C}$ (‰) <sup>b</sup>		$\varepsilon_{bulk,corr,C}$ (‰) <sup>c</sup>		$AKIE_{bulk,C}$ (-) <sup>d</sup>	
oxic												
acetochlor	47	± 25	53	± 27	31	± 17	-4.97	± 1.62	-5.23	± 1.09	1.075	± 0.008
S-metolachlor	61	± 10	151	± 83	29	± 8	-1.20	± 0.35	-1.19	± 0.19	1.018	± 0.001
anoxic												
acetochlor	69	± 16	47	± 12	59	± 16	-3.62	± 0.70	-3.51	± 0.38	1.053	± 0.003
S-metolachlor <sup>e</sup>	249	± 56	182	± 41	199	± 48	-1.87	± 0.58	-1.83	± 0.32	1.029	± 0.001

<sup>a</sup> Half-life time were calculated following a pseudo first-order kinetics:  $DT_{50} = \ln(2)/k_{obs}$ . Goodness of the linear fit ( $\ln(P(t)/P_0) = -k_{obs} \times t$ ) were  $R^2 > 0.7$  for dissipation and  $R^2 > 0.8$  for degradation. <sup>b</sup>  $\varepsilon$  derived from the Rayleigh plot (eq. 4.2) without any significant difference using all data or  $P(t)/P_0 > 0.2$ . Goodness of the linear fit were  $R^2 > 0.7$ . <sup>c</sup> Calculated using the system of eq. B22 to B28. <sup>d</sup> Calculated with eq. 4.3 where  $n = 14$  and  $15$  for acetochlor and S-metolachlor, respectively, and  $z = x = 1$ . <sup>e</sup> corresponding to  $P(t)/P_0 = 0.66$ , see Figure 4.1. Uncertainties correspond to 95% confidence intervals.



### **Water–sediment phase-transfer and implications for interpreting degradation kinetics**

The biodegradation rate constants ( $k_{deg}$ ) for each phase were estimated from the observed pesticide dissipation using the conceptual model developed and validated by Honti et al.<sup>19</sup> In this model (detailed in AB), pesticides are either freely dissolved in the water phase ( $P_w$ ), or sorbed to the organic fraction of the sediment ( $P_s$ ) consisting in dissolved and particulate organic carbon (Figure 4.2). The original conceptual model presented in Figure 4.2a has been developed according to OECD protocols, and validated for a wide range of experimental conditions (TOC between  $10^{-3}$  to  $300 \text{ mg C L}^{-1}$  and sediment-water ratio 1:3 to 1:1000) and molecules ( $\log K_{oc}$ , from 1 to 5).<sup>7, 13, 19</sup> Here, the model was simplified to focus on parent pesticides and the first generation of (Figure 4.2b).

The simplified model arises from the assumption that biodegradation exclusively occurs in water whereas sediment-bound pesticides are not available to biodegradation.<sup>42</sup> This assumption has been used since decades in regulatory testing<sup>43</sup> and simple pollutant fate modeling for various molecules and conditions.<sup>44</sup> In the present study, it is comforted by the absence of significant carbon isotope fractionation in the sediment, as described above. However, degrading microorganisms can be attached on the sediment surface and pesticide degradation may occur at the interface between sediment and water.<sup>45</sup>

In addition, TPs sorption was neglected because acetochlor and S-metolachlor TPs were not detected in the sediment phase, in agreement with TPs physico-chemical properties (octanol–water partition coefficient,  $P_{ow,p} > P_{ow,TPs}$  and  $K_{oc,p} > K_{oc,TPs}$ ).<sup>41</sup> Finally, the simplified model focuses on parent pesticides and the first generation of TPs to specifically derive phase-specific degradation rates and isotopic enrichment factors of parent pesticides. Comparatively, the OECD protocol also aims at identifying and quantifying TPs persistence, pesticide mineralization and formation of NERs, justifying a specific account for additional phases and processes.<sup>19</sup>

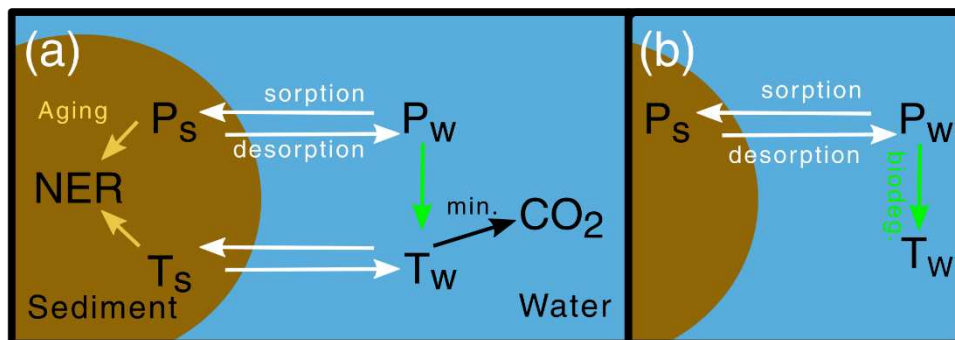


Figure 4.2. Conceptual models of pesticide phase-transfer and degradation in the water (w) and sediment (s) phase system. (a) Original model.<sup>13</sup> (b) Simplified model adopted in the present study. Species are  $P_s$ : pesticides sorbed on the sediment phase, including the dissolved and the particulate organic carbon,  $P_w$ : freely dissolved pesticides in the water phase,  $T_s$ : sum of transformation products sorbed on total organic carbon,  $T_w$ : sum of  $T$  freely dissolved in water phase,  $NER$ : non-extractable residues and  $CO_2$ : carbon dioxide. Arrows with the same color denote the same processes. *Min.*: mineralization.

The pesticide mass balance under closed system and steady-state conditions was established here from the simplified conceptual model (Figure 4.2b), and detailed in AB with eq. B10 to B18. The mass balance equation was rearranged to express the pseudo first-order degradation rate constants ( $k_{deg,w}$ ) as a function of the observed dissipation rate constants ( $k_{obs,w}$ ):

$$k_{deg,w} = k_{obs,w} \times [1 + K_{oc} \times (f_{oc} \times TSS + DOC)] \quad (4.4)$$

where  $K_{oc}$  is the organic carbon–water partitioning coefficient of the sediment. Since  $DOC \ll POC = f_{oc} \times TSS$  ( $DOC/POC = 0.3\%$ ) in our system, eq. 4.4 was simplified to eq. 4.5:

$$k_{deg,w} = k_{obs,w} \times [1 + K_{oc} \times f_{oc} \times TSS] \quad (4.5)$$

This assumption is valid for water–sediment systems with DOC concentrations lower than the threshold value defined in eq. 4.6:

$$DOC \leq \frac{CI \times (1 + K_{oc} \times f_{oc} \times TSS)}{K_{oc}} \quad (4.6)$$

where  $CI$  is the 95% confidence interval associated to  $k_{obs,w}$ . In our case, this simplification is valid for DOC concentrations lower than  $70 \text{ mg L}^{-1}$ , which is 10 to 70 times higher than the typical average river concentrations.<sup>21</sup> For higher DOC concentrations, eq. 4.4 remains valid

but measured pesticide concentrations in water should be corrected to account for partitioning between the freely dissolved fraction, feeding  $P_w$ , and the fraction sorbed on DOC, feeding  $P_S$ .

Corrections of  $DT_{50,w}$  ( $= \ln(2)/k$ ) to infer  $DegT_{50,w}$  in our system are provided in Table 4.1.  $k_{deg,w}$  are higher than  $k_{obs,w}$  because  $1 + K_{oc} \times f_{oc} \times TSS > 1$  (eq. 4.5), and depends on the TSS and/or the partitioning coefficient of pesticides.<sup>19</sup> Without considering the phase-transfer, biodegradation rate constants ( $k_{deg,w}$ ) would be underestimated by a factor ( $k_{deg,w}/k_{obs,w}$ ) of  $1.2 \pm 0.2$  and  $1.5 \pm 0.5$  for acetochlor, and of  $1.3 \pm 0.2$  and  $2.1 \pm 0.1$  for S-metolachlor under oxic and anoxic conditions, respectively. This emphasizes the need to account for phase-transfer when estimating  $k_{deg,w}$  of pesticides in water–sediment systems, especially under anoxic conditions.

### **Water–Sediment Phase-Transfer and Implications for Interpreting Isotope Signatures.**

The observed isotope signatures of pesticides in water ( $\delta^{13}C_{obs,w}$ ) may also be affected by phase-transfer. A sorption-based isotope effects may occur when the non-degraded pesticide fraction sorbed on the sediment progressively desorbs and mixes in water, while partitioning equilibrium is not achieved over degradation. This would decrease  $\delta^{13}C_{obs,w}$  during degradation and require a correction of  $\delta^{13}C_{obs,w}$ . To evaluate the potential effect of desorption on  $\epsilon_{bulk}$  values, we corrected acetochlor and S-metolachlor concentration and CSIA data accounting for the effect of phase-transfer (Table 4.1; AB, eq. B19 to B28).

In our case, the corrected isotopic enrichment factors ( $\epsilon_{bulk,corr}$ ) and  $\epsilon_{bulk}$  values did not significantly change ( $<0.3\%$ , Table 4.1). A negligible effect of pesticide desorption from sediment on  $\epsilon_{bulk}$  supports the notion that partitioning equilibrium is quasi-instantaneously achieved over degradation and isotope fractionation is limited through equilibrium<sup>16</sup> for ratios of degradation to desorption rate constant ( $k_{deg}/k_{des}$ ) lower than 0.02 ( $k_{des} < 2 \text{ d}^{-1}$ ).<sup>46</sup> We anticipate that the model remains valid under a ratio of  $k_{deg}/k_{des}$  lower than 0.1.<sup>47</sup> Beyond this domain, sorption-desorption kinetics should be considered in the model. To evaluate the impact of various types of sediment on the  $\epsilon_{bulk,corr}$ , a sensitivity analysis was carried out across a wide range of conditions ( $\epsilon_{bulk}$  between  $-0.5$  to  $-40\%$ ,  $\log K_{oc}$  between 1 to 6 and TOC between 0.5 to 500 mg L<sup>-1</sup>).<sup>41</sup> The analysis showed insignificant effect of pesticide phase-transfer between the sediment and the water on isotope fractionation ( $\epsilon_{bulk,corr} - \epsilon_{bulk} < 0.5\%$ ). This supports the idea that phase-transfer is associated with negligible isotope fractionation in water–sediment systems, and a correction of  $\epsilon_{bulk}$  is thus not needed under environmental conditions.

However, a correction of  $\delta^{13}C_{obs,w}$  may be necessary to follow the model terminology  $P_w$  and  $P_s$  (see above) when DOC concentrations are high and significantly contribute to the isotope mass balance. The threshold limit for a correction that account for DOC concentrations can be determined with an isotope mass balance as follows:

$$\delta^{13}C_{obs,w} = x_{p,DOC} \times \delta^{13}C_{DOC} + (1 - x_{p,DOC}) \times \delta^{13}C_w \quad (4.7)$$

where  $x_{p,DOC}$  is the mass fraction and  $\delta^{13}C_{DOC}$  ( $= \delta^{13}C_0$ ) the isotope signature of DOC-bound pesticides. Under the model assumption, the validity limit of the model to avoid accounting for the isotope signature of DOC-bound pesticides can be expressed using the partitioning equations (eq. B5 & B6) and eq. 4.7:

$$DOC \leq \frac{\Delta}{(\delta^{13}C_{DOC} - \Delta) \times K_{oc} \times f_{oc}} \quad (4.8)$$

where  $\Delta$  is the maximum isotope fractionation ( $\Delta = 0.5\%$ ) above which the isotope signature of DOC-bound pesticides ( $\delta^{13}C_{DOC}$ ) may significantly contribute to the pesticide isotope signature in water ( $\delta^{13}C_{obs,w}$ ). From eq. 4.8 a correction of the DOC term is not required to interpret CSIA data for pesticides with  $\log K_{oc}$  between 1 and 6,<sup>41</sup> and realistic DOC surface waters concentration between 5 and 20 mg L<sup>-1</sup>.<sup>21</sup> However, a correction of the DOC term is needed for the same range of  $\log K_{oc}$  and DOC concentrations higher than 300 mg L<sup>-1</sup>, which can be reached in active sludge of the wastewater treatment plants.<sup>48</sup>

### **Pesticide degradation pathways**

The carbon apparent kinetic isotope effects (AKIE<sub>C</sub>; eq. 4.3; Table 4.1) of acetochlor and *S*-metolachlor were calculated to compare isotope fractionation of different compounds and to interpret degradation pathways using  $\epsilon_{bulk}$  values. Similar AKIE<sub>C</sub> values and TPs patterns under oxic and anoxic conditions suggest an identical prevailing degradation pathway of acetochlor and *S*-metolachlor. AKIE<sub>C</sub> values of acetochlor (oxic:  $1.075 \pm 0.008$  and anoxic:  $1.053 \pm 0.003$ ) and *S*-metolachlor (oxic:  $1.018 \pm 0.001$  and anoxic:  $1.029 \pm 0.001$ ) are in the range of experimentally derived AKIE<sub>C</sub> for nucleophilic substitution degradations.<sup>36</sup> This is also in agreement with the predominance of acetochlor and *S*-metolachlor oxalinic acids as the major TPs (Figure 4.3). Nucleophile substitution pathway of acetochlor and *S*-metolachlor, primarily leading to the formation of oxalinic acids (Figure 4.3), has been previously elucidated via the Glutathione-*S*-transferase followed by an oxidation.<sup>49</sup> Ethanosulfonic acids, also produced via the Glutathione-*S*-transferase, were identified as secondary TPs produced under different environmental conditions.<sup>40,49,50</sup> Similar AKIE<sub>C</sub> values observed in a wetland column experiment (AKIE<sub>C</sub>, acetochlor =  $1.051 \pm 0.007$ ),<sup>31</sup> and soil batch experiments (AKIE<sub>C</sub>, *S*-metolachlor =  $1.023 \pm 0.001$ ),<sup>29</sup> suggest a similar degradation pathway or similar co-occurring pathways under distinct environmental conditions. In addition, the N isotope signature of

acetochlor and *S*-metolachlor in the water phase did not significantly change under oxic and anoxic conditions ( $1.2\text{‰} < |\Delta\delta^{15}N_{min,w}|$ ; AB, Table B5), supporting the proposed pathway. Indeed, N in acetochlor and *S*-metolachlor is positioned three atoms away from the reactive site, and only secondary isotope effect might be expected.

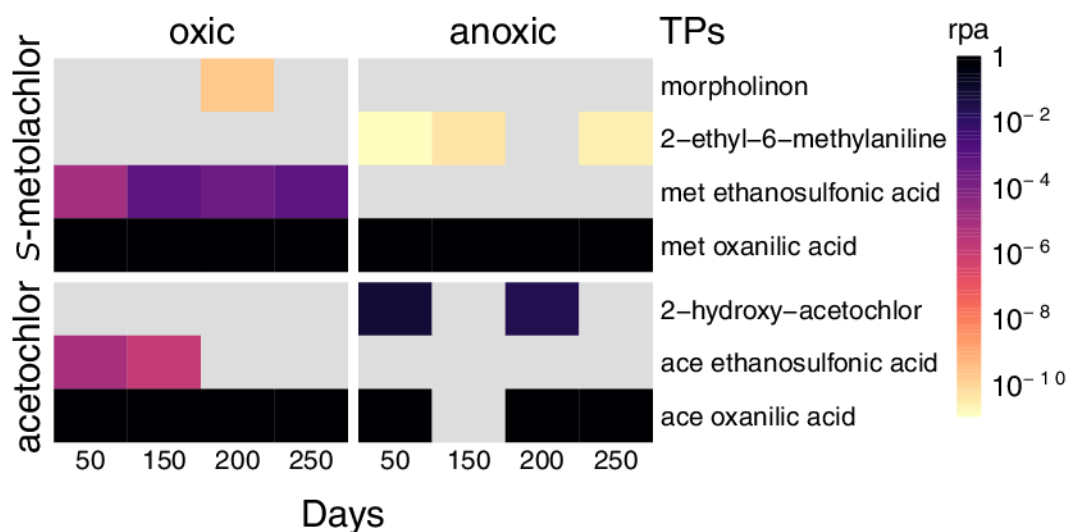


Figure 4.3. *S*-metolachlor and acetochlor transformation products (TPs) under oxic and anoxic conditions. Only confirmed structures (Level 1) are presented. The relative peak area (*rpa*) is defined for each TPs as the ratio of the peak area normalized by the response factor for one TP to the main TP for the same pesticide. Grey indicates absence of the TPs.

The contribution of acetochlor and *S*-metolachlor ethanosulfonic acids was low (*rpa* between  $10^{-2}$  to  $10^{-5}$ ) compared to previous studies showing that ethanosulfonic acid was only two to five time less produced than oxalinic acid.<sup>40, 49</sup> The semi-quantitative analysis of HR-MS/MS data also showed that TPs patterns under oxic and anoxic conditions slightly differed (Figure 4.3). Interestingly, acetochlor and *S*-metolachlor ethanosulfonic acids were not detected under anoxic conditions, although their formation also involves a *S*-cysteine conjugate intermediate, as for acetochlor and *S*-metolachlor oxalinic acids.<sup>49</sup> We hypothesize that some microorganisms use acetochlor and *S*-metolachlor ethanosulfonic acid as an alternative source of sulfur to growth under sulfate limiting conditions, such as those occurring in our anoxic batch experiments (AB, Figure B1).<sup>51, 52</sup> This idea is also supported by the confirmed formation of hydroxy acetochlor and the suggested formation of *N*-ethyl-*N*-(2-ethyl-6-methylphenyl)-2-hydroxyacetamide (L3;  $m/z$   $[M-H]^- = 221.1415$ ). These TPs may be formed as secondary hydroxy-TPs during microorganism sulfur assimilation, as observed previously with ethanesulfonate metazachlor, a TP of the chloroacetanilide herbicide metazachlor.<sup>53</sup> However, previous experiments with *S*-metolachlor under oxic nutrient-limiting conditions suggest (L3) the formation of the *N*-ethyl-*N*-(2-ethyl-6-methylphenyl)-2-hydroxyacetamide without any detection of the ethanosulfonic acid.<sup>54</sup> Altogether, the specific conditions of microbial

consumption of ethanesulfonate as a sulfur source remain unclear, although environmental implications are important because ethanosulfonic acids are more mobile than their parent pesticides and other TPs.<sup>55</sup>

### **Environmental implications for water–sediment studies**

Here we examined the dissipation of the two widely used chloroacetanilide herbicides acetochlor and *S*-metolachlor in water–sediment batch experiments under contrasted oxic and anoxic conditions. CSIA data and TPs identification complementarily allowed to identify possible degradation pathways and associated mechanisms. In water–sediment systems with two main phases, the dissipation of pesticides reflects the contribution of both biodegradation and phase-transfer. A simplified version of a conceptual model validated over a wide range of conditions and molecules facilitated the estimation and the interpretation of degradation rate constants and bulk isotopic enrichment factors ( $\epsilon_{bulk}$ ) associated with each phase. The simplified model is valid in closed steady-state laboratory systems when pesticides have a similar sorption affinity on the dissolved (DOC) and the particulate (POC) forms of organic carbon (detailed in AB). Steady-state conditions are fulfilled and the model remains valid when sorption kinetics are faster than biodegradation ( $k_{deg}/k_{des} < 0.1$ ). The  $k_{deg}/k_{des}$  ratio should carefully be estimated from experimental data before using the simplified model. However, a  $k_{deg}/k_{des}$  ratio lower than 0.1 is satisfied in 82% of experiments derived from pesticide degradation in the enviPath (n = 4716) database,<sup>11</sup> considering cases when  $k_{des}$  is lower than  $2 \text{ d}^{-1}$ .<sup>46</sup>

Most importantly, we anticipate that phase-transfer does not cause significant carbon isotope fractionation ( $\Delta\delta^{13}\text{C} < 0.5\text{‰}$ ) for a wide spectrum of environmental conditions and molecules. This is crucial since insignificant isotope fractionation during phase-transfer is a preliminary requirement to evaluate with CSIA the in situ pesticide degradation in water–sediment systems, including ponds, wetlands, rivers or wastewater treatment plants. The isotopic enrichment factors ( $\epsilon_{bulk}$ ) determined under representative conditions in laboratory experiments can be used to estimate biodegradation half-lives ( $DegT_{50,w}$ ) in different environmental systems, and thus can facilitate pesticide dissipation studies in surface waters. Since pesticide degradation can be evaluated with CSIA with limited or without information on pesticide concentrations or TPs, pesticide CSIA data may prove useful for quantifying and predicting pesticide degradation with reactive-transport modeling of the water-sediment system.

From a methodological point of view, we anticipate that sample preparation to limit the matrix effect, e.g., the dissolved or particulate carbon or nitrogen, before GC-IRMS measurements is necessary to apply CSIA in water–sediment systems. Bakkour et al.<sup>56</sup> evaluate that GC-IRMS injected sample containing larger DOC–pesticide ratio (mol/mol) higher than 80 might create a too large background signal for accurate isotope ratios measurements. However, this limitation can be overcome in the future with additional cleaning steps, including molecularly imprinted polymers,<sup>56</sup> or preparative high-pressure liquid chromatography<sup>57, 58</sup> to selectively extract the compound of interest. Altogether, we anticipate that CSIA can help in the future to elucidate pesticide degradation in specific phases of the water–sediment system, under both laboratory and field conditions, to eventually improve the prediction of pesticide behavior in surface waters.

## References

1. Maggi, F.; Tang, F. H. M.; la Cecilia, D.; McBratney, A., PEST-CHEMGRIDS, global gridded maps of the top 20 crop-specific pesticide application rates from 2015 to 2025. *Scientific Data* **2019**, *6*, 170.
2. Burri, N. M.; Weatherl, R.; Moeck, C.; Schirmer, M., A review of threats to groundwater quality in the anthropocene. *Sci. Total Environ.* **2019**, *684*, 136–154.
3. Schwarzenbach, R. P.; Egli, T.; Hofstetter, T. B.; von Gunten, U.; Wehrli, B., Global water pollution and human health. *Annu. Rev. Env. Resour.* **2010**, *35*, 109–136.
4. Malaj, E.; von der Ohe, P. C.; Grote, M.; Kuhne, R.; Mondy, C. P.; Usseglio-Polatera, P.; Brack, W.; Schafer, R. B., Organic chemicals jeopardize the health of freshwater ecosystems on the continental scale. *Proc. Natl. Acad. Sci. U.S.A.* **2014**, *111*, (26), 9549–9554.
5. Fenner, K.; Canonica, S.; Wackett, L. P.; Elsner, M., Evaluating pesticide degradation in the environment: Blind spots and emerging opportunities. *Science* **2013**, *341*, (6147), 752–758.
6. Ericson, J. F., An evaluation of the OECD 308 water/sediment systems for investigating the biodegradation of pharmaceuticals. *Environ. Sci. Technol.* **2007**, *41*, (16), 5803–5811.
7. Shrestha, P.; Junker, T.; Fenner, K.; Hahn, S.; Honti, M.; Bakkour, R.; Diaz, C.; Hennecke, D., Simulation studies to explore biodegradation in water–sediment systems: From OECD 308 to OECD 309. *Environ. Sci. Technol.* **2016**, *50*, (13), 6856–6864.
8. Ghattas, A.-K.; Fischer, F.; Wick, A.; Ternes, T. A., Anaerobic biodegradation of (emerging) organic contaminants in the aquatic environment. *Water Res.* **2017**, *116*, 268–295.

9. Vandermaesen, J.; Horemans, B.; Bers, K.; Vandermeeren, P.; Herrmann, S.; Sekhar, A.; Seuntjens, P.; Springael, D., Application of biodegradation in mitigating and remediating pesticide contamination of freshwater resources: state of the art and challenges for optimization. *Appl. Microbiol. Biotechnol.* **2016**, *100*, (17), 7361–7376.
10. Moser, A.; Wemyss, D.; Scheidegger, R.; Fencia, F.; Honti, M.; Stamm, C., Modelling biocide and herbicide concentrations in catchments of the Rhine basin. *Hydrol. Earth Syst. Sci.* **2018**, *22*, (8), 4229–4249.
11. Latino, D. A. R. S.; Wicker, J.; Gütlein, M.; Schmid, E.; Kramer, S.; Fenner, K., Eawag–Soil in enviPath: A new resource for exploring regulatory pesticide soil biodegradation pathways and half-life data. *Environ. Sci. Process. Impacts* **2017**, *19*, (3), 449–464.
12. Katagi, T., Pesticide behavior in modified water–sediment systems. *J. Pestic. Sci.* **2016**, *41*, (4), 121–132.
13. Honti, M.; Hahn, S.; Hennecke, D.; Junker, T.; Shrestha, P.; Fenner, K., Bridging across OECD 308 and 309 data in search of a robust biotransformation indicator. *Environ. Sci. Technol.* **2016**, *50*, (13), 6865–6872.
14. Escher, B. I.; Stapleton, H. M.; Schymanski, E. L., Tracking complex mixtures of chemicals in our changing environment. *Science* **2020**, *367*, (6476), 388–392.
15. Elsner, M.; Imfeld, G., Compound-specific isotope analysis (CSIA) of micropollutants in the environment — current developments and future challenges. *Curr. Opin. Biotechnol.* **2016**, *41*, 60–72.
16. Kopinke, F. D.; Georgi, A.; Voskamp, M.; Richnow, H. H., Carbon isotope fractionation of organic contaminants due to retardation on humic substances: Implications for natural attenuation studies in aquifers. *Environ. Sci. Technol.* **2005**, *39*, (16), 6052–6062.
17. Food and Agriculture Organization of the United Nations FAOSTAT. [www.fao.org/faostat/](http://www.fao.org/faostat/) (20<sup>th</sup> March **2019**).
18. Kiefer, K.; Müller, A.; Singer, H.; Hollender, J., New relevant pesticide transformation products in groundwater detected using target and suspect screening for agricultural and urban micropollutants with LC-HRMS. *Water Res.* **2019**, *165*, 114972.
19. Honti, M.; Fenner, K., Deriving persistence indicators from regulatory water–sediment studies - opportunities and limitations in OECD 308 data. *Environ. Sci. Technol.* **2015**, *49*, (10), 5879–5886.
20. Smith, E. J.; Davison, W.; Hamilton-Taylor, J., Methods for preparing synthetic freshwaters. *Water Res.* **2002**, *36*, (5), 1286–1296.
21. Raymond, P. A.; Spencer, R. G. M., Chapter 11 - Riverine DOM. In *Biogeochemistry of marine dissolved organic matter (Second edition)*, Hansell, D. A.; Carlson, C. A., Eds. Academic Press: Boston, **2015**; pp 509–533.
22. Maillard, E.; Imfeld, G., Pesticide mass budget in a stormwater wetland. *Environ. Sci. Technol.* **2014**, *48*, (15), 8603–8611.



23. OECD, Test No. 106: Adsorption – desorption using a batch equilibrium method. In *OECD Guidelines for the Testing of Chemicals, Section 1*, OECD Publishing: Paris, France, **2000**; p 45.
24. Borch, T.; Kretzschmar, R.; Kappler, A.; Cappellen, P. V.; Ginder-Vogel, M.; Voegelin, A.; Campbell, K., Biogeochemical redox processes and their impact on contaminant dynamics. *Environ. Sci. Technol.* **2010**, *44*, (1), 15–23.
25. Loch, A. R.; Lipka, K. A.; Carlson, D. L.; Chin, Y. P.; Traina, S. J.; Roberts, A. L., Nucleophilic aliphatic substitution reactions of propachlor, alachlor, and metolachlor with bisulfide (HS<sup>-</sup>) and polysulfides (S<sub>n</sub><sup>2-</sup>). *Environ. Sci. Technol.* **2002**, *36*, (19), 4065–4073.
26. OECD, Test No. 309: Aerobic mineralisation in surface water – simulation biodegradation test. In *OECD Guidelines for the Testing of Chemicals, Section 3*, Paris, France, **2004**; p 21.
27. Charlton, S. R.; Parkhurst, D. L., Modules based on the geochemical model PHREEQC for use in scripting and programming languages. *Computers & Geosciences* **2011**, *37*, (10), 1653–1663.
28. Schecher, W. D.; McAvoy, D. C. *MINEQL+: A chemical equilibrium program for personal computers*; Environmental Research Software: Hallowell, ME, US, **2001**.
29. Alvarez-Zaldívar, P.; Payraudeau, S.; Meite, F.; Masbou, J.; Imfeld, G., Pesticide degradation and export losses at the catchment scale: Insights from compound-specific isotope analysis (CSIA). *Water Res.* **2018**, *139*, 198–207.
30. Hammershøj, R.; Birch, H.; Redman, A. D.; Mayer, P., Mixture effects on biodegradation kinetics of hydrocarbons in surface water: Increasing concentrations inhibited degradation whereas multiple substrates did not. *Environ. Sci. Technol.* **2019**, *53*, (6), 3087–3094.
31. Elsayed, O. F.; Maillard, E.; Vuilleumier, S.; Nijenhuis, I.; Richnow, H. H.; Imfeld, G., Using compound-specific isotope analysis to assess the degradation of chloroacetanilide herbicides in lab-scale wetlands. *Chemosphere* **2014**, *99*, 89–95.
32. Ivdra, N.; Herrero-Martin, S.; Fischer, A., Validation of user- and environmentally friendly extraction and clean-up methods for compound-specific stable carbon isotope analysis of organochlorine pesticides and their metabolites in soils. *J. Chromatogr. A* **2014**, *1355*, 36–45.
33. Masbou, J.; Drouin, G.; Payraudeau, S.; Imfeld, G., Carbon and nitrogen stable isotope fractionation during abiotic hydrolysis of pesticides. *Chemosphere* **2018**, *213*, 368–376.
34. Jochmann, M. A.; Blessing, M.; Haderlein, S. B.; Schmidt, T. C., A new approach to determine method detection limits for compound-specific isotope analysis of volatile organic compounds. *Rapid Commun. Mass Spectrom.* **2006**, *20*, (24), 3639–3648.

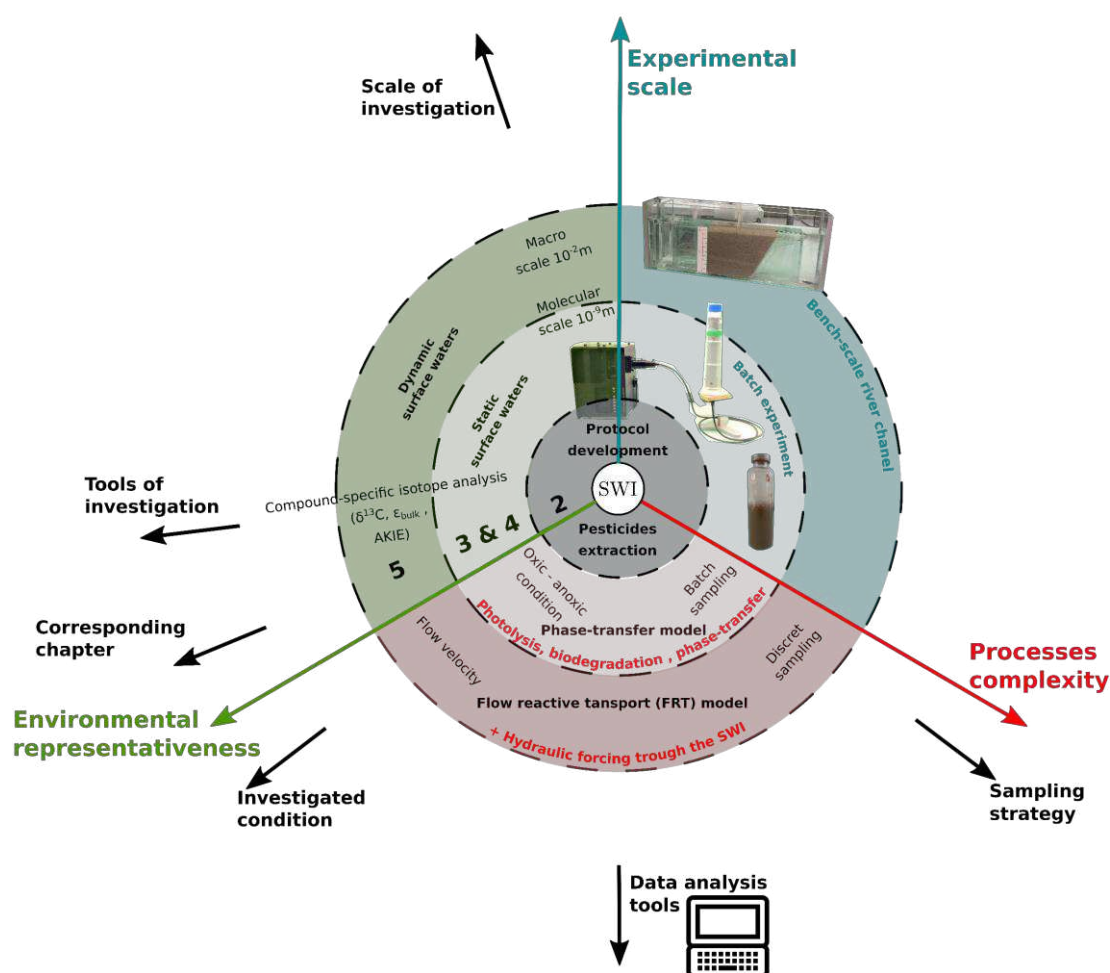
35. Scott, K. M.; Lu, X.; Cavanaugh, C. M.; Liu, J. S., Optimal methods for estimating kinetic isotope effects from different forms of the Rayleigh distillation equation. *Geochim. Cosmochim. Acta* **2004**, *68*, (3), 433–442.
36. Elsner, M.; Zwank, L.; Hunkeler, D.; Schwarzenbach, R. P., A new concept linking observable stable isotope fractionation to transformation pathways of organic pollutants. *Environ. Sci. Technol.* **2005**, *39*, (18), 6896–6916.
37. Villette, C.; Maurer, L.; Wanko, A.; Heintz, D., Xenobiotics metabolization in *Salix alba* leaves uncovered by mass spectrometry imaging. *Metabolomics* **2019**, *15*, (9), 122.
38. Schymanski, E. L.; Jeon, J.; Gulde, R.; Fenner, K.; Ruff, M.; Singer, H. P.; Hollender, J., Identifying small molecules via high resolution mass spectrometry: Communicating confidence. *Environ. Sci. Technol.* **2014**, *48*, (4), 2097–2098.
39. Gao, J.; Ellis, L. B. M.; Wackett, L. P., The University of Minnesota biocatalysis/biodegradation database: improving public access. *Nucleic Acids Res.* **2009**, *38*, (suppl 1), D488–D491.
40. Graham, W. H.; Graham, D. W.; deNoyelles, F.; Smith, V. H.; Larive, C. K.; Thurman, E. M., Metolachlor and alachlor breakdown product formation patterns in aquatic field mesocosms. *Environ. Sci. Technol.* **1999**, *33*, (24), 4471–4476.
41. Lewis, K. A.; Tzilivakis, J.; Warner, D. J.; Green, A., An international database for pesticide risk assessments and management. *Hum. Ecol. Risk Assess.* **2016**, *22*, (4), 1050–1064.
42. Knauer, K.; Homazava, N.; Junghans, M.; Werner, I., The influence of particles on bioavailability and toxicity of pesticides in surface water. *Integr. Environ. Assess. Manage.* **2017**, *13*, (4), 585–600.
43. ECHA, Chapter R.16: Environmental exposure estimation, version 3.0. In *Guidance on Information Requirements and Chemical Safety Assessment*, European Chemicals Agency: Helsinki, Finland, **2016**.
44. Schwarzenbach, R. P.; Gschwend, P. M.; Imboden, D. M., *Environmental organic chemistry*. third ed.; John Wiley & Sons: **2016**, p 1024.
45. Zumstein, M. T.; Helbling, D. E., Biotransformation of antibiotics: Exploring the activity of extracellular and intracellular enzymes derived from wastewater microbial communities. *Water Res.* **2019**, *155*, 115–123.
46. Site, A. D., Factors affecting sorption of organic compounds in natural sorbent/water systems and sorption coefficients for selected pollutants. A review. *J. Phys. Chem. Ref. Data* **2001**, *30*, (1), 187–439.
47. Anslyn, E. V.; Dougherty, D. A., Experiments related to thermodynamics and kinetics. In *Modern Physical Organic Chemistry*, book, University of science book, Ed. Sausalito, CA, US, **2006**; pp 421–441.

48. Mann, T.; Koglin, B.; Von Kienle, H.; Wegmann, U.; Weibrodt, W., Wastewater, 5. Physical Treatment. In *Ullmann's Encyclopedia of Industrial Chemistry*, Wiley: **2012**; Vol. 38, pp 685–710.
49. Feng, P. C. C., Soil transformation of acetochlor via glutathione conjugation. *Pestic. Biochem. Physiol.* **1991**, *40*, (2), 136–142.
50. Mersie, W.; McNamee, C.; Seybold, C.; Wu, J.; Tierney, D., Degradation of metolachlor in bare and vegetated soils and in simulated water–sediment systems. *Environ. Toxicol. Chem.* **2004**, *23*, (11), 2627–2632.
51. Zurrer, D.; Cook, A. M.; Leisinger, T., Microbial desulfonation of substituted naphthalenesulfonic acids and bezenesulfonic acids. *Appl. Environ. Microbiol.* **1987**, *53*, (7), 1459–1463.
52. Uria-Nickelsen, M. R.; Leadbetter, E. R.; Godchaux, W., Comparative aspects of utilization of sulfonate and other sulfur sources by *Escherichia coli* K12. *Arch. Microbiol.* **1994**, *161*, (5), 434–438.
53. Laue, H.; Field, J. A.; Cook, A. M., Bacterial desulfonation of the ethanesulfonate metabolite of the chloroacetanilide herbicide metazachlor. *Environ. Sci. Technol.* **1996**, *30*, (4), 1129–1132.
54. Gutowski, L.; Olsson, O.; Leder, C.; Kümmerer, K., A comparative assessment of the transformation products of *S*-metolachlor and its commercial product Mercantor Gold<sup>®</sup> and their fate in the aquatic environment by employing a combination of experimental and in silico methods. *Sci. Total Environ.* **2015**, *506-507*, 369–379.
55. Huntscha, S.; Singer, H.; Canonica, S.; Schwarzenbach, R. P.; Fenner, K., Input dynamics and fate in surface water of the herbicide metolachlor and of its highly mobile transformation product metolachlor ESA. *Environ. Sci. Technol.* **2008**, *42*, (15), 5507–5513.
56. Bakkour, R.; Bolotin, J.; Sellergren, B.; Hofstetter, T. B., Molecularly imprinted polymers for compound-specific isotope analysis of polar organic micropollutants in aquatic environments. *Anal. Chem.* **2018**, *90*, (12), 7292–7301.
57. Torrentó, C.; Bakkour, R.; Glauser, G.; Melsbach, A.; Ponsin, V.; Hofstetter, T.; Elsner, M.; Hunkeler, D., Solid-phase extraction method for stable isotope analysis of pesticides from large volume environmental water samples. *Analyst* **2019**, *144*, 2898–2908.
58. Schreglmann, K.; Hoeche, M.; Steinbeiss, S.; Reinnicke, S.; Elsner, M., Carbon and nitrogen isotope analysis of atrazine and desethylatrazine at sub-microgram per liter concentrations in groundwater. *Anal. Bioanal. Chem.* **2013**, *405*, (9), 2857–2867.

## Preface to Chapter 5

Chapter 4 underscores higher biodegradation rate at the water-sediment interface under oxic conditions than under anoxic conditions. As oxygen gradient into the river bed sediment is flow dependant,<sup>1</sup> we explore in Chapter 5 the effect of water flow velocity on reactive transport of pesticides in a recirculated bench-scale river channel (15 cm long).

At this bench-scale river channel, the investigation strategy combines pesticide concentration measurements, compound-specific isotopes analysis (CSIA) and flow-reactive-transport (FRT) might be further used to investigate dynamic system with larger complexity (molecules, DOC/POC, etc.).



1. Kaufman, M. H.; Cardenas, M. B.; Buttles, J.; Kessler, A. J.; Cook, P. L. M., Hyporheic hot moments: Dissolved oxygen dynamics in the hyporheic zone in response to surface flow perturbations. *Water Resour. Res.* **2017**, *53*, (8), 6642–6662.

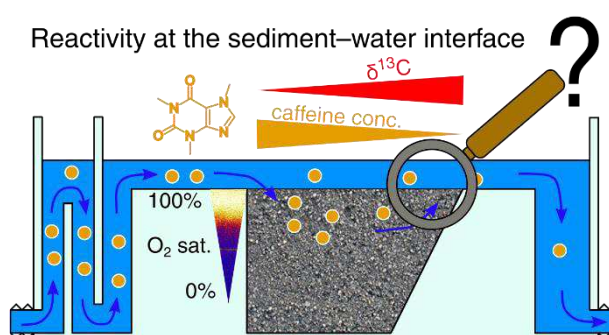


## Chapter 5

# Organic pollutant biodegradation at the sediment–water interface in a bench-scale river channel: insights of compound specific isotopes analysis (CSIA)

### Abstract

Hyporheic exchange flows (HEFs) has been identified as the main process influencing the biodegradation of organic pollutant in surface waters. However, knowledge about the interplay between HEFs, phase transfer and biodegradation at the sediment–water interface (SWI) remains scarce. Predictive modelling studies on horizontal and vertical flows driving pollutant fluxes exist, but they are rarely coupled with the reactivity, known to play a key role in the exchange processes.



Here, we designed a bench-scale river channel to investigate the effects of flow velocity on the transport of organic pollutants. We used caffeine as an organic model compound of human activity with chemical properties close to current agriculturally used pesticides ( $\log P_{ow} < 1$ , very low volatility and  $\log K_{OC}$  around two). We artificially designed an experiment with a very low dissolved (DOC) and particulate organic carbon (POC) to limit biodegradation in the water column. We examined the sorption and the biodegradation of caffeine in the hyporheic zone (HZ) with respect to HEFs under laminar flow with the help of compound specific isotopes analysis (CSIA). We conducted experimental studies combined with a flow-reactive-transport (FRT) modelling, to provide a better understanding on the physical processes.

Batch experiments showed a pseudo first-order kinetic rate constant of caffeine degradation ( $k_{deg}$ ) for the low (0.2:5) and high (1:5) sediment–water ratio between  $0.658 \pm 0.065$  and  $1.616 \pm 0.248$  day<sup>-1</sup> respectively. These kinetic values agreed with previous reported values for the sediment. Our results in the bench-scale river channel suggest that biodegradation prevailed in the water column, accounting for 85% of the initial mass, potentially coming from planktonic cells or soluble extracellular enzymes released by the sediment. Carbon isotope enrichment ( $\varepsilon_C = -0.59 \pm 0.10\text{‰}$ ) suggests a *N*-demethylation pathway which is consistent with the principal degradation pathway of the caffeine. Moreover, for low, medium and high laminar flows, we observed a flow-independence of the biodegradation rates of the caffeine which does not support the hypothesis that HEFs mainly drives the pollutant biodegradation activity.

We anticipate that our experimental design will provide a benchmark on the application of CSIA to interpret the transport and reactivity of organic pollutant at the SWI and to support future investigations of organic pollutant degradation in rivers.

---

This chapter is an edited version of: Droz, B., Drouin, G., Payraudeau, S., Fahs, M. & Imfeld, G. Organic pollutant biodegradation at the sediment–water interface: insights of CSIA at the bench-scale river channel drafted for Env. Sci. & Tech.

B.D. & G. D. contribute equally to this chapter.

## **Introduction**

Organic pollutants, such as pesticides, personal care products, pharmaceuticals and hormones enter in surface waters as point sources from wastewater treatment plants discharge and/or as non-point sources following pesticide applications on agricultural and urban areas. The export of organic pollutants threat aquatic ecosystems and drinking water resources.<sup>1</sup> In surface waters, e.g., rivers, lakes or wetlands, biodegradation, i.e., associated to microorganisms, was identified as the main degradation pathway of organic pollutants.<sup>2</sup> Among the different compartments and interfaces presents in surface waters, the sediment–water interface (SWI) in the sediment bed, called hyporheic zone (HZ), has been identified as the main reactive surface<sup>3-5</sup> where the microbial biofilm dominates the organic pollutant biodegradation.<sup>6</sup> In the water column, suspended solids also offer a specific surface allowing the development of microbial biofilms.<sup>7</sup> Finally, soluble extracellular or intracellular activity can also directly enhance biodegradation in the water column.<sup>8</sup> However, the water column may contain a lower abundance of planktonic microorganisms and a low amount of suspended solids. Therefore, the HZ dominates the degradation.<sup>9</sup> Despite this importance, key processes controlling the HZ organic pollutant biodegradation remained unresolved and were addressed only a in few laboratory studies under dynamic conditions.<sup>9-13</sup>

Hyporheic exchange flows (HEFs), i.e., in- and outflow from the HZ, are hypothesized to affect the organic pollutant transfer time across the HZ, and thus the organic pollutant biodegradation in surface waters.<sup>4, 14, 15</sup> The magnitude of the HEFs is controlled by sediment properties such as hydraulic conductivity and porosity,<sup>16</sup> as well as by hydrological conditions in rivers, including water flow velocity,<sup>17</sup> the succession of base flow and floods,<sup>18</sup> vertical surface-groundwater exchanges,<sup>19</sup> geomorphological variations of river bedforms<sup>12, 20</sup> and also the microbial diversity.<sup>13</sup> These vertical fluxes can sustain a redox gradient over the depth of the HZ, allowing a wide spectrum of possible transformation processes.<sup>21</sup> In addition, the propensity of an organic pollutant to sorb affects its availability to biodegradation in the HZ.<sup>22</sup> Sorption typically increases the organic pollutant residence time within the sediment bed,<sup>23, 24</sup> whereas it reduces the biodegradation availability.<sup>25</sup> Altogether, the complex interplay between hydraulic forcing, organic pollutant partitioning and degradative process currently limits our understanding of the fate of organic pollutants in surface waters.

A complementary approach to investigate the biodegradation process of organic pollutants is the use of compound-specific isotope analysis (CSIA). The CSIA is based on the change in the naturally occurring isotope ratio of an organic pollutant during the course of the degradation, called fractionation. It originates from the fact that light isotopes react slightly faster than the heavy ones at the reactive site.<sup>26</sup> It is generally assumed that no degradative process, i.e., involving no bond breaking or formation of new bonds, like transport and sorption, do not affect the isotope fractionation.<sup>27</sup> In addition, the organic pollutant biodegradation pathway generally modifies the stable isotope signature in a systematic way, and the extent of isotope fractionation may indicate the underlying biodegradation pathway.<sup>28</sup>



The use of CSIA to evaluate organic pollutant degradation has become an established tool in contaminated sites<sup>29-31</sup> and static meso-scale experiments such as a wetland and aquifer plume,<sup>32-35</sup> but was never used in water–sediment systems accounting for phase-transfer and biodegradation, in a dynamic environment such as a river.

Experimental bench-scale river model is particularly well-suited to investigate organic pollutant dissipation under dynamic conditions in water–sediment systems, accounting for phase-transfer and biodegradation, and characterizing the associated processes governing the pollutant transport at the SWI. However, direct observations do not allow us to decipher dissipation due to the transport processes, i.e., diffusion, dispersion, and the reactive processes, i.e., biodegradation, sorption. In this context, physically based flow-reactive-transport (FRT) models can couple three operators representing flow, pollutant transport and reactive processes across the SWI.<sup>17, 36</sup> In a companion paper,<sup>37</sup> we present a FRT model which parametrized the transport and the partitioning of tracers (NaCl and Foron Blue 291) during a lab-scale experiment. We observed that the exchange rates were quasi-proportional to the water column velocity. The model helps with capturing complex interactions between transport and pollutant partitioning to the sediment, whereas incorporation of the chemical reactivity to estimate the biodegradation still needs to be addressed.

In this study, we designed a bench-scale river channel to investigate the effect of flow velocity on organic pollutant transport and biodegradation at the SWI. Caffeine was used as an organic model compound of human activity<sup>38, 39</sup> with chemical properties close to current agriculturally used pesticides ( $\log P_{ow} < 1$ , very low volatility and  $\log K_{OC}$  around two). We artificially designed an experiment with a very low dissolved (DOC) and particulate organic carbon (POC) to limit biodegradation in the water column. We hypothesized that biodegradation mostly occurs at SWI in the pore water, across the oxic layer of the sediment. To test our hypothesis, we conducted experiments with representative water flow regimes of a small river (Strahler number  $< 2$ ). The respective contribution of organic pollutant transport and biodegradation to the overall organic pollutant dissipation was evaluated by coupling organic pollutant concentration measurements, CSIA and FRT modelling.

## **Materials and methods**

A list of all chemicals including suppliers and purities is provided in the Appendix C (AC). All solutions were made with ultrapure water ( $>18 \text{ M}\Omega \text{ cm}$ ). Experiments were carried out with a low alkalinity ( $<10 \text{ mg L}^{-1}$  of inorganic carbon) synthetic water<sup>40</sup> mimicking an agriculturally impacted surface water under low water flow velocity with low DOC (DOC =  $0.8 \pm 0.3 \text{ mg L}^{-1}$ ,  $\text{NO}_3^- = 21 \pm 1.5 \text{ mg L}^{-1}$ ).<sup>41</sup> Synthetic water was prepared one day before the experiment to ensure overnight carbonate dissolution equilibrium. Details on synthetic water preparation and hydrochemistry is provided in AC.

### **Sediment characterizations**

River bed sediment was collected with a shovel from the top 10 cm in the Avenheimerbach river (France,  $48^\circ40'08''\text{N}$ ,  $7^\circ33'50''\text{E}$ ), wet-sieved at 2 mm and stored wet at  $4^\circ\text{C}$  prior to the experiment. Effect of storage on soil microbial diversity was assumed to be negligible at this temperature.<sup>42</sup> A 95:5 ratio mixture between sediment and a pure sand ( $\text{SiO}_2 >98.7\%$ ) from the Kaltenhouse (K30, Quartz d'Alsace S.A, France) was used for the channel experiments. The blend enabled a microbial activity representative of real riverine systems in the sediment bed and ensured sufficient water conductivity to sustain oxygen gradient over the first top centimeters of the sediment. The physico-chemical composition of the blend was measured on the blend by NF/ISO method (details in AC) as follows: Clay 0.73% silt 3.1%, sand 96.2% and organic carbon ( $f_{oc}$ ) 0.095%, with a constant porosity between experiment ( $\Theta = 0.16 \pm 0.02$ ) and saturated conductivity ( $K_s$ ) of  $(4.4 \pm 2.2) \times 10^{-4} \text{ m s}^{-1}$ . Further sediment and blend properties are provided in the AC, Table C1.

### **Batch sorption and biodegradation experiments**

Batch experiments of sorption and biodegradation were conducted to determine the caffeine partitioning coefficient ( $K_d$ ) and oxic biodegradation kinetics rate and parametrize the FRT model described below. Batch sorptions were conducted following OECD 106 procedure<sup>43</sup> with the blend sediment and derived from a linear isotherm. Batch biodegradation experiments were conducted under oxic conditions at constant room temperature ( $20 \pm 5^\circ\text{C}$ ) as previously described (detail on Chap. 4). Two sets of experiments were conducted with two different sediment–water ratios (w/w) and two sediment compositions. A low sediment–water ratio (LSW; 0.2:5) was performed with the Avenheimerbach river sediment only to reflect the caffeine biodegradation rate of the water column containing low total suspended solid (TSS) under medium flow in a river system.<sup>44</sup> A high sediment–water ratio (HSW; 1:5) was performed with the 95:5 blend sediment, as for the channel experiment, to determine the biodegradation rate of caffeine within the river bed sediment. Experiments were carried out in

the dark and at natural constant  $pH$  ( $7.3 \pm 0.2$ ) to limit photolysis and hydrolysis, respectively. 30 mL of a caffeine aqueous solution ( $20 \text{ mg L}^{-1}$ ) were mixed in a 50 mL batch reactor (head space vial crimped with butyl/PTFE caps) with the corresponding amount of the blend sediment to reach the HSW and LSW ratios. The concentration of  $20 \text{ mg L}^{-1}$  was also used in the channel to allow a minimum caffeine mass for both quantification and CSIA. Comparatively, concentrations in wwtp effluents and rivers are 3 to 5 orders of magnitude lower.<sup>39, 45</sup> First, samples were collected after 1 day to ensure a steady state equilibrium of caffeine between water and sediment phase. At each sampling point (days 1, 2, 3, 4, 5, 6, 8, 11, 15 and 18),  $pH$  was recorded with an electrode ( $pH/cond$  multi 350i, WTW). The control hydrolysis experiment was made with synthetic water amended with a 50 mM phosphate buffer ( $\text{KH}_2\text{PO}_4/\text{Na}_2\text{HPO}_4$ ;  $pH = 8$ ). Degradation attributed to caffeine hydrolysis was up to 10% only after 100 days of incubation. The biodegradation rate was retrieved from a first-order dissipation rate considering the contribution of both biodegradation and phase-transfer between the sediment and the water phases, as previously described (detail on Chap. 4 and Appendix B). The model assumes that biodegradation exclusively occurs in the water, in closed steady-state laboratory systems, while the organic pollutant has the similar sorption affinity on dissolved (DOC) and particulate (POC) forms of organic carbon.

### **Bench-scale river channel**

The experiments were conducted in a continuous flow system with recirculated synthetic water (Figure 5.1). The system was consisted of a glass river channel and a 5 L mixing beaker connected together by viton tubing (Iso-versinic®,  $\varnothing_{\text{int.}}$ : 10 mm). The water flow and height were maintained at 20 mm during the experiment with a magnetic centrifuge pump (MD-15R, Iwaki). Channel size was 50 width  $\times$  380 long  $\times$  150 mm high. In the middle of the channel, there was a sediment bed (SB) defining the SWI (150 long  $\times$  100 mm high) and filled with the blended sediment (Figure 5.1). The  $pH$ , conductivity and temperature were continuously monitored with a multimeter (350i WTW), controlled by a self-made code in R<sup>46</sup> inside the mixing beaker. Dissolved oxygen ( $DO$ ) concentration along the water column and the SB was mapped along two vertical profiles (positions depicted in Figure 5.1) using 10 mm width foil sensors (SF-RPSu4, PreSens®), and continuously recorded (VisiSens TD, PreSens®).

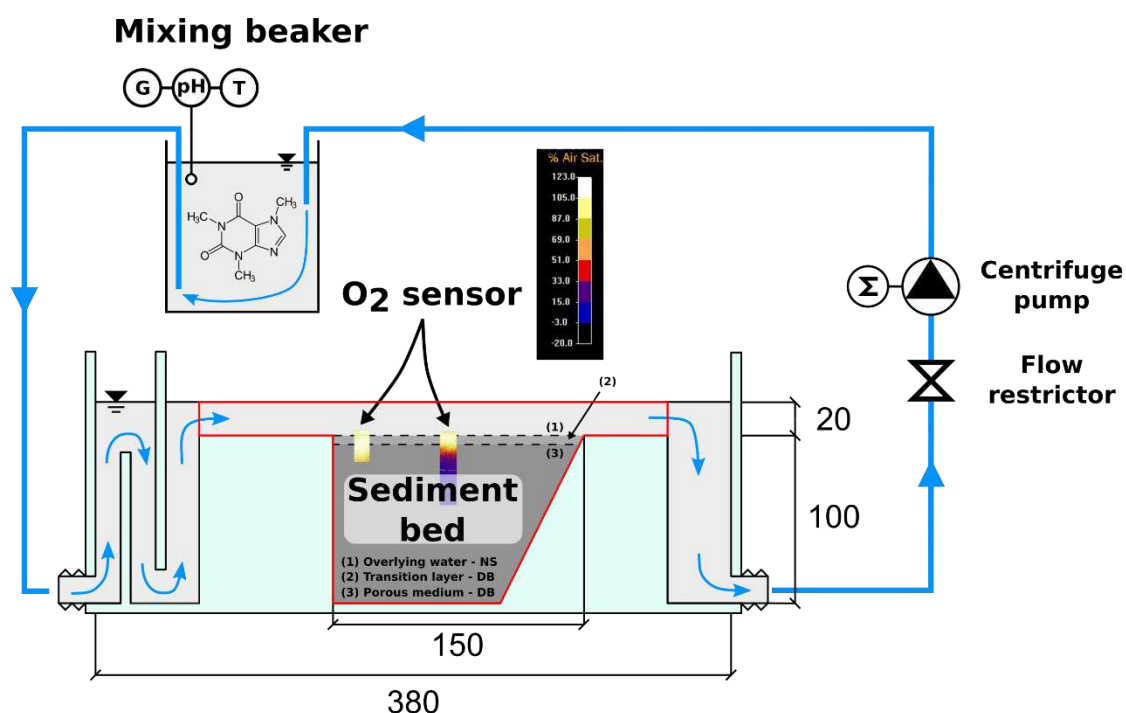


Figure 5.1. Scheme of the bench-scale river channel. Water is recirculated by a centrifuge pump via a mixing beaker used to ensure complete mixing of the experimental solution. The mixing beaker also allows to keep constant water height. Conductivity, pH and temperature are monitored to check stable experimental conditions.  $O_2$  foil sensors are represented at their actual size and display an example of results. The red contour frames the numerical domain. Scale are in mm.

### Dynamic biodegradation experiment

Three experiments were carried out at room temperature ( $20 \pm 5^\circ\text{C}$ ), with low, medium and high flows (Table 5.1), from  $1.12$  to  $4.79 \text{ cm s}^{-1}$ , observed in laminar conditions in small rivers, i.e., with Strahler order  $\leq 2$ . The column's water height in the channel was maintained at  $20 \text{ mm} \pm 5 \text{ mm}$ . Targeted flow velocities ensured laminar flow in the channel. Fume hood light was covered with aluminum stripe to limit exposition to light and avoid photolysis, although the half-life for caffeine degradation  $\approx 170 \text{ h}$ , and indirect photodegradation in our study was unlikely ( $k_{NO_3^-, caf.} = 8.46 \times 10^{-3} \text{ M}^{-1} \text{ s}^{-1}$ ; half-life  $\approx 67 \text{ h}$  for  $NO_3^- = 21 \text{ mg L}^{-1}$ ).<sup>47</sup> Before each new experiment the channel was filled with a new amount of the sediment blend ( $1.3 \pm 0.1 \text{ kg}$ ) and synthetic water ( $\approx 5 \text{ L}$ ). The flow and water height were then adjusted, followed by two to three days of pre-incubation to achieve a stable oxygen gradient in the SB. After reaching the equilibrium, a caffeine aqueous solution ( $6 \text{ mL}$ ;  $10 \text{ g L}^{-1}$ ) was added to the mixing beaker to obtain an initial concentration of  $20 \text{ mg L}^{-1}$  in the channel. Water was sampled with a syringe every one or two days at the outlet of the channel, and frozen ( $-20^\circ\text{C}$ ) prior to

its extraction within 2-3 days. Sample volumes were adjusted over time to obtain the necessary amount for CSIA.

*Table 5.1. Bench-scale river channel experimental conditions.*

	low-flow	medium-flow	high-flow
pH	7.7 ± 0.2	7.5 ± 0.3	8.1 ± 0.3
CaCO <sub>3</sub> (g s <sup>-1</sup> ) <sup>a</sup>	(0.117 ± 0.008) × 10 <sup>-7</sup>	(9.41 ± 0.01) × 10 <sup>-7</sup>	(9.87 ± 0.03) × 10 <sup>-7</sup>
temperature (°C)	20.2 ± 0.9	19.1 ± 0.4	20.7 ± 0.2
water height (mm) <sup>b</sup>	20 ± 2	20 ± 2	20 ± 2
v (cm s <sup>-1</sup> )	1.12 ± 0.04	3.17 ± 0.09	4.79 ± 0.04
Reynold number	124 ± 25	353 ± 69	533 ± 93
TSS (mg L <sup>-1</sup> ) <sup>c</sup>	<4.4	<4.4	<4.4
DOC (mg L <sup>-1</sup> )	0.8 ± 0.3	0.8 ± 0.3	0.8 ± 0.3

<sup>a</sup> Calculated from the relationship between conductivity and the change of cation–anion in water phase. <sup>b</sup> uncertainty estimated by continuous flow recording. <sup>c</sup> Estimate detection limit of TSS estimation on the linear relationship TSS = f(NTU) in AC, Figure C2.

Turbidity, as a proxy of TSS, and hydrochemistry, were recorded during the experiment to quantify potential mass exchanges between the sediment and the water column due to settling or riverbed sediment erosion. Nephelometric turbidity units (NTU) were then daily recorded with a turbidity meter (HI 88713, HANNA). Prior to the experiments, a significant linearity between NTU and TSS was established for the Avenheimerbach sediment (AC, Figure C2). Hydrochemistry, i.e., cation-anion contents, and DOC were measured in the mixing beaker for the three flow conditions, just before the caffeine injection, in the middle and at the end of the experiment. The sample was filtered at 0.45 µm with a CA filter. Cation–anion contents were measured by ionic chromatography (ICS-5000, Dionex/Thermo Fischer, US EPA 300.0). Dissolved organic/inorganic carbon (DOC/DIC) were analyzed by TOC analyzer (TOC-V-CPH Shimadzu, NF EN 1484). The evaporation rate of the system was periodically evaluated by weighting a beaker full of water similar to the mixing beaker. The mass balance of the system was corrected, to take in account the evaporation rate and the cumulative sample removals.

## **Caffeine extraction and quantification**

Water phase was filtered through 0.45  $\mu\text{m}$  on cellulose acetate (CA) filter. Caffeine on water phase was extracted by SPE using SolEx C18 cartridges (1 g phase, Dionex–Thermo Fischer) following in-house method (detail on Appendix B).<sup>48</sup> The extraction yield was  $110 \pm 10\%$  on six 100 mL samples containing between 1 to 1500  $\mu\text{g L}^{-1}$  of caffeine. Caffeine in the bench-scale river channel was quantified by gas chromatography–mass spectrometry up to 1  $\mu\text{g L}^{-1}$  (environmental quantification limit (EQL), equal to the analytical quantification limit divided by the extracted sample volume). Analytical reproducibility was determined by injecting a 500  $\mu\text{g L}^{-1}$  caffeine standard in each independent GC run. Relative reproducibility between measurements and standard concentrations was  $3.5 \pm 15.9\%$ .

## **Compound-specific isotope analysis (CSIA)**

Carbon and nitrogen isotope analysis were conducted according to established procedures for gas chromatography–isotope ratio mass spectrometry (GC-IRMS; detail on AC). Briefly,  $^{13}\text{C}/^{12}\text{C}$  and  $^{15}\text{N}/^{14}\text{N}$  isotope ratio values were measured in triplicate with a typical precision of  $\pm 0.5\text{‰}$  and  $\pm 1.0\text{‰}$  for C and N, respectively. Values were reported in delta notation per element ( $\delta^h E$ ), in parts per thousand (‰) relative to Vienna PeeDee Belemnite (V-PDB) and air standard, respectively.

$$\delta^h E = \frac{R(^h E/^l E)_{\text{sample}}}{R(^h E/^l E)_{\text{standard}}} - 1 \quad (5.1)$$

where  $\delta^h E$  is the isotope signature of the respective element ( $E$ ), and  $R(^h E/^l E)$  are the isotope ratios of heavy ( $h$ ) divided by light ( $l$ ) isotopes, in the sample or the standard. The  $\delta^h E$  linearity range of the caffeine measurement was defined as the range of injected mass of C and N respectively to which the  $\delta^{13}\text{C}$  and  $\delta^{15}\text{N}$  values of the compound stay within a  $\pm 0.5\text{‰}$  and  $\pm 1\text{‰}$  interval respectively<sup>49</sup>, and were established as 8 to 300 ng and 40 to 300 ng (150 to 4500 mV), for C and N, respectively. Initial caffeine isotope signature was evaluated by the GC-IRMS as follows:  $\delta^{13}\text{C}_{GC-IRMS,0} = -30.3 \pm 0.2\text{‰}$  and  $\delta^{15}\text{N}_{GC-IRMS,0} = -2.5 \pm 0.2\text{‰}$ , respectively. Trueness ( $\Delta\delta$ ) of the  $\delta^h E$  measurement was reported for the extraction procedure as  $\Delta\delta^h E$  ( $\Delta\delta^h E = \delta^h E_{\text{ext}} - \delta^h E_{GC-IRMS,0}$ ) where  $\delta^h E_{\text{ext}}$  was the isotope signature after extraction. Water extraction tests have shown insignificant carbon and nitrogen isotope fractionation ( $|\Delta\delta^{13}\text{C}_{\text{ext},w}| < 0.22$  and  $|\Delta\delta^{15}\text{N}_{\text{ext},w}| < 0.63$ ).

Bulk isotopic enrichment factors ( $\varepsilon_{bulk,E}$ ), that relate a change in  $^{13}\text{C}/^{12}\text{C}$  or  $^{15}\text{N}/^{14}\text{N}$  isotope ratios to the extent of degradation, were determined under representative conditions in the closed batch experiments and derived from the Rayleigh equation, eq. 5.2, without forcing the regression through the origin:<sup>50</sup>

$$\ln\left(\frac{\delta^h E(t) + 1}{\delta^h E_0 + 1}\right) = \varepsilon_{bulk,E} \times \ln(C(t)/C_0) \quad (5.2)$$

where  $\delta^h E_0$  and  $\delta^h E(t)$  represent the isotope signatures of an element  $E$  at time zero and  $t$  of the degradation respectively, while  $C(t)/C_0$  is the fraction of the remaining caffeine at time  $t$ .

To interpret and compare  $\varepsilon_{bulk,E}$  values in terms of underlying degradation pathways, apparent kinetic isotope effects ( $AKIE_E$ ) were calculated for each element to correct  $\varepsilon_{bulk,E}$  for isotope dilution, number of reactive sites and intramolecular isotopic competition in eq. 5.3:

$$AKIE_E \approx \frac{1}{1 + z \times \left(\frac{n}{x}\right) \times \frac{\varepsilon_{bulk,E}}{1000}} \quad (5.3)$$

where  $n$  is the total number of atoms of the element,  $x$  the number of atoms in reactive positions and  $z$  the number of atoms which are in intramolecular isotopic competition.<sup>28</sup>

## Flow reactive transport modelling

**General modelling approach** - Physically-based transport modelling is a promising complementary approach to CSIA to provide a mechanistic understanding of the processes governing reactivity at the SWI.<sup>51</sup> Here, we used a 2D flow-reactive-transport (FRT) model to account for transport (eq. 5.4) and linear kinetic sorption (eq. 5.5) described elsewhere<sup>37</sup> coupled with the first-order degradations as described by eq. 5.6:

$$\Theta \times \frac{\partial C_i}{\partial t} + \rho_{bulk} \times \frac{\partial S_i}{\partial t} + u \times \nabla C_i - \nabla \times (D_i \times \nabla C_i) = r_i \quad (5.4)$$

$$\frac{\partial S_i}{\partial t} = \alpha_i \times (K_{d,i} \times C_i - S_i) \quad (5.5)$$

$$r_i = -k_{j,i} \times C_i \quad (5.6)$$

$$\begin{aligned} D_i &= D_{m,i} \times I + D_{disp} \\ &= (\alpha_T \times |u| + D_m) \times \delta_{lm} \\ &+ (\alpha_L - \alpha_T) \times \frac{u_l \times u_m}{|u|} \quad l, m = 1, 2 \end{aligned} \quad (5.7)$$

where  $\Theta$  is the sediment porosity,  $C_i$  [ $\text{M}/\text{L}^3$ ] represents the dissolved concentration of species  $i$ ,  $S_i$  [ $\text{M}^0$ ] is its sorbed concentration controlled by  $K_{d,i}$ , the phase partitioning coefficient of

species  $i$  in  $[L^3/M]$ , and  $\alpha_i$  the first order rate of sorption  $[T^{-1}]$ .  $r_i$  is the first order reactive term of species  $i$  degraded by process  $j$  at rate  $k_{j,i}$ .  $\rho_{bulk}$  is the bulk density of the porous medium  $[M/L^3]$ ,  $D_i$  is the associated dispersion tensor  $[L^2/T]$ , accounting for molecular diffusion ( $D_{m,i}$ )  $[L^2/T]$ , and longitudinal ( $\alpha_L$ ) and transversal ( $\alpha_T$ ) dispersion  $[L]$ ,  $\delta_{lm}$  is the Kronecker function and  $r_i$  is the reactive term representing either sorption or degradation of species  $i$ . The velocity field  $u$  is computed before the transport via a coupled Navier–Stokes and Darcy–Brinkman system of equations, allowing to accurately reproduce velocity profiles at the SWI.<sup>37</sup>

**Isotope fractionation modelling** – Normal kinetic isotope effect, usually observed over contaminant degradation, reflects the slightly faster degradation rates of molecules containing the lightest isotopes ( $^lE$ ), as compared with the ones featuring the most abundant fraction of heavy isotopes ( $^hE$ ). The kinetic isotope fractionation factor ( $\alpha_C$ ), retrieved from laboratory degradation experiments expresses these kinetic differences. It relates the disappearance rates of heavy to light molecules, namely isotopologues, according to eq. 5.8:<sup>30</sup>

$$\alpha_C = 1 + \varepsilon_C = \frac{r^{hE}}{r^{lE}} \quad (5.8)$$

Thus, numerical modelling of isotope fractionation is abled through separate computation of both isotopologues undergoing distinct degradation rates as in eq. 5.9 ( $k^{lE}$  or  $k^{hE}$ ):<sup>52, 53</sup>

$$k^{hE} = (1 + \varepsilon_C) \times k^{lE} \quad (5.9)$$

The total concentration of caffeine can be described as the sum of heavy and light isotopologues ( $E_{tot} = ^lE + ^hE$ ).  $k^{lE}$  is assumed equal to the experimentally determined degradation rates as the natural abundance of  $^lE$  over  $^hE$  is about 99:1 for C and 99.6:0.4 for N.

**Oxygen consumption within the sediment** – The oxygen consumption rate in the sediment ( $k_{O_2}$ ) was monitored at 80 mm beneath the interface immediately after filling the channel with fresh sediment. Oxygen consumption in the sediment bed was attributed to diagenesis of organic matter and nutrient consumption (e.g., ammonium, nitrates, ...) in the blend sediment and the synthetic water.<sup>54</sup> Oxygen consumption within the sediment was modelled by a single first-order reaction term:<sup>17</sup>

$$\frac{d[O_2]}{dt} = k_{O_2} \times [O_2] \quad (5.10)$$

**Oxygen controlled degradation** – The preferential degradation of caffeine under oxic conditions was implemented via a hyperbolic formulation (e.g., Michaelis–Menten type), with a half-saturation constant for oxygen,  $K_M$   $[M L^{-3}]$  according to eq. 5.11. Since  $K_M$  was not available for caffeine oxic degradation,  $K_M$  equal to  $1 \mu\text{mol L}^{-1}$  was used as a default value,



often used in sediment diagenesis models for nitrification.<sup>55</sup> Considering the results presented below, simulations were not sensitive to this value. In this case, a simple first-order caffeine degradation without oxygen dependency would have led to equivalent results:<sup>56</sup>

$$k_{oxic} = k_{max,oxic} \times \frac{[O_2]}{[O_2] + K_M} \quad (5.11)$$

where  $k_{max,oxic}$  [ $T^{-1}$ ] refers to the experimentally determined oxidic degradation rate (i.e., 100% oxygen saturation =  $2.4 \times 10^{-4}$  M),  $[O_2]$  [ $M L^{-3}$ ] to the dissolved oxygen concentration. Then, a first-order reaction term was used to calculate caffeine concentration [ $Caf$ ]:

$$\frac{d[Caf]}{dt} = k_{oxic} \times [Caf] \quad (5.12)$$

For the degradation in the anoxic layers, we considered a constant rate of zero (infinite half-life), following the REACH guidelines,<sup>57</sup> and taking into account that the microbial catabolism pathway of caffeine is an oxidation pathway.<sup>58</sup> In the water column, 100% of oxygen saturation was reached, supporting prevailing oxidic degradation of caffeine. Parameters used in the model are summarized in the AC, Table C2.

## Results and discussion

### Caffeine sorption and degradation batch experiments

The sediment partitioning coefficient ( $K_d$ ) derived from a linear isotherm was equal to  $1.21 \pm 0.08$  L  $kg^{-1}$  for caffeine, or normalized to sediment organic carbon-water partitioning coefficient:  $K_{OC}$  equal to  $12.8 \pm 0.8$  L  $kg^{-1}$  C. Caffeine dissipation and degradation followed pseudo first-order kinetics in LSW and HSW batch experiments (Table 5.2).  $k_{dis}$  for LSW and HSW were  $0.641 \pm 0.064$  and  $1.614 \pm 0.248$  day<sup>-1</sup>, respectively suggesting faster dissipation rate with higher sediment–water ratios (Table 5.2).  $k_{deg}$  for LSW and HSW were  $0.658 \pm 0.065$  and  $1.616 \pm 0.248$  day<sup>-1</sup>, respectively, emphasizing a negligible contribution of sorption to the dissipation process with  $k_{diss} \approx k_{deg}$ . The  $k_{deg}$  values in our experiment ranged of previously estimated values made in the field for the sediments which were between 0.05 and 3.14 day<sup>-1</sup>.<sup>59, 60</sup> However, to the best of our knowledge, caffeine biodegradation rates had never been reported in mesocosms with water and sediment, as performed in the OECD 308 procedure.<sup>61</sup> Differences between kinetic rates for LSW and HSW infirm our hypothesis that the contributive microorganisms to biodegradation are proportional to the content of the total organic carbon (TOC = dissolved + particulate organic carbon).<sup>44</sup> Therefore, the normalized aerobic rate ( $k'_{bio} = k_{deg}/f_{oc}$ ) was higher under LSW ( $k'_{bio,LSW}$  of 6.93) than under HSW

( $k'_{bio,HSW}$  of 0.85). The dispersion of particles may increase the available amount of reactive sites associated to microorganism, resulting in a higher rate, constant in LSW.

*Table 5.2. Biodegradation batches' condition, dissipation and degradation kinetics and C-N isotope fractionation, and bulk enrichment factors at low (LSW) and high (HSW) sediment–water ratios.*

	LSW	HSW
s:w ratio	0.2:5	1:5
pH	7.3 ± 0.2	7.3 ± 0.2
TSS (g L <sup>-1</sup> )	4.53 ± 0.06	186 ± 13
$f_{oc}$ (%)	1.90	0.095 <sup>a</sup>
$k_{diss}$ (days <sup>-1</sup> )	0.641 ± 0.064	1.614 ± 0.248
$k_{degr}$ (days <sup>-1</sup> )	0.658 ± 0.065	1.616 ± 0.248
DegT <sub>50</sub> (days)	1.05 ± 0.21	0.43 ± 0.13
$\Delta\delta^{13}C$ (‰)	-4.98 ± 0.18	-3.80 ± 0.48
$\Delta\delta^{15}N$ (‰) <sup>b</sup>	<0.7	<0.7
$\epsilon_C$ (‰) <sup>c</sup>	-0.69 ± 0.07	-0.59 ± 0.10

<sup>a</sup> Calculated from the blend sediment–water ratio from the characterization in the AC, Table C1, <sup>b</sup> not significant, <sup>c</sup> coefficient of determination ( $R^2 > 0.9$ ).

Carbon isotope enrichment factor ( $\epsilon_C$ ) for caffeine in the water phase did not differ significantly under both conditions (Table 5.2; AC, Figure C3).  $AKIE_C$  values between  $1.005 \pm 0.001$  and  $1.004 \pm 0.001$  for LSW and HSW, respectively, were in the range of previous values for *N*-demethylation pathway, with an  $AKIE_C$  of  $1.002 \pm 0.002$ ,<sup>62, 63</sup> which is the main biodegradation pathway identified for caffeine (AC, Figure C1).<sup>58</sup> In contrast, the *N* fractionation was not significant ( $\Delta\delta^{15}N < 0.7\%$ ).

### **Influence of water flow on the depth of the oxic layer in sediment**

Simulated oxygen gradients fitted well with the observed gradients under both low, medium and high flow conditions (Figure 5.2, model parameter detailed in the AC, Table C2). This confirms the ability of the FRT model to reproduce the complex interplay between caffeine transport and biodegradation at the SWI. As hypothesized, the oxygen reached deeper sediment layers with increasing water flow. Under low flow conditions, the oxic layer extended by up to 10 mm below the SWI (Figure 5.2a). Under medium and high flow conditions, oxygen diffused up to 20 to 30 mm below the sediment surface (Figure 5.2b). Medium flow conditions displayed an intermediate oxygen penetration. Interestingly, under high flow conditions, the expansion of the oxic layer was not parallel to the sediment surface. Oxygen penetration was enhanced when entering the sediment bed. This is due to the flow regime in the bench-scale river channel, typical of rivers with bedforms (i.e., pumping flow).

While the bedforms generally strengthen mass exchange at the SWI,<sup>37 13</sup> they can also locally favour deeper oxic sediment layers.<sup>17</sup> This effect may enhance caffeine biodegradation in rivers featuring instream structures by creating successive and multiple zones of increased oxygen penetration.<sup>64</sup>

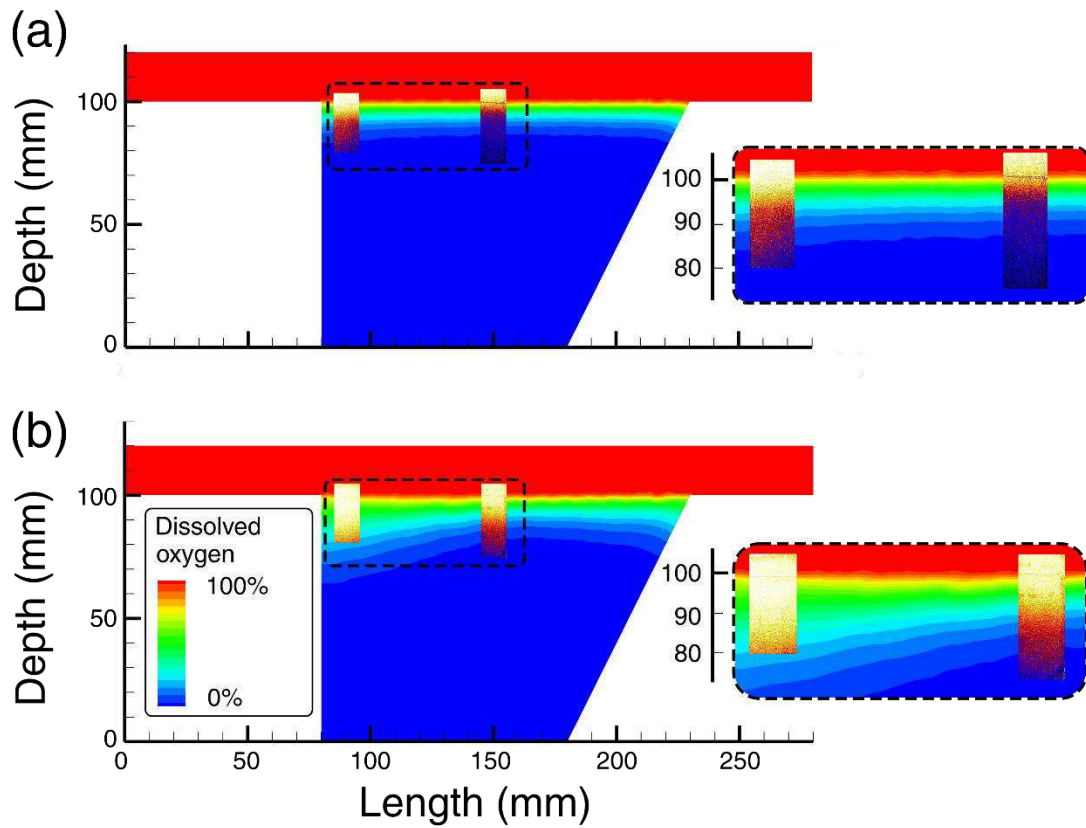


*Figure 5.2. Observed ( $O_2$  foil sensors) and simulated (whole domain mapping) oxygen gradients in the sediment bed under low (a) and high (b) flow.*

### **Influence of water flow on caffeine biodegradation at the SWI**

The water column hydrochemistry ( $\text{Na}^+$ ,  $\text{K}^+$ ,  $\text{Mg}^{2+}$ ,  $\text{Ca}^{2+}$ ,  $\text{Cl}^-$ ,  $\text{NO}_3^-$ ,  $\text{SO}_4^{2-}$ , DOC) remained constant during the experiment under all flow conditions, although a low dissolution of carbonate occurred (Table 5.1; AC, Figure C4). Carbonate dissolution could be estimated with the increase of conductivity but represented only 0.04 % of the initial sediment mass. This suggests a fairly stable system with minor changes in redox conditions within the sediment bed. Oxygen gradient within the sediment bed lightly fluctuated (approx.  $\pm 2$  mm) over the course of the experiments. TSS concentrations in the mixing beaker were systematically below the detection limit ( $<4.4$  mg  $\text{L}^{-1}$ ) in the water column.

Caffeine dissipation patterns were similar under all tested flow conditions (Figure 5.3). Time series could be decomposed into two main phases, as depicted by the shaded areas and the associated segments in Figure 5.3. For 1.5 days (phase 1) in each experiment, caffeine concentrations decreased slowly while carbon isotope signature remained fairly stable ( $\approx C_0 = 20$  mg  $\text{L}^{-1}$ , and  $\delta^{13}\text{C} -30.2 \pm 0.7\%$ ). Then, caffeine concentrations decreased up to 0 mg  $\text{L}^{-1}$  (EQL = 1  $\mu\text{g L}^{-1}$ ) while  $\delta^{13}\text{C}$  increased from the initial isotope signature up to  $-25.8 \pm 1.1\%$  within 1 to 2 days (phase 2). This was consistent with the change in concentrations and  $\delta^{13}\text{C}$  of the caffeine measured during the batch experiment. C-CSIA confirms that biodegradation was a major process of caffeine dissipation in the bench-scale river channel.

However, a detailed analysis of caffeine degradation in the bench-scale river channel was limited by the low temporal sampling resolution used during these experiments (about 1 day on average). Indeed, the rapid decrease of caffeine concentrations in phase 2 was only captured by one sampling point. In addition, the FRT model, as currently implemented, could not reproduce the two successive phases of the experimentally observed caffeine dissipation with a single set of parameters. Nonetheless, using different model parameterizations for phase 1 (transport only, no degradation) and phase 2 (transport and degradation), the FRT model allowed us to reproduce the observed caffeine degradation and isotope signature time-series. As the two different  $k_{deg}$  values for phases 1 and 2 reflected different degradation rates, this analysis helped understanding and identifying the variables driving caffeine dissipation at the SWI.

Phase 1 suggests a lag-phase of microbial activity at the beginning of the experiments. The slow concentration decreases during phase 1 emphasise caffeine penetration within the sediment and sorption with limited degradation. Indeed, it fitted with the numerical simulations, considering that caffeine did not undergo significant degradation during phase 1 (represented in the box ‘phase 1’ of Figure 5.3, with black lines). The absence of significant isotope fractionation also supports the fact that caffeine degradation was limited during phase 1. Microorganisms in contact with the new organic pollutants (caffeine was not quantified in the Avenheimerbach sediment and no waste-water water flow velocity existed upstream the

sampling points) may not immediately adapt, and need time to develop the ability to degrade new organic pollutants.<sup>65</sup>

As reported previously for atrazine degradation in soil columns, transient pollution (<1 day) punctually occurring, are likely not or only slightly biodegraded in the river sediment.<sup>66</sup> The same work also suggests that organic pollutant fate modelling under transient conditions should use a Monod kinetic accounting to target microbial population growth/decay rather than a first-order kinetics rate.

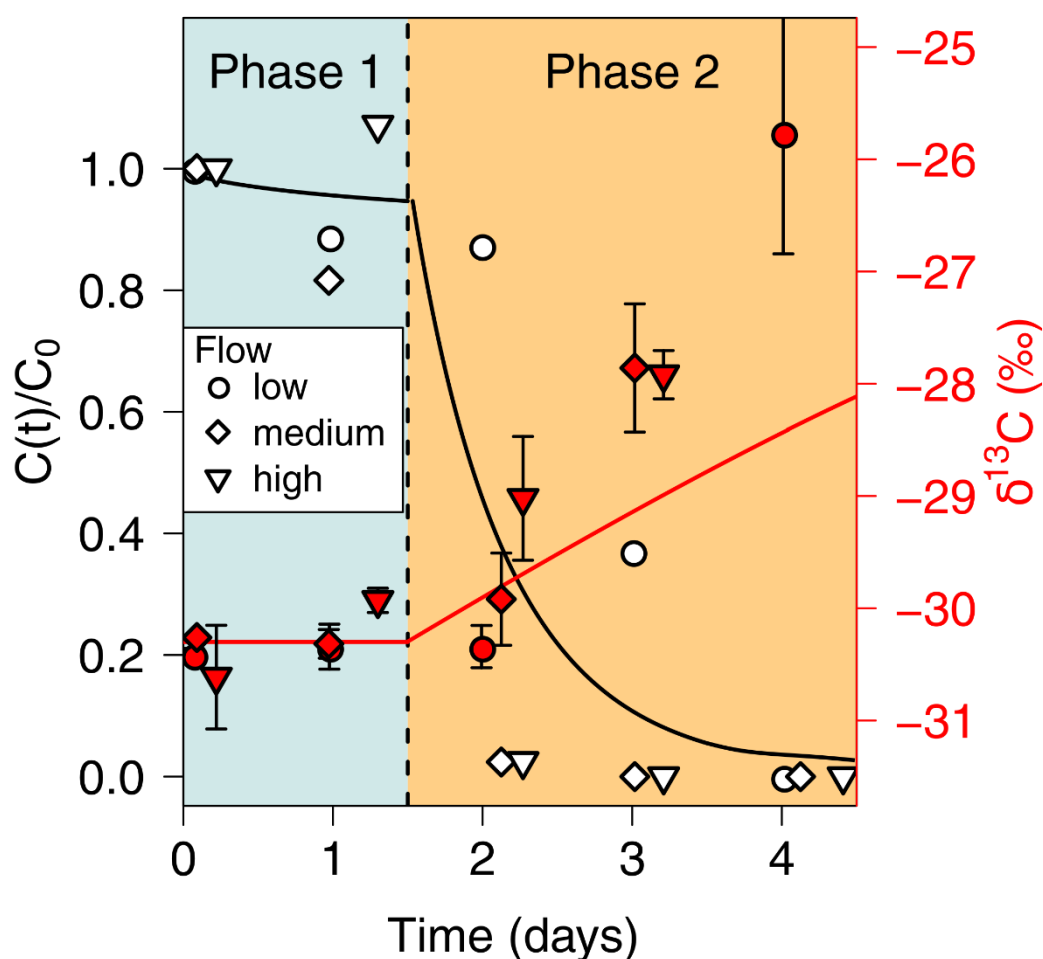


Figure 5.3. Observed (points) and simulated (lines) caffeine concentrations ( $C(t)/C_0$ , black) and isotope signatures ( $\delta^{13}C$ , red) for the low, medium and high flow conditions. Simulation results, provided here for the medium flow conditions, did not change much among the tested conditions.

In contrast, the rapid decrease of caffeine concentrations during phase 2, emphasized that biodegradation predominated in the water column rather than in the oxic layer of the sediment as originally hypothesized. According to the simulation results, a complete degradation of caffeine in 1 to 2 days in the water column, irrespective of the flow conditions,

can only be explained assuming biodegradation occurs in the water column (see the line featured in the box phase 2 of *Figure 5.3*). Indeed, the shallow oxic layer sediment may not allow sufficient contact of caffeine with the reactive zone to explain a complete degradation within 1 to 2 days. It is predicted that only 15% of the initial mass of caffeine will be degraded after 2 days when considering that biodegradation exclusively occurs in the oxic part of the sediment. Interestingly, the best simulation fit with the experimental results was obtained with a degradation rate in the water column corresponding to that which derived from the batch experiment with the smallest sediment–water ratio. This sediment–water ratio was the closest to the TSS concentrations in the bench-scale river channel.

Caffeine degradation in phase 2 was also confirmed by the observed and the simulated change of carbon isotope signatures of caffeine, reflecting a degradation extent larger than  $97 \pm 1\%$  ( $\epsilon_C = -0.69 \pm 0.07\text{‰}$ ) at the end of each experiment, as reproduced by the FRT model. Biodegradation of caffeine may either be supported by the formation of extracellular polymeric substance (EPS)-bound enzyme at the sediment surface or directly by biodegradation in the water column by soluble extracellular or intracellular enzymes. On the one hand, EPS-bound enzymes developing at the SWI may amplify biodegradation by retaining and concentrating highly diluted organic pollutants from the water column.<sup>6</sup> While EPS-bound enzymes can also develop around suspended particles or DOC,<sup>7</sup> our experiments contained an undetectable concentration of POC/DOC in any flow conditions which presume limited effect of EPS-bound enzymes to POC/DOC. On the other hand, planktonic microorganisms, i.e., not attached, or soluble extracellular enzyme activity may also directly promote biodegradation in the water column.<sup>8</sup> However, in such conditions, soluble extracellular biodegradation activity seems negligible, and EPS-bound enzymes represented only 20% of degradation by the intracellular activity for six tested antibiotics (amoxicillin, ampicillin, clindamycin, daptomycin, linezolid, and vancomycin) in the wastewater sludge.<sup>67</sup> Altogether, these observations support the initial assumption that higher water flows increase an/the oxic sediment layer, thereby enhancing caffeine biodegradation. They also highlight the need to numerically account for EPS-bound enzymes on suspended and soluble particles' transport within the water column and for further investigations about the relationships between soluble extracellular enzymes, TSS concentrations and organic pollutant degradation rates.

## **Environmental implications and perspectives**

Here, we present an investigation on the effect of flow velocity on organic pollutant transport and biodegradation at the SWI, using caffeine as an organic compound model of human activity. This preliminary analysis of experimental and numerical data emphasized that biodegradation patterns under low and high flow conditions did not significantly differ, although the oxygen gradients expanded as a function of the water flow velocity. The bench-

scale river channel coupled with the FRT model proved suited to identify compartments of preferential degradation at the SWI, and caffeine biodegradation prevailed in the water column. As biofilm attached (EPS plus intracellular enzyme) to suspended or bed sediment seems to dominate the biodegradation activity,<sup>6</sup> we had rather expected limited degradation in the water column in the experiment's conditions, i.e., very low POC/DOC (less than 0.8 mg L<sup>-1</sup>).<sup>12</sup> This observation only concerns the laminar conditions and advocates for testing the effect of different flows, DOC, POC, and for evaluating the microbial diversity, distribution and activity within the water column, to understand the variables driving organic pollutant degradation at the SWI. Altogether, this suggests that caffeine degradation, and hypothetically other organic compounds with similar sorption and biodegradation rates in rivers may be flow independent.

The FRT model proved suited to reproduce the oxic gradient at the SWI. As oxygen is a major control of organic matter, cycling at the SWI,<sup>54</sup> this model may be further used in different studies such as sediment diagenesis in water systems.<sup>68</sup> Analysis with the FRT model of the first phase 1, characterized by sorption and transport only, and of the second phase, with sorption, transport and biodegradation, emphasized the main processes controlling caffeine biodegradation in the bench-scale river channel. However, the FRT model could not reproduce the caffeine dissipation during both phases with only one  $k_{deg}$  value, suggesting that microbial equilibrium in the bench-scale river channel was not achieved when caffeine was spiked. Incorporating growth/decay of microbial populations, associated with degradation in the FRT model, might improve the prediction of biodegradation for these transient phases.

Our results highlighted the prevailing of caffeine biodegradation in the water column during phase 2, which could be attributed to EPS-bound enzymes on suspended or soluble particles stuck to the glass into the water, microbial development on the surface of the sediment and pipe of the experimental system, or a not yet understood abiotic degradation pathway. To our knowledge, water column biodegradation, hypothetically associated with soluble extra or intracellular enzyme activity has been already observed<sup>5, 9</sup> but never demonstrated. Bioassay measuring enzymatic degradation activity over the course of the experiment<sup>67, 69</sup> might help us with elucidating the location of the biodegradation activity, i.e., EPS-bound enzyme, soluble extracellular or intracellular activity at different locations, i.e., water column, porewater and sediment phase. This understanding will allow us to develop microbial activity modelling that would help with understanding processes occurring in the bench-scale river channel. Predictions of caffeine behavior with the FRT model may only be possible with a specific account of the dynamics of microbial degradation activities.

We observed two limitations in our experimental setup. Firstly, the low temporal sampling resolution of caffeine concentration measurements did not allow us to determine the kinetics and to delineate the two phases, thus hampering the interpretation of caffeine biodegradation process. A continuous online measurement of the organic pollutant concentration, for instance using fluorescence measurement, may overcome this problem in future experiments. Secondly, the low  $\epsilon$  value for the demethylation of caffeine severely

limited the detection of low extent of caffeine biodegradation (Appendix B, eq. B9). At least 72% of the caffeine should be biodegraded to reliably detect biodegradation with CSIA. To overcome this problem, another organic pollutant model, such as ibuprofen,<sup>34</sup> with a higher biodegradation rate ( $> 0.2 \text{ d}^{-1}$ ) would allow an optimal study in a laboratory time scale.

Overall, this study opens the door for more systematic investigations of environmental variables driving the organic pollutant dissipation in rivers because it relies on controlled and realistic experiment mimicking a river while combining caffeine concentration measurements, CSIA and FRT modelling. Although the microbial activity was not followed, the proposed experimental setup allows for more systematic investigations of organic pollutant transport and biodegradation at the SWI under more environmentally relevant conditions than the usual batch water–sediment systems (i.e., OECD 308).

## References

1. Escher, B. I.; Stapleton, H. M.; Schymanski, E. L., Tracking complex mixtures of chemicals in our changing environment. *Science* **2020**, *367*, (6476), 388–392.
2. Fenner, K.; Canonica, S.; Wackett, L. P.; Elsner, M., Evaluating pesticide degradation in the environment: Blind spots and emerging opportunities. *Science* **2013**, *341*, (6147), 752–758.
3. Writer, J. H.; Antweiler, R. C.; Ferrer, I.; Ryan, J. N.; Thurman, E. M., In-stream attenuation of neuro-active pharmaceuticals and their metabolites. *Environ. Sci. Technol.* **2013**, *47*, (17), 9781–9790.
4. Schaper, J. L.; Posselt, M.; Bouchez, C.; Jaeger, A.; Nuetzmann, G.; Putschew, A.; Singer, G.; Lewandowski, J., Fate of trace organic compounds in the hyporheic zone: Influence of retardation, the benthic biolayer, and organic carbon. *Environ. Sci. Technol.* **2019**, *53*, (8), 4224–4234.
5. Schaper, J. L.; Seher, W.; Nützmänn, G.; Putschew, A.; Jekel, M.; Lewandowski, J., The fate of polar trace organic compounds in the hyporheic zone. *Water Res.* **2018**, *140*, 158–166.
6. Battin, T. J.; Besemer, K.; Bengtsson, M. M.; Romani, A. M.; Packmann, A. I., The ecology and biogeochemistry of stream biofilms. *Nat. Rev. Microbiol.* **2016**, *14*, (4), 251–263.
7. De la Cruz Barrón, M.; Merlin, C.; Guilloteau, H.; Montargès-Pelletier, E.; Bellanger, X., Suspended materials in river waters differentially enrich class 1 integron- and IncP-1 plasmid-carrying bacteria in sediments. *Front. Microbiol.* **2018**, *9*, 1443.
8. Baltar, F., Watch out for the “living dead”: Cell-free enzymes and their fate. *Front. Microbiol.* **2018**, *8*, 2438.



9. Kunkel, U.; Radke, M., Biodegradation of acidic pharmaceuticals in bed sediments: Insight from a laboratory experiment. *Environ. Sci. Technol.* **2008**, *42*, (19), 7273–7279.
10. Li, Z.; Sobek, A.; Radke, M., Flume experiments to investigate the environmental Fate of Pharmaceuticals and Their Transformation Products in Streams. *Environ. Sci. Technol.* **2015**, *49*, (10), 6009–6017.
11. Mechelke, J.; Rust, D.; Jaeger, A.; Hollender, J., Enantiomeric fractionation during biotransformation of chiral pharmaceuticals in recirculating water-sediment test flumes. *Environ. Sci. Technol.* **2020**, *54*, (12), 7291–7301.
12. Jaeger, A.; Coll, C.; Posselt, M.; Mechelke, J.; Rutere, C.; Betterle, A.; Raza, M.; Mehrrens, A.; Meinikmann, K.; Portmann, A.; Singh, T.; Blaen, P. J.; Krause, S.; Horn, M. A.; Hollender, J.; Benskin, J. P.; Sobek, A.; Lewandowski, J., Using recirculating flumes and a response surface model to investigate the role of hyporheic exchange and bacterial diversity on micropollutant half-lives. *Environ. Sci. Process. Impacts* **2019**, *21*, (12), 2093–2108.
13. Posselt, M.; Mechelke, J.; Rutere, C.; Coll, C.; Jaeger, A.; Raza, M.; Meinikmann, K.; Krause, S.; Sobek, A.; Lewandowski, J.; Horn, M. A.; Hollender, J.; Benskin, J. P., Bacterial diversity controls transformation of wastewater-derived organic contaminants in river-simulating flumes. *Environ. Sci. Technol.* **2020**, *54*, (9), 5467–5479.
14. Zarnetske, J. P.; Haggerty, R.; Wondzell, S. M.; Baker, M. A., Dynamics of nitrate production and removal as a function of residence time in the hyporheic zone. *J. Geophys. Res.: Biogeosci.* **2011**, *116*, G01025.
15. Schaper, J. L.; Posselt, M.; McCallum, J. L.; Banks, E. W.; Hoehne, A.; Meinikmann, K.; Shanafield, M. A.; Batelaan, O.; Lewandowski, J., Hyporheic exchange controls fate of trace organic compounds in an urban stream. *Environ. Sci. Technol.* **2018**, *52*, (21), 12285–12294.
16. Hester, E. T.; Young, K. I.; Widdowson, M. A., Mixing of surface and groundwater induced by riverbed dunes: Implications for hyporheic zone definitions and pollutant reactions. *Water Resour. Res.* **2013**, *49*, (9), 5221–5237.
17. Kaufman, M. H.; Cardenas, M. B.; Buttles, J.; Kessler, A. J.; Cook, P. L. M., Hyporheic hot moments: Dissolved oxygen dynamics in the hyporheic zone in response to surface flow perturbations. *Water Resour. Res.* **2017**, *53*, (8), 6642–6662.
18. Dwivedi, D.; Steefel, C. I.; Arora, B.; Newcomer, M.; Moulton, J. D.; Dafflon, B.; Faybishenko, B.; Fox, P.; Nico, P.; Spycher, N.; Carroll, R.; Williams, K. H., Geochemical exports to river from the intrameander hyporheic zone under transient hydrologic conditions: East river mountainous watershed, Colorado. *Water Resour. Res.* **2018**, *54*, (10), 8456–8477.
19. Lansdown, K.; Heppell, C. M.; Trimmer, M.; Binley, A.; Heathwaite, A. L.; Byrne, P.; Zhang, H., The interplay between transport and reaction rates as controls on nitrate attenuation in permeable, streambed sediments. *J. Geophys. Res.: Biogeosci.* **2015**, *120*, (6), 1093–1109.

20. Briggs, M. A.; Lautz, L. K.; Hare, D. K., Residence time control on hot moments of net nitrate production and uptake in the hyporheic zone. *Hydrol. Process.* **2014**, *28*, (11), 3741–3751.
21. Meckenstock, R. U.; Elsner, M.; Griebler, C.; Lueders, T.; Stumpp, C.; Aamand, J.; Agathos, S. N.; Albrechtsen, H.-J.; Bastiaens, L.; Bjerg, P. L.; Boon, N.; Dejonghe, W.; Huang, W. E.; Schmidt, S. I.; Smolders, E.; Sørensen, S. R.; Springael, D.; van Breukelen, B. M., Biodegradation: Updating the concepts of control for microbial cleanup in contaminated aquifers. *Environ. Sci. Technol.* **2015**, *49*, (12), 7073–7081.
22. Liao, Z.; Lemke, D.; Osenbrück, K.; Cirpka, O. A., Modeling and inverting reactive stream tracers undergoing two-site sorption and decay in the hyporheic zone. *Water Resour. Res.* **2013**, *49*, (6), 3406–3422.
23. Ren, J.; Packman, A. I., Modeling of simultaneous exchange of colloids and sorbing contaminants between streams and streambeds. *Environ. Sci. Technol.* **2004**, *38*, (10), 2901–2911.
24. Ren, J. H.; Packman, A. I., Stream-subsurface exchange of zinc in the presence of silica and kaolinite colloids. *Environ. Sci. Technol.* **2004**, *38*, (24), 6571–6581.
25. Menz, J.; Müller, J.; Olsson, O.; Kümmerer, K., Bioavailability of antibiotics at soil–water interfaces: A comparison of measured activities and equilibrium partitioning estimates. *Environ. Sci. Technol.* **2018**, *52*, (11), 6555–6564.
26. Elsner, M., Stable isotope fractionation to investigate natural transformation mechanisms of organic contaminants: principles, prospects and limitations. *J. Environ. Monit.* **2010**, *12*, (11), 2005–2031.
27. Aelion, C. M.; Höhener, P.; Hunkeler, D.; Aravena, R., *Environmental isotopes in biodegradation and bioremediation*. CRC press: **2009**; p 450.
28. Elsner, M.; Zwank, L.; Hunkeler, D.; Schwarzenbach, R. P., A new concept linking observable stable isotope fractionation to transformation pathways of organic pollutants. *Environ. Sci. Technol.* **2005**, *39*, (18), 6896–6916.
29. Hermon, L.; Denonfoux, J.; Hellal, J.; Joulian, C.; Ferreira, S.; Vuilleumier, S.; Imfeld, G., Dichloromethane biodegradation in multi-contaminated groundwater: Insights from biomolecular and compound-specific isotope analyses. *Water Res.* **2018**, *142*, 217351–357226.
30. Hunkeler, D.; Meckenstock, R. U.; Lollar, B. S.; Schmidt, T. C.; Wilson, J. T. *A guide for assessing biodegradation and source identification of organic ground water contaminants using compound specific isotope analysis (CSIA)*; Environmental Protection Agency (EPA), US: **2008**; p 68.
31. Phillips, E.; Gilevska, T.; Horst, A.; Manna, J.; Seger, E.; Lutz, E. J.; Norcross, S.; Morgan, S. A.; West, K. A.; Mack, E. E.; Dworatzek, S.; Webb, J.; Lollar, B. S., Transformation of chlorofluorocarbons investigated via stable carbon compound-specific isotope analysis. *Environ. Sci. Technol.* **2019**, *54*, (2), 870–878

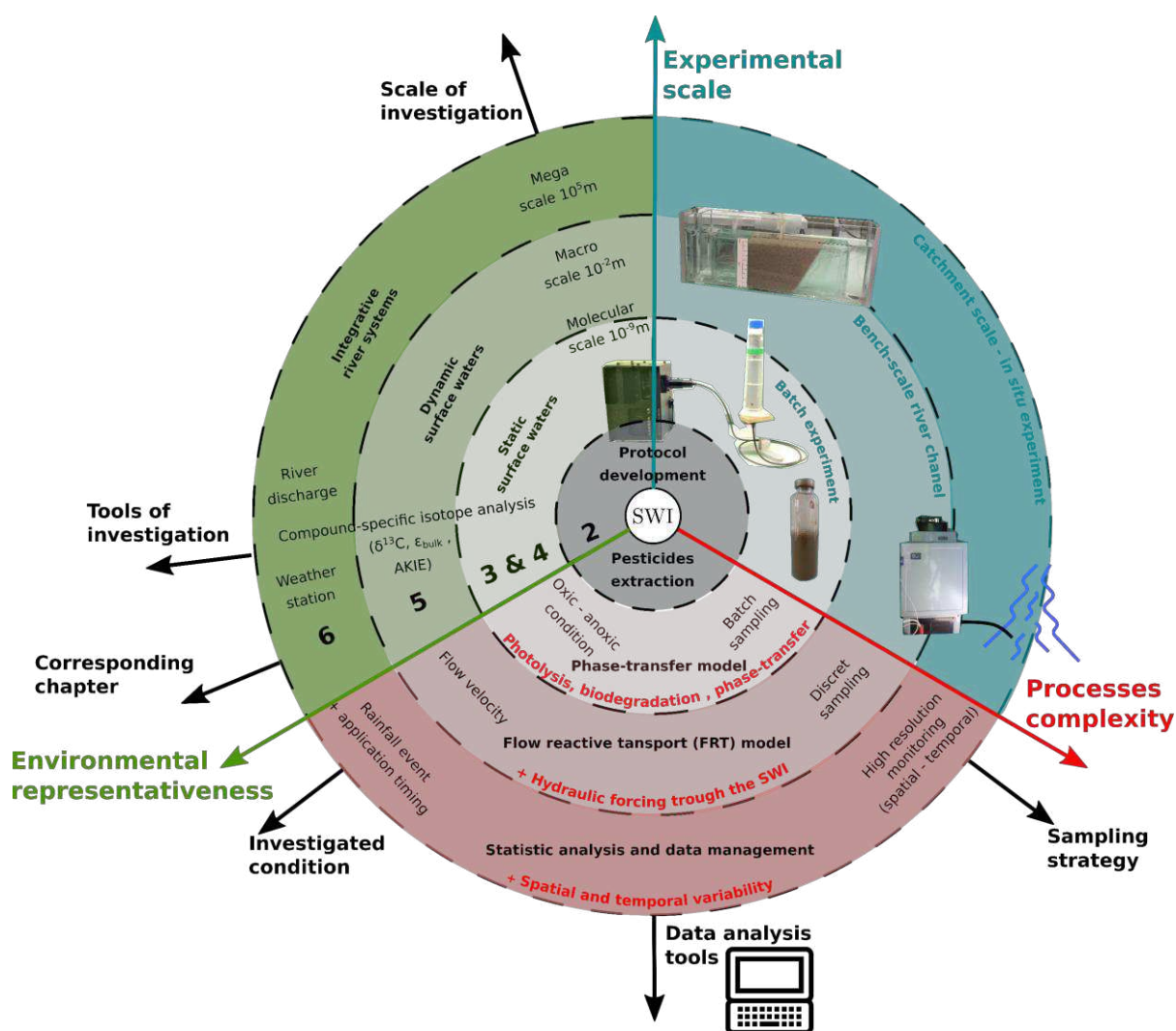
32. Elsayed, O. F.; Maillard, E.; Vuilleumier, S.; Nijenhuis, I.; Richnow, H. H.; Imfeld, G., Using compound-specific isotope analysis to assess the degradation of chloroacetanilide herbicides in lab-scale wetlands. *Chemosphere* **2014**, *99*, 89–95.
33. Hijosa-Valsero, M.; Matamoros, V.; Sidrach-Cardona, R.; Martín-Villacorta, J.; Bécares, E.; Bayona, J. M., Comprehensive assessment of the design configuration of constructed wetlands for the removal of pharmaceuticals and personal care products from urban wastewaters. *Water Res.* **2010**, *44*, (12), 3669–3678.
34. Schürner, H. K. V.; Maier, M. P.; Eckert, D.; Brejcha, R.; Neumann, C.-C.; Stumpp, C.; Cirpka, O. A.; Elsner, M., Compound-specific stable isotope fractionation of pesticides and pharmaceuticals in a mesoscale aquifer model. *Environ. Sci. Technol.* **2016**, *50*, (11), 5729–5739.
35. Blázquez-Pallí, N.; Shouakar-Stash, O.; Palau, J.; Trueba-Santiso, A.; Varias, J.; Bosch, M.; Soler, A.; Vicent, T.; Marco-Urrea, E.; Rosell, M., Use of dual element isotope analysis and microcosm studies to determine the origin and potential anaerobic biodegradation of dichloromethane in two multi-contaminated aquifers. *Sci. Total Environ.* **2019**, *696*, 134066.
36. Angot, P.; Goyeau, B.; Ochoa-Tapia, J. A., Asymptotic modeling of transport phenomena at the interface between a fluid and a porous layer: Jump conditions. *Phys. Rev. E* **2017**, *95*, (6), 063302.
37. Drouin, G.; Fahs, M.; Droz, B.; Younes, A.; Imfeld, G.; Payraudeau, S., Pollutant dissipation at the sediment–water interface: a robust discrete continuum numerical model and recirculating laboratory experiments. *Water Resour. Res.* **2020**, *submitted*.
38. Henderson, A.; Ng, B.; Landeweer, S.; Quinete, N.; Gardinali, P., Assessment of sucralose, caffeine and acetaminophen as anthropogenic tracers in aquatic systems across Florida. *Bull. Environ. Contam. Toxicol.* **2020**, *105*, 351–357.
39. Buerge, I. J.; Poiger, T.; Müller, M. D.; Buser, H.-R., Caffeine, an anthropogenic marker for wastewater contamination of surface waters. *Environ. Sci. Technol.* **2003**, *37*, (4), 691–700.
40. Smith, E. J.; Davison, W.; Hamilton-Taylor, J., Methods for preparing synthetic freshwaters. *Water Res.* **2002**, *36*, (5), 1286–1296.
41. Raymond, P. A.; Spencer, R. G. M., Chapter 11 - Riverine DOM. In *Biogeochemistry of marine dissolved organic matter (Second edition)*, Hansell, D. A.; Carlson, C. A., Eds. Academic Press: Boston, US, **2015**; pp 509–533.
42. Lee, Y.; Lorenz, N.; Dick, L.; Dick, R., Cold storage and pretreatment incubation effects on soil microbial properties. *Soil Sci. Soc. Am. J.* **2007**, *71*, (4), 1299–1305.
43. OECD, Test No. 106: Adsorption – desorption using a batch equilibrium method. In *OECD Guidelines for the Testing of Chemicals, Section 1*, OECD Publishing: Paris, France, **2000**, p 45.

44. Honti, M.; Hahn, S.; Hennecke, D.; Junker, T.; Shrestha, P.; Fenner, K., Bridging across OECD 308 and 309 data in search of a robust biotransformation indicator. *Environ. Sci. Technol.* **2016**, *50*, (13), 6865–6872.
45. Paíga, P.; Ramos, S.; Jorge, S.; Silva, J. G.; Delerue-Matos, C., Monitoring survey of caffeine in surface waters (Lis River) and wastewaters located at Leiria Town in Portugal. *Environ. Sci. Pollut. Res.* **2019**, *26*, (32), 33440–33450.
46. R Core Team R: A language and environment for statistical computing. <http://www.R-project.org> (2018).
47. Jacobs, L. E.; Weavers, L. K.; Houtz, E. F.; Chin, Y.-P., Photosensitized degradation of caffeine: Role of fulvic acids and nitrate. *Chemosphere* **2012**, *86*, (2), 124–129.
48. Masbou, J.; Drouin, G.; Payraudeau, S.; Imfeld, G., Carbon and nitrogen stable isotope fractionation during abiotic hydrolysis of pesticides. *Chemosphere* **2018**, *213*, 368–376.
49. Jochmann, M. A.; Blessing, M.; Haderlein, S. B.; Schmidt, T. C., A new approach to determine method detection limits for compound-specific isotope analysis of volatile organic compounds. *Rapid Commun. Mass Spectrom.* **2006**, *20*, (24), 3639–3648.
50. Scott, K. M.; Lu, X.; Cavanaugh, C. M.; Liu, J. S., Optimal methods for estimating kinetic isotope effects from different forms of the Rayleigh distillation equation. *Geochim. Cosmochim. Acta* **2004**, *68*, (3), 433–442.
51. Voermans, J. J.; Ghisalberti, M.; Ivey, G. N., A model for mass transport across the sediment-water Interface. *Water Resour. Res.* **2018**, *54*, (4), 2799–2812.
52. Van Breukelen, B. M.; Hunkeler, D.; Volkering, F., Quantification of sequential chlorinated ethene degradation by use of a reactive transport model incorporating isotope fractionation. *Environ. Sci. Technol.* **2005**, *39*, (11), 4189–4197.
53. Alvarez-Zaldívar, P.; Centler, F.; Maier, U.; Thullner, M.; Imfeld, G., Biogeochemical modelling of in situ biodegradation and stable isotope fractionation of intermediate chloroethenes in a horizontal subsurface flow wetland. *Ecol. Eng.* **2016**, *90*, 170–179.
54. Akbarzadeh, Z.; Laverman, A. M.; Rezanezhad, F.; Raimonet, M.; Viollier, E.; Shafei, B.; Van Cappellen, P., Benthic nitrite exchanges in the Seine River (France): An early diagenetic modeling analysis. *Sci. Total Environ.* **2018**, *628-629*, 580–593.
55. Soetaert, K.; Herman, P. M. J.; Middelburg, J. J., A model of early diagenetic processes from the shelf to abyssal depths. *Geochim. Cosmochim. Acta* **1996**, *60*, (6), 1019–1040.
56. Vanderborght, J.-P.; Wollas, R.; Bitten, G., Kinetic models of diagenesis in disturbed sediments. Part 2. Nitrogen diagenesis. *Limnol. Oceanogr.* **1977**, *22*, (5), 794–803.
57. ECHA, Chapter R.16: Environmental exposure estimation, version 3.0. In *Guidance on Information Requirements and Chemical Safety Assessment*, European Chemicals Agency: Helsinki, Finland, **2016**.

58. Mazzafera, P., Catabolism of caffeine in plants and microorganisms. *Front. Biosci.* **2004**, *9*, 1348–1359.
59. Bradley, P. M.; Barber, L. B.; Kolpin, D. W.; McMahon, P. B.; Chapelle, F. H., Biotransformation of caffeine, cotinine, and nicotine in stream sediments: Implications for use as wastewater indicators. *Environ. Toxicol. Chem.* **2007**, *26*, (6), 1116–1121.
60. Benotti, M. J.; Brownawell, B. J., Microbial degradation of pharmaceuticals in estuarine and coastal seawater. *Environ. Pollut.* **2009**, *157*, (3), 994–1002.
61. OECD, Test No. 308: Aerobic and anaerobic transformation in aquatic sediment systems. In *OECD Guidelines for the Testing of Chemicals, Section 3*, OECD Publishing: Paris, France, **2002**; p 19.
62. Skarpeli-Liati, M.; Pati, S. G.; Bolotin, J.; Eustis, S. N.; Hofstetter, T. B., Carbon, hydrogen, and nitrogen isotope fractionation associated with oxidative transformation of substituted aromatic *N*-alkyl amines. *Environ. Sci. Technol.* **2012**, *46*, (13), 7189–7198.
63. Penning, H.; Sorensen, S. R.; Meyer, A. H.; Aamand, J.; Elsner, M., C, N, and H isotope fractionation of the herbicide isoproturon reflects different microbial transformation pathways. *Environ. Sci. Technol.* **2010**, *44*, (7), 2372–2378.
64. Peter, K. T.; Herzog, S.; Tian, Z.; Wu, C.; McCray, J. E.; Lynch, K.; Kolodziej, E. P., Evaluating emerging organic contaminant removal in an engineered hyporheic zone using high resolution mass spectrometry. *Water Res.* **2019**, *150*, 140–152.
65. Bertrand, R. L., Lag phase is a dynamic, organized, adaptive, and evolvable period that prepares bacteria for cell division. *J. Bacteriol.* **2019**, *201*, (7), e00697–00718.
66. Cheyns, K.; Mertens, J.; Diels, J.; Smolders, E.; Springael, D., Monod kinetics rather than a first-order degradation model explains atrazine fate in soil mini-columns: Implications for pesticide fate modelling. *Environ. Pollut.* **2010**, *158*, (5), 1405–1411.
67. Zumstein, M. T.; Helbling, D. E., Biotransformation of antibiotics: Exploring the activity of extracellular and intracellular enzymes derived from wastewater microbial communities. *Water Res.* **2019**, *155*, 115–123.
68. Paraska, D. W.; Hipsey, M. R.; Salmon, S. U., Sediment diagenesis models: Review of approaches, challenges and opportunities. *Environ. Model. Software* **2014**, *61*, 297–325.
69. Cerro-Gálvez, E.; Sala, M. M.; Marrasé, C.; Gasol, J. M.; Dachs, J.; Vila-Costa, M., Modulation of microbial growth and enzymatic activities in the marine environment due to exposure to organic contaminants of emerging concern and hydrocarbons. *Sci. Total Environ.* **2019**, *678*, 486–498.

## Preface to Chapter 6

The previous chapters based on batch experiments and a bench-scale river channel underlined the advantage of CSIA to examine the occurrence of in situ degradation without preliminary knowledge on TPs and without a full mass-balance. The following chapter aims to validate the potential of CSIA to evaluate pesticide degradation with multiple sources of pesticides at the river and catchment scale, although it was never applied for surface water. Chapter 6 highlights the design and the results of a sampling campaign conducted from March to September 2019 at the Souffel catchment (Bas-Rhin, France; 120 km<sup>2</sup>). This step is the final scale to assess the feasibility and limits of CSIA to evaluate the degradation and to identify hotspots and hot-moments affecting the degradation of the targeted herbicide *S*-metolachlor, which is currently widely applied on the Souffel catchment.



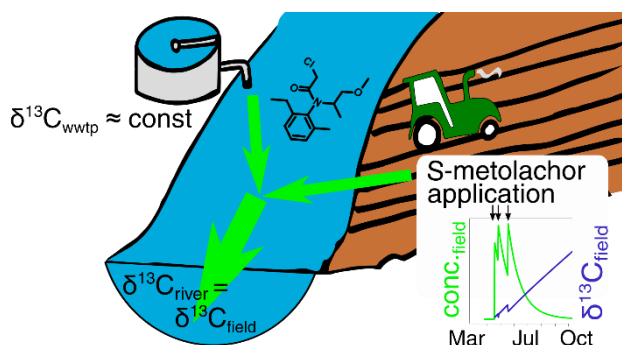


## Chapter 6

### Persistence of *S*-metolachlor in rivers: Insights from compound-specific isotope analysis (CSIA)

#### Abstract

Persistence of pesticides in surface water can threaten the quality of drinking water resources. A major challenge for water resource management is to quantify pesticide export, biodegradation and persistence at the catchment scale. Compound specific isotope analysis (CSIA) can provide quantitative estimates of pesticide biodegradation in soil and water as it is generally not affected by non-degradative processes, such as dilution, sorption, and volatilization. In this study, we combined a mass balance approach with pesticide CSIA to determine the source apportionment of *S*-metolachlor, a widely used chloroacetanilide herbicide, at the catchment scale during a growing season (March to October) and to evaluate its persistence along a river reach. Estimates of *S*-metolachlor persistence using CSIA agreed with the mass balance approach. The mass balance, accounting for the different compartments, showed that  $98.9 \pm 4.7\%$  ( $\bar{X} \pm \text{SD}$ ) of *S*-metolachlor was degraded in total, mainly in the field, with only  $12.3 \pm 3.1\%$  degraded in the river. In comparison, CSIA of *S*-metolachlor at the catchment outlet indicated that  $98 \pm 20\%$  of the applied pesticide was degraded over the four months. The wastewater treatment plants (WWTPs) contributed  $52 \pm 18\%$  of the input mass based on daily discharges, although identification of pesticide source origin remained difficult since isotope signatures of *S*-metolachlor for field and WWTP sources were similar. Altogether, our results show that pesticide CSIA allows to delineate sources and to estimate pesticide dissipation across a whole catchment. We anticipate that CSIA may help surface water management by supporting regulatory and monitoring strategies to prevent off-site transport from agricultural fields through evaluation of the contribution of river reaches to the overall pesticide dissipation at the catchment scale.





## **Introduction**

Up to  $2.6 \times 10^6$  tons of pesticides per year are used worldwide in conventional agricultural schemes.<sup>1</sup> Pesticides are ubiquitous in surface water and are commonly found in the ng to  $\mu\text{g}$  range, which may affect environmental health and the drinking water resources.<sup>2</sup> Pesticides may degrade or persist over decades in various environmental compartments such as topsoil, the water column and sediments.<sup>3,4</sup> While biodegradation has been identified as the major degradation process,<sup>5</sup> where, when, and how pesticide biodegradation occurs in agriculturally-impacted catchments remain fundamental, largely unresolved issues.

Overall, it remains difficult to track pesticide degradation under field conditions. Biodegradation studies are mostly conducted under laboratory conditions, while pesticide degradation is generally evidenced indirectly based on the identification of transformation products (TPs). The hyporheic zone (HZ) of rivers has been hypothesized as the most reactive zone for pollutant biodegradation, although direct evidence is currently lacking.<sup>6,7</sup> The HZ is characterized by a large spectrum of redox conditions<sup>8</sup> where pesticides in the aqueous phase can be degraded by freely dissolved or sediment-bound microorganisms.<sup>9-11</sup> However, despite efforts to understand dissipation processes at work in the HZ based on parent and TP measurements,<sup>9-15</sup> direct evidence of biodegradation in river systems, including conditions and locations of biodegradation, remains scarce.

In this context, compound-specific isotope analysis (CSIA) allows us to detect and possibly estimate the extent of biodegradation in the environment.<sup>16</sup> Pesticide molecules with lighter isotopes (e.g.,  $^{12}\text{C}$ ) are generally degraded at faster rates during a chemical transformation relative to their heavier counterparts (e.g.,  $^{13}\text{C}$ ), resulting a kinetic isotope effect. Consequently, the non-degraded, remaining fraction of pesticide is enriched in the heavier isotopologues. Hence, measuring the changes of the isotope signature (e.g.,  $\delta^{13}\text{C}$ ) over time allows us to evaluate the occurrence of degradation and, in some cases and if condition-specific isotopic enrichment factors have been determined, to quantify the extent of transformation. CSIA has been successfully used for two decades to evaluate the biodegradation of legacy industrial contaminants in groundwater.<sup>17</sup> More recently, pesticide CSIA has been used to evaluate degradation of the herbicide *S*-metolachlor in an agricultural setting.<sup>18</sup> In addition, isotope mixing models between sources using CSIA data can help to delineate source apportionment at the catchment scale.<sup>19</sup> However, pesticide CSIA has not been applied yet to elucidate the conditions and locations associated with pesticide biodegradation in river systems.<sup>20</sup>

The purpose of this study was to evaluate over a growing season the contribution of degradative and non-degradative processes leading to *S*-metolachlor dissipation at the river (total of 79 km length) and catchment scales ( $120 \text{ km}^2$ ), while accounting for the contribution of multiple sources, i.e., agricultural applications and wastewater treatment plants (WWTP), and the influence of successive hydrological events. *S*-metolachlor is a widely used herbicide,

ranked eighth in pesticides sold worldwide,<sup>21</sup> which has been applied homogeneously across agricultural parcels in the study catchment. We focused on the interpretation of factors controlling the dynamics of *S*-metolachlor off-site export from the fields into the river, and *S*-metolachlor dissipation processes in the river reaches. Mass balance, transit time analysis and *S*-metolachlor CSIA were combined to examine the contribution of biodegradation and source apportionment in the catchment.

## **Materials and methods**

### **Catchment description**

The outlet of the Souffel catchment (120 km<sup>2</sup>) is located 3 km northwest of Strasbourg (Bas-Rhin, France; 48° 38' 20" N, 7° 44' 35" E; Figure 6.1). The catchment is flat (average slope 2.4 ± 2.2%) with a total of 79 km of rivers composed of reaches varying from 1 to 3 Strahler orders (BD topo 2017, <http://www.ign.fr/>). The average annual rainfall from 1975 to 2018 at the Entzheim weather station (MeteoFrance, 48°32'24" N, 7°37'48" E) was 648 ± 91 mm, and 579 mm in 2019 (study year). The crop type of this catchment are homogeneously distributed and constituted 84.5% of the total area (Corine Land Cover 2012; v18.5.1; <http://land.copernicus.eu>). Corn and sugar beets were the main crops from 2015 to 2018, covering 51.2 ± 1.7% and 12.0 ± 0.5% of the agricultural area, respectively (National agricultural plot database – RPG, Registre Parcelaire Graphique, [www.ign.fr](http://www.ign.fr)) Both corn and sugar beets under conventional schemes receive applications of *S*-metolachlor-containing herbicide products (<https://ephy.anses.fr>, Mai 2019; Appendix D (AD), Table D1).

### **S-metolachlor applications**

A survey of pesticide application practices was conducted in 2019 for the 60 farmers who owned fields in a sub-catchment of the Souffel river (3.6 km<sup>2</sup> containing 94% of farmland; Figure 6.1). This sub-catchment is considered by local farming authorities as representative of the Souffel land use and farming practices. The survey covered 57% of the fields, with 43% potentially receiving *S*-metolachlor applications. Two successive doses of *S*-metolachlor, each ranging from 576 to 672 g ha<sup>-1</sup>, was applied on sugar beet fields on April 18 (± 1 days) and April 29 (± 2 days). A single dose of *S*-metolachlor, ranging from 160 to 1000 g ha<sup>-1</sup>, was applied on corn fields between May 14 and June 3 (median on May 20). These application doses and amounts are typical for climatic conditions and vegetation stages prevailing in 2019 in the Souffel catchment, as confirmed by local farmer advisers and pesticides sellers. *S*-metolachlor application amounts were thus extrapolated to the entire catchment (detailed in AD). Since the land use at the field scale was not yet available in 2019 for the entire catchment, a likelihood map was built from the three years of crop rotation from 2015 to 2018 (detailed in

AD). The likelihood map was validated based on the surveyed sub-catchment (<2% of variation between predicted and observed corn and sugar beet land uses). Modifications of crop rotations were identified in 2019 for the 120 km<sup>2</sup> catchment with the help of local farmer advisers. Different scenarios of *S*-metolachlor dose applications were considered using national regulations, local farmer recommendations and survey results (AD, Table D1).

## **Sampling locations**

Grab samples of river water, sediment and topsoil of sugar beet and corn fields were collected from March to October 2019 (March 13, April 2, Mai 15, June 12, July 17, August 21 and October 1) to cover the period of the *S*-metolachlor applications and the growing seasons of sugar beets and corn. Topsoil of sugar beet and corn fields were collected up to a distance of 100 m from the river at two locations in the surveyed sub-catchment (Figure 6.1; G10 and G11). At each location, four sub-samples were collected and thoroughly mixed to quantify dissipation of *S*-metolachlor over the season in the agricultural topsoil. Potential accidental releases of *S*-metolachlor from farms connected to the sewage network were screened by sampling outlets of the three WWTPs of the catchment (Figure 6.1, W1 to W3). Eleven sampling locations of water and river bed sediment were selected across the Souffel river (Figure 6.1, G1 to G11). G1 was close to the main Souffel spring, composed of 32% forest and 68% cropland. Locations G2 to G11 were selected via stratified random sampling<sup>22</sup> to obtain upstream agricultural land cover ranging from 84 to 94%. These 11 locations were used to estimate the dissipation and biodegradation of *S*-metolachlor from upstream to downstream.

## **Continuous sampling**

Finally, the outlet of the Souffel catchment (Figure 6.1, location A) was sampled between March 1 and October 1 (215 days) using a refrigerated sampler (ISCO 6712) connected to a flow proportional bubbler (module ISCO 730) to calculate the *S*-metolachlor loads at the catchment scale of 120 km<sup>2</sup>. Samples were then collected for defined discharge volumes, adapted weekly from 1500 m<sup>3</sup> to 960 m<sup>3</sup> to account for the progressive decrease of base-flow over the season. Discharge at the outlet was continuously measured with a radar flow meter (Vegapuls WL S 61, Vega), with an average precision of 15%. The sub-weekly water samples were collected weekly and merged into composite samples based on the hydrograph characteristics, i.e., base-flow and events merged separately. *pH*, conductivity and water temperature were recorded continuously at the same location with a multiparameter electrode (HI 9829, Hanna).

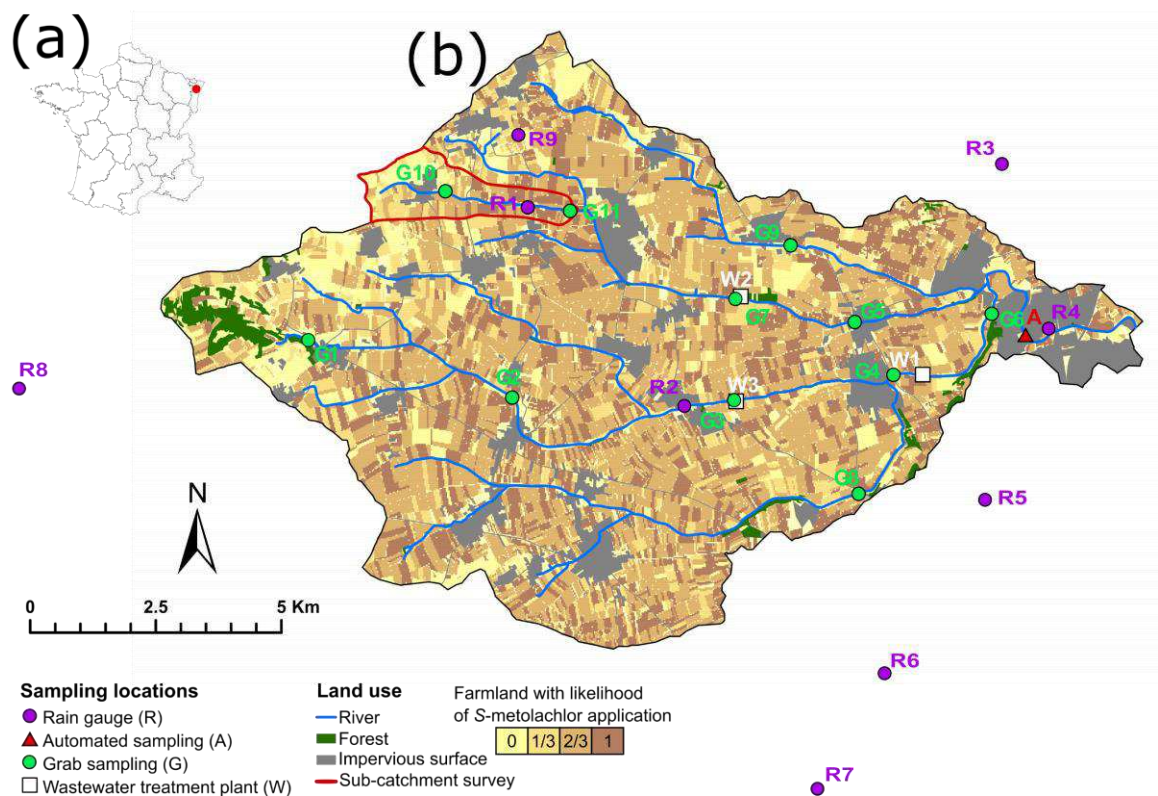


Figure 6.1. The Souffel catchment (b) located in France (a) with the sampling locations (in green, red and white) and the associated land use. Likelihood of *S*-metolachlor applications was estimated by averaging three years (2015 to 2017) of crop rotations and based on crops with reported *S*-metolachlor authorization (<https://ephy.anses.fr/>; corns, beets). Zero denotes an absence of *S*-metolachlor applications, while one stands for three potential applications within the three successive years.

### Grab sampling

Grab river water and wastewater samples were collected into 2 L HPDE bottles for *S*-metolachlor quantification and CSIA. Additional samples (150 mL) were collected in HPDE bottles and filtered on-site using 0.45  $\mu\text{m}$  cellulose acetate (CA) filters for further hydrochemical characterization (AD, Table D2). *pH*, conductivity and water temperature were recorded in the river (*pH*/cond multi 350i, WTW). River locations G1 to G11 were gauged using a handheld electromagnetic water flow meter (Nautilus C2000 / Sensa Z300, OTT) and the flow subsequently calculated using the velocity-area method. River velocities ( $v$ ) were converted to water discharge ( $Q$ ) using BAREME v8.2 (DREAL Auvergne-Rhone-Alpes). Due to low velocities during grab samples (from  $0.01 \text{ m s}^{-1}$  to  $1.36 \text{ m s}^{-1}$ ) and the small river sections, an uncertainty of  $16 \pm 8\%$  was calculated from the gauged data. River bed sediment samples (locations G2 to G11) were collected from the top five centimeters of the river bed using a clean scraper and transferred into plastic bags. A gravel river bed at G2 hampered

sediment sampling at this location. Water, sediment and topsoil samples were stored in a dark, sealed container at ~4 °C until *S*-metolachlor extraction, which was completed within two days following sample collection. Hourly rainfall data were collected in eight rain gauges (MétéoFrance, Strasbourg City and citizen data, [www.wunderground.com/weatherstation](http://www.wunderground.com/weatherstation)) covering the Souffel catchment area (R1 to R8 in Figure 6.1). Rainfall events were analyzed on R-v.3.5.0<sup>23</sup>) using hydromad v.0.9-26.<sup>24</sup>

### **S-metolachlor extraction and quantification**

The water samples from continuous and grab sampling were pre-filtered through qualitative filters (Grade 1, Whatman), and then filtered a second time through glass filters (GF/5, 0.4 µm average pore size, Macherey-Nagel), both using a bottle-top vacuum filtration unit. The filtrate was extracted and concentrated by solid-phase extraction (SPE – C18 cartridge) as previously described in Appendix B and elsewhere.<sup>25</sup> Filters were collected, dried at room temperature in a desiccator to determine the total suspended solid (TSS; AD, Table D2) and frozen prior to *S*-metolachlor extraction. 34% of filters ( $n = 93$ ) were selected to quantify solid-bound *S*-metolachlor based on the corresponding highest concentrations present in the aqueous phase and the mass of TSS on the filter in order to maximize possible quantification. *S*-metolachlor was extracted from the selected filters by solid liquid extraction as described in Appendix B. Topsoil and wet river bed sediment were homogenized and sieved through a 2 mm mesh, and then centrifuged at 2400 RCF for 20 min to remove excess water. Aliquots of topsoil and wet river bed sediment were collected for further characterization (AD, Table D2), and ~20 g equivalent dried mass of wet sediment or topsoil samples were extracted by solid liquid extraction, following the same procedure as for TSS. *S*-metolachlor concentrations were quantified with an established procedure for gas chromatography–mass spectrometry (GC-MS, detailed in Appendix B), with envQL (envQL, analytical detection limit of *S*-metolachlor divided by the concentration factor of the sample) ranging from 0.01 to 0.03 µg L<sup>-1</sup> for water and 0.4 to 2.5 µg kg<sup>-1</sup> for river bed sediment or topsoil, with an analytical reproducibility of 4.3%.

### **S-metolachlor loads and mass balance**

The *S*-metolachlor loads were calculated at the catchment outlet by multiplying the average *S*-metolachlor concentration by the integrated discharge for the sampling period range. Daily loads were calculated for each grab sampling event at both the river and WWTPs locations by multiplying the instantaneous concentrations by the discharge, which was measured with the handheld electromagnetic water flow meter and reported by the WWTPs managers, respectively. For the three reaches that receive WWTPs discharge (upstream locations G4, G7 and G3), mass mixing (eq. 6.1) was applied to the daily load of the WWTPs

( $L_{wwtp}$ ) and the upstream river ( $L_{river}$ ) to estimate the source apportionment of the WWTP ( $x_{wwtp}$ ):

$$x_{wwtp} = \frac{L_{wwtp}}{L_{wwtp} + L_{river}} \quad (6.1)$$

Mass conservation was assumed to estimate the source apportionment at the outlet considering a dilution by all river branch discharge.

A seasonal mass balance integrating the 214 days of the study was also attempted and compared with CSIA data, accounting for relevant processes identified in the catchment:

$$m_{app} + m_{stock\ y-1} + m_{wwtp} = m_{exp} + m_{vol} + m_{photo} + m_{hydro} + m_{wat,bio} + m_{soil,bio} + m_{res} \quad (6.2)$$

where  $m_{app}$  is the pesticide mass applied to the entire catchment following the application scenarios (detailed in AD, Table D1), and  $m_{stock\ y-1}$  is the residual pesticide stock from 2018 estimated for the 10 cm of topsoil before the first *S*-metolachlor application of 2019.  $m_{wwtp}$  is the effluent coming from WWTPs.  $m_{exp}$  is the exported load at the outlet of the catchment, estimated as previously described.  $m_{vol}$  and  $m_{photo}$  are the mass dissipated by the volatilization and the mass photodegraded, respectively (detailed in AD, Table D6).  $m_{hydro}$  is the mass degraded by hydrolysis and is considered to be negligible for *S*-metolachlor under field and river conditions.<sup>25</sup>  $m_{wat,bio}$  and  $m_{soil,bio}$  are the pesticide mass biodegraded at the river and at the field scales, following a first-order degradation rate as calculated in chapter 4 (Table 4.1) and elsewhere.<sup>18</sup>  $m_{res}$  is the residual *S*-metolachlor measured in soil after the 214 days.

### **S-metolachlor compound-specific isotope analysis (CSIA)**

Carbon *S*-metolachlor-specific isotope (C-CSIA) analyses were conducted according to established procedures for gas chromatography–isotope ratio mass spectrometry (GC-IRMS; detailed in Appendix B). Briefly,  $^{13}\text{C}/^{12}\text{C}$  isotope ratio values were measured in triplicate with a typical precision of  $\pm 0.5\%$  and reported as delta values ( $\delta^{13}\text{C}$ ) relative to the Vienna PeeDee Belemnite (V-PDB):

$$\delta^{13}\text{C} = \frac{R(^{13}\text{C}/^{12}\text{C})_{sample}}{R(^{13}\text{C}/^{12}\text{C})_{standard}} - 1 \quad (6.3)$$

where  $\delta^{13}\text{C}$  is the isotope signature of the carbon and  $R(^{13}\text{C}/^{12}\text{C})$  is the isotope ratio of  $^{13}\text{C}$  to  $^{12}\text{C}$  isotopes in a sample or a standard. The  $\delta^{13}\text{C}$  linearity range of the measurement was defined as the range of injected mass of C to which the  $\delta^{13}\text{C}$  values of the *S*-metolachlor stays

within  $\pm 0.5\text{‰}$ <sup>26</sup> and was established as 6 to 300 ng for C. The minimal change of isotope signature ( $\Delta\delta^{13}C_{min}$ ) in water above which isotope fractionation can be attributed to degradation was determined as the propagation of uncertainty associated with measurements and sample preparation (eq. B7).  $\Delta\delta^{13}C_{min}$  for water (w) and sediment (s) were, respectively, 0.95‰ and 1.77‰ for S-metolachlor.

With a calculated  $\varepsilon_{bulk,C} = -1.2 \pm 0.4\text{‰}$  for water derived from laboratory experiments (Table 4.1), the extent of biodegradation ( $B$ ) was calculated from the isotope signatures of water samples, as follow:

$$B = 1 - \left( \frac{\delta^{13}C(t) + 1}{\delta^{13}C_0 + 1} \right)^{1/\varepsilon_{bulk,C}} \quad (6.4)$$

S-metolachlor  $\delta^{13}C$  values were not measured in topsoil during our field investigation due to a strong matrix hampering reliable  $\delta^{13}C$  values. Consequently, the  $\delta^{13}C$  values were estimated from concentrations previously used in a model developed for similar agricultural clayey soils, accounting for the soil temperature and moisture (detailed in AD).<sup>18</sup>

Point and non-point source apportionment was also estimated whenever an isotope signature on the basis of the  $\Delta\delta^{13}C_{min}$ , considering a 95% confidence interval, could be identified in the source. The applicable stable isotope mixing approach as follows:

$$\delta^{13}C_{outlet} = x_{wwtp} \times \delta^{13}C_{wwtp} + (1 - x_{wwtp}) \times \delta^{13}C_{pred,river} \quad (6.5)$$

where  $\delta^{13}C_{outlet}$ ,  $\delta^{13}C_{wwtp}$ ,  $\delta^{13}C_{pred,river}$  are the isotope signatures measured at the outlet, at the WWTPs and the predicted signature from the agricultural input (Figure 6.5), respectively, and  $x_{wwtp}$  is the proportion of daily S-metolachlor load at the outlet coming from WWTPs.  $x_{wwtp}$  can be approximated with stable isotope mixing (eq. 6.6) as an alternative to mass mixing (eq. 6.1):

$$x_{wwtp} = \frac{\delta^{13}C_{outlet} - \delta^{13}C_{pred,river}}{\delta^{13}C_{wwtp} - \delta^{13}C_{pred,river}} \quad (6.6)$$

## **Results and discussion**

### **Catchment hydrological response**

The 2019 growing season, from March 1 to October 1, 2019, was characterized by 17 rainfall events (Figure 6.2a), defined as the cumulative volume of rainfall (>2 mm) separated by at least 24h of no rainfall. The rainfall events accumulated  $358 \pm 50$  mm ( $\bar{X} \pm$  SD between station R1 to R9) over the 215 days of the study. The period before the first reported applications of *S*-metolachlor was relatively dry (27.8 mm in 44 days). The discharge at the outlet was  $0.115 \pm 0.137$  m<sup>3</sup> s<sup>-1</sup> ( $\bar{X} \pm$  SD; Figure 6.2b) between March and October 2019 or  $0.83 \pm 0.98$  m<sup>3</sup> day<sup>-1</sup> ha<sup>-1</sup> when applied over the catchment area. This specific average discharge is one order of magnitude below that of the neighboring rivers to the north and the south of the study area for the same period ( $3.85$  m<sup>3</sup> day<sup>-1</sup> ha<sup>-1</sup> for the Zorn river and  $6.55$  m<sup>3</sup> day<sup>-1</sup> ha<sup>-1</sup> for the Bruche river, <http://www.hydro.eaufrance.fr>). Similar trends were observed for yearly average discharge (1980-2000) and can be explained by the location of the Souffel catchment in the Alsatian plain, which is relatively flat and without mountainous upstream terrain. This emphasize the limited capacity of the Souffel catchment to dilute pesticide loads compared to neighboring rivers. During each rainfall event the conductivity at the outlet dropped from the base flow conductivity of  $852 \pm 97$  down to  $133$  mS cm<sup>-1</sup>. An inverse correlation was observed between the discharge and the conductivity ( $R^2 = 0.53$ ;  $p < 0.01$ ) at the outlet, suggesting that rain water ( $\sigma < 0.03 \pm 0.01$  mS cm<sup>-1</sup>) that entered the river had a limited contact time with the topsoil, suggesting preferential flow paths in the subsurface.<sup>27</sup> The response time characterized by the time between the peak of a rainfall event (Figure 6.2a) and the peak of the associated discharge (Figure 6.2b) at the outlet was between 1.2 and 12 hours, which suggests fast runoff and/or sub-surface contributions to the river.<sup>28</sup> Hortonian runoff can occur when rainfall exceeds infiltration capacity. Runoff over the contributing area might be estimated by computing the topographic wetness index (TWI) of the catchment.<sup>29, 30</sup> The catchment has a very low TWI ( $6.5 \pm 1.4$   $\bar{X} \pm$  SD) with only 7.5% of the river bank associated with a TWI higher than 8.5, which suggests that only a limited area likely contributed to overland runoff (AD, Figure D1).<sup>31</sup> From March 1 to October 1, only rainfall events 9 and 15 were classified as heavy (>7.5 mm per hour),<sup>32</sup> while the 15 others were lighter ( $n = 14$ ; <2.5 mm per hour) or moderate ( $n = 1$ ; between 2.5 mm and 7.6 mm per hour). The intensity of rainfall patterns and the limited extent of contributing areas of overland flow suggest that sub-surface flow was the main contributor to the outlet discharge. Although, Hortonian runoff might contribute during rainfall events 9 and 15 (in June and August). Moreover, the non-correlation between TSS concentration at the outlet with the rainfall, and reported a mean of  $578 \pm 938$  mg L<sup>-1</sup> ( $\bar{X} \pm$  SD) with a maximum of 5,967 mg L<sup>-1</sup> (Figure 6.2b) supported the sub-surface flow contribution.



### Off-site transport of *S*-metolachlor

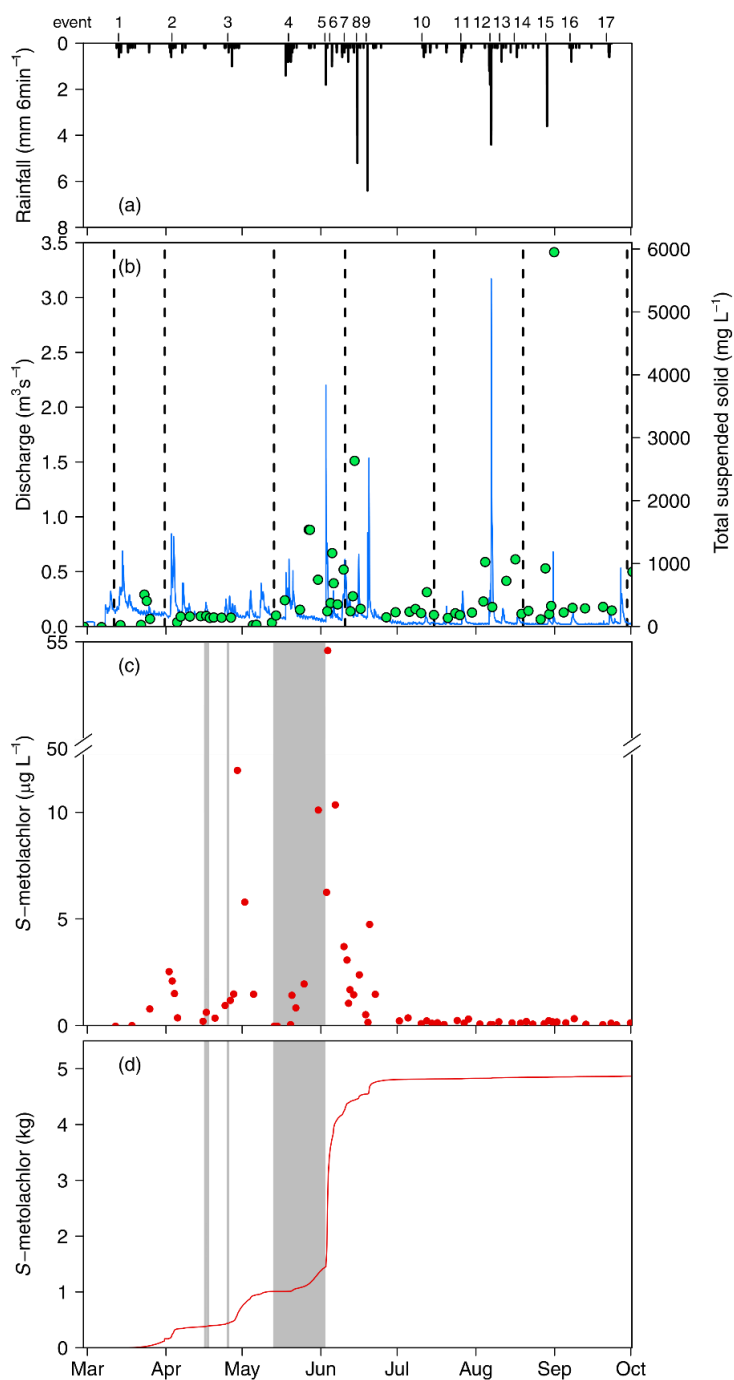


Figure 6.2. Dissolved *S*-metolachlor concentrations and loads at the outlet of the Souffel catchment in 2019 (location A in Figure 6.1) with (a) rainfall at location R1, (b) discharge (blue line), total suspended solids (green dots) and timing of the 7 grab sampling campaigns (dashed vertical line), (c) *S*-metolachlor concentrations in dissolved phase ( $n = 176$ ; red dots) with reported *S*-metolachlor application dates (in grey), and (d) cumulative load in dissolved phase.

Dissolved concentrations of *S*-metolachlor were quantified in 98% of the composite samples ( $n=61$ ; Figure 6.2c) at the outlet, ranging from 0.03 to 54.6  $\mu\text{g L}^{-1}$  over the course of the season with an average ( $\pm$  SD) of  $2.3 \pm 7.3 \mu\text{g L}^{-1}$ . *S*-metolachlor in the particulate phase were below the limit of detection ( $1.2 \mu\text{g kg}^{-1}$  TSS;  $n=35$ ). This suggests that Hortonian runoff and associated off-site transport of *S*-metolachlor by erosion had only a limited contribution to the total loads monitored from March to October 2019. This indicates that subsurface transport of dissolved *S*-metolachlor dominated during the study period.

Total *S*-metolachlor load exported from the Souffel catchment during the study period was  $4.87 \pm 1.00$  kg, while between  $4,909 \pm 116$  to  $9,224 \pm 217$  kg of *S*-metolachlor was applied, depending on the application scenario (AD, Table D3). Hence, it is estimated that from 0.04 to 0.12% of the applied *S*-metolachlor was exported from March 1 to October 1, which is similar to previous *S*-metolachlor export estimations made for a smaller catchment.<sup>33, 34</sup> As previously observed in a small catchment,<sup>35</sup> pesticide load export did not correlate with rainfall intensity, but was controlled by the interplay between dose and timing of pesticide applications, pesticide dissipation in topsoil and hydro-climatic characteristics.

More than 9% of the seasonal load was exported (Events 1 and 2; Table 6.1) before the first reported applications of *S*-metolachlor. This pre-application export could not be attributed to only the residual topsoil *S*-metolachlor from the previous year, which was estimated in the mass balance (AD, Table D3) to contribute only between 0.8 and 1.5% of the total seasonal export load. In addition, the background concentration of *S*-metolachlor in the river from the previous year was very low ( $<0.4 \mu\text{g L}^{-1}$ ).<sup>36</sup> This suggests a point or non-point source of *S*-metolachlor within the catchment in addition to the field applications. As underlined by the survey, three main *S*-metolachlor applications were performed by farmers, two on sugar beets and one later on corn fields (Figure 6.2c), which correspond to the relative surface area receiving *S*-metolachlor for a given application. Consequently, the combined rainfall events 3 and 4, and rainfall event 5 were responsible for 21 and 47%, respectively, of the total export, which corresponds to 19 and 81% of the surface that potentially received *S*-metolachlor. Worthy of note, the largest observed export occurred during rainfall event 5, a low intensity event ( $1.6 \pm 0.2 \text{ mm h}^{-1}$ ). Altogether, the *S*-metolachlor load dynamics suggests a transport-limited source dynamic (rainfall events 1 to 7)<sup>37</sup> until June 15, contributing to 91% of the seasonal load, followed by a mass-limited source dynamic<sup>38, 39</sup> with only 9% of the seasonal load (rainfall events 7 to 17) from June 15 to October 1.

**Table 6.1.** *S-metolachlor concentrations and load dynamics at the outlet of the Souffel catchment for the main rainfall events (export of 91% of the seasonal load).*

event	1+2	3 <sup>b</sup>	4	5	6 <sup>b</sup>	7
duration (hours) <sup>a</sup>	99 ± 24	101	80 ± 4	7 ± 6	1	42 ± 53
volume (mm) <sup>a</sup>	28 ± 14	11	26 ± 9	11 ± 8	2.6	18 ± 14
days since last application (d)	p.a.	8 <sup>c</sup>	20 <sup>d</sup>	15 <sup>e</sup>	17 <sup>e</sup>	21 <sup>e</sup>
mass applied (kg) <sup>f</sup>	0 (%)	248 ± 6 (2.5%)	495 ± 12 (5%)		4909 ± 116 (100%)	
max con. (µg L <sup>-1</sup> )	2.56	1.51	1.45	6.28	0.07	3.10
load (kg) <sup>g</sup>	0.44 (9%)	0.57 (12%)	0.44 (9%)	2.28 (47%)	0.44 (9%)	0.29 (5%)
max flow (m <sup>3</sup> s <sup>-1</sup> )	0.85	0.28	0.61	2.20	0.14	0.61

<sup>a</sup> considers rainfall gages R1, R2 and R9 only, <sup>b</sup> rainfall event detected only in R1, <sup>c, d, e</sup> consider application dates of April 18, April 29 and May 20, 2019, respectively, according to the survey of sub-catchment G11 (detailed in AD). <sup>f</sup> accounts for the realistic scenario (Table D1), percent of the total mass applied in parenthesis, <sup>g</sup> loads corresponding to the rainfall event, percent of the total load in parentheses. p.a. pre-application. Average flow discharge is 0.115 m<sup>3</sup> s<sup>-1</sup>.

### **S-metolachlor dissipation along the river during the season**

The grab sampling scheme was designed to investigate *S-metolachlor* dissipation in the river. Except for July, base-flow conditions were targeted for monthly sampling to avoid highly dynamic discharge conditions, which would hamper comparison of load discharges among the sampling locations. Similar monthly hydrological responses for the sampling locations were thus observed when comparing the normalized discharge, i.e., the discharge divided by the upstream area (AD, Figure D2).<sup>40</sup> No significant difference of the river hydrochemistry was observed between locations and sampling times (AD, Table D4; Tukey's test;  $p > 0.05$ ). However, significant differences were observed between river and WWTP outlet samples, with higher chloride, sodium and potassium concentrations observed in the WWTP outlets (Tukey's test;  $p < 0.01$ ). Conversely, nitrate concentrations in the river ( $\bar{X} \pm SD = 41.2 \pm 18.4 \text{ mg L}^{-1}$ ;  $n = 84$ ) were higher than those at the WWTP outlets ( $p < 0.01$ ;  $\bar{X} \pm SD = 16.2 \pm 18.0 \text{ mg L}^{-1}$ ;  $n = 21$ ). This indicates that a significantly larger proportion of nitrate comes from non-point sources versus WWTP effluent.

Dissolved concentrations of *S-metolachlor* were quantified in 73% and 100% of the river water grab ( $n = 78$ ) and wastewater ( $n = 21$ ) samples, respectively, ranging from 0.01 to 21.5 µg L<sup>-1</sup> and from 0.01 to 50.2 µg L<sup>-1</sup> during the season. *S-metolachlor* concentrations in the particulate phase were below the quantifiable limit in all samples (1.2 µg kg<sup>-1</sup> TSS;  $n = 18$ ). Finally, *S-metolachlor* was quantified in 11% of the sediment samples ( $n = 76$ ) ranging from 1.7 to 11.9 µg kg<sup>-1</sup>. The sub-catchment associated with sampling location G1 was comprised of 32% and 68% forest and farmland, respectively, and consequently was less impacted by *S-metolachlor* than any other sub-catchment, which were comprised of between 84 and 94% farmland. As expected, significantly lower dissolved *S-metolachlor* concentrations were

measured at G1, headwaters (Figure 6.1), than in any other locations ( $G2 \text{ to } G11 = 1.15 \pm 5.70 \mu\text{g L}^{-1}$  vs  $G1 = 0.10 \pm 0.22 \mu\text{g L}^{-1}$ ,  $\bar{X} \pm \text{SD}$ ;  $t$ -test;  $p < 0.01$ ) during the season.

*S*-metolachlor concentrations comparison between upstream and downstream were analyzed monthly over six months for the 11 river reaches defined by the sampling locations (G1 to G11) and the outlet A. Three distinct patterns were obtained (Figure 6.4a). For 90% of cases ( $n = 59$ ) the upstream-downstream concentrations did not vary, as underlined by the 1:1 slope (Figure 6.4a). This can be interpreted as a homogeneous release of *S*-metolachlor from each sub-catchment to the corresponding reach,<sup>41</sup> or by a balance between *S*-metolachlor lateral inputs to the reach and dissipation processes in the river. Significant increase from upstream to downstream, considering the 95% confidence interval for concentrations, was observed for only a few reaches and sampling dates ( $n = 5$ ). Concentrations significantly increased in two dissimilar cases. First, increased *S*-metolachlor concentrations between the spring (G1) and its downstream location (G2) resulted from *S*-metolachlor applications to fields in April. Secondly, the point source contribution of effluent from the three WWTPs into the connected reaches was observed, but only on April 2 (Figure 6.4a). Observations of a significant *S*-metolachlor contribution from WWTPs on April 2 can be attributed to the low background concentrations in the river before the main pesticide applications, and by subsequent accidental loads released during pesticide sprayer washing in farms connected to the sewage network. The final observed trend ( $n = 2$ ) was a significant decrease of *S*-metolachlor concentrations in the reaches between G2 and G3 on April 2 and G9 and the outlet in June. Overall, *S*-metolachlor dynamics of point and non-point sources over the course of the season can help to interpret *S*-metolachlor export in the catchment.

### **Point versus non-point sources apportionment**

The daily discharges from WWTPs contributed to  $52 \pm 18\%$  ( $\bar{X} \pm \text{SD}$ ) of the corresponding reach outlet discharge (Figure 6.3a). However, the WWTPs' contribution varied seasonally from 13% of the total reach discharge in spring and early fall up to 80% in summer. The total contribution of the three WWTP effluents at the outlet of the catchment corresponded to  $49 \pm 6\%$  of the total discharge during the high-flow period (March to June) and up to 100% during the low-flow period (July to September).

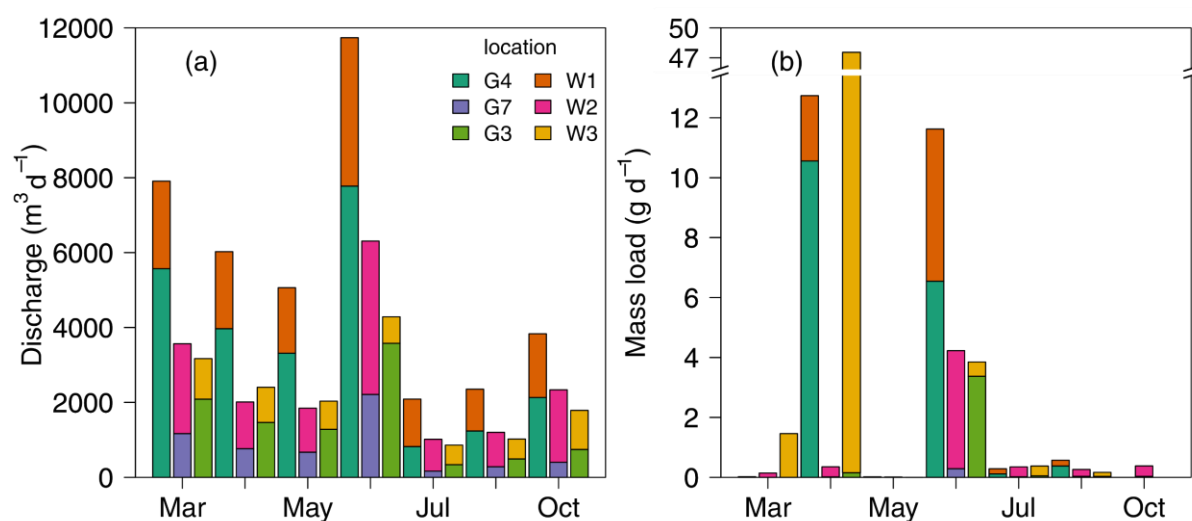


Figure 6.3. Contribution of river and WWTPs to the total reach discharge (a) and associated *S*-metolachlor loads (b) for monthly sampling. G4, G7 and G3 were located directly upstream of the effluents of WWTPs 1, 2 and 3, respectively. Note that G4 is downstream of G3, and W3 thus contributed to the G4 discharge.

The source apportionment of *S*-metolachlor loads, i.e., from WWTP effluents ( $x_{\text{wwtp}}$ ; eq. 6.1 and from upstream non-point agricultural sources ( $1 - x_{\text{wwtp}}$ ), was estimated using daily WWTP and outlet discharges and *S*-metolachlor concentrations.  $x_{\text{wwtp}}$  varied over the season and represented from 0 to 100% (53% on average) of the observed mass load at the outlet of the catchment. These estimations were in agreement with a previous investigation at WWTP W1, which estimated a  $x_{\text{wwtp}}$  of  $53 \pm 24\%$ , with a mass contribution on certain days of up to 100% during the 2015-2016 period.<sup>36</sup> We estimated that about 9% of the total offsite export of *S*-metolachlor observed during the rainfall events 1 and 2 in April (Table 6.1) originated from the WWTPs following early sprayer washing operations.

The monthly effluent sampling results from the WWTPs (Figure 6.3b) follows the catchment outlet load dynamic (Figure 6.2d), where exported mass was mainly observed from March to June. This suggests that the *S*-metolachlor load from the WWTPs was linked to releases during pesticide preparation or handling near farmhouses prior to field applications. Since dilution and biodegradation processes in river and source apportionment, i.e., non-point and point sources, cannot be teased apart based on upstream and downstream concentrations only, we applied *S*-metolachlor C-CSIA in parallel.

### **S-metolachlor isotope signature along the river**

$\delta^{13}\text{C}$  allowed us to estimate the S-metolachlor biodegradation in river and confirm S-metolachlor point and non-point source apportionment along the river and over the course of the season.  $\delta^{13}\text{C}$  was obtained for 25% ( $n = 25$ ), 48% ( $n = 32$ ) and 43% ( $n = 9$ ) of the grab, outlet and WWTP samples respectively, corresponding to the minimal mass of carbon required for accurate GC-IRMS analysis, i.e., higher than 20 ng. Upstream-downstream  $\delta^{13}\text{C}$ , including only nine reaches monitored in April and/or June (Figure 6.4b), suggested export of non-degraded S-metolachlor into the river in early April, since  $\delta^{13}\text{C}$  was similar to that of the S-metolachlor applied during the 2019 growing season (Figure 6.4b;  $\delta^{13}\text{C}_0 = -31.8 \pm 0.3\text{‰}$ , AD, Table D5). The  $\delta^{13}\text{C}$  of dissolved S-metolachlor in June suggested biodegradation (estimated to be about 60%, eq. 6.4 in reaches with or without wwtps effluents (Figure 6.4b). From April to October, the isotope signature collected at the wwtps remained constant ( $\delta^{13}\text{C}_{\text{wwtp}} = -29.76 \pm 0.97$ ;  $n = 9$ ), which was 2‰ heavier than the original signature. Hence, change of  $\delta^{13}\text{C}$  greater than 2‰ ( $\Delta\delta^{13}\text{C}_{\text{riv}} = \delta^{13}\text{C}_{\text{downstream}} - \delta^{13}\text{C}_{\text{upstream}}$ ) in June for the river reaches G6  $\rightarrow$  A, G5  $\rightarrow$  A and G9  $\rightarrow$  A (Figure 6.4b) could not be totally attributed to the wwtps. It suggests either that biodegradation occurred between the downstream and upstream part of the Souffel, or that a downstream point source of degraded S-metolachlor contributed more significantly than those in the upstream sub-catchments.

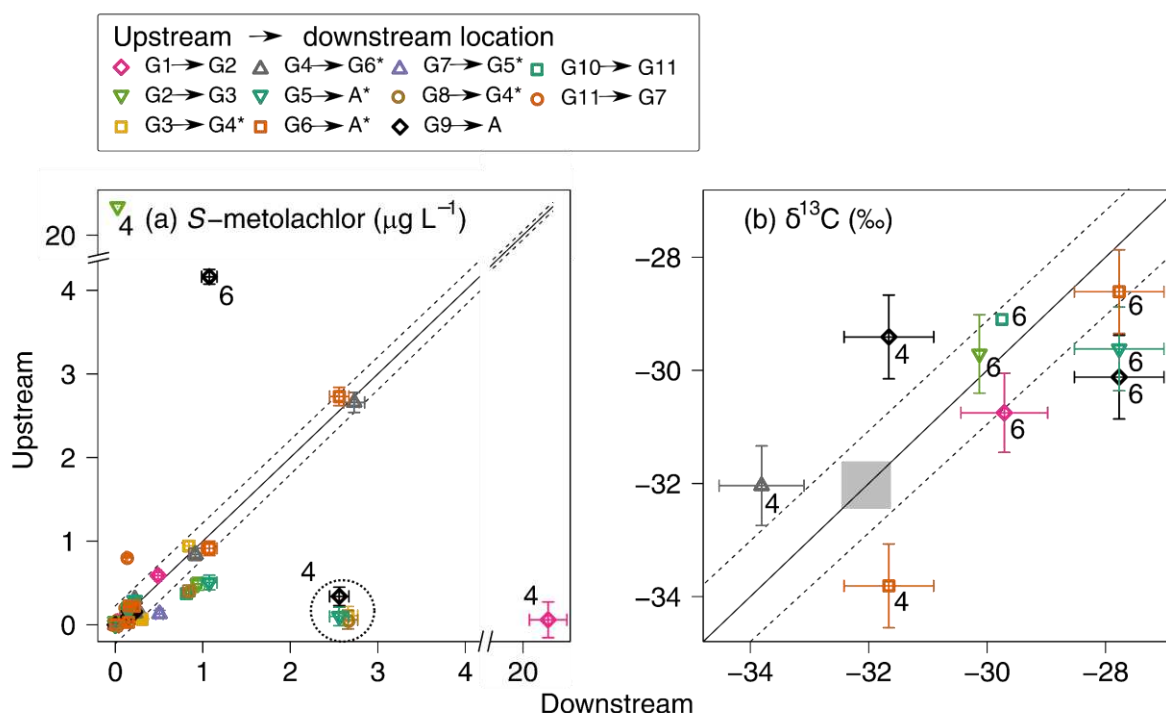


Figure 6.4. Upstream-downstream *S*-metolachlor (a) concentrations and (b) isotope signature ( $\delta^{13}\text{C}$ ) in April (label 4) and June (label 6). The black solid line indicates a 1:1 relationship and the dashed line the 95% confidence interval associated with the measurements. The grey zone represents the initial isotope signature of *S*-metolachlor application ( $\delta^{13}\text{C}_0 = -31.8 \pm 0.3\text{‰}$ , commercial formulation). Error bars indicate the propagation of uncertainty on triplicate measurements for concentration and  $\delta^{13}\text{C}$ , respectively. Asterisks (\*) highlight reaches with wwtp contribution.

### Degradation of *S*-metolachlor in the river reach

Extent of *S*-metolachlor degradation in a river can be calculated when the isotope signatures in the river are significantly higher ( $>\Delta\delta^{13}\text{C}_{\text{min}}$ ) than the source isotope signature from the topsoil on the field. Isotope signatures from the topsoil were found to follow a trend line over the course of the season after *S*-metolachlor application (Figure 6.5). Eighty five percent of the  $\delta^{13}\text{C}$  measurements in the river during the season were within the 95% confidence interval of the predicted uncertainty of the  $\delta^{13}\text{C}$  predicted for topsoil at locations G10 and G11. In addition, the average transit time to reach the outlet, which can be estimated using the water velocity, supports the interpretation of the *S*-metolachlor reactive transport in the water column and at the sediment–water interface (SWI). Transit times ranged from 2.4 hours to 8 days (for G2 in July), depending on the discharge and location, but were on average  $28 \pm 31$  hours ( $\bar{X} \pm \text{SD}$ ), which is far lower than the biodegradation half-life in the water column

( $DegT_{50,oxic} = 29 \pm 8$  days; Table 4.1) Altogether, these data advocate for a limited contribution of biodegradation in the river.

In addition to transit time, the horizontal and vertical hyporheic exchange flows (HEFs) may control the biodegradation at the river scale by facilitating mixing between nutrients necessary for bacterial activities, *S*-metolachlor in the water column and microbial degraders in the river bed sediment.<sup>10, 11</sup> The quantification of the HEFs along the 79 km of river reaches was not accessible in our study. However, multiple pieces of evidence support the idea that pesticide and water HEFs would be limited in the study river system. First, the river bed sediment was characterized as a silt loam sediment<sup>42</sup> (clay (<2  $\mu\text{m}$ ) =  $14.6 \pm 3.5\%$  ( $\bar{X} \pm \text{SD}$ ), silt (from 2 to 50  $\mu\text{m}$ ) =  $65.5 \pm 11.5\%$ , sand (from 50 to 2000  $\mu\text{m}$ ) =  $19.9 \pm 13.7\%$ ;  $n = 22$ ) with a low organic carbon content ( $C_{org} = 2.6 \pm 1.3\%$ ), suggesting very low permeability ( $K_s < 10^{-6} \text{ cm s}^{-1}$ ),<sup>43</sup> limiting HEFs.<sup>11, 44</sup> HEFs were considered to be not measurable under our experimental setup, but their contribution became evident during the low-discharge period (July to October) where the water mass balance between two river branches and their confluence was far from equal, and where the sum of the upstream wwtps' daily discharge was higher than the outlet discharge. For these low-flow periods in the downstream part of the catchment, a back-of-the-envelope calculation suggests an estimate of  $10 \pm 10\%$  volume infiltration. This estimation is in agreement with the high resolution comparison between area normalized daily discharges between locations G10 and G11 for the same period<sup>45</sup>, and comparable to similar river settings.<sup>11</sup> However, during this period low *S*-metolachlor concentrations were measured, therefore it is difficult to conclude whether the surface water–groundwater exchange was responsible for the removal of a significant mass of pesticides.

HEF dynamics can be related to the water table level of the Alsatian aquifer connected to the lower third of Souffel catchment. Moreover, *S*-metolachlor was detected in only 10% of river bed sediment samples at low concentrations (<12  $\mu\text{g kg}^{-1}$ ) during the season. This suggests that Souffel river bed sediment is probably not a main source or sink of *S*-metolachlor for the water column. Regular observations during grab sampling suggest that the sediment became rapidly anoxic with depth, reducing by a factor of seven the rate of biodegradation (Chap. 4). Finally, the low turbulence during base flow, the absence of tortuosity, waterfall and dams, as well as the low discharge of the Souffel river limit HEFs.<sup>46, 47</sup> Because of the low HEFs, the associated potential of *S*-metolachlor biodegradation is likewise limited. Altogether, CSIA and river reaches properties advocate for very limited biodegradation in the river, which could not be quantified with CSIA only.



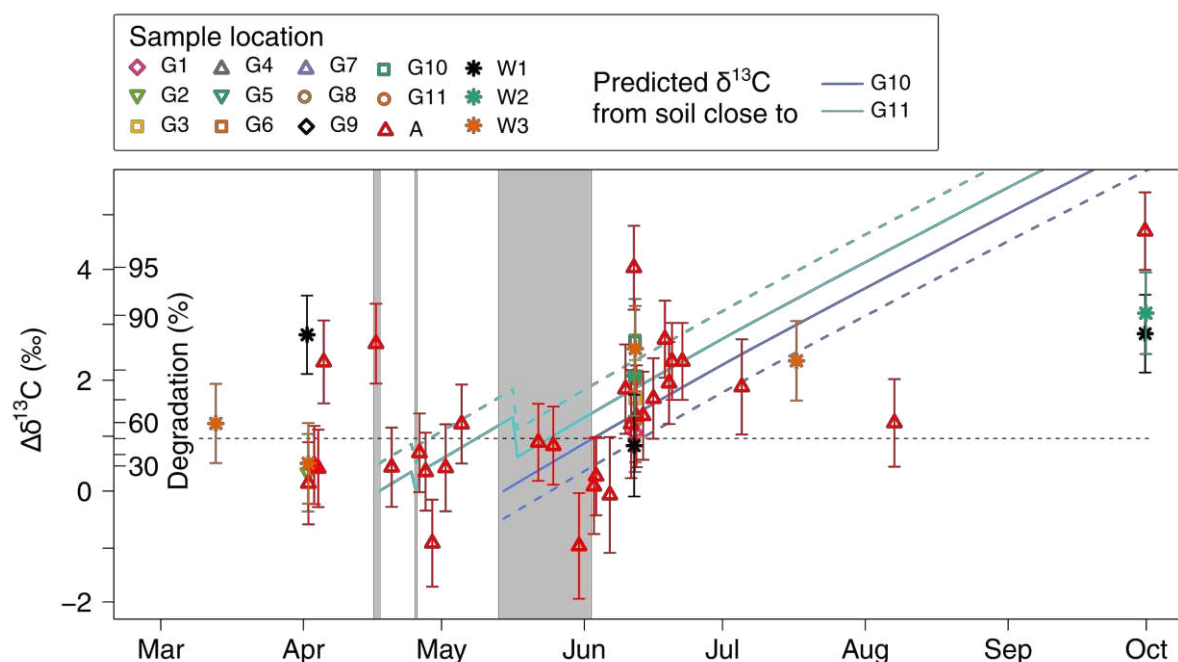


Figure 6.5. *S*-metolachlor carbon isotope fractionation ( $\Delta\delta^{13}\text{C} = \delta^{13}\text{C}(t) - \delta^{13}\text{C}_0$ ) over the growing season compared to the predicted topsoil  $\delta^{13}\text{C}$  (detailed in AD, Figure D3).<sup>18</sup> Colored dashed lines represent the predicted uncertainty of the topsoil  $\delta^{13}\text{C}$  estimate as the minimum  $\pm 0.5\%$ . The black dashed horizontal line represents the minimal change of isotope signature ( $\Delta\delta^{13}\text{C}_{\text{min}}$ , eq. B7) in water above which isotope fractionation can be attributed to degradation, i.e., the limit to detect biodegradation. The grey zone represents the approximate date of *S*-metolachlor application (AD, Table D5) defined from the farmer survey of the sub-catchment G11. Error bars account for the propagation of uncertainty associated with  $\Delta\delta^{13}\text{C}$ .

### Potential of the CSIA approach

A mass balance of *S*-metolachlor at the catchment scale for the entire season, i.e., from the date of applications to October, can be established based on previous laboratory studies, as well as field and river observations (eq. 6.3; AD, Table D3). At the field scale, the *S*-metolachlor volatilization in similar soil, climate and crop types was modeled (detailed in AD, Table D6) and accounts for from 2.2 to 5.5% of the applied product the day following application. The extent of off-site transport from the agricultural topsoil to surface and groundwaters was unknown at the catchment scale but was monitored and estimated to be less than 1% in an upstream reach (G10-G11),<sup>45</sup> and overall could be roughly estimated to be less than 0.1% of applied *S*-metolachlor in 2019. Consequently, transit time suggests limited biodegradation potential in the water column of the river, which is estimated to be  $2.7 \pm 2.3\%$  ( $\bar{X} \pm \text{SD}$ ). The extent of anoxic biodegradation in the SWI and photolysis in the water column of point and non-point sources were estimated to be 0.3 and 10%, respectively, according to the transit time and first-order kinetics. The *S*-metolachlor load at the outlet was estimated to

be between 0.05 to 0.1% of the *S*-metolachlor application. The mass balance was almost closed (<2%) and indicated that  $98.9 \pm 4.7\%$  ( $\bar{X} \pm \text{SD}$ ) of the applied *S*-metolachlor was degraded over the season, accounting for scenarios of uncertainty for *S*-metolachlor application.

This mass balance using monthly concentrations in topsoil, the river, and WWTPs, as well as continuous monitoring of *S*-metolachlor loads at the outlet, can be compared with the monthly data provided by CSIA at the catchment outlet. CSIA was able to capture biodegradation only since photolysis under simulated sunlight likely does not cause any isotope fractionation for *S*-metolachlor (Chap. 3). The extent of biodegradation measured using CSIA was similar in October with  $98 \pm 20\%$  ( $\bar{X} \pm \text{SD}$ ). The higher uncertainty reflects that of CSIA measurements. However, the uncertainty was largely compensated for by the limited amount of information needed to predict the extent of the biodegradation compared that necessary to establish a mass balance, which required not only more information but also several assumptions.

### **Environmental significance**

This study demonstrates the advantages of using CSIA to evaluate *S*-metolachlor biodegradation at an agricultural catchment scale using point and non-point source apportionment and outlet information only. We demonstrated that field topsoils act as the main reactive compartment, for which biodegradation explained more than 98.9% of the applied *S*-metolachlor mass reduction. With the 2019 climatic characteristics, *S*-metolachlor was mobilized under transport-limited dynamics until July, and then mass-limited transport corresponding to a large dissipation in topsoil. *S*-metolachlor degradation in the river,  $12.7 \pm 3.1\%$ , comprised mainly of photo- and bio-degradation, was limited, mainly due to a fast transit time and low hyporheic exchange flows (HEFs). Moreover, our results suggest that transport and dissipation of non-point source *S*-metolachlor at the catchment scale is mainly controlled by biodegradation in field topsoil. Hence, preventing pesticides from entering rivers is key to limiting pesticide contamination of water resources.

We also showed that *S*-metolachlor point sources linked to WWTP effluents can contribute from 50% up to more than 80% of the load at the outlet of the catchment over the course of the season. As *S*-metolachlor is approved and applied for only crop treatment purposes in Europe,<sup>48</sup> the presence of the *S*-metolachlor in the e WWTP effluents indicates occurrence of non-appropriate operations at the farm yards during filling or washing of sprayers and equipment.<sup>49</sup> From a regulatory point of view in France,<sup>50</sup> farms should be equipped with either filling-washing stations with separate systems to treat pesticides, or stand-alone pesticide collection stations. The contribution of this point source of *S*-metolachlor can be reduced, i.e., in term of concentration and detection frequency, mainly by using appropriate filling-washing infrastructure. The contribution of this point source was recently evaluated to be higher than recorded *S*-metolachlor concentrations in the effluents of 47% of the WWTPs in the US.<sup>51</sup>

While CSIA in rivers can provide an estimate of the extent of *S*-metolachlor biodegradation in the upstream catchment, several limitations should be addressed. Current limitations are mainly due to the low carbon enrichment factors associated with the biodegradation of *S*-metolachlor ( $\epsilon_C = -1.20 \pm 0.35\text{‰}$ ). The factors correspond to the minimal change of isotope signature in the water above which isotope fractionation can be attributed to degradation ( $\Delta\delta^{13}C_{min} = 0.95\text{‰}$ ; eq. B7; Table B5), which corresponds to 50% of biodegradation. Hence, minor degradation extents could not be detected. We anticipate that recent developments made in chlorine isotope analysis and its high enrichment factor ( $\epsilon_{Cl} = -9.70 \pm 2.9\text{‰}$ )<sup>52</sup> and development using MIPS<sup>53, 54</sup> on *S*-metolachlor will overcome those limitations and might allow us to detect an extent of biodegradation lower than 10% in the future.

From a river restoration point of view, the HEFs and transit times might be artificially enhanced or created to increase the extent of pesticide biodegradation at the river scale.<sup>55</sup> River restoration will also restore other key ecohydrological ecosystem functioning, such as habitat diversity and flood control.<sup>7, 56</sup> To increase biodegradation efficiency at the river scale, restoration should target re-meandering to restore tortuosity, which will not only enhance the transit time, but also create rugged bedform surfaces in time. Rugged bedform surfaces will produce high-pressure on the upstream side of the bedform, increasing both HEFs<sup>57</sup> and contact time between pesticides and microorganisms in the sediment bed.<sup>58</sup> In addition, restoration should also promote obstacles such as wood debris and small dams to increasing to increase HEFs by similar processes as the bedforms.<sup>59-61</sup> Finally, riparian restoration should be promote riverbank vegetation strip to create a buffer zone, thereby enhancing dissipation of pesticide loads from agricultural fields. To enhance the efficiency of the riverbank, natural or artificial amendments of organic matter (e.g., compost, biochar) should be promoted to create a reactive zone with significant microbial activity within the vadose zone.<sup>62</sup>

Finally, CSIA applied at the outlet can provide an estimate of the biodegradation extent in the catchment over the course of the agricultural season, and can be used to assess pesticide persistence, and eventually help water managers to address regulatory and monitoring strategies.

## References

1. Stehle, S.; Schulz, R., Agricultural insecticides threaten surface waters at the global scale. *Proc. Natl. Acad. Sci. U.S.A.* **2015**, *112*, (18), 5750–5755.
2. Schwarzenbach, R. P.; Egli, T.; Hofstetter, T. B.; von Gunten, U.; Wehrli, B., Global water pollution and human health. *Annu. Rev. Env. Resour.* **2010**, *35*, 109–136.

3. Rasmussen, J. J.; Wiberg-Larsen, P.; Baattrup-Pedersen, A.; Cedergreen, N.; McKnight, U. S.; Kreuger, J.; Jacobsen, D.; Kristensen, E. A.; Friberg, N., The legacy of pesticide pollution: An overlooked factor in current risk assessments of freshwater systems. *Water Res.* **2015**, *84*, 25–32.
4. Boxall, A. B. A.; Sinclair, C. J.; Fenner, K.; Kolpin, D.; Maud, S. J., When synthetic chemicals degrade in the environment. *Environ. Sci. Technol.* **2004**, *38*, (19), 368A–375A.
5. Fenner, K.; Canonica, S.; Wackett, L. P.; Elsner, M., Evaluating pesticide degradation in the environment: Blind spots and emerging opportunities. *Science* **2013**, *341*, (6147), 752–758.
6. Brunke, M.; Gonser, T., The ecological significance of exchange processes between rivers and groundwater. *Freshwat. Biol.* **1997**, *37*, 1–33.
7. Krause, S.; Lewandowski, J.; Grimm, N. B.; Hannah, D. M.; Pinay, G.; McDonald, K.; Martí, E.; Argerich, A.; Pfister, L.; Klaus, J.; Battin, T.; Larned, S. T.; Schelker, J.; Fleckenstein, J.; Schmidt, C.; Rivett, M. O.; Watts, G.; Sabater, F.; Sorolla, A.; Turk, V., Ecohydrological interfaces as hot spots of ecosystem processes. *Water Resour. Res.* **2017**, *53*, (8), 6359–6376.
8. Meckenstock, R. U.; Elsner, M.; Griebler, C.; Lueders, T.; Stumpp, C.; Aamand, J.; Agathos, S. N.; Albrechtsen, H.-J.; Bastiaens, L.; Bjerg, P. L.; Boon, N.; Dejonghe, W.; Huang, W. E.; Schmidt, S. I.; Smolders, E.; Sørensen, S. R.; Springael, D.; van Breukelen, B. M., Biodegradation: Updating the concepts of control for microbial cleanup in contaminated aquifers. *Environ. Sci. Technol.* **2015**, *49*, (12), 7073–7081.
9. Schaper, J. L.; Posselt, M.; Bouchez, C.; Jaeger, A.; Nuetzmann, G.; Putschew, A.; Singer, G.; Lewandowski, J., Fate of trace organic compounds in the hyporheic zone: Influence of retardation, the benthic biolayer, and organic carbon. *Environ. Sci. Technol.* **2019**, *53*, (8), 4224–4234.
10. Schaper, J. L.; Posselt, M.; McCallum, J. L.; Banks, E. W.; Hoehne, A.; Meinikmann, K.; Shanafield, M. A.; Batelaan, O.; Lewandowski, J., Hyporheic exchange controls fate of trace organic compounds in an urban stream. *Environ. Sci. Technol.* **2018**, *52*, (21), 12285–12294.
11. Kunkel, U.; Radke, M., Reactive tracer test to evaluate the fate of pharmaceuticals in rivers. *Environ. Sci. Technol.* **2011**, *45*, (15), 6296–6302.
12. Schaper, J. L.; Seher, W.; Nützmann, G.; Putschew, A.; Jekel, M.; Lewandowski, J., The fate of polar trace organic compounds in the hyporheic zone. *Water Res.* **2018**, *140*, 158–166.
13. Kunkel, U.; Radke, M., Fate of pharmaceuticals in rivers: Deriving a benchmark dataset at favorable attenuation conditions. *Water Res.* **2012**, *46*, (17), 5551–5565.
14. Lewandowski, J.; Putschew, A.; Schwesig, D.; Neumann, C.; Radke, M., Fate of organic micropollutants in the hyporheic zone of a eutrophic lowland stream: Results of a preliminary field study. *Sci. Total Environ.* **2011**, *409*, (10), 1824–1835.

15. Radke, M.; Ulrich, H.; Wurm, C.; Kunkel, U., Dynamics and attenuation of acidic pharmaceuticals along a river stretch. *Environ. Sci. Technol.* **2010**, *44*, (8), 2968–2974.
16. Elsner, M., Stable isotope fractionation to investigate natural transformation mechanisms of organic contaminants: principles, prospects and limitations. *J. Environ. Monit.* **2010**, *12*, (11), 2005–2031.
17. Hunkeler, D.; Meckenstock, R. U.; Lollar, B. S.; Schmidt, T. C.; Wilson, J. T. *A guide for assessing biodegradation and source identification of organic ground water contaminants using compound specific isotope analysis (CSIA)*; Environmental Protection Agency (EPA), US: **2008**; p 68.
18. Alvarez-Zaldivar, P. Pesticide degradation and transport at catchment scale Compound-specific isotope analysis and numerical modelling. Doctoral thesis, Laboratoire d'Hydrologie et de Géochimie de Strasbourg (LHyGeS), University of Strasbourg, Strasbourg, **2019**; p 202.
19. Lutz, S. R.; Van Breukelen, B. M., Combined source apportionment and degradation quantification of organic pollutants with CSIA: 2. Model validation and application. *Environ. Sci. Technol.* **2014**, *48*, (11), 6229–6236.
20. Elsner, M.; Imfeld, G., Compound-specific isotope analysis (CSIA) of micropollutants in the environment — current developments and future challenges. *Curr. Opin. Biotechnol.* **2016**, *41*, 60–72.
21. Food and Agriculture Organization of the United Nations FAOSTAT. [www.fao.org/faostat/](http://www.fao.org/faostat/) (20<sup>th</sup> March **2019**).
22. Forthofer, R. N.; Lee, E. S.; Hernandez, M., 6 - Study Designs. In *Biostatistics (Second Edition)*, Forthofer, R. N.; Lee, E. S.; Hernandez, M., Eds. Academic Press: San Diego, **2007**; pp 135–167.
23. R Core Team R: A language and environment for statistical computing. <http://www.R-project.org> (**2018**).
24. Andrews, F.; Guillaume, J. hydromad: Hydrological model assessment and development - R package version 0.9-26. <http://hydromad.catchment.org>.
25. Masbou, J.; Drouin, G.; Payraudeau, S.; Imfeld, G., Carbon and nitrogen stable isotope fractionation during abiotic hydrolysis of pesticides. *Chemosphere* **2018**, *213*, 368–376.
26. Jochmann, M. A.; Blessing, M.; Haderlein, S. B.; Schmidt, T. C., A new approach to determine method detection limits for compound-specific isotope analysis of volatile organic compounds. *Rapid Commun. Mass Spectrom.* **2006**, *20*, (24), 3639–3648.
27. Leu, C.; Singer, H.; Stamm, C.; Müller, S. R.; Schwarzenbach, R. P., Simultaneous assessment of sources, processes, and factors influencing herbicide losses to surface waters in a small agricultural catchment. *Environ. Sci. Technol.* **2004**, *38*, (14), 3827–3834.

28. Gericke, O. J.; Smithers, J. C., Direct estimation of catchment response time parameters in medium to large catchments using observed streamflow data. *Hydrol. Process.* **2017**, *31*, (5), 1125–1143.
29. Beven, K. J.; Kirkby, M. J., A physically based, variable contributing area model of basin hydrology / Un modèle à base physique de zone d'appel variable de l'hydrologie du bassin versant. *Hydrol. Sci. Bull.* **1979**, *24*, (1), 43–69.
30. Ali, G.; Birkel, C.; Tetzlaff, D.; Soulsby, C.; McDonnell, J. J.; Tarolli, P., A comparison of wetness indices for the prediction of observed connected saturated areas under contrasting conditions. *Earth Surf. Proc. Land.* **2014**, *39*, (3), 399–413.
31. Juracek, K. E. *Estimation of potential runoff-contributing areas in Kansas using topographic and soil information*; USGS: Lawrence, Kansas, US, **1999**; p 36.
32. Monjo, R., Measure of rainfall time structure using the dimensionless n-index. *Clim. Res.* **2016**, *67*, (1), 71–86.
33. Alvarez-Zaldívar, P.; Payraudeau, S.; Meite, F.; Masbou, J.; Imfeld, G., Pesticide degradation and export losses at the catchment scale: Insights from compound-specific isotope analysis (CSIA). *Water Res.* **2018**, *139*, 198–207.
34. Lefrancq, M.; Payraudeau, S.; Guyot, B.; Millet, M.; Imfeld, G., Degradation and transport of the chiral herbicide S-metolachlor at the catchment scale: Combining observation scales and analytical approaches. *Environ. Sci. Technol.* **2017**, *51*, (22), 13231–13240.
35. Imfeld, G.; Meite, F.; Wiegert, C.; Guyot, B.; Masbou, J.; Payraudeau, S., Do rainfall characteristics affect the export of copper, zinc and synthetic pesticides in surface runoff from headwater catchments? *Sci. Total Environ.* **2020**, *741*, 140437.
36. Agence de l'Eau Rhin-Meuse Système d'Information sur l'Eau Rhin-Meuse (SIERM). <https://rhin-meuse.eaufrance.fr> (**2020**).
37. Peter, K. T.; Hou, F.; Tian, Z.; Wu, C.; Goehring, M.; Liu, F.; Kolodziej, E. P., More than a first flush: Urban creek storm hydrographs demonstrate broad contaminant pollutographs. *Environ. Sci. Technol.* **2020**, *54*, (10), 6152–6165.
38. Musolff, A.; Schmidt, C.; Selle, B.; Fleckenstein, J. H., Catchment controls on solute export. *Adv. Water Resour.* **2015**, *86*, 133–146.
39. Fairbairn, D. J.; Arnold, W. A.; Barber, B. L.; Kaufenberg, E. F.; Koskinen, W. C.; Novak, P. J.; Rice, P. J.; Swackhamer, D. L., Contaminants of emerging concern: Mass balance and comparison of wastewater effluent and upstream sources in a mixed-use watershed. *Environ. Sci. Technol.* **2016**, *50*, (1), 36–45.
40. Shaw, S. B.; Beslity, J. O.; Colvin, M. E., Working toward a more holistic set of hydrologic principles to teach non-hydrologists: Five simple concepts within catchment hydrology. *Hydrol. Process.* **2019**, *33*, 2258–2262.

41. Gericke, O. J.; Smithers, J. C., Review of methods used to estimate catchment response time for the purpose of peak discharge estimation. *Hydrol. Sci. J.* **2014**, *59*, (11), 1935–1971.
42. Gerakis, A.; Baer, B., A computer program for soil textural classification. *Soil Sci. Soc. Am. J.* **1999**, *63*, 807–808.
43. Ren, X.; Zeng, G.; Tang, L.; Wang, J.; Wan, J.; Liu, Y.; Yu, J.; Yi, H.; Ye, S.; Deng, R., Sorption, transport and biodegradation – An insight into bioavailability of persistent organic pollutants in soil. *Sci. Total Environ.* **2018**, *610-611*, 1154–1163.
44. Morrice, J. A.; Valett, H. M.; Dahm, C. N.; Campana, M. E., Alluvial characteristics, groundwater–surface water exchange and hydrological retention in headwater streams. *Hydrol. Process.* **1997**, *11*, (3), 253–267.
45. Drouin, G. Micropollutant dissipation at the sediment-water interface by coupling modelling and compound-specific isotope analysis. Doctoral thesis, Laboratoire d'Hydrologie et de Géochimie de Strasbourg (LHyGeS), University of Strasbourg, Strasbourg, **2020**; 294.
46. Voermans, J. J.; Ghisalberti, M.; Ivey, G. N., A model for mass transport across the sediment-water Interface. *Water Resour. Res.* **2018**, *54*, (4), 2799–2812.
47. Jaeger, A.; Posselt, M.; Betterle, A.; Schaper, J.; Mechelke, J.; Coll, C.; Lewandowski, J., Spatial and temporal variability in attenuation of polar organic micropollutants in an urban lowland stream. *Environ. Sci. Technol.* **2019**, *53*, (5), 2383–2395.
48. European Commission EU pesticides database.  
<http://ec.europa.eu/food/plant/pesticides/eu-pesticides-database> (18<sup>th</sup> January **2019**).
49. Gerecke, A. C.; Schärer, M.; Singer, H. P.; Müller, S. R.; Schwarzenbach, R. P.; Sägesser, M.; Ochsenein, U.; Popow, G., Sources of pesticides in surface waters in Switzerland: Pesticide load through waste water treatment plants—current situation and reduction potential. *Chemosphere* **2002**, *48*, (3), 307–315.
50. Le Foll, S.; Royal, S.; Sapin, M.; Touraine, M., Arrêté du 4 mai 2017 relatif à la mise sur le marché et à l'utilisation des produits phytopharmaceutiques et de leurs adjuvants visés à l'article L. 253-1 du code rural et de la pêche maritime. *Journal Officiel de la République Française - Lois et décrets* **2017**, *108*, 115.
51. Sutton, R.; Xie, Y.; Moran, K. D.; Teerlink, J., Occurrence and sources of pesticides to urban wastewater and the environment. In *Pesticides in Surface Water: Monitoring, Modeling, Risk Assessment, and Management*, American Chemical Society: **2019**; Vol. 1308, pp 63–88.
52. Ponsin, V.; Torrentó, C.; Lihl, C.; Elsner, M.; Hunkeler, D., Compound-specific chlorine isotope analysis of the herbicides atrazine, acetochlor and metolachlor. *Anal. Chem.* **2019**, *91*, (22), 14290–14298.

53. Zhang, L.; Han, F.; Hu, Y.; Zheng, P.; Sheng, X.; Sun, H.; Song, W.; Lv, Y., Selective trace analysis of chloroacetamide herbicides in food samples using dummy molecularly imprinted solid phase extraction based on chemometrics and quantum chemistry. *Anal. Chim. Acta* **2012**, *729*, 36–44.
54. Wang, Y.; Jin, X.; Zhao, D.; Guo, X.; Li, R., Molecularly imprinted solid-phase extraction coupled with gas chromatography for the determination of four chloroacetamide herbicides in soil. *Anal. Methods* **2015**, *7*, (15), 6411–6418.
55. Peter, K. T.; Herzog, S.; Tian, Z.; Wu, C.; McCray, J. E.; Lynch, K.; Kolodziej, E. P., Evaluating emerging organic contaminant removal in an engineered hyporheic zone using high resolution mass spectrometry. *Water Res.* **2019**, *150*, 140–152.
56. Lewandowski, J.; Arnon, S.; Banks, E.; Batelaan, O.; Betterle, A.; Broecker, T.; Coll, C.; Drummond, J. D.; Gaona Garcia, J.; Galloway, J.; Gomez-Velez, J.; Grabowski, R. C.; Herzog, S. P.; Hinkelmann, R.; Höhne, A.; Hollender, J.; Horn, M. A.; Jaeger, A.; Krause, S.; Löchner Prats, A.; Magliozzi, C.; Meinikmann, K.; Mojarrad, B. B.; Mueller, B. M.; Peralta-Maraver, I.; Popp, A. L.; Posselt, M.; Putschew, A.; Radke, M.; Raza, M.; Riml, J.; Robertson, A.; Rutere, C.; Schaper, J. L.; Schirmer, M.; Schulz, H.; Shanafield, M.; Singh, T.; Ward, A. S.; Wolke, P.; Wörman, A.; Wu, L., Is the hyporheic zone relevant beyond the scientific community? *Water* **2019**, *11*, (11), 2230.
57. Elliott, A. H.; Brooks, N. H., Transfer of nonsorbing solutes to a streambed with bed forms: Theory. *Water Resour. Res.* **1997**, *33*, (1), 123–136.
58. Jaeger, A.; Coll, C.; Posselt, M.; Mechelke, J.; Rutere, C.; Betterle, A.; Raza, M.; Mehrrens, A.; Meinikmann, K.; Portmann, A.; Singh, T.; Blaen, P. J.; Krause, S.; Horn, M. A.; Hollender, J.; Benskin, J. P.; Sobek, A.; Lewandowski, J., Using recirculating flumes and a response surface model to investigate the role of hyporheic exchange and bacterial diversity on micropollutant half-lives. *Environ. Sci. Process. Impacts* **2019**, *21*, (12), 2093–2108.
59. Krause, S.; Klaar, M. J.; Hannah, D. M.; Mant, J.; Bridgeman, J.; Trimmer, M.; Manning-Jones, S., The potential of large woody debris to alter biogeochemical processes and ecosystem services in lowland rivers. *WIREs Water* **2014**, *1*, (3), 263–275.
60. Blaen, P. J.; Kurz, M. J.; Drummond, J. D.; Knapp, J. L. A.; Mendoza-Lera, C.; Schmadel, N. M.; Klaar, M. J.; Jäger, A.; Folegot, S.; Lee-Cullin, J.; Ward, A. S.; Zarnetske, J. P.; Datry, T.; Milner, A. M.; Lewandowski, J.; Hannah, D. M.; Krause, S., Woody debris is related to reach-scale hotspots of lowland stream ecosystem respiration under baseflow conditions. *Ecohydrology* **2018**, *11*, (5), e1952.
61. Herzog, S. P.; Higgins, C. P.; Singha, K.; McCray, J. E., Performance of engineered streambeds for inducing hyporheic transient storage and attenuation of resazurin. *Environ. Sci. Technol.* **2018**, *52*, (18), 10627–10636.
62. Ulrich, B. A.; Vignola, M.; Edgehouse, K.; Werner, D.; Higgins, C. P., Organic carbon amendments for enhanced biological attenuation of trace organic contaminants in biochar-amended stormwater biofilters. *Environ. Sci. Technol.* **2017**, *51*, (16), 9184–9193.



*Persistence of S-metolachlor in rivers: Insights from compound-specific isotope analysis (CSIA)*

## **Chapter 7**

### **General conclusion**

#### **Introduction**

The overall goal of this thesis was to improve interpretation of pesticide dissipation at the sediment–water interface (SWI) where degradation, phase transfer and transport processes co-occur at different temporal and spatial scales in surface water. In this context, compound-specific isotope analysis (CSIA) may help to tease apart pesticide biodegradation from other dissipation processes and to identify degradation pathways.

Based on the current knowledge, presented in the Chap. 1, our thesis aimed to address the following gaps concerning pesticide dissipation at the SWI:

- 1. How can isotope signatures reflect ongoing direct and indirect photolysis processes?**
- 2. What is the extent of biodegradation in the water–sediment system?**
- 3. How does water flow velocity influence pesticide dissipation and the contribution of non-degradative and degradative processes in the water column and in the hyporheic zone (HZ)?**
- 4. What are the potential and limits of CSIA to evaluate pesticide degradation and persistence in rivers under environmental conditions during a growing season?**

In a first section, these four questions are situated in the context of the multi-scale and multi-compartment approach developed in this thesis (Figure 7.1). Then, the main findings and implications of this thesis are discussed in two distinct sections, with an emphasis on the gradient of the investigation scale in terms of both processes complexity and environmental representativeness. The limits of our approach and expected improvements for further investigation of pesticide dissipation understanding at the SWI are eventually addressed in Chap. 8.

## A compartment system

In this thesis, pesticide degradation pathways at the SWI were investigated to tease apart pesticide biodegradation from other dissipation processes while identifying degradation pathways. A series of experiments was set up to scale up from batch experiments to an investigation at the catchment scale, with an intermediate scale consisting of a bench scale river channel (Figure 7.1 & Figure 1.7). With a corresponding increase in complexity of the investigated processes and the associated environmental representativeness to increasing investigated scales, insights could be gained regarding pesticide dissipation in both rivers and at the catchment scale (Figure 7.1). The lab-scale experiments developed in this thesis, presented in Chap. 2 through 5, examined the effects of elementary processes before addressing a combination of different processes under controlled conditions. These elementary experiments provided a set of degradation kinetic rates and associated isotope signatures, which are required to disentangle the contribution of each degradation process and the overall dissipation at the SWI at larger scales.

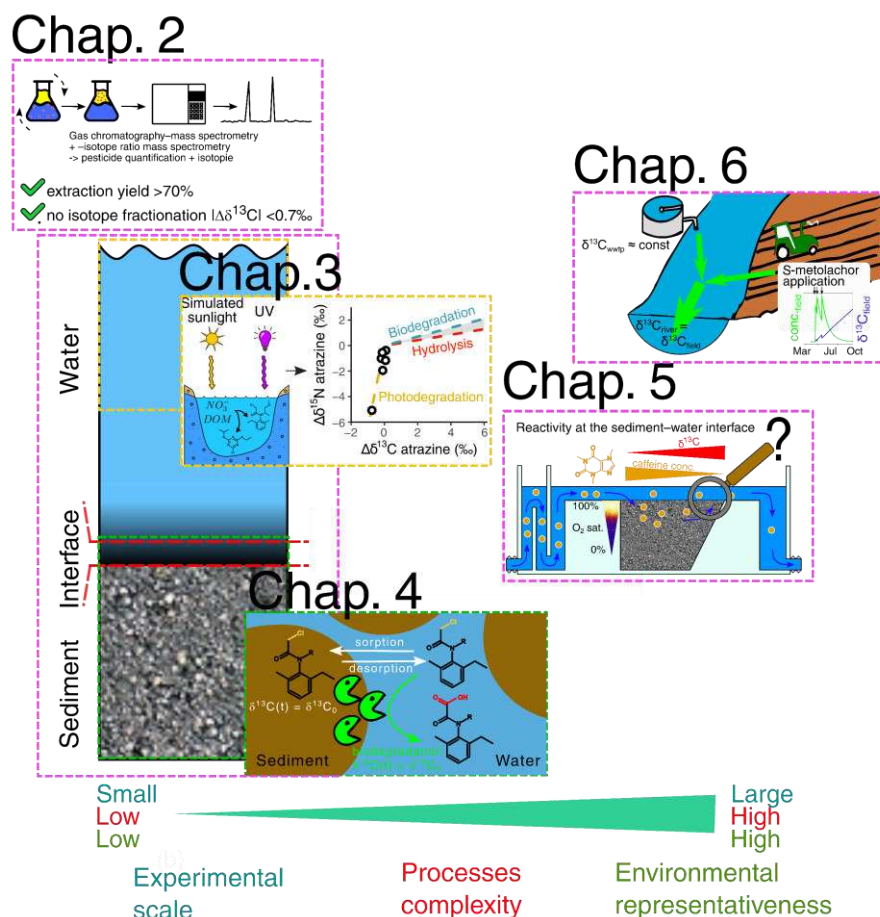


Figure 7.1. Overview of the developed approach from smaller to larger spatial scale, with corresponding increasing complexity and environmental representativeness. The dashed color boxes indicate the targeted SWI compartment and the corresponding scale of investigation in each chapter.

Chap. 2 described the development and improvement of N and C-CSIA methods for a panel of targeted pesticides and key environmental compartments: water, sediment and soil. For the targeted pesticides (atrazine, terbutryn, acetochlor, *S*-metolachlor and metalaxyl) the extraction methods were improved by increasing the extraction yield to larger than 70%, with no significant isotope fractionation for C ( $|\Delta\delta^{13}\text{C}| < 0.7\text{‰}$ ) for sediment and soil samples. Including previous analytical development of the research group,<sup>1, 2</sup> this methodological development was adopted to extract, quantify and derive C and N isotope signatures of pesticides for the different scales and chapters of this thesis.

Chap. 3 targeted the question **1. How can isotope signatures reflect ongoing direct and indirect photolysis processes?** To address this question, the carbon and nitrogen isotope fractionations during direct and indirect UV and simulated sunlight photodegradation of the herbicides atrazine and *S*-metolachlor batch experiments were investigated. The significance of this study notably relies on the use of synthetic water mimicking agriculturally impacted surface waters ( $\text{NO}_3^- > 20 \text{ mg L}^{-1}$  and  $\text{DOM} = 5 \text{ mg C L}^{-1}$ ). In Chap. 4, the question **2. What is the extent of biodegradation in the water–sediment system?** was targeted. To address the issue, the complexity of the experimental design was increased to examine two simultaneous processes: biodegradation and phase transfer, i.e., sorption and desorption. The contribution of these two processes to acetochlor and *S*-metolachlor dissipation in water–sediment systems under both oxic and anoxic conditions was examined. Indeed, both degradation and phase-transfer contributed to an apparent decrease of pesticide concentration in the closed system of batch experiments. An original combination of C-CSIA, transformation products (TPs) identification by high resolution tandem mass spectrometry (HR-MS/MS) and a phase–transfer model was used to tease apart degradative and non-degradative processes in these closed systems.

Chap. 5 deals with question **3. How does water flow velocity impact pesticide dissipation and the contribution of non-degradative and degradative processes in the water column and in the HZ?** A bench-scale river channel was designed to investigate the effect of flow velocity on the reactive transport of caffeine, an organic compound associated with anthropogenic activity. At the SWI, I examined both sorption and biodegradation of caffeine in the hyporheic zone (HZ) with respect to horizontal hyporheic exchanges flows (HEFs) under laminar flow conditions with the help of CSIA and flow-reactive-transport (FRT) modelling. Finally, in Chap. 6, question **4. What are the potential and limits of CSIA to evaluate pesticide degradation and persistence in rivers under environmental conditions during a growing season?** was investigated. Knowledge of the main dissipation processes, associated rates and isotope fractionation derived from lab-scale experiments under controlled conditions (Chap. 2 to 5) were used to evaluate *S*-metolachlor persistence along a river (Souffel, Bas-Rhin) during a growing season (March to October 2019) (Chap. 6).

## Key findings for the sediment–water interface

**Isotope signatures of direct and indirect photolysis processes.** The core of this PhD revolved around evaluating the benefit and limits of the CSIA approach to estimate the extent of degradation and to identify the degradation pathway at the SWI using elementary experiments in the laboratory. The absence of carbon isotope fractionation for both direct and indirect photolysis under simulated sunlight of atrazine and *S*-metolachlor (Chap. 3) compared to the significant C fractionation for biodegradation of these compounds (Chap. 4) underlined the potential of CSIA to disentangle these two destructive processes simultaneously occurring in surface water. Most importantly, our results indicate that photo-induced C and N isotope fractionation and degradation depends on the irradiation wavelength, i.e., with UV or simulated sunlight lamps, as suggested elsewhere.<sup>3</sup> From an experimental point of view, this difference advocates for a more systematic use of simulated sunlight lamps to derive more environmentally representative isotope fractionation and degradation rates to extrapolate pesticide photolysis extent in surface waters at an environmental scale, i.e., river scale. Similar conclusions were already made for diclofenac<sup>4</sup> and sulfamethoxazole<sup>3</sup>. Moreover, pesticide photodegradation is limited to the photic zone where the light penetration is inversely proportional to the amount of dissolved or particulate matter present in water and can be calculated.<sup>5</sup> This limits the photodegradation of pesticides to the upper centimeter, especially during high particulate loading associated with flood events.<sup>6</sup> In addition, large dissolved organic matter content ( $>5 \text{ mg L}^{-1}$ ), depending on its optical properties, can slow down the extent of photodegradation<sup>7</sup>, whereas nitrate might increase the extent of photodegradation.<sup>8</sup> One unique aspect of our investigation was a set of photolysis experiments carried out under realistic conditions of agriculturally impacted water, i.e., with high nitrate concentrations ( $>20 \text{ mg L}^{-1}$ ) and moderate dissolved organic carbon ( $\sim 5 \text{ mg C L}^{-1}$ ), which was not often available in literature<sup>9</sup>, and improved the environmental representativeness and potential for scale-up from laboratory to river scale.

**Biodegradation at the water–sediment system.** In literature, changes of isotope signature by non-destructive processes such as rate-limiting mass transfer<sup>10</sup> and repetitive sorption<sup>11</sup> have been reported. The results obtained in Chap. 4 showed that carbon isotope fractionation of the targeted pesticides is not significantly affected by phase transfer, i.e., sorption/desorption in the water–sediment system. A sensitivity analysis underlined that this statement can be generalized for a wide spectrum of representative SWI conditions and molecules. These results demonstrated that isotope signatures of pesticides at the SWI were only altered when destructive processes occurred, as initially postulated. This constitutes a major consideration when scaling up investigations to include more complex processes at the SWI and in predicting degradation at the environmental river-scale with the help of CSIA.

**The water–sediment system conditions** (oxic-anoxic, pH, temperature, etc.) may favor different transformation pathways, limit degradation to one specific process, e.g., enzymatic activity, and/or influence the rate of degradation.<sup>12, 13</sup> In particular, the gradient between oxic and anoxic conditions present at the SWI can separate the aerobic and anaerobic microbial activities, which may in turn impact the biodegradation rate.<sup>14</sup> However our results from the two contrasting conditions, i.e., oxic vs anoxic, advocates for the ubiquitous potential of biodegradation via the glutathione transferase pathway. This pathway has been previously identified for chloroacetanilide biodegradation<sup>15</sup> regarding to the ubiquity presence of the glutathione transferase in the bacteria domain.<sup>16</sup> Interestingly, carbon isotopic enrichment factors ( $\epsilon_C$ ) were similar to those obtained from agricultural soil<sup>17</sup> and lab-scale wetland column experiments<sup>2</sup> which suggests that chloroacetanilides have similar biodegradation pathways occurring across different environmental compartments and conditions. Consequently, the  $\epsilon_C$  derived from the elementary laboratory experiments could be applied to estimate the extent of biodegradation at the environmental scale. In contrast, prediction of the extent of degradation based on the rate of degradation derived from laboratory experiments should be always corrected accounting for the environmental variables. For instance, oxic degradation is generally faster than anoxic degradation, which uses weaker electron acceptors, e.g. Mn,  $\text{NO}_3^-$ , Fe,  $\text{SO}_4^{2-}$ , than oxygen.<sup>18</sup> In soil, it has been shown that the biodegradation rate follows the Arrhenius law as a function of temperature and soil moisture<sup>19, 20</sup>. Deviation from the Arrhenius law has been observed for temperatures lower than 20°C due to the composition and activity of microbial communities.<sup>21</sup> Altogether, our results advocate for the use of CSIA, which seems more robust in an up-scaling approach, i.e., with similar  $\epsilon_C$ , to predict the extent of degradation than the use of lab-scale degradation rates, which is the “traditional method” to evaluate pesticide degradation in surface water.

**Water flow velocity impacts pesticide dissipation at the SWI.** In Chap. 5, a bench-scale river channel was used to increase the complexity of the system and to be more representative of the river dynamics than static batch experiments. This design allowed us to consider the reactive transport of pesticides across different compartments, i.e., the water-column, the SWI and the riverbed sediment layer constituting the HZ, with different extents of pesticide degradation. Indeed, faster degradation of organic compounds was generally observed in the oxic top layer of the HZ.<sup>22</sup> We observed that the water column could also play a significant role as it accounted for 85% of the total caffeine biodegradation of the system. The significant contribution of the water column compared to the sediment suggests a microbial equilibrium established under and above the SWI, which was favored in our experiment by the thin water layer characterizing our experimental setup. This also raises new questions about the role of the microbial compartments in pesticide biodegradation in a river. This observation will require further experimental investigations to understand current gaps of knowledge regarding the reactivity of the water column. New experiments are proposed in the next Chapter (Chap. 8) to address this gap. Although these results may not be directly extrapolated to S-metolachlor, which is less soluble and more persistent than caffeine, these experiments underlined that the water layers close to the SWI, i.e., riverbed and river banks, can also be

hot-spots of biodegradation. Consequently, according to our results, the water column reactivity may be underestimated when using lab-derived  $DT_{50}$  for water for scaled-up predictions of the extent of degradation in surface water at a river scale.

**Pesticide degradation and persistence under environmental conditions in rivers during a growing season.** Using the CSIA developments (Chap. 2), the lab-scale knowledge about degradation processes, i.e., degradation rate and associated isotope fractionation (Chap. 3 to 5), and previous investigations at the field scale,<sup>23, 24</sup> the dissipation and persistence of *S*-metolachlor in a 120-km<sup>2</sup> catchment (Chap. 6) were evaluated. Under environmental conditions, i.e., dynamic discharge and turbidity in a river, we could tease apart, with the help of C-CSIA, the contribution of the photo- and bio-degradation processes in the river from upstream to downstream. Photo- and bio-degradation processes were observed in the river to be  $2.7 \pm 2.3\%$  and  $10 \pm 3\%$ , respectively, of the applied *S*-metolachlor. Degradation of *S*-metolachlor mainly occurred in field soils, which accounted for  $98.9 \pm 4.7\%$  of the applied *S*-metolachlor before it entered the river network. These results, obtained with C-CSIA data from both sediment and river water, emphasize that the contribution of the river to degradation was minor compared to that of field soils. The results advocate for preventive actions to reduce pesticide runoff from the fields or to enhance hyporheic exchange and reactivity during river restoration, e.g., by promoting obstacles such as wood debris and small dams.<sup>25</sup>

## **Implications**

**Improve representativeness during elementary degradation experiments.** Our results in Chap. 3 advocate for using simulated sunlight more regularly instead of UV lamps when characterizing photodegradation to produce more robust rates, thereby enhancing up-scaling to river systems. Indeed, our results confirmed that the degradation pathways are light wavelength specific,<sup>3, 4, 26</sup> and the rate of degradation, the transformation product or the isotopic enrichment factor calculated from inappropriate settings may lead to misinterpretation of prevailing processes in water–sediment systems.<sup>27</sup> For instance, the use of UV lamps instead of simulated sunlight may overestimate the role of direct and indirect photodegradation pathways in water containing DOM.<sup>28</sup> As pesticide photodegradation might be a significant degradation process in the top layer of rivers, photolysis rates must be derived under realistic conditions (sunlight, DOM and nitrate) to support in situ dissipation evaluation.<sup>29</sup> Similarly, in Chap. 4 & 5, we increased the complexity of investigated processes and showed that the phase transfer, transport and degradation under dynamic conditions should be systematically accounted for via more representative setups, i.e., closer to environmental river conditions. Consequently, degradation rate constants derived from these dynamic lab-scale setups are more generally applicable across scales to predict degradation of pesticides.<sup>27, 30</sup> Finally, the dependency of degradation rates on environmental variables, such as temperature, pH, and oxic conditions, demand that the experimental setups reasonably cover the ranges of these variables to enhance scaling-up from laboratory to environmental scales.

**Complementary tools to investigate degradation.** As the complexity increases throughout the chapters, the need for modelling and additional tools increases to support the interpretation of the dataset generated. Indeed, the simultaneous occurrence of processes involved in the reactive transport of pesticides, i.e., sorption and degradation in closed systems (Chap. 4) and sorption, degradation and transport in dynamic systems (Chap. 5), required modelling tools to confirm or exclude the contribution of a process or a compartment to the observed dissipation. In the case of simultaneous sorption – degradation occurrence, these two processes can be modeled and solved analytically, whereas in dynamic systems at larger scales, reactive transport that incorporates CSIA should be processed through an FRT model with adapted numerical schemes to reduce equifinality and computational time.<sup>31</sup>

Transformation product identification provided complementary evidence for the interpretation of degradation pathways, (Chap. 3 & 4) as previously shown.<sup>32</sup> However, comparison of transformation products from photodegradation and biodegradation also showed that transformation products are not necessarily associated with a specific degradation pathway. As an example, oxalinic acids were the main transformation products of *S*-metolachlor found in almost all investigated conditions in Chap. 3 and 4. Conversely, C stable isotope fractionation may reflect almost exclusively *S*-metolachlor biodegradation in the water–sediment system and may more specifically underpin occurring pathways for surface water investigations.

Finally, at environmental scales, single-element CSIA data are often not sufficient to elucidate the complexity of the system and might be coupled with a mass balance approach. Consequently, preliminary knowledge of the elementary degradation pathways, i.e., hydrolysis, photolysis, biodegradation and their associated kinetic rate constants, is needed to establish a mass balance calculation.

**Advocating for multi-element CSIA.** Advantages of the multi or at least dual element isotope plots to identify photodegradation pathways were illustrated in Chap. 3. However, the choice of the elements targeted for CSIA should be specific to the pesticide based on knowledge of the degradation reactions. For instance, as observed throughout the chapters of this thesis, the primary degradation pathway for chloroacetanilide (hydrolyse, photolyse, biodegradation) involved systematic bond breaking of the C–Cl bond. Consequently, future developments should combine C and Cl CSIA. In addition, to better interpret the degradation pathway during lab scale experiments, dual element CSIA presents some advantages for the environmental scale. For instance, the selection of an appropriate isotopic enrichment factor ( $\epsilon$ ) retrieved from the laboratory experiment to calculate the extent of degradation at river scale should be made on expert knowledge. In contrast, dual isotope plots allow direct pathway identification from the data gathered from environmental samples as the slope of the dual plots indicate  $\epsilon_{E_1}/\epsilon_{E_2}$ , where  $E_1$  and  $E_2$  are the two elements measured. In addition, to resolve the extent of degradation and source apportionment at the same time without using mass balances, at least two elements should be measured to be able to resolve the system of equations.<sup>33, 34</sup>



Consequently, dual plots will become necessary for further environmental investigations, but the choice of elements analyzed will be critical and constrained by the preliminary knowledge of the degradation pathways examined at the lab scale.

## References

1. Masbou, J.; Drouin, G.; Payraudeau, S.; Imfeld, G., Carbon and nitrogen stable isotope fractionation during abiotic hydrolysis of pesticides. *Chemosphere* **2018**, *213*, 368–376.
2. Elsayed, O. F.; Maillard, E.; Vuilleumier, S.; Nijenhuis, I.; Richnow, H. H.; Imfeld, G., Using compound-specific isotope analysis to assess the degradation of chloroacetanilide herbicides in lab-scale wetlands. *Chemosphere* **2014**, *99*, 89–95.
3. Willach, S.; Lutze, H. V.; Eckey, K.; Löppenberg, K.; Lüling, M.; Wolbert, J.-B.; Kujawinski, D. M.; Jochmann, M. A.; Karst, U.; Schmidt, T. C., Direct photolysis of sulfamethoxazole using various irradiation sources and wavelength ranges — insights from degradation product analysis and compound-specific stable isotope analysis. *Environ. Sci. Technol.* **2018**, *52*, (3), 1225–1233.
4. Maier, M. P.; Prasse, C.; Pati, S. G.; Nitsche, S.; Li, Z.; Radke, M.; Meyer, A.; Hofstetter, T. B.; Ternes, T. A.; Elsner, M., Exploring trends of C and N isotope fractionation to trace transformation reactions of diclofenac in natural and engineered systems. *Environ. Sci. Technol.* **2016**, *50*, (20), 10933–10942.
5. Schwarzenbach, R. P.; Gschwend, P. M.; Imboden, D. M., *Environmental organic chemistry*. third ed.; John Wiley & Sons: **2016**; p 1024.
6. Fono, L. J.; Kolodziej, E. P.; Sedlak, D. L., Attenuation of wastewater-derived contaminants in an effluent-dominated river. *Environ. Sci. Technol.* **2006**, *40*, (23), 7257–7262.
7. Leresche, F.; von Gunten, U.; Canonica, S., Probing the photosensitizing and inhibitory effects of dissolved organic matter by using *N,N*-dimethyl-4-cyanoaniline (DMABN). *Environ. Sci. Technol.* **2016**, *50*, (20), 10997–11007.
8. Vione, D.; Minella, M.; Maurino, V.; Minero, C., Indirect photochemistry in sunlit surface waters: Photoinduced production of reactive transient species. *Chem. Eur. J.* **2014**, *20*, (34), 10590–10606.
9. Remucal, C. K., The role of indirect photochemical degradation in the environmental fate of pesticides: A review. *Environ. Sci. Process. Impacts* **2014**, *16*, (4), 628–653.
10. Ehrl, B. N.; Kundu, K.; Gharasoo, M.; Marozava, S.; Elsner, M., Rate-limiting mass transfer in micropollutant degradation revealed by isotope fractionation in chemostat. *Environ. Sci. Technol.* **2018**, *53*, (3), 1197–1205.

11. Kopinke, F.-D.; Georgi, A.; Roland, U., Isotope fractionation in phase-transfer processes under thermodynamic and kinetic control – Implications for diffusive fractionation in aqueous solution. *Sci. Total Environ.* **2018**, *610–611*, 495-502.
12. Boxall, A. B. A.; Sinclair, C. J.; Fenner, K.; Kolpin, D.; Maud, S. J., When synthetic chemicals degrade in the environment. *Environ. Sci. Technol.* **2004**, *38*, (19), 368A–375A.
13. Boye, K.; Noël, V.; Tfaily, M. M.; Bone, S. E.; Williams, K. H.; Bargar, John R.; Fendorf, S., Thermodynamically controlled preservation of organic carbon in floodplains. *Nat. Geosci.* **2017**, *10*, 415.
14. Brune, A.; Frenzel, P.; Cypionka, H., Life at the oxic-anoxic interface: microbial activities and adaptations. *FEMS Microbiol. Rev.* **2000**, *24*, (5), 691–710.
15. Feng, P. C. C., Soil transformation of acetochlor via glutathione conjugation. *Pestic. Biochem. Physiol.* **1991**, *40*, (2), 136–142.
16. Allocati, N.; Federici, L.; Masulli, M.; Di Ilio, C., Glutathione transferases in bacteria. *FEBS J.* **2009**, *276*, (1), 58–75.
17. Alvarez-Zaldívar, P.; Payraudeau, S.; Meite, F.; Masbou, J.; Imfeld, G., Pesticide degradation and export losses at the catchment scale: Insights from compound-specific isotope analysis (CSIA). *Water Res.* **2018**, *139*, 198–207.
18. Ghattas, A.-K.; Fischer, F.; Wick, A.; Ternes, T. A., Anaerobic biodegradation of (emerging) organic contaminants in the aquatic environment. *Water Res.* **2017**, *116*, 268–295.
19. Dinelli, G.; Accinelli, C.; Vicari, A.; Catizone, P., Comparison of the persistence of atrazine and metolachlor under field and laboratory conditions. *J. Agric. Food. Chem.* **2000**, *48*, (7), 3037–3043.
20. Meite, F.; Alvarez-Zaldívar, P.; Crochet, A.; Wiegert, C.; Payraudeau, S.; Imfeld, G., Impact of rainfall patterns and frequency on the export of pesticides and heavy-metals from agricultural soils. *Sci. Total Environ.* **2018**, *616–617*, 500–509.
21. Meynet, P.; Davenport, R. J.; Fenner, K., Understanding the dependence of micropollutant biotransformation rates on short-term temperature shifts. *Environ. Sci. Technol.* **2020**, *54*, (19), 12214–12225.
22. Lewandowski, J.; Arnon, S.; Banks, E.; Batelaan, O.; Betterle, A.; Broecker, T.; Coll, C.; Drummond, J. D.; Gaona Garcia, J.; Galloway, J.; Gomez-Velez, J.; Grabowski, R. C.; Herzog, S. P.; Hinkelmann, R.; Höhne, A.; Hollender, J.; Horn, M. A.; Jaeger, A.; Krause, S.; Löchner Prats, A.; Magliozzi, C.; Meinikmann, K.; Mojarrad, B. B.; Mueller, B. M.; Peralta-Maraver, I.; Popp, A. L.; Posselt, M.; Putschew, A.; Radke, M.; Raza, M.; Riml, J.; Robertson, A.; Rutere, C.; Schaper, J. L.; Schirmer, M.; Schulz, H.; Shanafield, M.; Singh, T.; Ward, A. S.; Wolke, P.; Wörman, A.; Wu, L., Is the hyporheic zone relevant beyond the scientific community? *Water* **2019**, *11*, (11), 2230.

23. Meite, F. Transformation et transport des pesticides inorganiques et de synthèse dans les sols de bassins versants agricoles. Doctoral thesis, Laboratoire d'Hydrologie et de Géochimie de Strasbourg (LHyGeS), l'université de Strasbourg, Strasbourg, **2018**; 367.
24. Alvarez-Zaldivar, P. Pesticide degradation and transport at catchment scale Compound-specific isotope analysis and numerical modelling. Doctoral thesis, Laboratoire d'Hydrologie et de Géochimie de Strasbourg (LHyGeS), University of Strasbourg, Strasbourg, **2018**; p 202.
25. Peter, K. T.; Herzog, S.; Tian, Z.; Wu, C.; McCray, J. E.; Lynch, K.; Kolodziej, E. P., Evaluating emerging organic contaminant removal in an engineered hyporheic zone using high resolution mass spectrometry. *Water Res.* **2019**, *150*, 140–152.
26. Hensen, B.; Olsson, O.; Kummerer, K., The role of irradiation source setups and indirect phototransformation: Kinetic aspects and the formation of transformation products of weakly sunlight-absorbing pesticides. *Sci. Total Environ.* **2019**, *695*, 133808.
27. Katagi, T., Pesticide behavior in modified water–sediment systems. *J. Pestic. Sci.* **2016**, *41*, (4), 121–132.
28. Apell, Jennifer N.; McNeill, K., Updated and validated solar irradiance reference spectra for estimating environmental photodegradation rates. *Environ. Sci. Process. Impacts* **2019**, *21*, (3), 427–437.
29. Radke, M.; Ulrich, H.; Wurm, C.; Kunkel, U., Dynamics and attenuation of acidic pharmaceuticals along a river stretch. *Environ. Sci. Technol.* **2010**, *44*, (8), 2968–2974.
30. Honti, M.; Hahn, S.; Hennecke, D.; Junker, T.; Shrestha, P.; Fenner, K., Bridging across OECD 308 and 309 data in search of a robust biotransformation indicator. *Environ. Sci. Technol.* **2016**, *50*, (13), 6865–6872.
31. Van Breukelen, B. M.; Prommer, H., Beyond the Rayleigh equation: Reactive transport modeling of isotope fractionation effects to improve quantification of biodegradation. *Environ. Sci. Technol.* **2008**, *42*, (7), 2457–2463.
32. Huntscha, S.; Hofstetter, T. B.; Schymanski, E. L.; Spahr, S.; Hollender, J., Biotransformation of benzotriazoles: Insights from transformation product identification and compound-specific isotope analysis. *Environ. Sci. Technol.* **2014**, *48*, (8), 4435–4443.
33. Lutz, S. R.; Van Breukelen, B. M., Combined source apportionment and degradation quantification of organic pollutants with CSIA: 1. Model derivation. *Environ. Sci. Technol.* **2014**, *48*, (11), 6220–6228.
34. Lutz, S. R.; Van Breukelen, B. M., Combined source apportionment and degradation quantification of organic pollutants with CSIA: 2. Model validation and application. *Environ. Sci. Technol.* **2014**, *48*, (11), 6229–6236.

## **Chapter 8**

### **Perspectives and implications**

#### **General consideration**

According to the state of the art addressed at the beginning of this thesis, the understanding of pesticide degradation is currently limited due to the unresolved complexity of the interplay between water flow velocity and microbial dynamics, and the physico-chemical properties of pesticides. In particular, the impact of drivers of water flow dynamics (e.g., water flow velocity and sediment bedforms) on the hyporheic exchange flows (HEFs) and on the capacity of pesticide dissipation at the sediment–water interface (SWI) remained unclear.<sup>1, 2</sup> Altogether, the results of this, PhD including the development of the bench-scale river channel, serve as an opportunity to investigate dynamic processes involving pollutant biodegradation at the SWI. It raises three specific questions that can be addressed in future studies, as described in a set of experiments presented in the following sections:

1. Is pesticide biodegradation river flow-dependent?
2. What is the effect of dissolved and particulate organic carbon (DOC/POC) on pesticide biodegradation under hydrological and sediment transport dynamics in a river?
3. Which microbial compartments (soluble extracellular enzyme, extracellular polymeric substance (EPS)-bound enzyme, planktonic cell) are mainly involved in pesticide biodegradation in a river?

Compound-specific stable isotope analysis (CSIA) of organic micropollutants in the SWI applied across different scales as well as the complexity of the investigation emphasized some potential applications and limitations in its ability to evaluate the contribution of pesticide dissipation processes in water–sediment systems. The potential applications and limitations were addressed at different scales of investigation, which include laboratory batch experiments (Chap. 3 & 4), bench-scale river channel models (Chap. 5) and catchment scale environmental investigations (Chap. 7). Throughout this thesis project, I have been faced with the current limitations of the sensitivity associated with CSIA measurements. To overcome this limitation, the general strategy was to concentrate the sample during the preparation, which also co-concentrated the environmental matrix, e.g., natural organic compounds. As observed (Chap. 2, 3, 4 & 6) during this Ph.D., this environmental matrix in samples greatly hampered C-CSIA measurements, and even more so N-CSIA measurements. This reduced the accuracy and precision of the estimated biodegradation and source apportionment at the river scale within

the current analytical framework. I discuss below some conceptual and analytical aspects to circumvent this limitation in the future.

In the two sections below, I present a potential future experimental investigation of pesticide dissipation at the SWI under water flow velocity conditions to elucidate the unresolved complexity of the interplay between water flow and microbial dynamics by addressing the three questions above. Then, in a second section, I provide a roadmap to address pesticide-CSIA limitations and strategies to overcome the environmental matrix observed in our thesis project with emphasis on future research questions about organic compound fate at the SWI.

## **Towards future investigation of pesticide dissipation at the SWI**

The interplay between surface and groundwater flows, pesticide partitioning between dissolved and sorbed phases, biogeochemical conditions, and microbial compartments involved in the degradative processes at the SWI remain poorly understood. Despite recent investigations<sup>1-3</sup>, this represents a current gap to understand and predict pesticide dissipation at the river scale. Teasing apart the contribution of each of these components at the SWI reactivity might be possible under controlled and replicable experiments at the laboratory scale.

**Examining how flow affects biodegradation.** HEFs, i.e., in- and outflow from the hyporheic zone (HZ), are hypothesized to be the major drivers of the reactivity of pesticide biodegradation in surface water.<sup>4-6</sup> Although frequently studied, the impact of water flow dynamic drivers (e.g., water flow velocity and sediment bedforms) on HEFs and on the capacity of pesticide dissipation at the SWI remains difficult to investigate. In this Ph.D. thesis, tracer experiments and numerical evidence<sup>2</sup> underlined that river flows can significantly affect organic compound exchanges across the SWI and the depth of the oxic layer in the sediment. However, the estimated biodegradation of caffeine at the SWI obtained in Chap. 5 appeared to be flow-independent, i.e., no difference in the biodegradation rates for the three laminar water flow velocities tested. In addition, I observed a significant contribution of biodegradation in the water column compared to that in the sediment, even though the concentration of DOC/POC was observed to be low in the water phase. As DOC/POC was hypothesized has carry on the biodegradation activity in water column.<sup>7</sup> These results suggested that for laminar flow in rivers, biodegradation of non-persistent and soluble micropollutants might be flow independent, having limited interactions with riverbed sediments or suspended particles. However, I hypothesized that for higher flow regimes pesticide transport by river flow might be favored over pesticide incorporation into the HZ, thereby decreasing reactivity due to a lower contact time.

**Emphasizing the role of DOC/POC and microorganisms at the SWI.** The experiment in Chap. 5 underscored the need for fundamental understanding of the microbial dynamics and associated biodegradation at the river scale, i.e., in the water column and in the HZ. Based on our current understanding, water column biodegradation was hypothesized to be mainly related to DOC and POC-sorbed microorganisms<sup>7</sup> or associated with dissolved enzymes or planktonic microorganisms in water.<sup>6, 8</sup> However, to the best of our knowledge, no explanation about the water column reactivity has been validated. A current challenge to quantifying the contribution of soluble enzymes or planktonic microorganisms in river is related to the limited amount of soluble extracellular enzyme material in surface water.<sup>9</sup> In comparison, EPS-bound enzymes attached to suspended or sediment bed material might constitute 65 to 80% of the microbial mass in rivers.<sup>10</sup> In WWTP sludge, EPS-bound enzymes have been shown to play the major role in organic pollutant biodegradation, i.e., up to 90%, compared to soluble extracellular enzymes.<sup>11</sup> To the best of our knowledge, the only clear demonstration of soluble extracellular enzymes in the environment is in the case of hydrocarbon plumes in seawater where microorganism blooms release soluble extracellular enzymes.<sup>12</sup> Indeed, current knowledge cannot fully explain the biodegradation observed in water columns without significant DOC or POC concentrations. Consequently, this lack of knowledge on the microbial dynamic hampers the parametrization of the biodegradation rate in the water column in flow-reactive-transport (FRT) models.

Thus, I proposed to design a future experiment to examine how the microbial dynamics across the SWI and associated biodegradation activity are affected by water flow velocities. I anticipate that the answer will have a huge impact across different fields (ecology, environmental chemistry, hydrology)<sup>13</sup> and will serve to improve interpretation of organic pollutant biodegradation reactivity in surface water.

Our working hypotheses are that biodegradation activity is dominated by the intracellular or EPS-bound enzyme on suspended and dissolved organic material,<sup>14</sup> and that organic matter can act as a substrate for microbial growth.<sup>15</sup> A positive relationship may be drawn between DOC or POC and biodegradation activity, as showed in static experiments.<sup>16</sup> The goal of such a study would be to establish a quantitative relationship between the water flow velocity and the biodegradation rates over a broad spectrum of experimental conditions.

I propose to test different DOC, POC and DOC/POC conditions under several water flow velocities in the bench-scale river channel presented in Chap. 5. The set-up could be slightly modified to measure continuously the concentration of the tested organic pollutant in the water column, using continuous flow-through fluorimetry. In addition, bacteria dynamics could also be measured in-situ by online flow cytometry.<sup>17</sup> This would allow us to obtain a higher time resolution that could be adjusted to the biodegradation rate of the targeted pollutant and microbial activity. A mixture of micropollutants with small half-live values e.g., caffeine, diclofenac, ibuprofen, parathion, benzotriazole, etc. would reduce experiment duration. This would allow for many replicate experiments since experimental reproducibility is crucial here. The FRT developed and presented in Chap. 5 could be adapted to account for the transport of dissolved and particulate organic matter, as well as bacterial growth, to incorporate possible lag phases, as observed in Chap. 5.<sup>2</sup> To generalize our findings, soluble extracellular, extracellular polymeric substance (EPS)-bound and intracellular enzymes could be separated to assess the protease and peptidase activities of the resulting enzyme pools using established protocols.<sup>10-12</sup> Such a dataset may help to understand the microbial dynamics of the different phases of the SWI across diverse hydro-sedimentary conditions. In addition, the development of a module including predictive tools for microbial dynamics can improve the design of adapted river restoration scenarios to enhance biodegradation of anthropogenic pollution.

## **Compound-specific stable isotope analysis (CSIA) of organic micropollutants in the sediment-water interface (SWI): potential application, limits and implications**

The use of CSIA in the field has the advantage of being able to identify degradation without needing to complete a mass balance or identify transformation products. The principal concept of CSIA is fairly simple and has been used to demonstrate biodegradation in aquifers<sup>18-20</sup> and laboratory studies for decades.<sup>21</sup> Each degradation pathway exhibits a specific isotopic enrichment factor ( $\epsilon$ ), allowing us to evaluate the degradation extent and pathways from isotopic data (Chap. 3 to 5). In addition, source appointment may be quantified to some extent. In the presented case study (Chap. 6), the quantification of the extent of degradation was limited by the low carbon  $\epsilon$  associated with degradation of *S*-metolachlor ( $\epsilon_C = -1.20 \pm 0.35\text{‰}$ ), and the minimal change of isotopic ratios ( $\Delta\delta^{13}C_{min} = 0.95\text{‰}$ ) above which isotope fractionation could be considered as degradation (eq. B7). Hence the biodegradation extent (eq. 6.4) could only be detected after 50% biodegradation, and minor degradation amounts could not be detected.

Thirdly, during this thesis project, I have faced several limits to measure C-CSIA and N-CSIA (Chap. 2 & 4) from field and experimental samples containing a high level of dissolved organic matter (DOM). This matrix effect resulted from sample preparation to concentrate pesticides for CSIA measurement, which simultaneously co-concentrated the DOM matrix. Gas chromatography–isotope ratio mass spectrometry (GC-IRMS) measurements were in some cases hampered by the large amount of organic matter, resulting in a large GC-IRMS background signal and overlapping peaks of targeted pesticides.

As DOM contained a lot of C, N, P, and S, I anticipate that chlorine might be a key element to examine micropollutant degradation pathways at the SWI since i) chlorine is a common constitutive element of a variety of micropollutants, such as pesticide, plastics, solvents, or pharmaceuticals, ii) bond cleavage resulting from the biodegradation often involves C–Cl bonds, resulting in a primary isotope effect on chlorine,<sup>22</sup> iii) this element is rarely abundant in the DOM matrix and measurements will be less affected by a matrix effect,<sup>23</sup> iv) it has a naturally large isotopic ratio which facilitates its measurement ( $^{37}\text{Cl}/^{35}\text{Cl}$  is about 32%),<sup>24</sup> and v) the limit to detect biodegradation with CSIA is anticipated to be lower than with C. For instance, for *S*-metolachlor, recent developments in chlorine isotope analysis and its high enrichment factor ( $\epsilon = -9.70 \pm 2.9\text{‰}$ )<sup>25</sup> can overcome the limitations in detecting biodegradation and might allow future pesticide degradation detection lower than 10%. However, chlorine isotope analysis currently suffers from unresolved bottlenecks, discussed in recent reviews,<sup>22, 26</sup> and presented as a practical point of view in the section below.

In summary, before attempting in-situ analysis of pesticide degradation in surface water, analytic development capabilities for dual element CSIA with limited matrix interference should be consolidated. Dual-element CSIA will improve quantification and pathway evaluation of pesticide degradation presented in Chap. 1. Major improvements regarding measurement sensitivity or/and sample preparation to reduce DOM-matrix effect should be made to address micropollutant degradation at the SWI by CSIA. This aspect is addressed in the following section.



## **Toward the chlorine isotope measurement**

Today, on-line carbon isotope measurement has become available in many laboratories and has been widely used for assessing pesticide degradation in the field. In contrast, chlorine isotope measurement is rarely available and suffers from unresolved challenges. Diverse methods are available to measure stable chlorine isotopes, including GC–high-temperature conversion (HTC)–IRMS,<sup>27</sup> GC–inductively coupled plasma (ICP)–high resolution mass spectrometer (HRMS)<sup>28</sup> and GC–quadrupole mass spectrometer (qMS).<sup>25</sup>

GC-HTC-IRMS requires a dedicated GC-IRMS device due to the production of the analyte gas HCl, which could degrade the device and hamper proper measurements of other elements, which is extremely costly for routine analysis. However, analysis with GC-HTC-IRMS allows for direct data comparison and validation with other techniques.<sup>27, 29</sup>

GC-ICP-HRMS is able to resolve the Cl-isotopologue  $^{37}\text{Cl}^+$  ( $m/z = 36.9659$ ) from the mass interference of argon plasma  $^1\text{H}^{36}\text{Ar}^+$  ( $m/z = 36.9754$ ). However, ICP ionization was originally designed for heavy elements ( $> 40$  amu) which have lower ionization potential than Cl.<sup>30, 31</sup> Consequently, the yield of ionization of Cl is lower than for heavy elements which reduces the signal intensity, can increase the difficulty for the GC-ICP-HRMS obtain accurate and precise results, and makes the sensitivity comparable to GC-qMS for chlorine isotope application. Finally, a practical limitation is that ICP-HRMS was not traditionally built for GC coupling, and software for data acquisition might not always allow transient signals to calculate the isotope ratio.<sup>32, 33</sup> These two practical limitations might be overcome by trigger synchronization between GC and ICP-HRMS and external analysis workflow, which would require intense development in the laboratory.

In comparison, GC-qMS is the most financial and versatile tool available for routine analysis all laboratories. The tool also has the advantage of having a generally integrated workflow, which enables isotopic ratio estimation and processing of a routinely large number of samples. Good laboratory practice concerning chlorine isotope analysis has already been addressed and includes multiple injections ( $n = 8$  to  $10$ ) of the sample, extensive bracketing by a molecularly identical isotopic reference material with known  $\delta^{37}\text{Cl}$  and intensive optimization of peak integration parameters.<sup>34</sup>

One disadvantage of the GC-qMS isotope application is that the analytic gas is dependent on the organic compound as the analyte are a mass fragment of the organic compound molecule containing Cl. Consequently, several molecularly identical isotopic reference materials with known  $\delta^{37}\text{Cl}$  should be established for a large spectrum of  $\delta$  values to implement the regular reference standard strategy of CSIA.<sup>35</sup> The establishment of in-house Cl reference material is crucial and challenging for new molecule investigation, but has been recently accomplished for acetochlor and *S*-metolachlor.<sup>36</sup> The authors provide the synthesis method to generate in-house reference material, which could potentially be applied to a large spectrum of Cl-containing organic compounds and open new avenues for CSIA application. However, in-house reference material  $\delta$  values must be validated by inter-laboratory consensus measurement with reference comparison between GC-qMS versus GC-ICP-HRMS and/or GC-HTC-IRMS.<sup>29</sup>

To conclude, new method development will be needed for chlorine isotope investigation to offer new insights into pesticide degradation at the field scale for new organic compounds. GC-qMS  $\delta^{37}\text{Cl}$  is the most affordable method, with a low method development cost and similar accuracy and sensitivity to the reference method (GC-HTC-IRMS), that can be used for new applications. However, there is a crucial need to establish suitable reference material with inter-laboratory consensus and reference method validations beforehand.

### **Improving sample preparation, accuracy, reproducibility, and sensitivity for CSIA measurements**

Sample preparation for GC-IRMS measurement should meet the following criteria: i) the pesticides extraction should produce at least a 70% yield, ii) the extraction and following preparation should not induce significant isotopic fractionation of the target element, which should be at least lower than the typical precision for the considered element (Table 1.1), iii) the sample should be sufficiently concentrated to enable measurement of the target element, iv) a complete separation of the individual pesticides should be achieved, and v) the absence of matrix effects, which could cause background interference in the measurements, should be demonstrated. In this thesis, for a mixture of pesticides, I have addressed the two first points with C-CSIA (Chap. 2). Criterion iv) is very important because the two isotopologues were found to elute differently, where the heavier appear slightly earlier on the gas chromatogram.<sup>37</sup> If the two associated pesticides peaks overlap, the  $\delta$  values of both would be altered.<sup>38</sup> However, this point was largely covered by the good laboratory practice of properly separating two organic compounds<sup>39</sup> in the GC and was not considered to be limiting. Criteria iii) and v) are related since the common analytical strategy is to concentrate the sample to meet the requirement of typical sensitivity of the measured element, which increases the matrix concentration and potential associated measurement pitfall. Two complementary strategies could be envisaged to resolve both problems simultaneously. This includes (i) more

sophisticated sample post-cleaning to remove DOM-matrix interference, and (ii) an improvement of the sensitivity of the device to allow lower accurate measurements.

### *Improving sample preparation to remove matrix interference*

DOM from surface water contains a large amount of dissolved carbon and nitrogen, up to 10 and 0.5 ppm respectively.<sup>40,41</sup> They are partially removed during the extraction procedure using SPE cartridges (Chap. 3) but the residual dissolved C and N allow for accurate CSIA measurement. Briefly, DOM could co-elute with the pesticides and create background during chromatography. As they are combusted together, i.e., DOM and pesticides, to allow IRMS measurement, the observed  $\delta$  value will reflect the  $\delta$  value of the pesticide together with that of the DOM matrix. Several strategies to eliminate the DOM matrix have been discussed in the literature, such as preparative high-performance liquid chromatography (HPLC),<sup>42</sup> size exclusion chromatography (SEC),<sup>43</sup> two-dimensional gas chromatography–isotope ratio (2D-GC)<sup>44, 45</sup> and molecularly imprinted polymers (MIPs).<sup>46, 47</sup> However, I anticipate that preparative HPLC would remove background around the peak but not necessarily that attached to the peak itself during chromatographic separation. SEC has never been tested for CSIA applications but should work in the case of the DOM matrix from river water, which has a minimum molecular mass difference of 2 kDa from the extracted compounds. Consequently, the method will be probably not suitable for WWTP samples, which could contain a large DOC content (up to 30 ppm),<sup>48</sup> but also a large amount of compounds that have a similar order of molecular mass (100-1000 Da).<sup>49</sup>

2D-GC has been evaluated for CSIA application including benzene, toluene, ethylbenzene, and xylenes (BTEX) in environmental samples with high matrix loads (level not reported),<sup>45</sup> steroid analysis in urine<sup>50</sup> and C4 and C5 saturated compounds in smoke samples.<sup>51</sup> These three examples demonstrate the feasibility of 2D-GC-IRMS to remove matrix interference with the same typical uncertainty and sensitivity as the regular GC-IRMS. One criticism concerning 2D-GC-IRMS is an increase of GC run time by at least a factor two. However, the issues remain regarding the feasibility of surface water samples with DOC loads of about 10 ppm or complex mixtures of DOC in WWTP effluent.

MIPs have gained a large interest over the past several years<sup>47</sup> and constitute the most promising way to remove the DOM matrix and enable pesticide analysis<sup>52, 53</sup>, with successful measurement of samples originally associated with a large matrix. To our knowledge, MIPs have never been used for pesticide CSIA applications, but a proof of concept has been demonstrated for 1*H*-benzotriazole (from dishwashing detergent). Bakkour et al.<sup>54</sup> report a high efficiency of selective extraction of 1*H*-benzotriazole from WWTP effluent with DOC loads up to 28 ppm. The authors reported an average fractionation of C and N from its original value ( $\Delta\delta^{13}\text{C}$  and  $\Delta\delta^{15}\text{N}$ ) of  $0.6 \pm 0.4\%$  and  $-1.4 \pm 1.3\%$  which matches the analytical uncertainty of typical measurements by GC-IRMS for C, although is fairly high for N. However, attainment of some reproducible and accurate values, although they may be less precise, for N could be still an advantage compared to no attainable values when using dual-element CSIA.

To sum up, 2D-GC and MIPs constitute the most promising cleaning methods for further pesticide CSIA studies to remove DOM matrices and produce more accurate and reproducible GC-IRMS measurements. In both cases, extract cleaning should be added as an additional step in the developed extraction method (Chap. 2) to decrease the matrix effect. The drawback of this strategy will be an increase in the overall sample analysis workflow time, and thus a decrease in overall sample processing within the same timeframe. Finally, the strategy to improve DOM matrix cleaning has been discussed for water extract to compare feasibility of different practices and to give examples from the literature. However, the same strategy could also be applied to soil/sediment extract to remove the DOM matrix.<sup>53</sup>

#### *Custom-made devices for higher sensitivity of accurate isotopic measurement*

It is also important to mention that the low instrumental sensitivity, typically 0.1 to 5 nmol and 1 to 10 nmol for carbon and nitrogen, respectively, is one of the major limitations for CSIA environmental application.<sup>55</sup> Increasing instrumental sensitivity will open new avenues for applications constrained by sampling volumes, while reducing interference in GC-IRMS from the sample matrix. Consequently, increasing the instrument sensitivity without diminishing, or even increasing, the high analytical precision should be a priority for further development. To our knowledge, the focus of recent studies has largely concerned applications of CSIA, sample preparation and sampling strategy rather than analytical measurement improvement. Common GC-IRMS were developed in the early 1990's without major improvements until today.<sup>56</sup> One major improvement was to use a custom-made combustion oven with a better temperature controller and optimized conditions.<sup>57-59</sup> Recently, a single combined reactor (P/N 1255321, NiO tube and CuO-NiO-Pt wires, Thermo Fischer Scientific) was promoted for CSIA for compounds less volatile and more recalcitrant to combustion such as atrazine and dichlobenil.<sup>60</sup> This has the obvious advantage for routine analysis of C of having a single combined reactor, compared to the traditional GC-IRMS with two reactors, one for oxidation one for reduction. One disadvantage of a single reactor may be its less versatile setup than the traditional GC-IRMS, meaning that tuning will be not possible. For instance, in the case of nitrogen isotopic measurement, the oxidation of an organic compound to  $N_xO_y$  is followed by a reduction of  $N_xO_y$  to form  $N_2$ , analyzed by the IRMS. The reduction zone, in the case of a single reactor, should have sufficient reductive capacity to scavenge the oxygen surplus coming from the oxidation and reduced  $N_xO_y$ . Conversely, insufficient oxygen will not allow proper combustion of the organic compound. In addition, reduction is often optimized with a lower temperature than oxidation<sup>57, 59</sup> which is difficult to control in a single oven.

To our knowledge only two initiatives to lower the IRMS sensitivity have been made. They both have start by modifying a regular instrument. The Naohiko Ohkouchi group was able to improve the sensitivity by about 160-340 and 30 times for both nitrogen and carbon isotopic measurements.<sup>61</sup> They made different improvements to the device, including replacing the nafion water trap by a custom-made trap, and improving the electric flow control valves for pulse injection by a leak-tight four-port valve to lower the  $N_2$  background. More recently the Katherine H. Freeman group was able to improve the sensitivity up to 30 pmol of carbon.<sup>62</sup>

They used a combination of improvements including microfluidic valves, hand-made capillary combustion reactors, narrow capillary transfer lines and cryogenic water traps.

To conclude, I anticipate that custom-made devices for CSIA application will be more popular in the future and will offer new perspective to enable more accurate, reproducible and sensitive stable isotope measurements. However, while some custom-made adjustments can be done easily, e.g., combustion reactors and water traps, most of them need engineering skills and require intensive development, e.g., capillary valves.

## References

1. Posselt, M.; Mechelke, J.; Rutere, C.; Coll, C.; Jaeger, A.; Raza, M.; Meinikmann, K.; Krause, S.; Sobek, A.; Lewandowski, J.; Horn, M. A.; Hollender, J.; Benskin, J. P., Bacterial diversity controls transformation of wastewater-derived organic contaminants in river-simulating flumes. *Environ. Sci. Technol.* **2020**, *54*, (9), 5467–5479.
2. Drouin, G.; Fahs, M.; Droz, B.; Younes, A.; Imfeld, G.; Payraudeau, S., Pollutant dissipation at the sediment–water interface: a robust discrete continuum numerical model and recirculating laboratory experiments. *Water Resour. Res.* **2020**, *sub*.
3. Mechelke, J.; Rust, D.; Jaeger, A.; Hollender, J., Enantiomeric fractionation during biotransformation of chiral pharmaceuticals in recirculating water-sediment test flumes. *Environ. Sci. Technol.* **2020**, *54*, (12), 7291–7301.
4. Zarnetske, J. P.; Haggerty, R.; Wondzell, S. M.; Baker, M. A., Dynamics of nitrate production and removal as a function of residence time in the hyporheic zone. *J. Geophys. Res.: Biogeosci.* **2011**, *116*, G01025.
5. Schaper, J. L.; Posselt, M.; Bouchez, C.; Jaeger, A.; Nuetzmann, G.; Putschew, A.; Singer, G.; Lewandowski, J., Fate of trace organic compounds in the hyporheic zone: Influence of retardation, the benthic biolayer, and organic carbon. *Environ. Sci. Technol.* **2019**, *53*, (8), 4224–4234.
6. Schaper, J. L.; Posselt, M.; McCallum, J. L.; Banks, E. W.; Hoehne, A.; Meinikmann, K.; Shanafield, M. A.; Batelaan, O.; Lewandowski, J., Hyporheic exchange controls fate of trace organic compounds in an urban stream. *Environ. Sci. Technol.* **2018**, *52*, (21), 12285–12294.
7. De la Cruz Barrón, M.; Merlin, C.; Guilloteau, H.; Montargès-Pelletier, E.; Bellanger, X., Suspended materials in river waters differentially enrich class 1 integron- and IncP-1 plasmid-carrying bacteria in sediments. *Front. Microbiol.* **2018**, *9*, 1443.
8. Kunkel, U.; Radke, M., Biodegradation of acidic pharmaceuticals in bed sediments: Insight from a laboratory experiment. *Environ. Sci. Technol.* **2008**, *42*, (19), 7273–7279.

9. Fillinger, L.; Zhou, Y.; Kellermann, C.; Griebler, C., Non-random processes determine the colonization of groundwater sediments by microbial communities in a pristine porous aquifer. *Environ. Microbiol.* **2019**, *21*, (1), 327–342.
10. Romaní, A.; Fund, K.; Artigas, J.; Schwartz, T.; Sabater, S.; Obst, U., Relevance of polymeric matrix enzymes during biofilm formation. *Microb. Ecol.* **2008**, *56*, 427–436.
11. Zumstein, M. T.; Helbling, D. E., Biotransformation of antibiotics: Exploring the activity of extracellular and intracellular enzymes derived from wastewater microbial communities. *Water Res.* **2019**, *155*, 115–123.
12. Cerro-Gálvez, E.; Sala, M. M.; Marrasé, C.; Gasol, J. M.; Dachs, J.; Vila-Costa, M., Modulation of microbial growth and enzymatic activities in the marine environment due to exposure to organic contaminants of emerging concern and hydrocarbons. *Sci. Total Environ.* **2019**, *678*, 486–498.
13. Lewandowski, J.; Arnon, S.; Banks, E.; Batelaan, O.; Betterle, A.; Broecker, T.; Coll, C.; Drummond, J. D.; Gaona Garcia, J.; Galloway, J.; Gomez-Velez, J.; Grabowski, R. C.; Herzog, S. P.; Hinkelmann, R.; Höhne, A.; Hollender, J.; Horn, M. A.; Jaeger, A.; Krause, S.; Löchner Prats, A.; Magliozzi, C.; Meinikmann, K.; Mojarrad, B. B.; Mueller, B. M.; Peralta-Maraver, I.; Popp, A. L.; Posselt, M.; Putschew, A.; Radke, M.; Raza, M.; Riml, J.; Robertson, A.; Rutere, C.; Schaper, J. L.; Schirmer, M.; Schulz, H.; Shanafield, M.; Singh, T.; Ward, A. S.; Wolke, P.; Wörman, A.; Wu, L., Is the hyporheic zone relevant beyond the scientific community? *Water* **2019**, *11*, (11), 2230.
14. Battin, T. J.; Besemer, K.; Bengtsson, M. M.; Romani, A. M.; Packmann, A. I., The ecology and biogeochemistry of stream biofilms. *Nat. Rev. Microbiol.* **2016**, *14*, (4), 251–263.
15. Meile, C.; Scheibe, T. D., Reactive transport modeling of microbial dynamics. *Elements* **2019**, *15*, (2), 111–116.
16. Honti, M.; Hahn, S.; Hennecke, D.; Junker, T.; Shrestha, P.; Fenner, K., Bridging across OECD 308 and 309 data in search of a robust biotransformation indicator. *Environ. Sci. Technol.* **2016**, *50*, (13), 6865–6872.
17. Besmer, M. D.; Weissbrodt, D. G.; Kratochvil, B. E.; Sigrist, J. A.; Weyland, M. S.; Hammes, F., The feasibility of automated online flow cytometry for in-situ monitoring of microbial dynamics in aquatic ecosystems. *Front. Microbiol.* **2014**, *5*.
18. Sherwood Lollar, B.; Slater, G. F.; Ahad, J.; Sleep, B.; Spivack, J.; Brennan, M.; MacKenzie, P., Contrasting carbon isotope fractionation during biodegradation of trichloroethylene and toluene: Implications for intrinsic bioremediation. *Org. Geochem.* **1999**, *30*, (8, Part 1), 813–820.
19. Aelion, C. M. H., Patrick Hunkeler, daniel; Aravena, R., *Environmental isotopes in biodegradation and bioremediation*. CRC press: **2009**; p 450.
20. Hermon, L.; Denonfoux, J.; Hellal, J.; Joulain, C.; Ferreira, S.; Vuilleumier, S.; Imfeld, G., Dichloromethane biodegradation in multi-contaminated groundwater: Insights from biomolecular and compound-specific isotope analyses. *Water Res.* **2018**, *142*, 217351–357226.

21. Elsner, M.; Imfeld, G., Compound-specific isotope analysis (CSIA) of micropollutants in the environment — current developments and future challenges. *Curr. Opin. Biotechnol.* **2016**, *41*, 60–72.
22. Zimmermann, J.; Halloran, L. J. S.; Hunkeler, D., Tracking chlorinated contaminants in the subsurface using compound-specific chlorine isotope analysis: A review of principles, current challenges and applications. *Chemosphere* **2020**, *244*, 125476.
23. LaRowe, D. E.; Van Cappellen, P., Degradation of natural organic matter: A thermodynamic analysis. *Geochim. Cosmochim. Acta* **2011**, *75*, (8), 2030–2042.
24. Brand, W. A.; Coplen, T. B.; Vogl, J.; Rosner, M.; Prohaska, T., Assessment of international reference materials for isotope-ratio analysis (IUPAC Technical Report). *Pure Appl. Chem.* **2014**, *86*, (3), 425–467.
25. Ponsin, V.; Torrentó, C.; Lihl, C.; Elsner, M.; Hunkeler, D., Compound-specific chlorine isotope analysis of the herbicides atrazine, acetochlor and metolachlor. *Anal. Chem.* **2019**, *91*, (22), 14290–14298.
26. Ojeda, A. S.; Phillips, E.; Sherwood Lollar, B., Multi-element (C, H, Cl, Br) stable isotope fractionation as a tool to investigate transformation processes for halogenated hydrocarbons. *Environ. Sci. Process. Impacts* **2020**, *22*, 567–582.
27. Renpenning, J.; Kümmel, S.; Hitzfeld, K. L.; Schimmelmann, A.; Gehre, M., Compound-specific hydrogen isotope analysis of heteroatom-bearing compounds via gas chromatography–chromium-based high-temperature conversion (Cr/HTC)–isotope ratio mass spectrometry. *Anal. Chem.* **2015**, *87*, (18), 9443–9450.
28. Van Acker, M. R. M. D.; Shahar, A.; Young, E. D.; Coleman, M. L., GC/multiple collector-ICPMS method for chlorine stable isotope analysis of chlorinated aliphatic hydrocarbons. *Anal. Chem.* **2006**, *78*, (13), 4663–4667.
29. Bernstein, A.; Shouakar-Stash, O.; Ebert, K.; Laskov, C.; Hunkeler, D.; Jeannotat, S.; Sakaguchi-Soder, K.; Laaks, J.; Jochmann, M. A.; Cretnik, S.; Jager, J.; Haderlein, S. B.; Schmidt, T. C.; Aravena, R.; Elsner, M., Compound-specific chlorine isotope analysis: A comparison of gas chromatography/isotope ratio mass spectrometry and gas chromatography/quadrupole mass spectrometry methods in an interlaboratory study. *Anal. Chem.* **2011**, *83*, (20), 7624–7634.
30. Vanhaecke, F.; Balcaen, L.; Malinovsky, D., Use of single-collector and multi-collector ICP-mass spectrometry for isotopic analysis. *J. Anal. At. Spectrom.* **2009**, *24*, (7), 863–886.
31. Weiss, D.; Rehkämper, M.; Schoenberg, R.; McLaughlin, M.; Kirby, J.; Campbell, P.; Arnold, T.; Chapman, J.; Peel, K.; Gioia, S., Application of nontraditional stable-isotope systems to the study of sources and fate of metals in the environment. *Environ. Sci. Technol.* **2008**, *42*, (3), 655–664.
32. Horst, A.; Renpenning, J.; Richnow, H.-H.; Gehre, M., Compound specific stable chlorine isotopic analysis of volatile aliphatic compounds using gas chromatography hyphenated with multiple collector inductively coupled plasma mass spectrometry. *Anal. Chem.* **2017**, *89*, (17), 9131–9138.

33. Renpenning, J.; Horst, A.; Schmidt, M.; Gehre, M., Online isotope analysis of  $^{37}\text{Cl}/^{35}\text{Cl}$  universally applied for semi-volatile organic compounds using GC-MC-ICPMS. *J. Anal. At. Spectrom.* **2018**, *33*, (2), 314–321.
34. Aeppli, C.; Holmstrand, H.; Andersson, P.; Gustafsson, O., Direct compound-specific stable chlorine isotope analysis of organic compounds with quadrupole GC/MS using standard isotope bracketing. *Anal. Chem.* **2010**, *82*, (1), 420–426.
35. Werner, R. A.; Brand, W. A., Referencing strategies and techniques in stable isotope ratio analysis. *Rapid Commun. Mass Spectrom.* **2001**, *15*, (7), 501–519.
36. Lihl, C.; Renpenning, J.; Kümmel, S.; Gelman, F.; Schürner, H. K. V.; Daubmeier, M.; Heckel, B.; Melsbach, A.; Bernstein, A.; Shouakar-Stash, O.; Gehre, M.; Elsner, M., Toward improved accuracy in chlorine isotope analysis: synthesis routes for in-house standards and characterization via complementary mass spectrometry methods. *Anal. Chem.* **2019**, *91*, (19), 12290–12297.
37. Brenna, J. T.; Corso, T. N.; Tobias, H. J.; Caimi, R. J., High-precision continuous-flow isotope ratio mass spectrometry. *Mass Spectrom. Rev.* **1997**, *16*, (5), 227–258.
38. Hayes, J. M.; Freeman, K. H.; Popp, B. N.; Hoham, C. H., Compound-specific isotopic analyses: A novel tool for reconstruction of ancient biogeochemical processes. *Org. Geochem.* **1990**, *16*, (4), 1115–1128.
39. *Gaz chromatography GC troubleshooting guide*; Phenomenex: **2014**.
40. Raymond, P. A.; Spencer, R. G. M., Chapter 11 - Riverine DOM. In *Biogeochemistry of marine dissolved organic matter (Second edition)*, Hansell, D. A.; Carlson, C. A., Eds. Academic Press: Boston, US, **2015**; pp 509–533.
41. International Humic Substances Society <http://humic-substances.org/> (**2020**),
42. Torrentó, C.; Bakkour, R.; Glauser, G.; Melsbach, A.; Ponsin, V.; Hofstetter, T.; Elsner, M.; Hunkeler, D., Solid-phase extraction method for stable isotope analysis of pesticides from large volume environmental water samples. *Analyst* **2019**, *144*, 2898–2908.
43. Sandron, S.; Rojas, A.; Wilson, R.; Davies, N. W.; Haddad, P. R.; Shellie, R. A.; Nesterenko, P. N.; Kelleher, B. P.; Paull, B., Chromatographic methods for the isolation, separation and characterisation of dissolved organic matter. *Environ. Sci. Process. Impacts* **2015**, *17*, (9), 1531–1567.
44. Amaral, M. S. S.; Nolvachai, Y.; Marriott, P. J., Comprehensive two-dimensional gas chromatography advances in technology and applications: Biennial update. *Anal. Chem.* **2020**, *92*, (1), 85–104.
45. Ponsin, V.; Buscheck, T. E.; Hunkeler, D., Heart-cutting two-dimensional gas chromatography–isotope ratio mass spectrometry analysis of monoaromatic hydrocarbons in complex groundwater and gas-phase samples. *J. Chromatogr. A* **2017**, *1492*, 117–128.
46. Martín-Esteban, A., Molecularly-imprinted polymers as a versatile, highly selective tool in sample preparation. *TrAC, Trends Anal. Chem.* **2013**, *45*, 169–181.



47. Pichon, V.; Delaunay, N.; Combès, A., Sample preparation using molecularly imprinted polymers. *Anal. Chem.* **2020**, *92*, (1), 16–33.
48. Michael-Kordatou, I.; Michael, C.; Duan, X.; He, X.; Dionysiou, D. D.; Mills, M. A.; Fatta-Kassinos, D., Dissolved effluent organic matter: Characteristics and potential implications in wastewater treatment and reuse applications. *Water Res.* **2015**, *77*, 213–248.
49. Petrie, B.; Barden, R.; Kasprzyk-Hordern, B., A review on emerging contaminants in wastewaters and the environment: Current knowledge, understudied areas and recommendations for future monitoring. *Water Res.* **2015**, *72*, 3–27.
50. Tobias, H. J.; Sacks, G. L.; Zhang, Y.; Brenna, J. T., Comprehensive two-dimensional gas chromatography combustion isotope ratio mass spectrometry. *Anal. Chem.* **2008**, *80*, (22), 8613–8621.
51. Nara, H.; Nakagawa, F.; Yoshida, N., Development of two-dimensional gas chromatography/isotope ratio mass spectrometry for the stable carbon isotopic analysis of C<sub>2</sub>–C<sub>5</sub> non-methane hydrocarbons emitted from biomass burning. *Rapid Commun. Mass Spectrom.* **2006**, *20*, (2), 241–247.
52. Hu, X.; Dai, G.; Huang, J.; Jin, H.; Yu, Y.; Liang, Y., Preparation and characterization of metolachlor molecularly imprinted polymer coating on stainless steel fibers for Solid-Phase Microextraction. *Anal. Lett.* **2011**, *44*, (7), 1358–1370.
53. Wang, Y.; Jin, X.; Zhao, D.; Guo, X.; Li, R., Molecularly imprinted solid-phase extraction coupled with gas chromatography for the determination of four chloroacetamide herbicides in soil. *Anal. Methods* **2015**, *7*, (15), 6411–6418.
54. Bakkour, R.; Bolotin, J.; Sellergren, B.; Hofstetter, T. B., Molecularly imprinted polymers for compound-specific isotope analysis of polar organic micropollutants in aquatic environments. *Anal. Chem.* **2018**, *90*, (12), 7292–7301.
55. Hofstetter, T. B.; Schwarzenbach, R. P.; Bernasconi, S. M., Assessing transformation processes of organic compounds using stable isotope fractionation. *Environ. Sci. Technol.* **2008**, *42*, (21), 7737–7743.
56. Hofstetter, T. B.; Berg, M., Assessing transformation processes of organic contaminants by compound-specific stable isotope analysis. *TrAC, Trends Anal. Chem.* **2011**, *30*, (4), 618–627.
57. Meyer, A. H.; Penning, H.; Lowag, H.; Elsner, M., Precise and accurate compound specific carbon and nitrogen isotope analysis of atrazine: Critical role of combustion oven conditions. *Environ. Sci. Technol.* **2008**, *42*, (21), 7757–7763.
58. Spahr, S.; Bolotin, J.; Schleucher, J.; Ehlers, I.; von Gunten, U.; Hofstetter, T. B., Compound-specific carbon, nitrogen, and hydrogen isotope analysis of *N*-nitrosodimethylamine in aqueous solutions. *Anal. Chem.* **2015**, *87*, (5), 2916–2924.
59. Spahr, S.; Huntscha, S.; Bolotin, J.; Maier, M. P.; Elsner, M.; Hollender, J.; Hofstetter, T. B., Compound-specific isotope analysis of benzotriazole and its derivatives. *Anal. Bioanal. Chem.* **2013**, *405*, (9), 2843–2856.

60. Reinnicke, S.; Juchelka, D.; Steinbeiss, S.; Meyer, A.; Hilkert, A.; Elsner, M., Gas chromatography/isotope ratio mass spectrometry of recalcitrant target compounds: performance of different combustion reactors and strategies for standardization. *Rapid Commun. Mass Spectrom.* **2012**, *26*, (9), 1053–1060.
61. Ogawa, N.; Nagata, T.; Kitazato, H.; Ohkouchi, N., Ultra-sensitive elemental analyzer/isotope ratio mass spectrometer for stable nitrogen and carbon isotope analyses. *Earth, Life and Isotopes* **2010**, 339-353.
62. Baczynski, A. A.; Polissar, P. J.; Juchelka, D.; Schwieters, J.; Hilkert, A.; Summons, R. E.; Freeman, K. H., Picomolar-scale compound-specific isotope analyses. *Rapid Commun. Mass Spectrom.* **2018**, *32*, (9), 730–738.



## Appendix A

### Supporting information to chapter 3

#### Supporting materials and methods

##### List of chemicals

**Pesticides.** *S*-metolachlor (2-chloro-*N*-(2-ethyl-6-methylphenyl)-*N*-((2*S*)-1-methoxypropan-2-yl)acetamide), atrazine (6-chloro-4-*N*-ethyl-2-*N*-propan-2-yl-1,3,5-triazine-2,4-diamine) and metolachlor d<sub>11</sub> were analytical grade (Pestanal, >99.9%, Sigma-Aldrich®, St Louis, MO, USA).

**Transformation products of *S*-metolachlor and atrazine.** *S*-metolachlor ethanesulfonic acid (ESA - sodium 2-((2-ethyl-6-methylphenyl)(1-methoxy-2-propanyl)amino)-2-oxoethanesulfonate), *S*-metolachlor oxanilic acid (OXA - 2-(2-ethyl*N*-(1-methoxypropan-2-yl)-6-methylanilino)-2-oxoacetic acid), metolachlor CGA 37735 (*N*-(2-ethyl-6-methylphenyl)-2-hydroxyacetamide), 2-hydroxy-atrazine (A-OH - 2-(ethylamino)-6-(propan-2-ylamino)-1*H*-1,3,5-triazin-4-one), desethylatrazine (DEA; 6-chloro-2-*N*-propan-2-yl-1,3,5-triazine-2,4-diamine), desisopropylatrazine (DIA; 6-chloro-2-*N*-ethyl-1,3,5-triazine-2,4-diamine), atrazine-desethyl-2-hydroxy (A-DOH - (6*Z*)-4-Imino-6-(isopropylimino)-1,4,5,6-tetrahydro-1,3,5-triazin-2-ol) were analytical grade (>98%, Sigma-Aldrich®, St Louis, MO, USA). Hydroxy-metolachlor (Met-OH - *N*-(2-ethyl-6-methylphenyl)-2-hydroxy-*N*-(1-methoxypropan-2-yl)acetamide) was purchased as reference standard for GC in ACN from LGC Standards (Molsheim, France).

**Actinometer.** *p*-nitroanisole (PNA) and pyridine (anhydrous, >99.8%) were analytical grade (>97%).

**Solvents and other chemicals:** The solvents dichloromethane (DCM), acetonitrile (ACN) and ethyl acetate (EtOAc) were HPLC grade purity (>99.9%). All the pre-cited chemicals as well as magnesium sulfate heptahydrate (BioUltra, ≥99.5%), calcium chloride hexahydrate (BioUltra, ≥99.0%), calcium nitrate tetrahydrate (≥99.0%), potassium phosphate monobasic (BioUltra, ≥99.5%) and sodium phosphate dibasic (BioUltra, ≥99.5%) used for buffer solution and synthetic water preparation were purchased from Sigma-Aldrich® (St Louis, MO, USA).

Table A1. Chemical composition of irradiation solutions

parameter	unit	value <sup>a</sup>	analytical method	irradiation solution
pH	-	7.9 ± 0.2	electrode	All
DOC <sup>b</sup>	mg L <sup>-1</sup>	5.4 ± 0.2	TOC analyzer	SRFA & TOT
cations				
NH <sub>4</sub> <sup>+</sup>		n.p.	IC	NIT & TOT
Na <sup>+</sup>		9.9 ± 0.5	IC	NIT & TOT
K <sup>+</sup>	mg L <sup>-1</sup>	0.71 ± 0.04	IC	NIT & TOT
Mg <sup>2+</sup>		1.47 ± 0.07	IC	NIT & TOT
Ca <sup>2+</sup>		13.4 ± 0.7	IC	NIT & TOT
anions				
Cl <sup>-</sup>		12.0 ± 0.6	IC	NIT & TOT
NO <sub>3</sub> <sup>-</sup>	mg L <sup>-1</sup>	20.5 ± 1.0	IC	NIT & TOT
SO <sub>4</sub> <sup>2-</sup>		5.6 ± 0.3	IC	NIT & TOT

<sup>a</sup> Analytical uncertainties reported correspond to one standard deviation over triplicate measurements. <sup>b</sup> DOC concentrations measured in UW were <0.2 mg C L<sup>-1</sup>, which limited any effect of dissolved organic matter in direct photodegradation experiments (DIR and DIR254). n.p. not present, DOC: dissolved organic carbon.

### Organic matter photobleaching

DOM photoirradiation reduces its light absorbance properties. The control experiment showed that the decrease of light absorbance at  $\lambda = 254$  nm was less than 20% after >310 hours of irradiation. SRFA photosensitizing and light absorption effects were thus assumed constant across the experiments in TOT solutions. Also, the composition of SRFA did not change over irradiation as evidenced by its steady absorption spectrum.

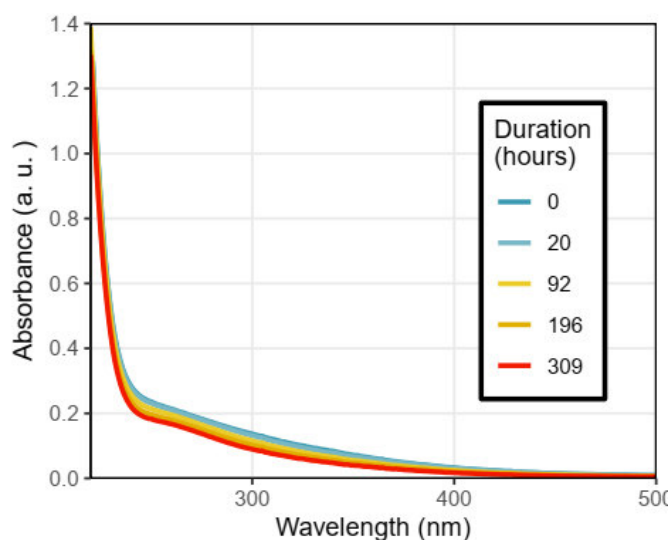


Figure A1. Temporal changes of absorbance of the TOT solution caused by organic matter photobleaching.

**PNA/Pyr actinometer system**

A PNA (30  $\mu\text{M}$ )/pyridine (10 mM) actinometer system was used to measure mean light intensity during experiments.<sup>1,2</sup> Values of wavelength independent quantum yields ( $\Theta_{PNA}$ ) of  $3.19 \times 10^{-3} \text{ mol E}^{-1}$  were used from Laszakovits et al.<sup>1</sup> To account for a closed irradiation system (i.e., aluminium foil covering the quartz vial walls and assumed to reflect light without absorption), it was assumed that chemicals absorbed all of the incident light and the decay of PNA as expressed in eq. A1:<sup>3</sup>

$$\frac{dC_{PNA}}{dt}(\lambda) = \frac{\epsilon(\lambda)}{\sum_{\lambda} \epsilon(\lambda)} \times \Theta_{PNA} \times F_W(\lambda) \quad (\text{A1})$$

with  $\frac{dC_{PNA}}{dt}$  the observed pseudo first-order decaying rate of PNA,  $\Theta_{PNA}$  the wavelength independent PNA quantum yield,  $\frac{\epsilon(\lambda)}{\sum_{\lambda} \epsilon(\lambda)}$  the relative fraction of light absorbed by PNA at wavelength  $\lambda$  also provided by Laszakovits et al.<sup>1</sup> and  $F_W(\lambda)$  the relative photon irradiance of the lamp at wavelength  $\lambda$ .

$$\frac{dC_{PNA}}{dt} = \sum_{\lambda} \left( \frac{\epsilon(\lambda)}{\sum_{\lambda} \epsilon(\lambda)} \times \Theta_{PNA} \times F_W(\lambda) \right) \quad (\text{A2})$$

eq. A2 and  $F_W(\lambda)$  and  $\frac{\epsilon(\lambda)}{\sum_{\lambda} \epsilon(\lambda)}$  were computed over the range of validity for the PNA/Pyr system  $\lambda \in [290,400]$  nm.

Table A2. Irradiation conditions with Xenon arc lamp and correction factors used to estimate photodegradation rates.

light interval ( $\Delta\lambda$ )	VIS (360 < $\lambda$ < 830 nm)		UVA (320 < $\lambda$ < 400 nm)		UVB (280 < $\lambda$ < 320 nm)		total ( $I_{tot}$ )	correction factor <sup>b</sup>	
	Intensity <sup>a</sup>	absolute mW cm <sup>-2</sup>	relative %	absolute mW cm <sup>-2</sup>	relative %	absolute mW cm <sup>-2</sup>	relative %		absolute mW cm <sup>-2</sup>
experiment									
ATZ - DIR		16.4	68.4	6.8	28.3	0.8	3.4	24.0	0.63
ATZ - NIT		8.5	66.3	4.0	31.1	0.3	2.6	12.8	1.18
ATZ - SRFA		7.1	68.4	3.0	28.7	0.3	2.9	10.4	1.45
ATZ - TOT		12.9	64.1	6.7	33.4	0.5	2.5	20.2	0.75
SMET - DIR		13.1	68.0	5.6	28.9	0.6	3.1	19.3	0.78
SMET - NIT		6.2	70.5	2.4	27.1	0.2	2.4	9.9	1.52
SMET - SRFA		9.6	66.9	4.2	29.6	0.5	3.5	13.3	1.14
SMET - TOT		6.9	69.2	2.8	27.8	0.3	3.0	10.8	1.40
mean irradiation		10.1	67.7	4.4	29.4	0.4	2.9	15.1	
standard deviation		3.7	2.0	1.8	2.0	0.2	0.4	5.3	

<sup>a</sup> Light intensity are reported as the arithmetic mean of light measurements at the beginning and the end of the respective experiments. Relative light intensities stand for the contribution of each wavelength interval (VIS, UVA, UVB) to the whole irradiation,  $I_{relative} = \frac{I_{\lambda}}{\sum_{i \in \{VIS, UVA, UVB\}} I_{\lambda_i}}$ .

<sup>b</sup> Correction of degradation rates were performed according to the correction factors with the averaged total light intensity  $\overline{I_{tot}} = 15.1 \text{ mW cm}^{-2}$  as the reference value divided by individual total light intensities,  $F_k = \overline{I_{tot}}/I_{tot}$ .

### Light spectrum homogeneity within the light-proof box

Light homogeneity within the light-proof box varied between 80 and 120% of relative irradiation intensity taking the mean intensity value as a reference. The LP Hg lamp was temporarily replaced by medium pressure Hg lamp emitting at  $\lambda = 365 \text{ nm}$  and was used to irradiate 11 beakers filled with 50 mL of PNA (30  $\mu\text{M}$ )/Pyridine (10 mM) actinometers and evenly distributed within the light-proof box. After four hours, the remaining concentration of PNA was measured in each beaker and the variations in the irradiation intensity were retrieved by comparing the mean value of  $k_{pE}$  with individual values computed from eq. A3.<sup>1,2</sup>

$$\ln\left(\frac{[PNA](t)}{[PNA]_0}\right) = k_{pE} \times t \quad (\text{A3})$$

$k_{pE}$  stands for the pseudo first order reaction rate of PNA and is linearly proportional to the incident irradiance.

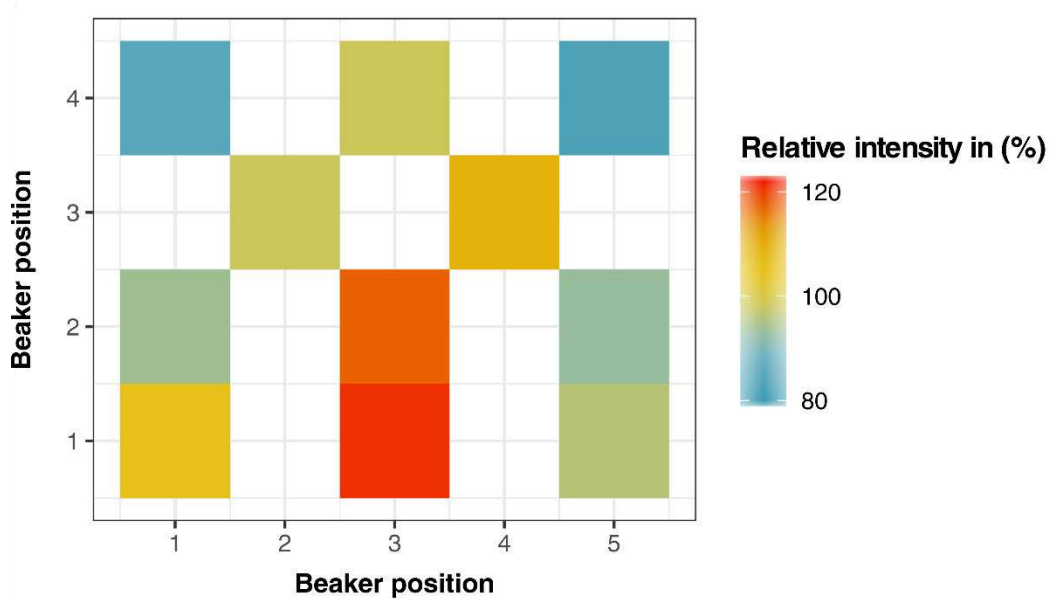


Figure A2. Spatial distribution of irradiation intensity within the light-proof box. Transparent places correspond to empty spaces where the irradiation intensity was not measured within the light-proof box.

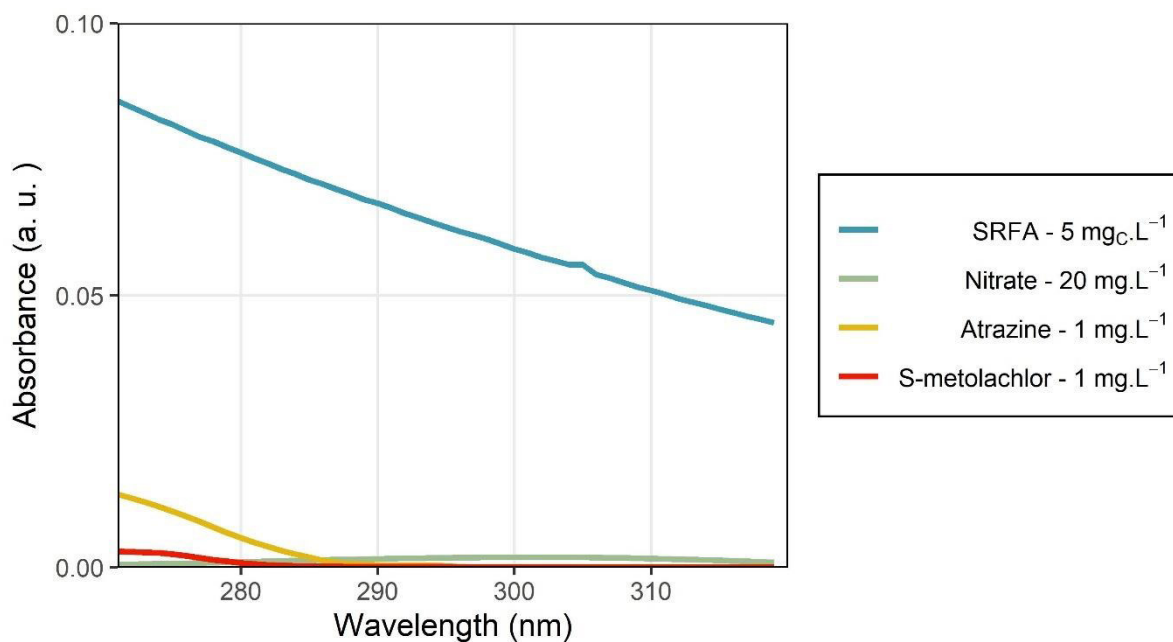


Figure A3. Absorption spectra of atrazine, S-metolachlor, nitrates and SRFA at experimental concentrations. The absorption spectra for nitrates was extracted from Gaffney et al.<sup>4</sup>



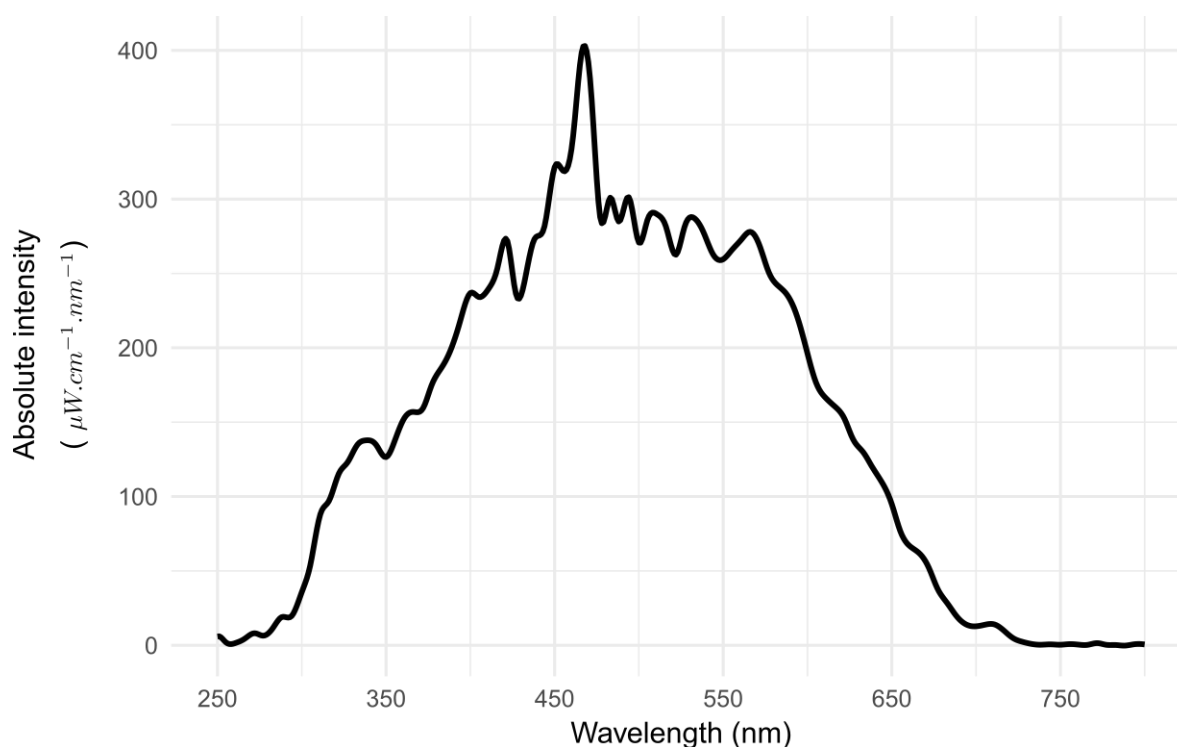


Figure A4. Absolute light intensity as a function of the wavelength for the Xenon Arc Lamp as measured in the quartz tube after the liquid light guide. The light spectrum was characterized with a calibrated spectroradiometer ILT 900C (International Light®) at a wavelength resolution of 1 nm. Significant irradiation ( $I(\lambda) > 0.1 \times I_{mean}$ ) ranged from [270;720] nm.

### Prediction of degradation rates and identification of dominant photodegradation pathways

The effective contribution of nitrates and DOM as photosensitizers can be inferred from eq. A4. The observed degradation rates were composed of the sum of elemental photo-oxidation processes (e.g., direct,  $HO\cdot$  and  ${}^3DOM^*$  mediated).<sup>5-7</sup> The contribution of carbonate radicals ( $CO_3^{\bullet-}$ ) as potential relevant photosensitizer was not included here because Vionne et al.<sup>8</sup> highlighted the limited oxidation of atrazine and anilines with  $CO_3^{\bullet-}$  under sunlight irradiation even in carbonate rich waters (sum of  $[HCO_3^-]$  and  $[CO_3^{2-}] \approx 10$  times higher than in our conditions).<sup>8</sup> Accordingly, eq. A4 can be simplified to eq. A5. However, carbonates were considered as significant quenchers of  $HO\cdot$ .<sup>5</sup>

$$\frac{dC}{dt} = -k_{obs} \times C \quad (A4)$$

$$\frac{dC}{dt} = - \left( k_{dir} + k_{HO\cdot} \times [HO\cdot]_{SS} + k_{{}^3DOM^*} \times [{}^3DOM^*]_{SS} + k_{CO_3^{\bullet-}} \times [CO_3^{\bullet-}] + k_{1O_2} \times [{}^1O_2] \right) \times C$$

$$\frac{dC}{dt} = - \left( k_{dir} + k_{HO\bullet} \times [HO\bullet]_{SS} + k_{^3DOM^*} \times [^3DOM^*]_{SS} + k_{^1O_2} \times [^1O_2]_{SS} \right) \times C \quad (A5)$$

$C$  stands for pesticide concentration,  $k_{obs}$  for the observed degradation rate ( $s^{-1}$ ), which is expressed as the sum of direct ( $k_{dir}$ ) and selected indirect processes ( $k_{HO\bullet}$ ,  $k_{^3DOM^*}$ ,  $k_{^1O_2}$ ). The latter degradation rates are second order and depend on the steady state concentrations of the associated short-lived reactive intermediates ( $[^3DOM^*]_{SS}$ ,  $[^1O_2]_{SS}$  and  $[HO\bullet]_{SS}$ ).

### Calculation of short-lived reactive intermediates steady state concentrations

Estimating the steady state concentrations of short-lived reactive intermediates requires identification of the main photosensitizers promoting and scavenging radicals and short-lived species and to determine the amount of light absorbed by each photosensitizers. The latter step accounts for competition for light irradiance between the different light-absorbing dissolved species as well as corrections for light attenuation.

### Identification of main photosensitizers

Main short-lived reactive intermediates involved in pesticide photodegradation ( $^3DOM^*$ ,  $^1O_2$  and  $HO\bullet$ ) were formed through photosensitizer irradiation, respectively fulvic substances and nitrates.<sup>9</sup>  $^3DOM^*$  and  $^1O_2$  originates from irradiation of DOM and  $HO\bullet$  from irradiation of DOM and nitrates.<sup>3</sup> Fulvic acids such as SRFA also have the ability to scavenge  $HO\bullet$  and  $^1O_2$ .<sup>10</sup> These species are short-lived and their concentrations in water are balanced by their ratio of production over quenching as expressed in eq. A6 to A8.<sup>3</sup>

$$[HO\bullet]_{SS} \quad (A6)$$

$$= S(\lambda) \times \frac{\Phi_{HO\bullet,NO_3^-} \times k_{a,NO_3^-} \times [NO_3^-] + \Phi_{HO\bullet,DOM} \times k_{a,DOM} \times [DOM]}{k_{HO\bullet,DOM} \times [DOM] + k_{HO\bullet,HCO_3^-} \times [HCO_3^-] + k_{HO\bullet,CO_3^{2-}} \times [CO_3^{2-}]}$$

$$[^1O_2]_{SS} = S(\lambda) \times \frac{\Phi_{^1O_2,DOM} \times k_{a,^1O_2} \times [DOM]}{k_{d,^1O_2}} \quad (A7)$$

$$[^3DOM^*]_{SS} = S(\lambda) \times \frac{\Phi_{^3DOM^*,DOM} \times k_{a,DOM} \times [DOM]}{k_{^3DOM^*,O_2} \times [O_2]} \quad (A8)$$

$\Phi_{R,Sens}$  refers to the quantum yield of formation of short-lived reactive intermediates ( $R$ ) by the photosensitizer ( $Sens$ ) expressed in  $\text{mol E}^{-1}$ ,  $k_{a,Sens}$  stands for the rate constant of light absorption by  $Sens$  over the whole light spectrum considered and is expressed in  $\text{E mol}^{-1} \text{s}^{-1}$  and  $k_{R,Sens}$  is the second-order rate constant of consumption of  $R$  by  $Sens$  in  $\text{mol}^{-1} \text{L s}^{-1}$ .  $k_{d,^1O_2}$

refers to the first-order reaction rate of  $^1\text{O}_2$  with water and is expressed in  $\text{s}^{-1}$ .  $[\text{O}_2]$  was set to  $2.4 \times 10^{-4} \text{ M}$  corresponding to the aqueous saturation at  $20^\circ\text{C}$ .

Although it is in principle possible to evaluate  $[\text{}^3\text{DOM}^*]_{\text{ss}}$  using eq. A8, there are some uncertainties in the literature about the value of  $\Phi_{\text{}^3\text{DOM}^*}$ . We chose to evaluate  $[\text{}^3\text{DOM}^*]_{\text{ss}}$  using the following expression:  $[\text{}^3\text{DOM}^*]_{\text{ss}} \approx [\text{}^1\text{O}_2]_{\text{ss}} / f_{\Delta}$ , where  $f_{\Delta}$  is the fraction of  $^3\text{DOM}^*$  that produces  $^1\text{O}_2$ . We chose a value of 0.34 for  $f_{\Delta}$  based on data for a Suwannee River natural organic matter isolate from the IHSS.<sup>11</sup>

Second-order rate constant for the reaction between atrazine or *S*-metolachlor and  $^3\text{DOM}^*$  can be found in Zeng et al.<sup>5</sup> They were determined by multiplying measured pseudo-first order reaction constant by the estimated  $[\text{}^3\text{DOM}^*]_{\text{ss}}$ . As the  $[\text{}^3\text{DOM}^*]_{\text{ss}}$  reported in Zeng et al.<sup>5</sup> were manifestly underestimated (it does not follow the expression  $[\text{}^3\text{DOM}^*]_{\text{ss}} \approx [\text{}^1\text{O}_2]_{\text{ss}} / f_{\Delta}$ ), it was necessary to correct the reported constant by recalculating them. We achieved that by recalculating  $[\text{}^3\text{DOM}^*]_{\text{ss}}$  in Zeng et al.<sup>5</sup> Then we calculated the corrected second-order rate constant between atrazine or *S*-metolachlor and  $^3\text{DOM}^*$  as the reported second-order rate constant divided by the recalculated  $[\text{}^3\text{DOM}^*]_{\text{ss}}$  and multiplied by the reported  $[\text{}^3\text{DOM}^*]_{\text{ss}}$ .

Table A3. Kinetic parameters for formation and consumption of short-lived reactive intermediates.

		units	ref.
quenching rates			
$k_{\text{HO}\cdot, \text{DOM}}$	$1.6 \times 10^8$	$\text{M}^{-1}\text{s}^{-1}$	A
$k_{\text{HO}\cdot, \text{HCO}_3^-}$	$1 \times 10^7$	$\text{M}^{-1}\text{s}^{-1}$	B
$k_{\text{HO}\cdot, \text{HCO}_3^{2-}}$	$4 \times 10^8$	$\text{M}^{-1}\text{s}^{-1}$	B
$k_{\text{}^3\text{DOM}^*, \text{O}_2}$	$2 \times 10^9$	$\text{M}^{-1}\text{s}^{-1}$	C
$k_{\text{d}, \text{}^1\text{O}_2}$	$1.5 \times 10^5$	$\text{s}^{-1}$	C, D
quantum yield of formation			
$\Phi_{\text{HO}\cdot, \text{NO}_3^-}$	$1 \times 10^{-2}$	-	E
$\Phi_{\text{HO}\cdot, \text{DOM}}$	$1.65 \times 10^{-5}$	-	F
$\Phi_{\text{}^3\text{DOM}^*, \text{DOM}}$	$4.2 \times 10^{-4}$	-	F
$\Phi_{\text{}^1\text{O}_2, \text{DOM}}$	$6.54 \times 10^{-2}$	-	F
second-order rate constants for reactions			
atrazine			
$k_{\text{HO}\cdot, \text{atr}}$	$2.7 \times 10^9$	$\text{M}^{-1}\text{s}^{-1}$	G
$k_{\text{}^1\text{O}_2, \text{atr}}$	$2.0 \times 10^5$	$\text{M}^{-1}\text{s}^{-1}$	G
$k_{\text{}^3\text{DOM}^*, \text{atr}}$	$1.2 \times 10^9$	$\text{M}^{-1}\text{s}^{-1}$	G
<i>S</i> -metolachlor			
$k_{\text{HO}\cdot, \text{met}}$	$6.9 \times 10^9$	$\text{M}^{-1}\text{s}^{-1}$	G
$k_{\text{}^1\text{O}_2, \text{met}}$	$4.4 \times 10^5$	$\text{M}^{-1}\text{s}^{-1}$	G
$k_{\text{}^3\text{DOM}^*, \text{met}}$	$9.8 \times 10^8$	$\text{M}^{-1}\text{s}^{-1}$	G
Ref. A <sup>12</sup> , B <sup>8, 13</sup> , C <sup>7</sup> , D <sup>10, 14</sup> , E <sup>14</sup> , F <sup>15</sup> , G. <sup>5</sup>			

### Calculation of light absorption rates and screening factors

Calculations were performed over the spectral range  $\lambda \in [270 - 320 \text{ nm}]$  as it corresponds to the range of significant absorbance for all dissolved species with respect to the emission spectrum of the Xenon arc lamp. As the light path length changed over repetitive samplings, an average path length of 15 cm was chosen as representative across the experiments. Changes in the actual path length would only significantly affect the absolute predicted degradation rates while the relative contribution of different processes would remain unaffected.

The screening factor was computed in its wavelength dependant form. We assumed the light to travel straight through the quartz vial and to be insensitive to light scattering as in eq. A9.<sup>16</sup> Depending on the water composition,  $Sens_i$  referred to a combination of DOM,  $NO_3^-$ , atrazine and *S*-metolachlor. We introduced  $S(\lambda)$  to calculate the rate of light absorption as shown in eq. A10.<sup>6</sup>

$$S(\lambda) = \frac{1 - e^{-2.303 \times \sum(\epsilon_i(\lambda) \times [Sens]_i) \times l}}{2.303 \times \sum(\epsilon_i(\lambda) \times [Sens]_i) \times l} \quad (\text{A9})$$

$$k_{a,Sens} = \sum S(\lambda) \times \frac{A_i(\lambda)}{A_{tot}(\lambda)} \times E_0 \times (1 - 10^{-A_{tot}(\lambda)}) \quad (\text{A10})$$

### Supporting Results

Predicted degradation rates and relative contributions of each short-lived reactive intermediates to the overall photodegradation are provided in Table A4. The prediction generally fitted with the observation of a systematic decrease in degradation rates in the presence of DOM, although predicted values of absolute degradation rates were more uncertain. The predicted degradation rates proved extremely sensitive to the average path length while the relative contribution of each photodegradation pathways was left completely unaffected by this parameter. The best fit to experimental data was obtained with an average path length of 8 cm (relatively lower than the actual value estimated at 15 cm). Predicted data were only compared with each other. Note that  $k_{dir}$  was not computed and that we used the observed values of degradation rates in UW instead. Indeed,  $k_{dir}$  strongly depends on the experimental setup, as shown by the wide range of reaction quantum yield for direct photodegradation gathered in Zeng et al.<sup>5</sup> for atrazine and *S*-metolachlor with different light sources.

Table A4. Comparison of predicted and observed degradation rates and presentation of the predicted contribution of each short-lived reactive intermediate to the overall photodegradation.

pesticide	condition	predicted contribution (%)				k <sub>deg</sub> (d <sup>-1</sup> )		obs / pred (%)
		direct	HO•	<sup>1</sup> O <sub>2</sub>	<sup>3</sup> DOM*	obs	pred	
atrazine	DIR	100	0	0	0	0.57	0.57	100
	NIT	25	75	0	0	0.46	0.94	49
	SRFA	34	22	2	42	0.14	0.12	117
	TOT	17	62	1	20	0.30	0.15	200
S- metolachlor	DIR	100	0	0	0	0.28	0.28	100
	NIT	5	95	0	0	0.28	5.11	5
	SRFA	8	54	4	33	0.09	0.10	90
	TOT	3	87	1	9	0.11	0.21	52

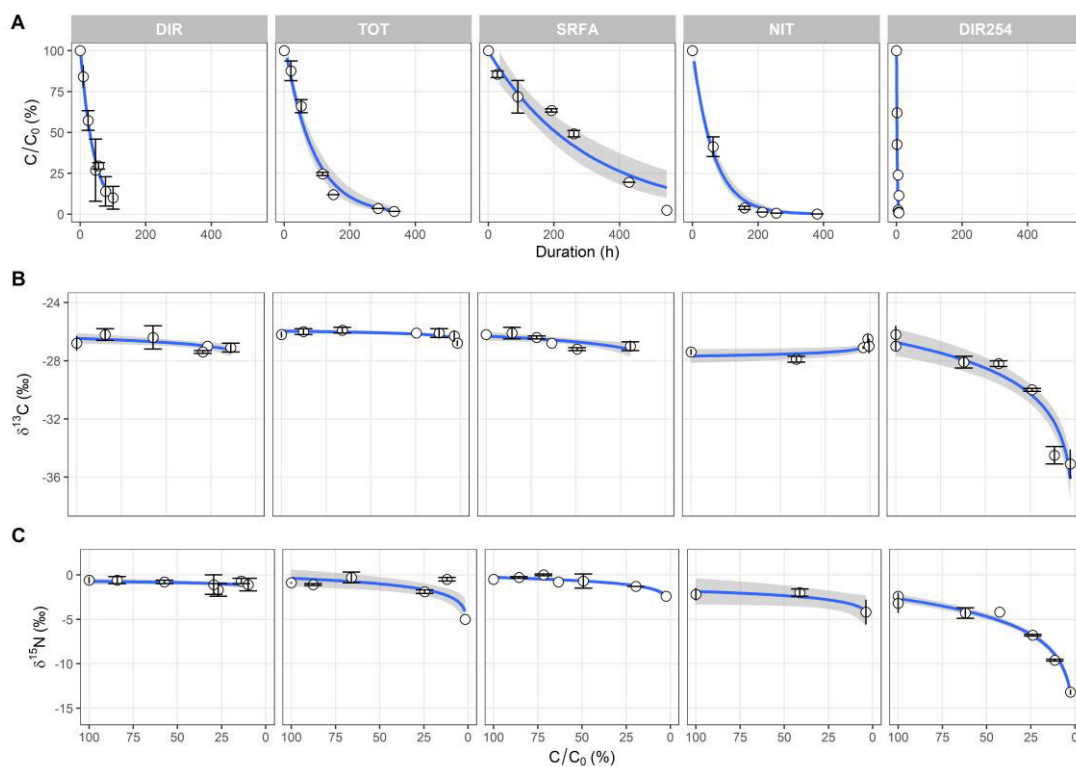


Figure A5. Observed degradation kinetics (A) and Rayleigh plots for carbon (B) and nitrogen (C) for atrazine.

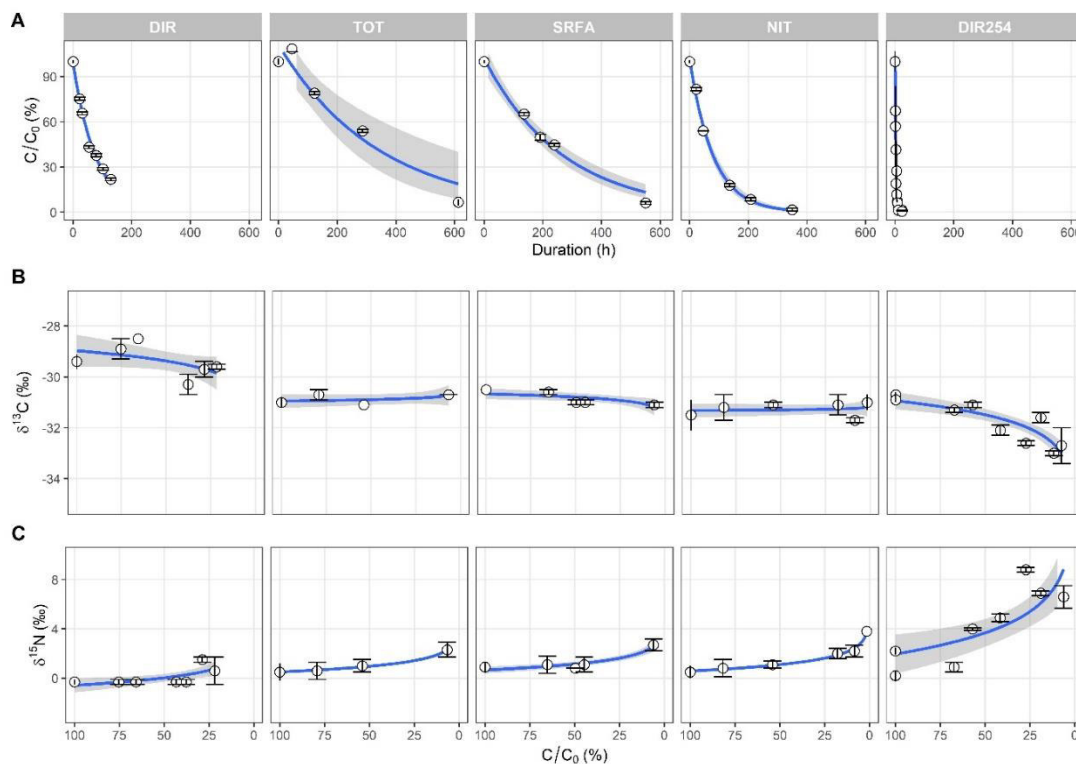


Figure A6. Observed degradation kinetics (A) and Rayleigh plots for carbon (B) and nitrogen (C) for S-metolachlor.

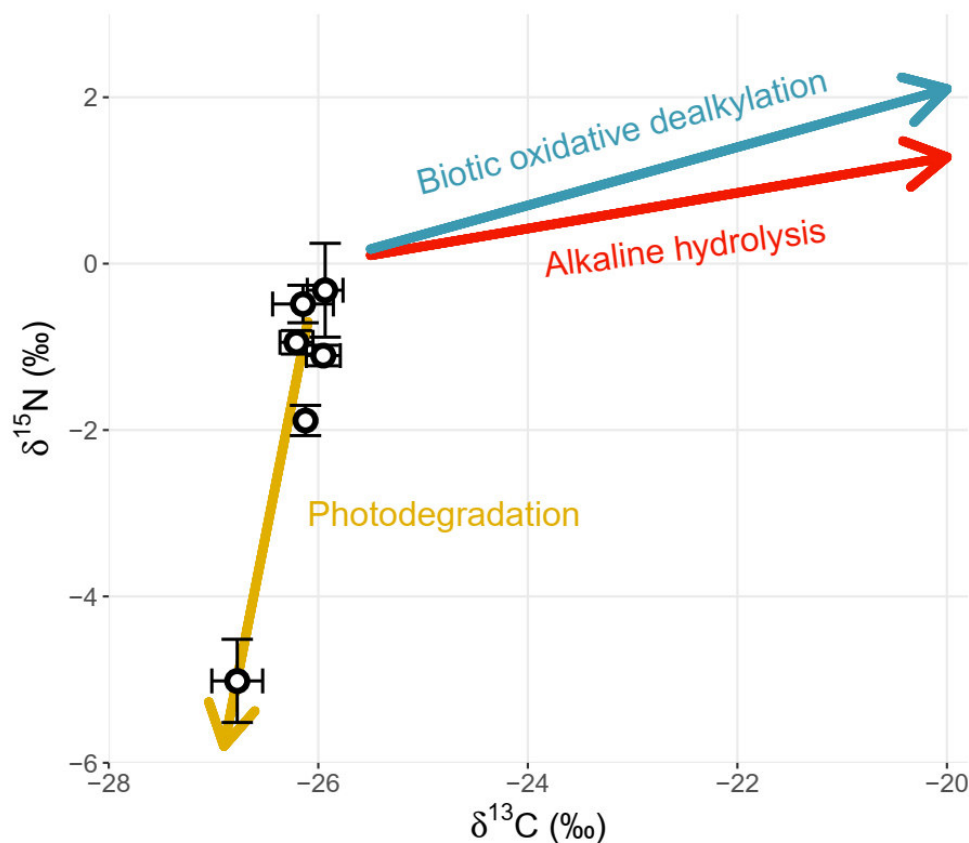


Figure A7. Dual C and N isotope plot for atrazine reflecting contrasted enrichment patterns between biotic oxidative dealkylation by the bacterial strain *Rhodococcus* sp. NI86/21,<sup>17</sup> abiotic alkaline hydrolysis at pH equal to 12<sup>18</sup> and photodegradation in agriculturally impacted surface waters, with points representing the C and N enrichments observed in the presence of nitrates and dissolved organic matter (DOM).

Atrazine photodegradation footprint is mainly carried by changes in N stable isotope composition, whereas the others degradative processes occurring in surface waters are mostly reflected by changes of C stable isotope composition.<sup>19</sup>

## Appendix B

### Supporting information to chapter 4

#### Abbreviations

*NER*, non-extractable residue

$V_w$ , volume of the water phase (L)

$V_{tot}$ , volume total of the system (water and sediment; L)

$DegT_{50,w} = \ln(2)/k_{deg,w}$ , degradation half-life in water (d)

$DT_{50,s} = \ln(2)/k_{obs,s}$ , dissipation half-life in sediment (d)

$DT_{50,w} = \ln(2)/k_{obs,w}$ , dissipation half-life in water (d)

$k_{obs,w}$  pseudo first-order dissipation rate constant in water ( $d^{-1}$ )

$k_{obs,s}$  pseudo first-order dissipation rate constant in sediment ( $d^{-1}$ )

$k_{deg,w}$ , pseudo first-order biodegradation rate constant in water ( $d^{-1}$ )

*TSS*, concentration of total suspended solids ( $kg L^{-1}$ )

*DOC*, concentration of dissolved organic carbon ( $kg C L^{-1}$ )

*DIC*, concentration of dissolved inorganic carbon ( $kg C L^{-1}$ )

*COD*, chemical oxygen demand ( $kg O_2 L^{-1}$ )

$f_{oc}$ , content of sediment organic carbon (w/w)

$POC = f_{oc} \times TSS$ , concentration of particulate organic carbon ( $kg C L^{-1}$ )

$TOC = DOC + POC$ , concentration of total organic carbon ( $kg C L^{-1}$ )

$K_d$ , sediment partitioning coefficient ( $L kg^{-1}$ )

$K_{oc}$ , sediment organic carbon-water partitioning coefficient ( $L kg^{-1}$ )

$P_s$ , pesticide concentration in the sediment phase ( $\mu g kg^{-1}$ )

$P_w$ , freely dissolved pesticide concentration in the water phase ( $\mu g L^{-1}$ )

$P(t)/P_0$ , fraction of remaining pesticides as a function of time t

$m_{p,w}$ , pesticide mass in the water phase

$m_{p,s}$ , pesticide mass in the sediment phase

$dm_{p,w}/dt$ , derivative of pesticide mass in the water phase

$dm_{T,w}/dt$ , derivative of transformation products mass in the water phase

$dm_{p,s}/dt$ , derivative of the pesticide mass in the sediment phase

$dm_{T,s}/dt$ , derivative of the transformation products mass in the sediment phase

$dP_w/dt$  derivative of pesticide concentration in the water phase

$\delta^h E_0, \delta^h E_t$ , stable isotope signature (‰) of element *E* at time zero or t, respectively



## Supporting materials and methods

### Chemicals reagents

Pesticide mixture compounds: atrazine (6-chloro-4-*N*-ethyl-2-*N*-propan-2-yl-1,3,5-triazine-2,4-diamine), acetochlor (2-chloro-*N*-(ethoxymethyl)-*N*-(2-ethyl-6-methylphenyl)acetamide), metalaxyl (methyl 2-(*N*-(2-methoxyacetyl)-2,6-dimethylanilino)propanoate), *S*-metolachlor (2-chloro-*N*-(2-ethyl-6-methylphenyl)-*N*-((2*S*)-1-methoxypropan-2-yl)acetamide), metolachlor-*d*<sub>11</sub> and terbutryn (2-*N*-tert-butyl-4-*N*-ethyl-6-methylsulfanyl-1,3,5-triazine-2,4-diamine) were purchased in highest available purity (>99%; Pestanal®, Sigma–Aldrich, St. Louis, USA).

Commercially available transformation products of selected pesticides: carboxylic acid metalaxyl (2-((1-Carboxyethyl)(methoxyacetyl)amino)-3-methylbenzoic acid), demethylmetalaxyl (*N*-(2,6-Dimethylphenyl)-*N*-(methoxyacetyl)alanine), *S*-metolachlor ethanesulfonic acid (MET ESA; sodium 2-((2-ethyl-6-methylphenyl)(1-methoxy-2-propanyl)amino)-2-oxoethanesulfonate), *S*-metolachlor oxanilic acid (MET OXA; 2-(2-ethyl-*N*-(1-methoxypropan-2-yl)-6-methylanilino)-2-oxoacetic acid), acetochlor ethanesulfonic acid (ACE ESA; sodium 2-(*N*-(ethoxymethyl)-2-ethyl-6-methylanilino)-2-oxoethanesulfonate), 2-hydroxy-atrazine (HA; 2-(ethylamino)-6-(propan-2-ylamino)-1*H*-1,3,5-triazin-4-one), desethylatrazine (DEA; 6-chloro-2-*N*-propan-2-yl-1,3,5-triazine-2,4-diamine), desisopropylatrazine (DIA; 6-chloro-2-*N*-ethyl-1,3,5-triazine-2,4-diamine), atrazine-desethyl-2-hydroxy ((6*Z*)-4-Imino-6-(isopropylimino)-1,4,5,6-tetrahydro-1,3,5-triazin-2-ol), metolachlor CGA 37913 (2-(2-ethyl-6-methylanilino)propan-1-ol), 2-ethyl-6-methylaniline, metolachlor CGA 37735 (*N*-(2-ethyl-6-methylphenyl)-2-hydroxyacetamide), metolachlor MFCD01034341 (*N*-(2-Ethyl-6-methylphenyl)acetamide) were purchased in A.C.S-grade reagents (>98%) from Sigma–Aldrich (USA). Acetochlor oxanilic acid (ACE OXA; 2-(*N*-(ethoxymethyl)-2-ethyl-6-methylanilino)-2-oxoacetic acid), deethylterbutryn (2-*N*-tert-butyl-6-methylsulfanyl-1,3,5-triazine-2,4-diamine), terbutylazine-2-hydroxy (2-(tert-butylamino)-6-(ethylamino)-1*H*-1,3,5-triazin-4-one), terbutryn sulfoxide (2-*N*-tert-butyl-4-*N*-ethyl-6-methanesulfinyl-1,3,5-triazine-2,4-diamine), desethylhydroxyterbutryne (2-amino-6-(tert-butylamino)-1*H*-1,3,5-triazin-4-one) were purchased in highest available purity (>99%) from TechLab (Metz, France). Terbutryn sulfoxide (2-*N*-tert-butyl-4-*N*-ethyl-6-methanesulfinyl-1,3,5-triazine-2,4-diamine) were purchased in highest available purity (>97%) from MicroCombiChem (Wiesbaden, Germany). 2-hydroxy-acetochlor (*N*-(ethoxymethyl)-*N*-(2-ethyl-6-methylphenyl)-2-hydroxyacetamide), metolachlor CGA 40919 (4-(2-ethyl-6-methylphenyl)-5-methylmorpholin-3-one) and hydroxy-metolachlor (*N*-(2-ethyl-6-methylphenyl)-2-hydroxy-*N*-(1-methoxypropan-2-yl)acetamide) were purchased as reference standard for GC in ACN from LGC Standards (Molsheim, France).

Solvent and reagents: dichloromethane (DCM), acetonitrile (ACN), ethanol (EtOH), ethylacetate (EtOAc) and pentane in HPLC grade purity (>99.9%), anhydrous magnesium sulphate (MgSO<sub>4</sub>; technical grade reagent, >97%), calcium nitrate tetrahydrate

(Ca(NO<sub>3</sub>)<sub>2</sub>·4H<sub>2</sub>O), magnesium sulfate heptahydrate (MgSO<sub>4</sub>·7H<sub>2</sub>O), calcium chloride dihydrate (CaCl<sub>2</sub>·2H<sub>2</sub>O), sodium bicarbonate (NaHCO<sub>3</sub>), potassium dihydrogen phosphate (KH<sub>2</sub>PO<sub>4</sub>), disodium hydrogen phosphate (Na<sub>2</sub>HPO<sub>4</sub>) were purchased in A.C.S-grade reagents (≥99%) were purchased from Sigma–Aldrich. Primary-secondary amine (PSA; P/N 52738, bonded silica) was purchased from Supelco (Bellefonte, USA). All aqueous solutions were prepared with ultrapure water (>18 MΩ cm).

Synthetic water was prepared after Smith, et al.<sup>20</sup> from the Esthwaite lake soft water recipe. Two 50 fold concentrated stock solutions, were prepared with (i) 3 mg L<sup>-1</sup> Ca(NO<sub>3</sub>)<sub>2</sub>·4H<sub>2</sub>O, 15 mg L<sup>-1</sup> MgSO<sub>4</sub>·7H<sub>2</sub>O, 20 mg L<sup>-1</sup> CaCl<sub>2</sub>·2H<sub>2</sub>O, and (ii) 30 mg L<sup>-1</sup> NaHCO<sub>3</sub>. (i) was dissolved into the require amount of ultrapure water, and (ii) was added under continuous stirring of the solution. Synthetic water was used after reaching equilibrium for CO<sub>2</sub> and constant *pH* (<24 hours). Synthetic water was filter-sterilized through 0.2 μm cellulose acetate (CA) syringe filter. Triplicate measurement by ionic chromatography was (mg L<sup>-1</sup>): 8.9 ± 0.5 Na<sup>+</sup>, 6.2 ± 0.7 Ca<sup>2+</sup>, 1.5 ± 0.1 Mg<sup>2+</sup>, 10.3 ± 0.6 Cl<sup>-</sup>, 1.8 ± 0.7 NO<sub>3</sub><sup>-</sup>, 6.2 ± 0.3 SO<sub>4</sub><sup>2-</sup>, 3.8 ± 0.5 DIC and 1.6 ± 0.2 DOC.

### **Sediment sampling and properties**

The 10 first cm of the bed sediment were collected from an experimental stormwater wetland (Rouffach, France, 47°57'43" N, 7°17'26" E).<sup>21</sup> A total of ten sub-samples, each of 2 kg per location, were successively collected with a shovel cleaned with ultrapure water, acetone and wiped at 10 random spots. The ten sub-samples were then pooled together and thoroughly homogenized with the shovel.

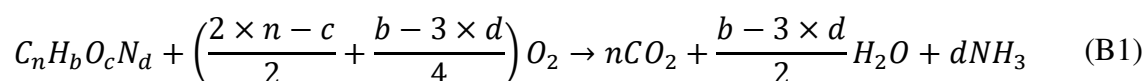
Physico-chemical parameters were measured following standard analytical procedures (NF/ISO) from homogenized sediment samples, dried at 105°C and sieved to 2 mm. Residual humidity (*RH*) was measured by mass difference after drying to constant mass (ISO 11465). *pH* was measured in a 1:5 (w/w) total suspended sediment (*TSS*)-ultrapure water ratio (*pH*<sub>H<sub>2</sub>O</sub>) or 0.01 mol L<sup>-1</sup> CaCl<sub>2</sub> solution (*pH*<sub>CaCl<sub>2</sub></sub>; ISO 10390). Cation exchange capacity (*CEC*) was measured by the cobaltihexamine chloride extraction method (ISO 23470). Bulk density (*BD*) was measured using the core method (ISO 11272) from a core sample of soil with a known volume cylinder (48 cm<sup>3</sup>) collected from the field and weighted. Total carbon and organic carbon content for the sediment (*f*<sub>OC</sub>) were measured by combustion on a CHN elementary analyzer (FLASH 2000 NC-Thermo Fisher Scientific; ISO 10694) with a precision of ± 2%. Before organic carbon measurement, the sediment was decarbonated by acid fumigation.<sup>22</sup> Organic matter was measured by the weight loss on ignition method at 375°C during 16 h (in-house method). Particle size distribution was measured by laser diffraction methods in water mode (LS230, Beckmann Coulter; ISO 13320) and converted into three texture class contents following the World Reference Base (WRB) of soil:<sup>23</sup> clay <2 μm, silt from 2 to 50 μm, and sand from 50 to 2000 μm. First, several phases were sequentially removed by solid-liquid extraction: i) organic matter was extracted by proportion of 1:3 (v/v) H<sub>2</sub>O<sub>2</sub> at 60°C, ii)

flocculants cation was extract by proportion of KCl 1:50 (v/v) or HCl 1:20 (v/v), depending on the presence or absence of carbonate, iii) desegregation of particle was made by adding a 1:1 (v/v) solution of natrium hexametaphosphate 0.55%. Major elements (Si, Al, Mg, Ca, Fe, Mn, Na, K) were measured on a dried and powdered sediment using an agate disk mill (<250 µm). Sample were prepared as follows: alkaline fusion procedure (NF ISO 14869-2) following by a total dissolution in nitric acids:glycerol solution (0.7:4 mol L<sup>-1</sup>) and measurements by inductively coupled plasma optical emission spectrometry (ICP-OES, ICAP6500, Thermo Fisher Scientific).

## Hydrochemistry

Cation-anion contents were measured from a sub-sample filtered at 0.2 µm with a CA filter of the water phase by ionic chromatography (ICS-5000, Dionex/Thermo Fischer, US EPA 300.7/300.0). DOC/DIC, COD and UV-Visible light absorbance measurements were performed using a separate sample filtered at 0.45 µm with a CA filter. DOC/DIC were analyzed at selected sampling times (0, 15, 200 and 300 days) by TOC analyzer (TOC-V-CPH Shimadzu, NF EN 1484). COD is measured photometrically using test kit (P/N 985036, Nanocolor, range between 3 and 150 mg L<sup>-1</sup> O<sub>2</sub> Macherey-Nagel) at days 0 and 300 for oxic and anoxic condition. The anoxic sample was prepared and transferred into the photometrically tube under Ar (<0.2 mg L<sup>-1</sup> O<sub>2</sub>) using glovebox (GP[concept], Jacomex).

Mean oxidation state for the C ( $\bar{O}x$ ) was estimated according to the relation between  $DOC^*$  and  $COD^*$  (\* stands for molar concentrations).<sup>24</sup> Considering an unknown organic compound with the formula  $C_nH_bO_cN_d$  and assuming oxidation sate of -3 for nitrogen, -2 for oxygen and +1 for hydrogen. The total oxidation (no NO<sub>x</sub> formation) of the compound follows the stoichiometry of the eq. B1,



Then the balance for oxidation number of the neutral compound can be written as eq. B2:

$$n\bar{O}x + b - 2 \times c - 3 \times d = 0 \quad (\text{B2})$$

Using the stoichiometric coefficient of eq. B1 and the balance for oxidation number (eq. B2), the system could be resolved and gave eq. B3:

$$\bar{O}x = 4 \times \left(1 - \frac{COD^*}{DOC^*}\right) \quad (\text{B3})$$

UV-Visible light absorbance measurements were used as a proxy of chromophore and moieties modification on the DOC.<sup>25</sup> Absorbance at 254 and 280 nm were record for day 0 and 300 on UV-1700 pharmaSpec (Shimadzu) spectrophotometers using a quartz glass cuvettes (10 mm path lengths). Specific ultraviolet absorbance (SUVA;  $L \text{ mg}^{-1} \text{ C} \cdot \text{m}^{-1}$ ) was calculated for 254 and 280 nm to eq. B4, where  $A(\lambda)$  is the sample absorbance at a given wavelength ( $\lambda$ ) and  $l$  (m) is the path length.

$$SUVA(\lambda) = \frac{A(\lambda)}{l \times DOC} \quad (\text{B4})$$

### Batch sorption isotherm

Batch sorption experiments were conducted at room temperature ( $20 \pm 5^\circ\text{C}$ ) and in the dark to avoid photolysis, following OECD Guideline 106<sup>26</sup>. Batch sorption was carried out with the sediment used for the biodegradation experiments. Three conditions were tested: (i) sorption on non-autoclaved sediment with the pesticide mixture, (ii) sorption on autoclaved sediment with the pesticide mixture, and (iii) sorption on non-autoclaved sediment with the individual pesticides. The difference between (i) and (ii) enabled to evaluate the effect of autoclaving on sorption properties in abiotic control experiments. Difference between (i) and (iii) enabled to assess the effect of pesticide mixture on sorption compared to sorption of a single pesticide. Sediment was dried at  $40^\circ\text{C}$ , sieved at 2 mm and stored in dark before sorption experiments. In a 50 mL polypropylene (PP) centrifuge tube, 5 g of dried sediment were mixed with 30 mL of  $\text{CaCl}_2$  (0.01M) and vortex 20 sec. Tubes were spiked with the pesticide mixture stock to obtained an initial concentration of 0.75, 1, 2.5, 5, 7.5 and  $10 \text{ mg L}^{-1}$  pesticides and flushed with  $\text{N}_2$  until ACN evaporation. Centrifuge tubes were shaken (orbital shaker 80 rpm) for 24 h. The centrifuges tubes were then centrifuged at 2400 RCF 20 min. The water phase was collected and filtered successively through  $0.45 \mu\text{m}$  and  $0.2 \mu\text{m}$  CA syringe filter. Pesticide extraction, quantification and CSIA were carried out as for the biodegradation experiment. Control experiments without TSS showed no sorption (>95% of recovery) on the PP centrifuge tube within the range of concentrations and the time scale of the sorption experiments. Sorption experiments were best fitted with a linear model, compare to Freundlich or Langmuir model, following:

$$P_s = K_d \times P_w \quad (\text{B5})$$

Sorption was compared among experiment under the assumption that organic carbon content is causally related to pesticide sorption capacity. The sediment organic carbon-water partitioning coefficient ( $K_{OC}$ ) were calculated for each experiment following:

$$K_{OC} = K_d \times f_{oc}^{-1} \quad (\text{B6})$$

### **Water-sediment extraction and effect on stable isotope signature of pesticides**

Pesticides were extracted from water phase by solid phase extraction (SPE) using SolEx C18 cartridges (1 g, Dionex-Thermos Fischer Scientific) on an AutoTrace 280 SPE system (Dionex-Thermos Fischer Scientific) following a modified US EPA method.<sup>27, 28</sup> Briefly, the extraction cartridge was conditioned by washing successively with EtOH (5 mL), ACN (5 mL), and ultrapure water (10 mL). Sample was loaded on the cartridge and dried under nitrogen flux for 10 min. The pesticide mixture was eluted by 5 mL of EtOAc followed by 5 mL of ACN. The extracts were dried under nitrogen stream at room temperature and then re-suspended into ACN up to 1 mL. By vortexing the residues were collected and transfer into a 1.5 mL glass gas chromatography (GC) vials before measurements.

Pesticides were extracted from sediment phases by solid-liquid extraction protocol modified from Ivdra, et al.<sup>29</sup> Briefly, the wet sediment (5 g dry mass) previously transferred into a centrifuge tube was extracted with 3 mL pentane:DCM (3:1, v/v) in centrifuge tubes, vortexed 5 s followed by 5 min into ultrasonic bath (Branson 5510, 40 kHz). Then, centrifuge tubes were vortexed for 1 min and centrifuged at 2400 RCF 20 min. The supernatant was transferred into an amber glass vial and extraction procedure was repeated an additional two times. The three supernatants were pooled together and dried under a gentle nitrogen stream at room temperature and then re-suspended into ACN up to 1 mL, before vortexing to collect residues on the glassware. The RH and impurity were removed by adding in each vial about 75 mg of anhydrous  $\text{MgSO}_4$  and 13 mg of PSA. Vials were vortexed for 30 s, centrifuged at 2400 RCF 5 min and the supernatant transferred into a 1.5 mL glass GC vials before measurements.

Extraction efficiencies and stable isotope fractionation induced by the extraction protocol were evaluated from water and sediment samples. For the water phase, 100 mL of synthetic water was spiked with the pesticide mixture stock to reach concentrations between 1 and 1500  $\mu\text{g L}^{-1}$  for each pesticide. Six successive concentrations were tested, including 1, 5, 10, 50, 500 and 1500  $\mu\text{g L}^{-1}$ . Pesticides were extracted from water samples as described above.

For sediment samples, 5 g of sediment dried at 40 °C were put into a 15 mL centrifuge tubes and adjusted up to 100% w/w RH with ultrapure water. Sediment samples were spiked with the pesticide mixture stock to reach concentration from 0.5 to 150  $\mu\text{g g}^{-1}$ . Ten successive

concentrations were tested, including 0.5, 5, 10, 20, 30, 40, 50, 75, 100, 125 and 150  $\mu\text{g g}^{-1}$ . The spiked sediment samples were vortexed for 3 min to ensure homogenization. Sediment samples were incubated for 7 days in the dark at 4°C before extraction. Pesticide extraction from sediment samples was carried out as described above. Each tested condition was performed in duplicate. Additionally, a blank series with no sediment were spiked as previously described to evaluate whether pesticide sorption occurred during extraction. A series of abiotic control experiments was set-up in parallel to quantify potential abiotic degradation or volatilization losses during the 7 days of sediment incubation. Sediment samples were autoclaved twice (24 h intervals). The extraction protocol for sediment samples was applied as described above.

### **Pesticide quantification**

Pesticide quantification was performed using a gas chromatography (GC, Trace 1300, Thermo Fisher Scientific) coupled with a mass spectrometer (MS, ISQ™, Thermo Fisher Scientific) equipped with a TG-5MS column (30 m  $\times$  0.25 mm ID, 0.25  $\mu\text{m}$  film thickness, Thermo Fisher Scientific). The sample (1.5  $\mu\text{L}$ ) and GC internal standard (metolachlor- $\text{d}_{11}$ ; 1  $\mu\text{L}$  at 300  $\mu\text{g L}^{-1}$ ) were injected simultaneously via a split/splitless injector. Injector was set at 280°C with a split flow rate of 6  $\text{mL min}^{-1}$  and a helium carrier gas flow rate of 1.5  $\text{mL min}^{-1}$ . The GC oven program consisted of a 1 min hold time at 50°C, heating at 30°C  $\text{min}^{-1}$  to 160°C, heating at 4°C  $\text{min}^{-1}$  to 220°C, heating at 30°C  $\text{min}^{-1}$  to 300°C, followed by a 1 min hold time at 300°C. The MS transfer line and source were heated at 320°C. Eluted pesticides were identified by their specific masses in a selective ion mode (SIM). Instrumental detection limits (IDLs) and instrument quantification limits (IQLs) were determined by multiple blank and standard injection, respectively, ( $n = 5$ ) at the lowest concentration giving a signal-to-noise (S/N) ratio of three. IDLs and IQLs were around 8 and 45  $\mu\text{g L}^{-1}$ , respectively (Table B5). Calibration was made using a pesticide mixture from 25 up to 750  $\mu\text{g L}^{-1}$ . Analytical reproducibility, analytical uncertainty due to matrix effect from water and sediment samples, are provided in Table B5.

### **Compound-specific isotope analysis (CSIA)**

For carbon and nitrogen CSIA, GC-isotope ratio mass spectrometry (IRMS) system consisted of a GC (TRACE™ Ultra) coupled via a GC combustion interface (IsoLink/Conflow IV) to an IRMS (DeltaV, both from Thermo Fisher Scientific). Between 1 and 3  $\mu\text{L}$  of samples were injected via a split/splitless injector. Injector was set at 250°C with a split flow rate of 30  $\text{mL min}^{-1}$  and a helium carrier gas flow rate of 1.5  $\text{mL min}^{-1}$  into a TG-5MS column (60 m  $\times$  0.25 mm ID, 0.25  $\mu\text{m}$  film thickness). For C, the GC oven program consisted of a 1 min hold time at 50°C, heating at 15°C  $\text{min}^{-1}$  to 150°C, heating at 2°C  $\text{min}^{-1}$  to 250°C, heating at 20°C  $\text{min}^{-1}$  to 300°C, followed by a 1 min hold time at 300°C. For N, the GC oven program consisted of a 1 min hold time at 50°C, heating at 20°C  $\text{min}^{-1}$  to 150°C, heating at 10°C  $\text{min}^{-1}$  to 300°C, followed by a 4 min hold time at 300°C. For both elements, target compounds were combusted to the analyte gases ( $\text{CO}_2$  and  $\text{N}_2$ ) in a single combined reactor (P/N 1255321, NiO tube and

CuO-NiO-Pt wires, Thermo Fischer Scientific) operated at 1000°C. For N, liquid N<sub>2</sub> was used for cryogenic trapping of CO<sub>2</sub>. The MS transfer line and source were heated at 320°C. To validate the measurement quality, samples were bracketed with two standard measurements before and after a series of measurements. First standard was a BTEX standard of known isotope signature (Benzene, Toluene, Ethylbenzene and o-Xylene 15 µL of each in 50 mL of *n*-Pentane) or an international reference material AIEA600 (Caffeine; 150 mg L<sup>-1</sup> in acetone) for C and N respectively. Pure solid powder of pesticides were measured as the reference isotope signatures by elemental analyzer IRMS (Flash EA IsoLink™ CN IRMS, Thermo Fisher Scientific). Values were  $\delta^{13}C_{EA-IRMS} = -29.02 \pm 0.03\text{‰}$ ,  $\delta^{15}N_{EA-IRMS} = -2.43 \pm 0.41\text{‰}$  for the acetochlor and  $\delta^{13}C_{EA-IRMS} = -30.60 \pm 0.07\text{‰}$ ,  $\delta^{15}N_{EA-IRMS} = -0.52 \pm 0.10\text{‰}$  for the S-metolachlor.

The minimal change of isotope signature ( $\Delta\delta^h E_{min}$ ), before which isotope fractionation can be attributed to degradation, was determined as the propagation of uncertainties associated with measurements and sample preparation<sup>30</sup> and calculated as follow:

$$\Delta\delta^h E_{min} = \sqrt{\sigma_{ea}^2 + \sigma_s^2 + \sigma_{au}^2} + \Delta\delta^{13}C_{ext} \quad (\text{B7})$$

where  $\sigma_{ea}^2$ ,  $\sigma_s^2$  and  $\sigma_{au}^2$  are the uncertainty associate with the triplicate measurement of the initial product by an elemental analyzer IRMS (0.5‰ and 0.7‰ for C and N respectively), the sample uncertainty associated with the triplicate measurement and the maximal analytical uncertainty of the GC-IRMS (0.5‰ and 1.0‰ for C and N respectively), respectively.  $\Delta\delta^{13}C_{ext}$  is the trueness of the  $\delta^{13}C$  measurement associated with the extraction procedure, as previously determined (Table B5).

The extent of pesticide biodegradation ( $B$ ) can be estimated from the inverse form of the Rayleigh equation and using  $\varepsilon$  values determined under representative conditions in laboratory experiments:<sup>31</sup>

$$B = 1 - \left( \frac{\delta^{13}C(t) + 1}{\delta^{13}C_0 + 1} \right)^{1/\varepsilon_{bulk,C}} \quad (\text{B8})$$

Consequently, the limit of detection to evaluate the extent of biodegradation ( $B \geq 1 - P(t)/P_0$ ), was determined as follows:

$$B \geq 1 - e^{\Delta/\varepsilon} \quad (\text{B9})$$

where  $\Delta$  correspond to the minimal change of isotope signature ( $\Delta\delta^h E_{min}$ ) above which isotope fractionation was can be attributed to degradation, as previously calculated in eq. B7 and provided in Table B5.

## Mass balance accounting for the phase-transfer model

A pesticide mass balance was established from the two-phase conceptual model to tease apart (Figure 4.2) destructive and non-destructive processes contributing to pesticide dissipation in a water–sediment system with two phases. First, the pesticide mass balance was used to estimate the half-life of degradation ( $DegT_{50}$ ) from the observed half-life of the dissipation ( $DT_{50}$ ) for each phase. Then, the conceptual model was used to evaluate the effect of desorption of isotopically lighter, non-degraded pesticide from the sediment phase to the water phase on the isotopic enrichment factor ( $\epsilon$ ) in order to correct if necessary the extent of the biodegradation in the water phase, accounting for phase-transfer.

### A) Estimation of the Rate Constant of the Degradation ( $k_{deg,w}$ )

The pesticide mass balance relies on nine assumptions described below which set the boundaries of the developed framework. As compared with previous studies,<sup>32-34</sup> we closed the mass balance only for the pesticide itself as the other species (i.e., non-extractable residues - NER, formation of CO<sub>2</sub> over mineralization, sum of TPs) were not quantified and targeted in our study.

1. The system is closed and masses are conserved.
2. The water–sediment system with two phases is defined similarly as in a previous study:<sup>34</sup> the water phase (subscript w) is assumed to contain only the aqueous freely dissolved species ( $P_w$ ), and the sediment phases (subscript s) contains the bounded fraction of the (i.e., particulate and dissolved organic carbon -  $P_s$ ).
3. Species are bounded exclusively on organic carbon because the studied pesticides are not charged at the experiment  $pH$  and thus do not result in ionic charge interactions with minerals.<sup>3</sup> Pesticides thus sorb to organic carbon present in the dissolved (DOC) and the particulate (POC) forms.
4. Sorption on DOC and POC were assumed equivalent, with sediment organic carbon–water partitioning coefficient ( $K_{oc}$ ) remaining unaffected by the type of organic matter as well as the  $pH$  of the water phase.<sup>35</sup>
5. Considering the experimental duration, the system is assumed under steady state condition. This is supported by two aspects:
  - i) A constant  $P_s/P_w$  ratio all along the experiment which corresponded to  $K_d$  values obtained in separate batch isotherm experiments (Table B4). It advocates for a fully established sorption equilibrium at any time.
  - ii) Stable hydrochemical characteristics across the experiment, suggesting constant water redox condition over the experiment.
6. The sum of all transformation products (TPs) is considered as a single species.
7. The system shaking is assumed sufficient to maintain fully mixed conditions, i.e., the dissipation processes are homogeneous in the system over space and time. This is supported by a volume ratio between the total ( $V_{tot}$ ) and by the water phase ( $V_w$ ) close to one



( $V_{tot}/V_w$  is equal to 0.96) which indicates that the sediment is in sufficient low concentration to allow homogenous suspension by shaking.

8. Pesticide degradation in the sediment phase is negligible during the experiment. This is supported by the isotope signature showing no significant isotope fractionation in the sediment phase (Figure 4.1). This follows the general assumption than sorbed species are not or less available for degradation<sup>3</sup> or in other term species should be in fully dissolved to be bioavailable for microorganism.<sup>36, 37</sup>
9. Hydrolysis does not occur at the experimental  $pH$  for the species of interest.<sup>18</sup>

The pesticide mass balance equation (eq. B10) as follows:

$$m_{p,system} = m_{p,w} + m_{p,s} \quad (B10)$$

The degradation during the experiment  $\frac{dm_{p,system}}{dt}$  is assumed to fit to a pseudo first-order degradation kinetic in the water phase, eq. B11,

$$\frac{dm_{p,system}}{dt} = -k_{deg,w} \times t \times V_w \quad (B11)$$

Under steady state condition,  $m_{p,s}$  is expressed by the partitioning between the two phases following eq. B5 and can be re-written as eq. B12,

$$m_{p,s} = K_d \times m_{p,w} \times TSS \quad (B12)$$

once reinjected in eq. B10, giving eq. B13.

$$m_{p,system} = m_{p,w} \times (1 + K_d \times TSS) \quad (B13)$$

Then, the variation of pesticide mass in sediment phase can be expressed as a function of  $K_{oc}$  (eq. B6) and the total organic carbon concentration (eq. B14; TOC) following our assumption four, where TOC is the sum of POC and DOC:

$$\begin{aligned} K_d \times TSS &= K_{oc} \times TOC \\ TOC &= POC + DOC = f_{oc,s} \times TSS + DOC \end{aligned} \quad (B14)$$

So eq. B13 becomes eq. B15,

$$m_{p,system} = m_{p,w} \times [1 + K_{oc} \times (f_{oc,s} \times TSS + DOC)] \quad (B15)$$

Finally, assuming the observed dissipation of the pesticide in the water phase follows a pseudo first-order reaction as

$$\frac{dm_{p,w}}{dt} = -k_{obs,w} \times t \times V_w \quad (B16)$$

This gives:

$$\frac{dm_{p,system}}{dt} = \frac{dm_{p,w}}{dt} \times [1 + K_{oc} \times (f_{oc,s} \times TSS + DOC)] \quad (B17)$$

Combining eq. B11, B15 and B17 lead to the expression of the effective,

$$k_{deg,w} = k_{obs,w} \times [1 + K_{oc} \times (f_{oc,s} \times TSS + DOC)] \quad (B18)$$

However, as our system DOC and POC originated from the same source of sediment (i.e., DOC dissolved from POC), the sum of POC and DOC remained constant over time in agreement with observations (see section above). Additionally, DOC was negligible because i) it accounts for only 0.3% (DOC/POC; w/w) of the sediment phase, which is equivalent to  $2 \times 10^{-3}\%$  of the total sorbed pesticide mass of the system, ii) accounting DOC would propagate a variance of  $\pm 0.1 \text{ d}^{-1}$  over the  $k_{deg,w}$  which is far below the uncertainty associated to the calculation of the  $k_{deg,w}$  which is  $\pm 11 \text{ d}^{-1}$ , iii) TSS losses during the extraction process, less than 2%, which is higher than the fraction of DOC contained within the system. By consequence we could use the simplified eq. B19:

$$k_{deg,w} = k_{obs,w} \times [1 + K_{oc} \times f_{oc,s} \times TSS] \quad (B19)$$

### B) Impact of Phase Transfer on Isotopic Enrichment Factor ( $\epsilon$ )

Following the same assumptions and using the water–sediment system conceptual model developed above for the degradation, we calculated a corrected isotopic enrichment factor ( $\epsilon_{bulk,corr}$ ) accounting for both phase-transfer and degradation on the water phase. A constant isotope signature over time (equal to  $\delta^{13}\text{C}_0$ ) of the sorbed fraction of acetochlor and *S*-metolachlor suggested the absence of significant degradation in the sediment phase.

Under closed system assumption, experimental  $\epsilon_{bulk,E}$  values for an element  $E$  is determined following the Raleigh equation (eq. B20),<sup>31</sup>

$$\ln\left(\frac{\delta^h E(t) + 1}{\delta^h E_0 + 1}\right) = \epsilon_{bulk,E} \times \ln\left(\frac{m_{p,w}}{m_{p,0}}\right) \quad (B20)$$

where  $m_{p,0}$  and  $m_{p,w}$  are the initial and the remaining mass of the pesticide in water. In our water–sediment system with two phases,  $m_{p,w}$  corresponds to the freely dissolved fraction and  $m_{p,0}$  the initial dissolved pesticide mass at the equilibrium:

$$m_{p,w} = m_{p,system} - m_{p,s} \quad (B21)$$

$$\ln\left(\frac{\delta^h E(t) + 1}{\delta^h E_0 + 1}\right) = \varepsilon_{bulk,E} \times \ln\left(\frac{m_{p,system} - m_{p,s}}{m_{p,0}}\right) \quad (B22)$$

Accordingly,  $\varepsilon_{bulk,E}$  is not linearly correlated to  $\ln\left(\frac{m_{p,w}}{m_{p,0}}\right)$  anymore and cannot be derived from a simple linear regression.  $\varepsilon_{bulk,E}$  could not be analytically expressed as a function of  $m_{p,w}$  only. By consequence, we used a stepwise calculation expressing  $m_{p,system} - m_{p,s}$  according to the equivalent pesticide mass remaining in the water phase undergoing degradation. This calculation accounts for the mass of pesticide desorbed from the sediment ( $m_{p,s \rightarrow w}(t)$ ), and the mass of pesticide remaining in the water phase at each time step ( $m_{p,w}(t)$ ) which can be expressed as the fraction of pesticide ( $f_{p,s \rightarrow w}$ ) desorbing from the sediment to the total over time, as follows:

$$f_{p,s \rightarrow w} = \frac{m_{p,s \rightarrow w}(t)}{m_{p,s \rightarrow w}(t) + m_{p,w}(t)} \quad (B23)$$

Iterative correction scheme is necessary as  $m_{p,s \rightarrow w}$  at time  $t$  depend of the  $t - 1$  values (eq. B24):

$$m_{p,s \rightarrow w}(t) = m_{p,s \rightarrow w}(t - 1) - m_{p,deg} \quad (B24)$$

where the theoretical pesticide mass degraded in water phase ( $m_{p,deg}$ ) is recalculated based on a pseudo first-order previously corrected such eq. B25:

$$m_{p,deg} = P_w \times V_w \times e^{-k_{deg} \times t} \quad (B25)$$

Theoretically, the isotope signatures follow additive properties.<sup>38</sup> At each time step the measured  $\delta^h E_{meas}$  reflects isotope signatures of the pesticide in the water phase and that the pesticide fraction desorbed from the sediment to the water phase, following eq. B26:

$$\delta^h E_{meas} = f_{p,s \rightarrow w} \times \delta^h E_s + (1 - f_{p,s \rightarrow w}) \times \delta^h E_w \quad (B26)$$

As no degradation was observed in the sediment phase,  $\delta^h E_s$  is assumed to be constant over time and equal to the  $\delta^h E_0$ . By using the system of eq. B22 to B26 we could express eq. B27:

$$\frac{\delta^h E_w(t) + 1}{\delta^h E_0 + 1} = \frac{\delta^h E_{meas} - f_{p,s \rightarrow w} \times \delta^h E_0}{1 - f_{p,s \rightarrow w}} + 1 \quad (B27)$$

which could be reinjected into a modified Raleigh eq. B28:

$$\ln\left(\frac{\delta^h E_w(t) + 1}{\delta^h E_0 + 1}\right) = \varepsilon_{bulk,corr} \times (-k_{deg} \times t) \quad (\text{B28})$$

Finally, the  $\varepsilon_{bulk,corr}$  is numerically resolved using eq. B23 with a time step equivalent to 30,000 iterations ( $\Delta t$  equal to 0.01 day) into the linear system of eq. B27 & B28. Good fit was obtained after 10,000 iterations using a convergence criterion of 0.01. Convergence criterion is defined as Querin, et al.<sup>39</sup> as the variation of an objective value in the last 10 iteration,

$$cc_i = \frac{|\sum_{i-9}^{i-5} OV_i - \sum_{i-4}^i OV_i|}{\sum_{i-4}^i OV_i} \quad (\text{B29})$$

where  $i$  is the number of iterations,  $OV_i$  is the objective value in the  $i$  iteration.

## Supporting results and discussion

### Sediment characteristics

The sediment (Table B1) was classified as silt loam<sup>40</sup> with a low content of organic carbon and carbonate.<sup>41</sup> The C/N ratio of the sediment suggests a carbon limitation environment for microbial growth.<sup>42, 43</sup> Elemental composition analysis emphasizes that silica was the main mineral constituent followed by calcium.

Table B1. Sediment characteristics.

	day 0		day 300
	non-autoclaved	autoclaved	non-autoclaved
residual humidity (w/w)	0.37 ± 0.03		
$pH_{H_2O}$	7.5 ± 0.5		
$pH_{CaCl_2}$	7.2 ± 0.5		
CEC (cmol g <sup>-1</sup> )	14.3 ± 2.8		
BD (g cm <sup>-3</sup> )	1.7 ± 0.1		
clay (< 2µm; %)	21.2 ± 2.5		19.3
silt (2 - 50 µm; %)	67.4 ± 2.5		65.5
sand (50 - 2000 µm; %)	11.4 ± 4.3		15.2
$f_{oc}$ (%) <sup>a</sup>	2.3 ± 2.1	1.2	2.0
C/N <sup>a</sup>	7.2 ± 1.5	9.3	7.0
C <sub>min</sub> (%) <sup>a</sup>	3.9 ± 0.5	4.9	4.0
OM (%)	17.0		
SiO <sub>2</sub> (%)	52.9		
Al <sub>2</sub> O <sub>3</sub> (%)	7.4		
MgO (%)	1.5		
CaO (%)	13.4		
Fe <sub>2</sub> O <sub>3</sub> (%)	2.9		
MnO (%)	0.076		
TiO <sub>2</sub> (%)	0.44		
Na <sub>2</sub> O (%)	1.0		
K <sub>2</sub> O (%)	1.7		
P <sub>2</sub> O <sub>5</sub> (%)	0.30		

Uncertainties correspond to the standard deviation (SD) from triplicate measurements. CEC,  $f_{oc}$ , C<sub>min</sub>, OM refer to cation exchange capacity, fraction of organic carbon, mineral carbon and organic matter, respectively. <sup>a</sup>Measurements of  $f_{oc}$ , C/N and C<sub>min</sub> are associated with an analytical uncertainty of 2%. Elementary analysis by ICP-OES measurements is reported for its most abundant oxide form.

**Hydrochemistry**

Table B2. Change from days 0 to 300 of the dissolved organic carbon content ( $\Delta\text{DOC}$ ), specific ultraviolet absorbance ( $\text{SUVA}_{254/280}$ ) and mean carbon oxidation state ( $\bar{O}x$ ) in biodegradation experiments.

times (days)	$\Delta\text{DOC}$ (ppm)	$\text{SUVA}_{254/280}$ ( $\text{L mg}^{-1} \text{C m}^{-1}$ ) <sup>a</sup>		$\bar{O}x$ <sup>b</sup>	
	0 → 300	0	300	0	300
oxic	10 ± 5	4.2 ± 0.0 /	6.3 ± 0.0 /	-0.48 ±	-0.45
		9.5 ± 2.4	12.0 ± 1.6	0.02	
anoxic	19 ± 4	n.m. <sup>c</sup>	n.m. <sup>c</sup>	n.m. <sup>c</sup>	-0.14

<sup>a</sup> Calculated with eq. B4. <sup>b</sup> Calculated with eq. B3, propagation of uncertainty associated with the measurement is typically ±0.3.<sup>24</sup> <sup>c</sup> n.m. not measured but considered as similar as under oxic conditions at time zero. Uncertainties correspond to the standard deviation (SD) of triplicate measurements.

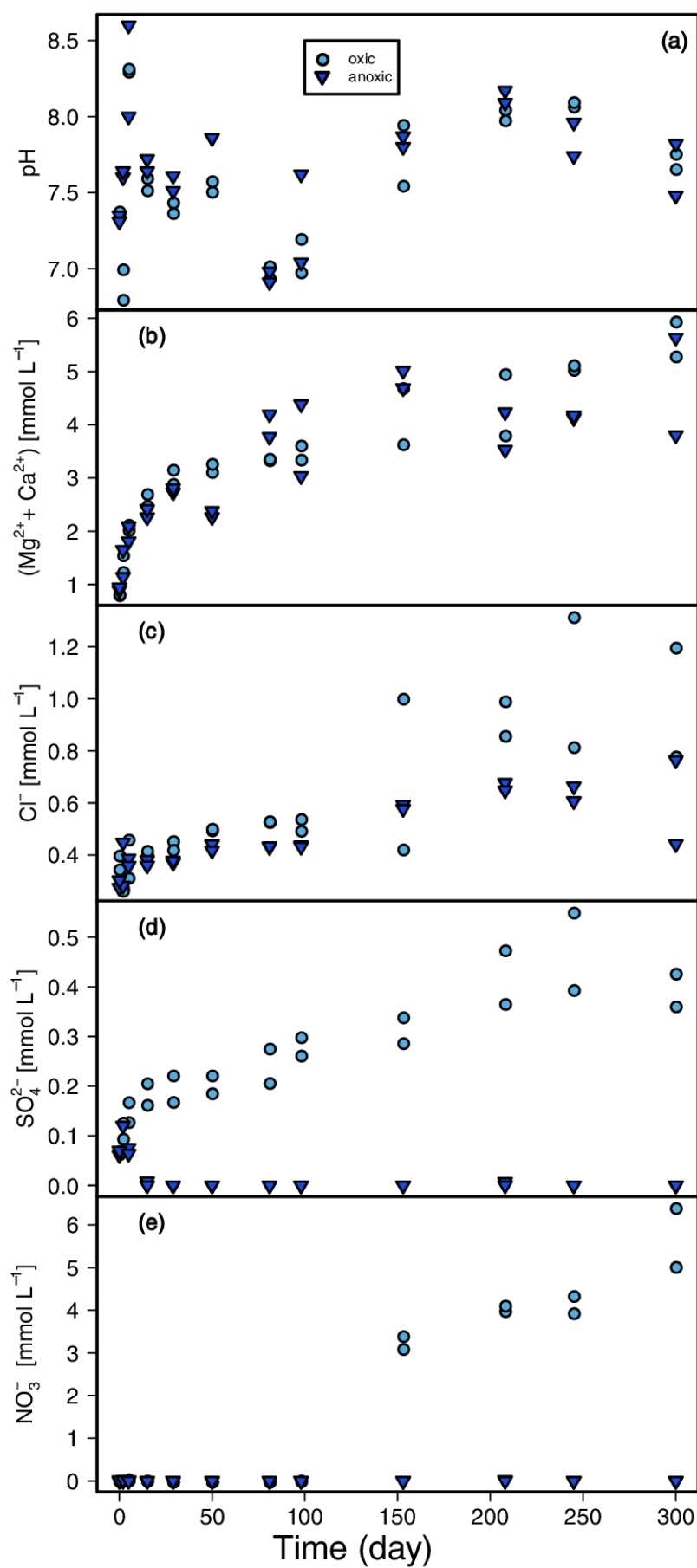


Figure B1. Changes of hydrochemistry during biodegradation experiments. (a) pH, (b) magnesium-calcium (Mg<sup>2+</sup> + Ca<sup>2+</sup>), (c) chloride (Cl<sup>-</sup>), (d) sulfate (SO<sub>4</sub><sup>2-</sup>) and (e) nitrate (NO<sub>3</sub><sup>-</sup>) concentration.

## Control experiment

Table B3. Change from days 0 to 300 of the pesticide remaining fraction ( $P(t)/P_0$ ) and carbon isotope signatures ( $\delta^{13}C$ ) in the control experiment.

	atrazine	terbutryn	acetochlor	S-metolachlor	metalaxyl
oxic autoclaved ( $n=8$ )					
$\Delta(P(t)/P_0)_w$	$1.01 \pm 0.11$	$1.13 \pm 0.25$	$1.15 \pm 0.14$	$1.07 \pm 0.09$	$1.11 \pm 0.11$
$\Delta(P(t)/P_0)_s$	$1.04 \pm 0.12$	$0.87 \pm 0.12$	$0.95 \pm 0.11$	$0.93 \pm 0.07$	$1.09 \pm 0.22$
$\Delta\delta^{13}C_w$ (‰)	$0.22 \pm 0.81$	$-0.58 \pm 0.51$	$0.81 \pm 2.17$	$-0.63 \pm 0.78$	$-1.56 \pm 0.31$
$\Delta\delta^{13}C_s$ (‰)	n.m.	n.m.	n.m.	n.m.	n.m.
anoxic autoclaved ( $n=8$ )					
$\Delta(P(t)/P_0)_w$	$1.13 \pm 0.14$	$1.56 \pm 0.38$	$1.20 \pm 0.19$	$1.11 \pm 0.20$	$1.05 \pm 0.11$
$\Delta(P(t)/P_0)_s$	$0.98 \pm 0.07$	$0.82 \pm 0.20$	$0.90 \pm 0.08$	$0.95 \pm 0.05$	$0.96 \pm 0.17$
$\Delta\delta^{13}C_w$ (‰)	$-0.10 \pm 0.36$	$0.05 \pm 2.98$	$-1.12 \pm 0.12$	$-0.54 \pm 2.11$	$-2.05 \pm 0.31$
$\Delta\delta^{13}C_s$ (‰)	n.m.	n.m.	n.m.	n.m.	n.m.
hydrolysis autoclaved (pH=8; $n=10$ )					
$\Delta(P(t)/P_0)_w$	$0.88 \pm 0.10$	$0.83 \pm 0.12$	$0.94 \pm 0.08$	$0.94 \pm 0.11$	$1.23 \pm 0.42$

w: water phase, s: sediment phase, n.m.: not measured. <sup>a</sup> CSIA of pesticides in autoclaved sediment show up a large matrix effect which do not enable the measurement. Uncertainties correspond to the standard deviations of  $n$  samples collected over time.

## Batch sorption experiment

Table B4. Pesticide sediment partitioning coefficients

	batch sorption experiments (OECD 106)	biodegradation experiment	
	$K_d$ (L kg <sup>-1</sup> ) <sup>a</sup>	$P_s/P_w$ ratio (L kg <sup>-1</sup> ) <sup>b</sup>	
sediment non-autoclaved and pesticide in mixture ( $n = 11$ ; pH=7.5)			
atrazine	$4.1 \pm 5.7$	oxic ( $n = 10$ )	anoxic ( $n = 10$ )
terbutryn	$21.6 \pm 5.8$	$1.4 \pm 0.9$	$0.8 \pm 0.4$
acetochlor	$5.8 \pm 2.3$	$12.9 \pm 9.0$	$13.3 \pm 11.1$
S-metolachlor	$6.6 \pm 1.7$	$4.3 \pm 3.4$	$2.4 \pm 1.3$
metalaxyl	$0.6 \pm 0.4$	$3.8 \pm 2.3$	$2.6 \pm 0.8$
sediment non-autoclaved and one pesticide at the time ( $n = 8$ ; pH=7.5)			
atrazine	$2.1 \pm 1.4$		
terbutryn	$15.7 \pm 2.0$		

Uncertainties correspond to the 95% confidence interval (C.I.) from  $n$  replicate measurements. <sup>a</sup> Data were fitted by linear relationship between sorbed pesticides and pesticides in water phase (eq. B5). The coefficient of determination ( $R^2$ ) of linear  $K_d$  fitting ranged from 0.66 to 1.00 ( $R^2$  average = 0.90). <sup>b</sup>  $P_s/P_w$  ratio were not considered when the  $P_w$  value ranged below the propagation of uncertainty of the  $P_s/P_w$  ratio (division by zero when  $P_w \rightarrow 0$ ). This threshold corresponds in average to  $92 \pm 2\%$  of dissipation.



## Method validation and limits

Table B5. Extraction efficiency, qualitative and quantitative limit of the analytical methods.

	atrazine	terbutryn	acetochlor	S-metolachlor	metalaxyl
solid-liquid extraction on the non-autoclaved sediment					
recovery (% , n=22)	88.7 ± 18.0	86.9 ± 18.8	91.6 ± 22.4	88.1 ± 20.3	76.0 ± 18.8
$\Delta\delta^{13}\text{C}_{\text{ext,s}}$ (‰, n=12) <sup>a</sup>	-0.28 ± 0.49	0.06 ± 1.87	-0.17 ± 0.22	-0.55 ± 1.00	0.61 ± 0.94
$\Delta\delta^{13}\text{C}_{\text{min,s}}$ (‰) <sup>b</sup>	1.13	2.06	0.91	1.77	1.79
$\Delta\delta^{15}\text{N}_{\text{ext,s}}$ (‰, n=5) <sup>a</sup>	-0.10 ± 1.08	0.69 ± 0.91	1.20 ± 0.40	1.58 ± 0.60	1.86 ± 0.43
$\Delta\delta^{15}\text{N}_{\text{min,s}}$ (‰) <sup>b</sup>	1.39	1.83	2.01	2.51	2.69
solid-liquid extraction on the autoclaved sediment					
recovery (% , n=22)	85.1 ± 27.7	76.6 ± 31.4	86.5 ± 29.6	81.2 ± 29.5	75.5 ± 26.3
$\Delta\delta^{13}\text{C}_{\text{ext,s}}$ (‰, n=12) <sup>a</sup>	-0.83 ± 0.37	1.40 ± 0.79	-0.84 ± 0.30	-1.23 ± 0.32	2.38 ± 0.36
$\Delta\delta^{13}\text{C}_{\text{min,s}}$ (‰) <sup>b</sup>	1.63	2.46	1.61	2.01	3.17
solid phase extraction (SPE)					
recovery (% , n=4)	108.3 ± 11.7	107.7 ± 12.6	121.9 ± 14.2	115.9 ± 12.2	125.4 ± 14.4
$\Delta\delta^{13}\text{C}_{\text{ext,w}}$ (‰, n=4) <sup>a</sup>	0.40 ± 0.60	0.09 ± 0.24	-0.12 ± 0.41	0.11 ± 0.45	0.92 ± 0.74
$\Delta\delta^{13}\text{C}_{\text{min,w}}$ (‰) <sup>b</sup>	1.33	0.83	0.94	0.95	1.95
$\Delta\delta^{15}\text{N}_{\text{ext,w}}$ (‰, n=4) <sup>a</sup>	0.48 ± 0.96	1.96 ± 1.32	0.68 ± 0.73	0.85 ± 0.90	1.14 ± 1.09
$\Delta\delta^{15}\text{N}_{\text{min,w}}$ (‰) <sup>b</sup>	1.67	3.46	1.70	1.99	2.44
gas chromatography mass spectrometer (GC-MS)					
IDLs ( $\mu\text{g L}^{-1}$ ) <sup>c</sup>	4.52 ± 0.10	2.48 ± 0.38	2.31 ± 0.61	7.42 ± 0.38	0.81 ± 0.08
IQLs ( $\mu\text{g L}^{-1}$ ) <sup>c</sup>	41.6 ± 1.3	45.3 ± 1.2	33.2 ± 1.6	30.5 ± 1.1	39.3 ± 2.6
anal. rep. (%) <sup>d</sup>	2.34 ± 0.01	4.42 ± 0.02	5.60 ± 0.03	4.30 ± 0.04	7.18 ± 0.18
wat. anal. prec. (%) <sup>e</sup>	11.7 ± 0.1	12.6 ± 0.1	14.2 ± 0.2	12.2 ± 0.1	14.4 ± 0.2
sed. anal. prec. (%) <sup>e</sup>	19.9 ± 0.1	21.9 ± 0.1	23.6 ± 0.2	23.7 ± 0.1	23.1 ± 0.2
gas chromatography isotopic ratio mass spectrometer (GC-IRMS)					
C range lin. (ng C) <sup>f</sup>	10 - 300	10 - 300	20 - 300	20 - 300	20 - 300
(mg L <sup>-1</sup> )	11 - 336	11 - 321	16 - 240	16 - 236	15 - 232
N range lin. (ng N) <sup>f</sup>	40 - 300	40 - 300	40 - 300	40 - 300	40 - 300
(mg L <sup>-1</sup> )	72 - 538	86 - 642	449 - 3367	472 - 3541	465 - 3486

Uncertainties correspond to the standard deviation (SD) from *n* replicate measurements. <sup>a</sup> Trueness ( $\Delta\delta$ ) of the  $\delta^h E$  measurement for each pesticide was verified for the extraction procedure and reported as  $\Delta\delta^h E$  ( $\Delta\delta^h E = \delta^h E_{GC-IRMS} - \delta^h E_{EA-IRMS}$ ) where  $\delta^h E_{GC-IRMS}$  was the of isotope signatures measured by GC-IRMS and  $\delta^h E_{EA-IRMS}$  was isotope signatures determined independently for a pure solid by elemental analyzer IRMS (Flash EA IsoLink™ CN IRMS, Thermo Fisher Scientific). <sup>b</sup> Minimal change of isotope ratios  $\Delta\delta^h E_{min}$  before fractionation was attributed to degradation and were calculated by the propagation of uncertainty, eq. B7. <sup>c</sup> Instrumental detection limits (IDLs) and instrument quantification limits (IQLs) were determined by multiple blank and standard injection, respectively, (*n* = 5) at the lowest concentration giving a signal-to-noise (S/N) ratio of three. <sup>d</sup> Analytical reproducibility is determined by injecting a 500  $\mu\text{g L}^{-1}$  calibration standard in five independent GC runs; reported as the ratio between SD of the five measurement and the concentration of the standard.<sup>44</sup> <sup>e</sup> Analytical accuracy associated with the matrix effect of water (wat.) and sediment (sed.) samples was evaluated by five independent GC runs (*n* = 5) of the similar spike sample at 300  $\mu\text{g L}^{-1}$  and reported as the ratio between measured and spiked values. <sup>f</sup> Range of linearity with the lowest values corresponding to the limit for precise isotope analysis (LPIA) was calculated using a moving mean procedure with set intervals of  $\pm 0.5\%$  and  $\pm 1\%$  around this moving mean for C and N respectively.<sup>45</sup> Corresponding concentrations are given in mg L<sup>-1</sup> for a 2  $\mu\text{L}$  injection. Limit of extraction capability was estimated as the lowest spike amount which could be extracted with a recovery >70%, corresponding to 0.05  $\mu\text{g}$  of pesticide for the SPE and 2.5  $\mu\text{g}$  for the solid-liquid extraction.

## Pesticides Dissipation

Dissipation in water were 2 to 6 times faster under oxic conditions than under anoxic conditions, although acetochlor dissipation rate constant did not differ among conditions (Figure B2). Dissipation rate constants in water and sediment were similar, under the same conditions, based on the 95% C.I. However, dissipation of *S*-metolachlor under oxic condition was faster in water, whereas dissipation of atrazine and metalaxyl under anoxic conditions was faster in the sediment.

Insignificant changes in carbon stable isotope signature were observed (obs) in water and sediment after 300 days for atrazine ( $\Delta\delta^{13}C_{obs} < 1.0\text{‰}$ ) and metalaxyl ( $\Delta\delta^{13}C_{obs} < 0.7\text{‰}$ ). Terbutryn was mainly found in the sediment, and low concentration in the water phase hampered CSIA measurements. By consequence, CSIA data obtained for atrazine, terbutryn and metalaxyl were not further analyzed, and only data for acetochlor and *S*-metolachlor were considered.

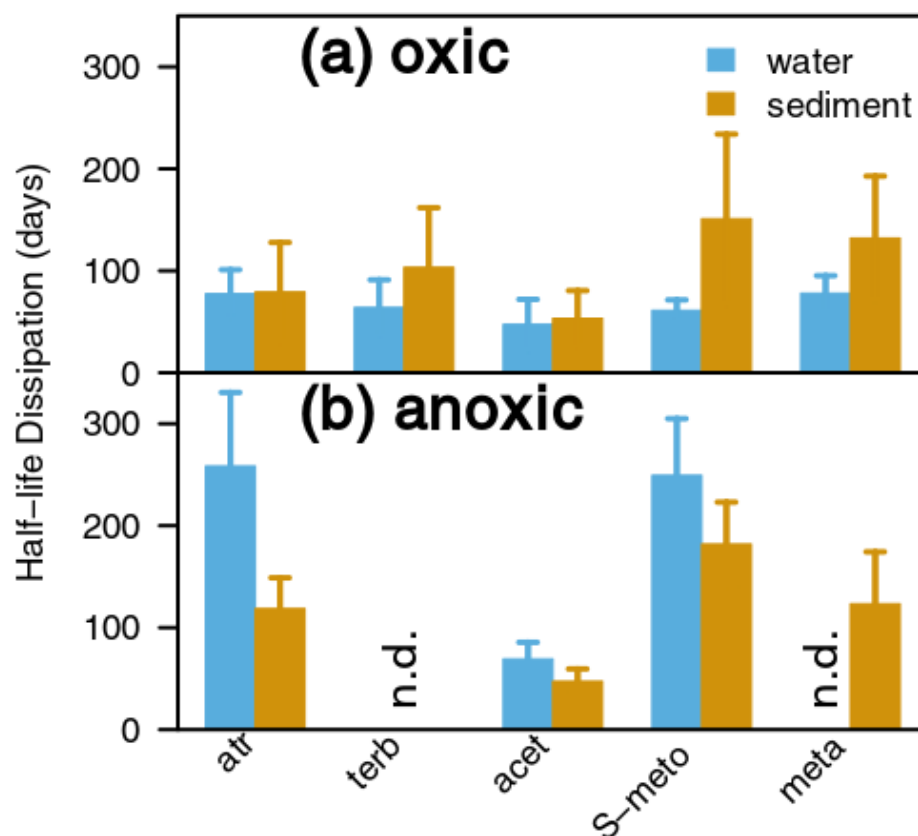


Figure B2. Half-life dissipation ( $DT_{50}$ ) for atrazine (atr), terbutryn (terb), acetochlor (acet), *S*-metolachlor (*S*-meto) and metalaxyl (meta) under (a) oxic and (b) anoxic conditions in the water and the sediment phases. Metalaxyl did not follow a strict pseudo first-order kinetics (goodness on linear fit  $\ln(P(t)/P_0) = -k_{obs} \times t$  was  $R^2 = 0.6$ ) in both phases. n.d.: not determined due to insufficient degradation ( $P(t)/P_0 > 0.5$ ) to calculate a  $DT_{50}$ .

**Transformation products analysis**

*Table B6. Suspect list of parent compound and transformation product identified from the literature and screened by liquid chromatography (LC) coupled to an Impact-II (Bruker, Germany) quadrupole time of flight (Q-TOF) to perform high resolution mass spectrometry (HR-MS/MS).*

*Electronic Appendix available pre-publishing on the CNRS website at <https://seafiler.unistra.fr/f/485d381c52114599be21/?dl=1>*

## Appendix C

### Supporting information to chapter 5

#### Supporting materials and methods

##### Chemicals reagents

Solvent and reagents including: dichloromethane (DCM), acetonitrile (ACN), ethanol (EtOH) and ethylacetate (EtOAc) in HPLC grade purity (>99.9%), calcium nitrate tetrahydrate ( $\text{Ca}(\text{NO}_3)_2 \cdot 4\text{H}_2\text{O}$ ), magnesium sulfate heptahydrate ( $\text{MgSO}_4 \cdot 7\text{H}_2\text{O}$ ), calcium chloride dihydrate ( $\text{CaCl}_2 \cdot 2\text{H}_2\text{O}$ ), sodium bicarbonate ( $\text{NaHCO}_3$ ), potassium dihydrogen phosphate ( $\text{KH}_2\text{PO}_4$ ), disodium hydrogen phosphate ( $\text{Na}_2\text{HPO}_4$ ) and caffeine ( $\text{C}_8\text{H}_{10}\text{N}_4\text{O}_2$ ) were purchased in A.C.S.-grade reagents ( $\geq 99\%$ ) from Sigma–Aldrich.

##### Synthetic water preparation and characterization

The preparation of the synthetic water followed the Esthwaite lake soft water recipe.<sup>20</sup> Two stock solutions, 50 fold concentrated, were made with (i)  $40 \text{ mg L}^{-1} \text{Ca}(\text{NO}_3)_2 \cdot 4\text{H}_2\text{O}$ ,  $15 \text{ mg L}^{-1} \text{MgSO}_4 \cdot 7\text{H}_2\text{O}$ ,  $20 \text{ mg L}^{-1} \text{CaCl}_2 \cdot 2\text{H}_2\text{O}$  and (ii)  $30 \text{ mg L}^{-1} \text{NaHCO}_3$ . (i) was dissolved into the required amount of ultrapure water and (ii) was added under continuous stirring of the solution. The use of sodium bicarbonate is likely to end up in dissolved  $\text{CO}_2$  excess or deficit which was balanced with 24 h vigorous stirring prior to the experiment. *pH* was measured time to time during these 24h to check for stability. Then the synthetic water was filtrated at  $0.2 \mu\text{m}$  using a cellulose acetate (CA) filter. The hydrochemistry of the synthetic water was measured prior to each experiment by ionic chromatography (ICS-5000, Dionex/Thermo Fischer, US EPA 300.0) and TOC analyzer (TOC-V-CPH Shimadzu, NF EN 1484), and was in average ( $n = 4; \pm \text{SD}$ ) in  $\text{mg L}^{-1}$ :  $\text{Na}^+ 8.2 \pm 0.9$ ,  $\text{K}^+ 0.05 \pm 0.01$ ,  $\text{Mg}^{2+} 2.7 \pm 0.3$ ,  $\text{Ca}^{2+} 10 \pm 2$ ,  $\text{Cl}^- 9.7 \pm 0.5$ ,  $\text{NO}_3^- 21 \pm 1.5$ ,  $\text{SO}_4^{2-} 10.7 \pm 0.6$ , DOC  $0.8 \pm 0.3$  and DIC  $4.5 \pm 0.1$ .

**Sediment properties**

Table C1. Sediment properties.

	river sediment	sand	blend
$\Theta$ (w/w) <sup>a</sup>	0.33 ± 0.02		0.16 ± 0.02
$\rho_{\text{bulk}}$ (g cm <sup>-3</sup> ) <sup>a</sup>			2.29 ± 0.05
$K_s$ (m s <sup>-1</sup> ) <sup>a</sup>			(4.4 ± 2.2) × 10 <sup>-4</sup>
clay (< 2µm; %)	14.53	0	0.7 <sup>b</sup>
silt (2 - 50 µm; %)	62.06	0	3.1 <sup>b</sup>
sand (50 - 2000 µm; %)	23.41	100	96.2 <sup>b</sup>
$d_{10}$ (µm)	0.93	352	
$d_{50}$ (µm)	22.5	527	
$d_{90}$ (µm)	198	771	
$f_{oc}$ (%)	1.9	0.0	0.095 <sup>b</sup>
OM (%)		0.06	0.15
SiO <sub>2</sub> (%) <sup>c</sup>		98.7	98.4
Al <sub>2</sub> O <sub>3</sub> (%) <sup>c</sup>		0.38	0.58
MgO (%) <sup>c</sup>		0.04	0.03
CaO (%) <sup>c</sup>		0.26	0.16
Fe <sub>2</sub> O <sub>3</sub> (%) <sup>c</sup>		<0.03	0.09
MnO (%) <sup>c</sup>		<0.0002	0.0036
TiO <sub>2</sub> (%) <sup>c</sup>		0.015	0.028
Na <sub>2</sub> O (%) <sup>c</sup>		<0.07	<0.07
K <sub>2</sub> O (%) <sup>c</sup>		<0.1	<0.1
P <sub>2</sub> O <sub>5</sub> (%) <sup>c</sup>		<0.004	<0.004

Sand and blend refer to Kaltenhouse sand (K30, Quartz d'Alsace S.A, France) and a blend containing 95% K30 and 5% of sediment collected in the Avenheimerbach river (France, 48°40'08"N, 7°33'50"E).  $\Theta$ ,  $\rho_{\text{bulk}}$ ,  $K_s$ ,  $f_{oc}$ , OM refer to porosity, bulk density, saturated conductivity, fraction of organic carbon and organic matter respectively.  $d_{10}$ , 50 and 90 are 10,50, 90% of the portion of particles with smaller diameters than this value. <sup>a</sup> Uncertainty is reported as the 75% percentile from 20 measurements, <sup>b</sup> calculated values from the sediment measurements are based on the blending with sand, <sup>c</sup> elementary analysis with ICP-OES is reported for the most abundant oxide form.

### Caffeine biodegradation pathway

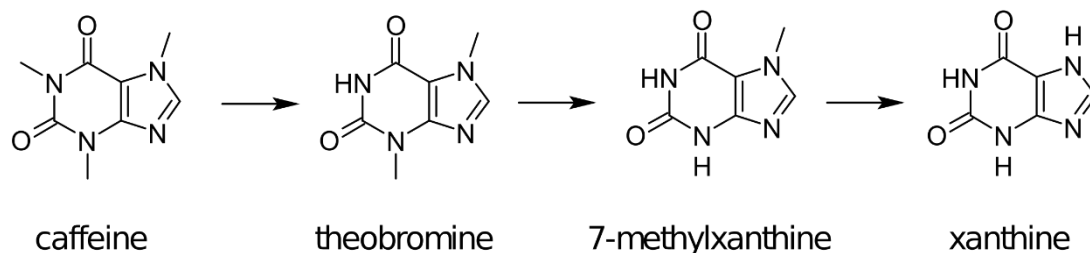


Figure C1. Oxic biodegradation pathway of caffeine.<sup>46</sup>

### Relationship between the nephelometric turbidity units (NTU) and the total suspended solid (TSS)

500 g of the river sediment were mixed with 1 L of tape water and settled for 30 min. Several aliquots from the upper part were collected and diluted in up to 0.1 to 5 L of tape water to generate a series of measurable turbidity samples from 1 to 300 NTU, measured with a turbidity meter (HI 88713, HANNA). Then, the sample was filtered through a glass filter (GF/5, 0.4  $\mu\text{m}$  average pore size, Macherey–Nagel), the filter was dried until constant mass at 105°C and weight. Residues on the filter were considered as part of the initial total suspended solid in the sample.

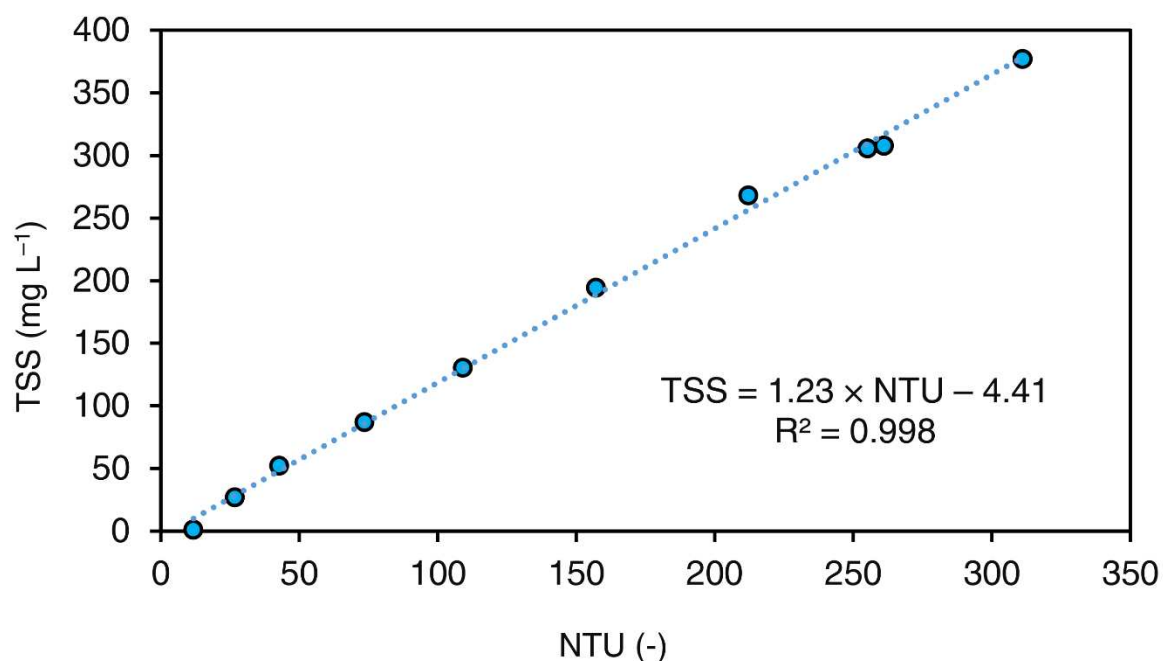


Figure C2. Relationship between the nephelometric turbidity units (NTU) record with a turbidity meter (HI 88713, HANNA) and the total suspended solids (TSS) measured by weighting.

### Rayleigh plots

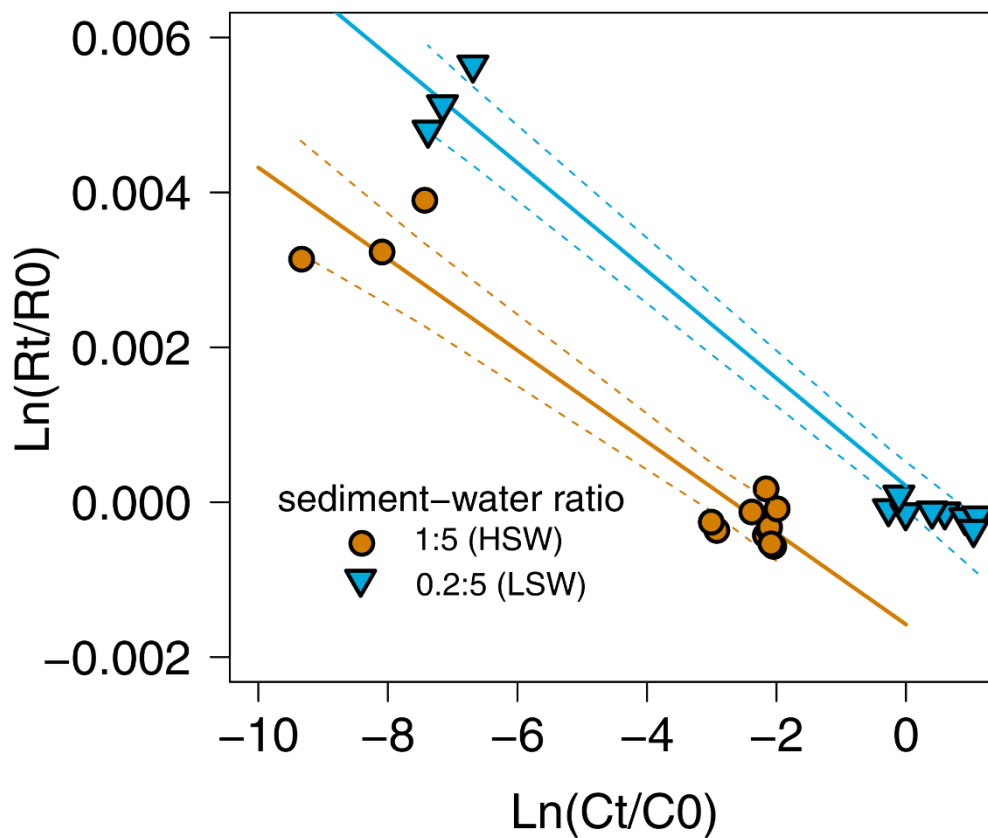


Figure C3. Logarithmic Rayleigh plot for the caffeine batch biodegradation experiment. Solid and dash lines express the linear fit and the 95% confidence interval of the Rayleigh equation.

### Prediction of carbonate dissolution using the conductivity

Relationship between measured conductivity and predicted conductivity ( $\kappa$ ) could be dressed with the cation-anion measurement (Figure C3):

$$\kappa = \sum_{i=1}^n (C_i \times \Lambda_i) \quad (C1)$$

where the  $C_i$  was the molar concentration ( $\text{mol L}^{-1}$ ) of each cation-anion and  $\Lambda_i$  the respective molar conductivity ( $\text{mS m}^2 \text{mol}^{-1}$ ). Cation-anion measurement during the experiment shows no difference except for carbonate. As a consequence, conductivity could be used as a proxy of aqueous carbonate concentration change over time ( $\Delta C_{\text{CaCO}_3}(t)$ ):

$$\Delta C_{\text{CaCO}_3}(t) = \Delta \kappa(t) \quad (C2)$$

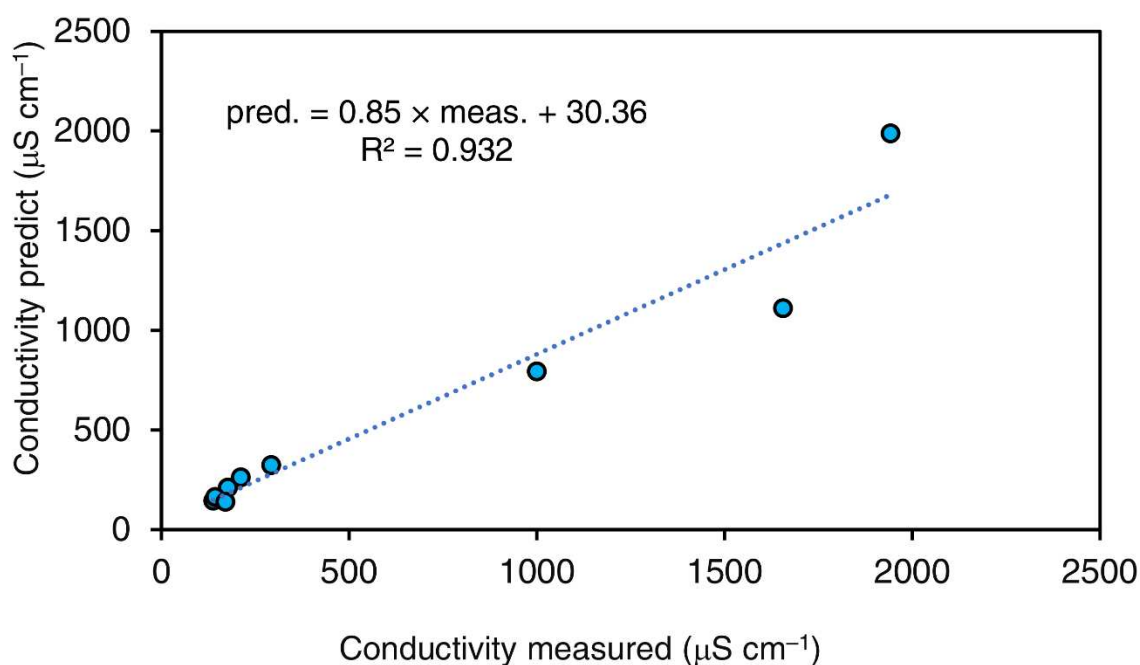


Figure C4. Relationship between the measured and the predicted conductivity from the sum of the cation–anion molar content, multiplied by the molar conductivity.



**Flow reactive transport model parameters***Table C2. Flow reactive transport model parameters.*

Hydraulic parameters - flow and transport		ref.
mesh (nb triangle / max size (mm))	5606 /4	
$\alpha_L$ (m)	0.01	Drouin et al.
$\alpha_T$ (m)	$\alpha_L \times 0.1$	
$\Theta$ (w/w) <sup>a</sup>	$0.16 \pm 0.02$	in this study
$K_s$ (m s <sup>-1</sup> ) <sup>a</sup>	$(4.4 \pm 2.2) \times 10^{-4}$	
Reactive parameters - caffeine and oxygen		
$k_{O_2}$ (s <sup>-1</sup> )	$(2.0 \pm 1.4) \times 10^{-2}$	in this study
$k_d$ (s <sup>-1</sup> )	$8.3 \times 10^{-5}$	Price
$D_{caf}$ (m <sup>2</sup> s <sup>-1</sup> )	$8 \times 10^{-10}$	
$K_M$ ( $\mu\text{mol L}^{-1}$ )	1	Soetaert et al.

<sup>a</sup> uncertainty are reported as the 75% percentile from 20 measurements. Ref. Drouin<sup>47</sup>, Price<sup>48</sup>, Soetaert et al.<sup>49</sup>

## Appendix D

### Supporting information to chapter 6

#### Supporting material and methods

##### Likelihood of crop rotation and S-metolachlor application dose

Agricultural fields that could potentially receive S-metolachlor applications were identified by cross-referencing information on types of crops that typically receive S-metolachlor applications (<https://ephy.anses.fr>, Table D1) and fields identified in the national farming survey (Registre Parcelaire Graphique - RPG, [www.ign.fr](http://www.ign.fr)) from 2015 to 2018. A typical three-year crop rotation was observed. The stability of this three-year crop rotation was compared in terms of corn and sugar beet percentages for two successive periods: from 2015 to 2017 and from 2016 to 2018. The likelihood of observing a change in parcel usage from corn or sugar beet only differed by 1% between these 2 periods and concerned only 32% of the farming area. Additionally, an insignificant (<0.1%) overall change in land use, i.e., farmland versus urban surface, was observed for each sub-catchment from 2015 to 2018. For each agricultural field, three scenarios were considered: the maximum legal dose of S-metolachlor containing product, hereafter called maximal; a scenario following local farming recommendations (<https://alsace.chambre-agriculture.fr/>), hereafter called economic (Table D1); and a scenario based on farmer surveys, hereafter called realistic. S-metolachlor application quantities were calculated for each field from Table D1 and applied over the three-year rotation farming practice.

Table D1. Main crops type and S-metolachlor application at the Souffel catchment.

field type	proportion of crop type (%) <sup>a</sup>	S-metolachlor application (g ha <sup>-1</sup> yr <sup>-1</sup> )		
		maximal <sup>b</sup>	economic <sup>c</sup>	realistic min-max <sup>d</sup>
sugar Beet	12.0 ± 0.5	576	384	576 - 672
corn	51.2 ± 1.7	1920	1280	160 - 1000
wheat	20.4 ± 1.9			
others cereals	1.3 ± 0.2			no application
meadow	5.9 ± 0.2			
vegetable (zucchini, pumpkin, squash, beans)	0.2	1500		not in survey
soja / sorgho / sunflower	0.2	1344		
divers (tabac, hops,...)	8.7			no application

<sup>a</sup> Calculated from the Registre Parcelaire Graphique ([www.ign.fr](http://www.ign.fr)) from 2015 to 2018 ( $\bar{X} \pm SD$ ). S-metolachlor applications are reported and then applied based on field type (<https://ephy.anses.fr/>); <sup>b</sup> follow regulatory limits, <sup>c</sup> based on local farming recommendations (<https://alsace.chambre-agriculture.fr/>) and <sup>d</sup> based on sampling results from s the G11 sub-catchment.

Table D2. Analytic methods description.

characterization	methods in brief	reference
water		
pH/conductivity/temperature	Electrode measurement (pH/cond multi 350i, WTW).	
water velocity	Handheld electromagnetic water flow meter (Nautilus C2000 / Sensa Z300, OTT).	
total suspended solid (TSS)	Sample filtered with a bottle-top vacuum filtration unit through a glass filter (GF/5, 0.4 µm average pore size, Macherey-Nagel) and dried at room temperature in a dessicator.	modified NF872
bulk density	Weigh a soil field sample that as a cylindrical known volume (48 cm <sup>3</sup> , core method).	ISO 11272
dissolved organic carbon (DOC) / dissolved inorganic carbon (DIC)	Sample is passed through a 0.25 µm cellulose acetate filter, then dissolved organic carbon is oxidized into CO <sub>2</sub> and detected by infrared spectrometry (TOC-V CPH, Shimadzu).	NF EN 1484
iron (Fe <sup>2+</sup> , Fe <sup>3+</sup> )	Presence/absence of iron is measured by semi-quantitative strip (P/N 1.16982.0001, Reflectoquant®, Merck) with reflectometer (P/N 1.16970.0001, Merck). If presence, UV-vis spectrophotometric measurement is made at 511 nm after reaction with 1,10-phenanthroline to form a red complex (P/N 1.00796.0001, Spectroquant®, Merck).	DIN 38406-1
cations/anions ( Na <sup>+</sup> , K <sup>+</sup> , Mg <sup>2+</sup> , Ca <sup>2+</sup> , NH <sub>4</sub> <sup>+</sup> , Cl <sup>-</sup> , NO <sub>3</sub> <sup>-</sup> , SO <sub>4</sub> <sup>2-</sup> , PO <sub>4</sub> <sup>3-</sup> )	Ion chromatography analysis (ICS-5000, Dionex/Thermo Fischer). Bromide can be measured if there is a low sulfate content.	US EPA 300.7/300.0
nitrite (NO <sub>2</sub> <sup>-</sup> )	Presence/absence of nitrite is measured by semi-quantitative strip (P/N 1.16973.0001, Reflectoquant®, Merck) with reflectometer (P/N 1.16970.0001, Merck). If present, UV-vis spectrophotometric measurement is made at 536 nm after Reaction with <i>N</i> -(1-naphthyl)ethylenediamine dihydrochloride to form a red-violet azo complexe (P/N 1.14776.0002, Spectroquant®, Merck).	DIN 26777
minor element (Mn, Cu, Si, Al, Fe, Zn, Ti, P)	Sample filtered through 0.25 µm, digest 1 mL sample by HNO <sub>3</sub> (50 mL, 69%) and oxalic acid (50 mL, 1 M), aqueous phase measure by inductively coupled plasma-optical emission spectrometry (ICP-OES, ICAP6500, Thermo Fisher).	In house method
sediment		
residual humidity (RH) content	Sample dried until constant mass at 105°C.	ISO 11465
pH <sub>H2O</sub> / pH <sub>CaCl2</sub>	Electrode measurement of 1:5 w/w sediment:water or 0.01 M CaCl <sub>2</sub> .	ISO 10390
organic carbon (f <sub>OC</sub> ) / inorganic carbon (C <sub>inorg</sub> )	Total combustion by elementary analyzer (CHN, FLASH 2000 NC, Thermo Fisher). Prior to organic carbon measurement, sample was decarbonated by HCl fumigation C <sub>inorg</sub> = total C - f <sub>OC</sub> .	ISO 10694, A
particule size fraction (0.1 µm to 2 mm)	Sample was pre-treated with a proportion 1:3 (v/v) of H <sub>2</sub> O <sub>2</sub> at 60 °C to degrade organic matter, KCl 1:50 (v/v) or HCl 1:20 (v/v) was added if the sample contained carbonate or no carbonate respectively to extract flocculent cations and 1:1 (v/v) solution of Natrium hexametaphosphate 0.55% was added to disperse the particles. Measurement performed by laser granulometer in aqueous mode (LS230, Beckmann Coulter).	ISO 13320
elementary analysis (Na, K, Mg, Ca, Ti, Mn, Fe, Al, Si)	Sample prepare by fusion alkaline with lithium tetraborate and analysed by inductively coupled plasma-optical emission spectrometry (ICP-OES, ICAP6500, Thermo Fisher).	NF ISO 14869-2

Ref. A<sup>22</sup>

**Pesticide mass balance**

Table D3. Attempted mass balance at the catchment scale: agricultural field and river.

	unit	mean $\pm$ standard deviation (min-max)	
area	km <sup>2</sup>	120	
application area <sup>a</sup>	km <sup>2</sup>	64.5 $\pm$ 2.2	
<i>S</i> -metolachlor application and stock in the soil			
stock in the soil (top 10 cm) before applications <sup>b</sup>	kg	7.49 $\pm$ 0.26	
maximal scenario (likelihood)	kg	9224 $\pm$ 217	
economic scenario (likelihood)	kg	6159 $\pm$ 146	
realistic scenario (survey)	kg	4909 $\pm$ 116	
stock in the soil (top 10 cm) after 214 days <sup>b</sup>	kg	38.2 $\pm$ 1.3	
hydrology <sup>c</sup>			
outflow discharge (0–214 days)	m <sup>3</sup> day <sup>-1</sup>	8800 $\pm$ 9050	(1400-72,270)
erosion <sup>c</sup>			
TSS export (0–214 Days)	t	720	
<i>S</i> -metolachlor export in runoff/discharge <sup>c</sup>			
dissolved export (0–214 days)	kg	4.87 $\pm$ 1.00	
particulate export (0–214 days)	kg	n.o.	
total export (dissolve and particulate) (0-214 days) <sup>d</sup>	%	(0.04 - 0.12)	
wwtp <i>S</i> -metolachlor load <sup>e</sup>			
	%	49 $\pm$ 6	
	kg	2.4 $\pm$ 0.8	
dissipation process in the river stretch			
sorption in sediment bed		n.o.	
hydrolysis (0–214 days)		n.o.	
hyporheic exchange		n.m.	
photolysis (0–214 days)	%	10.4 $\pm$ 2.9	
	g	506 $\pm$ 23	
river biodegradation (0–214 days)	%	2.7 $\pm$ 2.3	
	g	131 $\pm$ 20	
dissipation process in the agricultural field			
volatilization (0-36h after application)	%	(2.2 - 5.5)	
field biodegradation (0-214 days)	%	98.9 $\pm$ 4.7	
	kg	(4740 - 9337)	
remaining mass unaccounted for <sup>d</sup>			
	kg	(91 - 142)	
	%	1.50 - 1.90	

<sup>a</sup> calculated on the basis of Table D1. <sup>b</sup> extrapolated from the topsoil data in the vicinity of G10 and G11 ( $n = 2$ ). <sup>c</sup> data from the outlet of the catchment ( $n = 67$ ), <sup>d</sup> range covered by the three scenarios. <sup>e</sup> estimated from grab sampling ( $n = 7 \times 3$  locations). n.o. not occurring, n.m. not measurable.

## Hydrochemistry

Table D4. Water composition during grab sampling at each location ( $\bar{X} \pm SD$ ; n = 7 per location).

loc.	pH (-)	cond. (mS cm <sup>-1</sup> )	T (°C)	TSS (mg L <sup>-1</sup> )	DOC (mg L <sup>-1</sup> )	NH <sub>4</sub> <sup>+</sup> (mg L <sup>-1</sup> )	Na <sup>+</sup> (mg L <sup>-1</sup> )	K <sup>+</sup> (mg L <sup>-1</sup> )	Mg <sup>2+</sup> (mg L <sup>-1</sup> )	Ca <sup>2+</sup> (mg L <sup>-1</sup> )	Cl <sup>-</sup> (mg L <sup>-1</sup> )	NO <sub>3</sub> <sup>-</sup> (mg L <sup>-1</sup> )	SO <sub>4</sub> <sup>2-</sup> (mg L <sup>-1</sup> )	HCO <sub>3</sub> <sup>-</sup> (mg L <sup>-1</sup> )	CO <sub>3</sub> <sup>2-</sup> (mg L <sup>-1</sup> )
G1	9.0 ± 0.7	0.931 ± 0.023	14.2 ± 2.2	105 ± 102	1.54 ± 0.48	0 ± 0	6.8 ± 0.4	2.4 ± 0.3	56 ± 2	130 ± 14	26 ± 2	56 ± 2	169 ± 18	301 ± 114	53 ± 45
G2	8.5 ± 1.1	1.190 ± 0.122	16.4 ± 3.2	82 ± 112	1.87 ± 0.54	0.082 ± 0.162	10.5 ± 1.4	4.9 ± 0.6	41 ± 5	185 ± 24	31 ± 4	41 ± 5	364 ± 58	326 ± 103	41 ± 62
G3	8.9 ± 0.8	1.057 ± 0.301	16.5 ± 3.1	181 ± 197	3.58 ± 1.92	0.337 ± 0.769	25.6 ± 34.5	8.0 ± 7.3	34 ± 16	143 ± 53	51 ± 30	34 ± 16	231 ± 116	320 ± 92	71 ± 90
G4	8.1 ± 0.5	1.165 ± 0.104	13.3 ± 3.9	580 ± 708	5.83 ± 5.26	10.35 ± 7.372	29.1 ± 9.9	8.7 ± 2.0	26 ± 7	158 ± 9	53 ± 6	26 ± 7	234 ± 47	382 ± 117	57 ± 122
G5	8.2 ± 0.5	0.900 ± 0.162	14.1 ± 3.4	136 ± 93	4.91 ± 1.14	0.379 ± 0.487	54.2 ± 22.9	12.3 ± 4.5	37 ± 13	111 ± 29	89 ± 33	37 ± 13	75 ± 11	383 ± 109	11 ± 14
G6	7.8 ± 0.4	1.061 ± 0.157	13.0 ± 3.9	784 ± 976	6.97 ± 6.62	7.768 ± 5.572	43.9 ± 16.8	11.8 ± 3.8	24 ± 9	132 ± 16	71 ± 20	24 ± 9	181 ± 29	397 ± 85	4 ± 5
G7	8.3 ± 0.5	0.837 ± 0.339	14.7 ± 2.8	108 ± 167	2.87 ± 0.53	0.673 ± 1.261	20.0 ± 4.9	4.1 ± 1.5	52 ± 11	140 ± 18	61 ± 7	52 ± 11	81 ± 9	443 ± 72	19 ± 27
G8	8.5 ± 0.3	0.831 ± 0.044	15.0 ± 3.9	149 ± 222	3.62 ± 0.55	0.531 ± 0.978	27.0 ± 3.4	8.1 ± 3.3	31 ± 4	114 ± 18	66 ± 8	31 ± 4	77 ± 10	371 ± 65	16 ± 10
G9	8.4 ± 0.4	1.076 ± 0.066	14.2 ± 3.6	57 ± 51	5.25 ± 4.96	0.194 ± 0.339	36.1 ± 40.2	8.2 ± 5.2	35 ± 15	158 ± 46	78 ± 52	35 ± 15	179 ± 66	396 ± 93	14 ± 19
G10	8.8 ± 0.8	1.056 ± 0.141	15.4 ± 0.9	20 ± 15	2.23 ± 0.93	0.866 ± 2.049	12.1 ± 1.1	4.6 ± 1.5	70 ± 14	158 ± 27	33 ± 4	70 ± 14	187 ± 40	345 ± 116	62 ± 67
G11	8.9 ± 0.8	0.943 ± 0.261	15.0 ± 1.5	273 ± 551	3.84 ± 2.12	0.228 ± 0.503	10.8 ± 2.6	3.8 ± 0.8	65 ± 17	143 ± 45	37 ± 12	65 ± 17	147 ± 56	305 ± 113	65 ± 70
W1	7.4 ± 0.4	0.937 ± 0.208	16.8 ± 4.1	11 ± 6	8.32 ± 5.92	0.6 ± 0.793	96.8 ± 25.8	19.3 ± 4.5	13 ± 12	58 ± 14	134 ± 36	13 ± 12	65 ± 15	267 ± 81	3 ± 7
W2	7.7 ± 0.6	0.923 ± 0.197	17.1 ± 4.6	81 ± 140	8.10 ± 2.99	8.863 ± 20.74	84.9 ± 21.7	22.6 ± 6.1	22 ± 21	69 ± 14	104 ± 24	22 ± 21	72 ± 12	311 ± 85	43 ± 109
W3	8.3 ± 1.2	1.169 ± 0.201	17.1 ± 4.4	184 ± 263	6.36 ± 3.51	26.23 ± 20.13	58.6 ± 36.1	13.6 ± 6.2	14 ± 21	108 ± 65	76 ± 28	14 ± 21	150 ± 136	429 ± 157	24 ± 35
A	7.4 ± 0.3	0.967 ± 0.175	14.5 ± 2.2	488 ± 473	5.19 ± 1.84	4.365 ± 2.535	47.8 ± 19.1	11.8 ± 3.6	25 ± 13	110 ± 23	75 ± 24	25 ± 13	131 ± 30	351 ± 99	1 ± 1

## Data availability

Raw data on hydrochemistry, S-metolachlor concentration and isotopic signature, for the grab and the continuous data. Flow and rainfall measurement data are temporarily available prior to publication with meta data at <https://seafiler.unistra.fr/f/6bba477035584a96881c/?dl=1>

### Wetness index

Topographical wetness index (TWI) was used to identify contributing areas prone to generate overland flow.<sup>30</sup> The European Digital Elevation Model (EU-DEM, v1.1, <https://land.copernicus.eu>) at 25 m resolution for the year 2011 was used to calculate TWI using SAGA-GIS 2.3.2+ through RSAGA package v1.3.0.

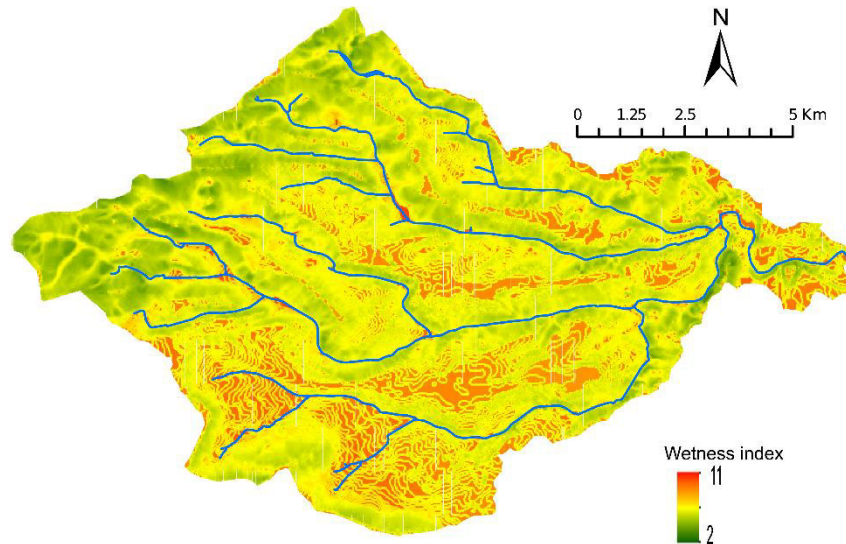


Figure D1. Topographical wetness index (TWI) of the Souffel catchment.

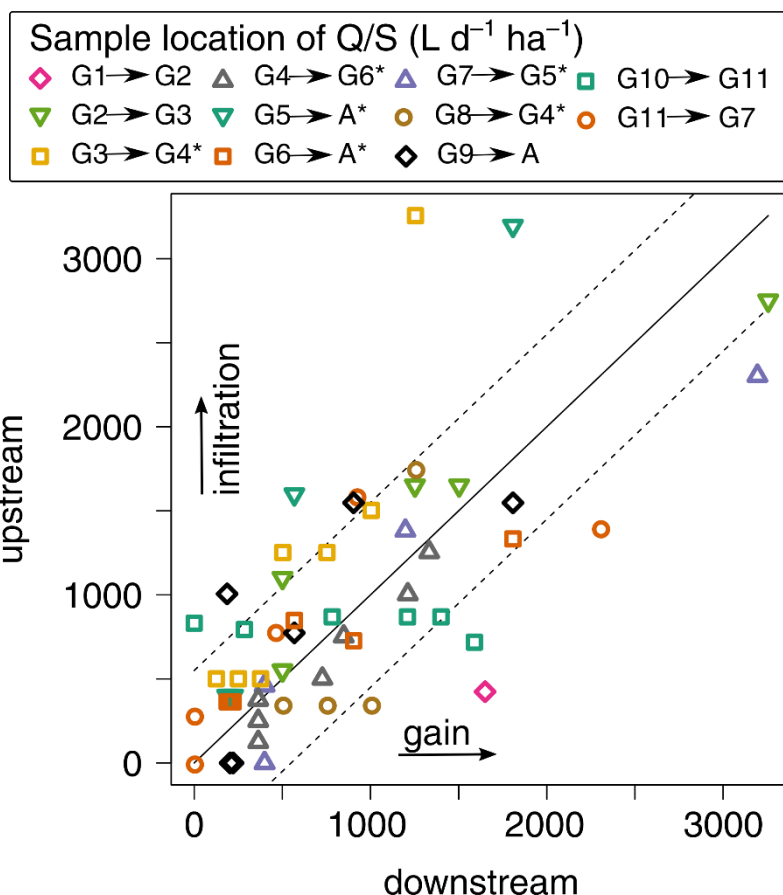


Figure D2. Upstream and downstream normalized flow,<sup>50</sup> i.e., discharge divide by surface of the corresponding sub-catchment, for all grab sampling events. Solid line indicates a 1:1 relationship and dashed line the 95% confidence interval considering a measured flow with 30% uncertainty. Asterisks (\*) highlight reaches with WWTP contribution.

### Concentration change of S-metolachlor within topsoil

During the 2019 campaign, S-metolachlor concentrations in topsoil were measured but the associated  $\delta^{13}C$  values could not be measured due to matrix effects. Therefore,  $\delta^{13}C$  was modeled from measured S-metolachlor concentrations in topsoils as measured and validated in a similar agricultural headwater catchment.<sup>51</sup>

Briefly, S-metolachlor biodegradation in topsoils is calculated from a corrected first-order constant ( $k_{dyn}$ ) accounting for the observed topsoil temperature ( $T_{obs}$ ) and moisture ( $\theta_{obs}$ ), as follows:<sup>52</sup>

$$k_{dyn} = k_{Ref} \times f_T \times f_\theta \quad (D1)$$

where  $f_T$  and  $f_\theta$  are the factors that account for the influence of the topsoil temperature and moisture (w/w). The factors for the influence of topsoil temperature follow the Arrhenius laws as follows:<sup>53</sup>

$$f_T = \begin{cases} 0 & \text{if, } T_{\text{obs}} \leq T_{\text{ref}} \\ \frac{T_{\text{obs}} - T_{\text{ref}}}{5} \times e^{\frac{E_a}{R} \times \left( \frac{1}{T_{\text{ref}}} - \frac{1}{T_{\text{obs}}} \right)} & \text{if, } T_{\text{ref}} < T_{\text{obs}} \leq (T_{\text{ref}} + 5) \\ e^{\frac{E_a}{R} \times \left( \frac{1}{T_{\text{ref}}} - \frac{1}{T_{\text{obs}}} \right)} & \text{if, } T_{\text{obs}} > (T_{\text{ref}} + 5) \end{cases} \quad (\text{D2})$$

where  $T_{\text{ref}}$  is the reference temperature (293.15 K) in Kelvin,  $E_a$  is the *S*-metolachlor activation energy ( $2.391 \times 10^3 \text{ J mol}^{-1}$ ) and  $R$  is the gas constant ( $8.314 \text{ J mol}^{-1} \text{ K}^{-1}$ ).<sup>54</sup>

The relation to soil moisture follows:<sup>53</sup>

$$f_\theta = \left( \frac{\theta_{\text{obs}}}{\theta_{\text{ref}}} \right)^{\beta_\theta} \quad (\text{D3})$$

where  $\beta_\theta$  is a calibration constant and  $\theta_{\text{ref}}$  the reference water content, which was set at 0.5 and 0.2, respectively.  $\theta_{\text{obs}}$  and  $T_{\text{obs}}$  for the growing season were obtained for the 0-20 cm topsoil at a 8 km spatial resolution for the year 2019 by the national weather service (<https://publitheque.meteo.fr>) computed by a daily soil water budget model.<sup>55</sup>

Initial *S*-metolachlor concentrations in topsoils were estimated from application rates reported in the farmer surveys. *S*-metolachlor doses were assumed to be present within the top 10 cm of topsoil.<sup>56</sup> Bulk soil density was set at  $1.29 \text{ kg dm}^{-3}$  according to the soilgrid data for the agricultural area within the catchment.<sup>57</sup>

Isotope fractionation was predicted from the *S*-metolachlor biodegradation in topsoils (Table D3) using the Rayleigh equation, considering  $\epsilon_c = -1.4 \pm 0.4\%$  and the  $\delta^{13}\text{C}_0$  as the signature from the commercial product (Table D5).<sup>30</sup>



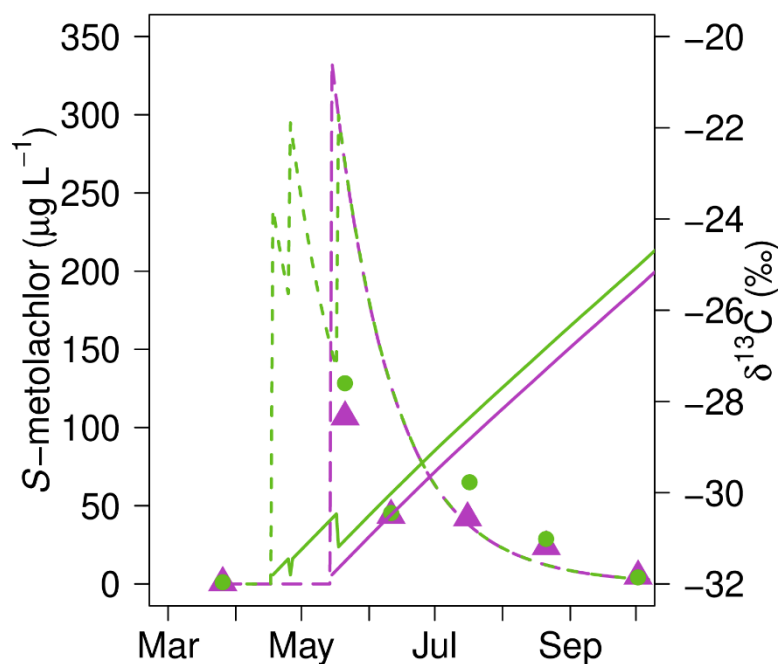


Figure D3. Comparison of measured and predicted *S*-metolachlor topsoil concentrations around G10 (purple) and G11 (green). Points stand for the measured and dashed lines for the predicted concentrations. Solid lines correspond to the predicted isotope fractionation.

Table D5. Isotope signature ( $\delta^{13}\text{C}$ ) of commercial products containing *S*-metolachlor.

commercial name	$\delta^{13}\text{C}$ (‰)	<i>n</i>
Dual Gold <sup>a</sup>	$-31.9 \pm 0.2$	4
Camix <sup>a</sup>	$-31.7 \pm 0.2$	4
Mercantor Gold <sup>a</sup>	$-31.3 \pm 0.2$	4
Mercantor Gold <sup>b</sup>	$-32.2 \pm 0.5$	3
<i>S</i> -Metolastar <sup>a</sup>	$-32.1 \pm 0.2$	5
<b>average</b>	<b><math>-31.8 \pm 0.3</math></b>	

Uncertainties correspond to the SD from *n* measurements. Measured in <sup>a</sup> this study and <sup>b</sup> Alvarez-Zaldivar et al.<sup>30</sup>

### Estimation of the volatilization after application

Percent volatilization after application was estimated based on the semi-empirical physical based model developed from Hippelein and McLachlan<sup>58</sup> and generalized over 224 molecules including *S*-metolachlor by Davie-Martin, et al.<sup>59</sup> Briefly, the authors had developed a multiphase partitioning approach based on soil–air ( $K_{\text{soil-air}}$ ) and water–air ( $K_{\text{water-air}}$ )

partition coefficients for the topsoil. Air temperature and moisture combined with topsoil relative moisture and organic carbon content are the principal parameters accounting for variation of the rate of the volatilization in the model, which was consistent with observations made in agricultural fields.<sup>60, 61</sup> The volatilization was only considered to take place for 36 h following application as observed in the field.<sup>60, 61</sup> Table D6 summarizes the parameter values used in the model to calculate the volatilization after each reported application. The predicted contribution of volatilization accounts for 2.2 to 5.5% mass loss of applied *S*-metolachlor within 36 h after the application.

Table D6. Local parameters used for the volatilization estimation.

parameter	values	reference
temperature (min-max)	5.7-20.9°C	www.meteo-offenheim.fr
relative humidity (annual average)	77%	www.meteo-offenheim.fr
bulk density	1.29 kg L <sup>-1</sup>	Soilgrid - A
soil organic carbon	0-50%	Soilgrid - A
soil depth <sup>a</sup>	50 cm	B
soil moisture	min-max 0-100% average: 28%	http://land.copernicus.eu - C

<sup>a</sup> topsoil depth average where >80% of the *S*-metolachlor total amount in topsoil was found within 1-2 weeks following application. Ref. A<sup>57</sup>, B<sup>62-64</sup>, C<sup>65</sup>

## Estimation of photodegradation at the Souffel river

Photodegradation extent was estimated as following<sup>3, 66</sup>. Briefly,

1. Ratio of day-average surface solar intensities  $L(330\text{nm})$  measured during solar simulating photodegradation experiments (Chap. 3) and the Souffel River estimate from the Greifensee (Switzerland, 47°21'59"N 8°39'42"E).<sup>67</sup>

Solar simulator:  $L_{\text{sim}}(330\text{nm}) = 6.05 \times 10^{-2} \text{ mE cm}^{-2} \text{ day}^{-1}$

Souffel river:  $L_{\text{river}}(330\text{nm}) = 4.34 \times 10^{-2} \text{ mE cm}^{-2} \text{ day}^{-1}$

2. Depth of the photic zone in the Souffel river

The photic zone is defined as follows:

$$A = \log(I_0/I) = 1.3 \quad (D4)$$

where  $A$  was the absorbance and  $I$  the intensity, respectively.

$$A_{330\text{nm}} = \alpha_{330} \times Z_{\text{photic}},$$

where  $\alpha_{330}$  was the beam attenuation coefficient ( $6 \text{ m}^{-1}$  for muddy river water) and  $Z_{\text{photic}}$  the depth of the photic zone.

$$S = \frac{(1 - e^{-\alpha_{330} \times Z_{\text{photic}}})}{\alpha_{330} \times Z_{\text{photic}}} \quad (D5)$$

where  $S$  was the screening factor to account for DOM sorption.

$$k_{\text{phot,river}} = \frac{k_{\text{phot,sim}}}{L_{\text{sim}}/L_{\text{river}}} \times S \quad (D6)$$

where  $k_{\text{phot,river}}$  and  $k_{\text{phot,sim}}$  were the photodegradation rate in the river and the photodegradation rate during the solar simulating photodegradation under nitrate conditions (Table A4).  $k_{\text{phot,sim}}$  under nitrate conditions ( $k_{\text{phot,sim}} = (1.3 \pm 0.1) \times 10^{-6} \text{ s}^{-1}$ ) could be considered to be the maximum photodegradation because no dissipation by dissolved organic matter was taken into account. Therefore, the photodegradation might be slightly overestimated.

## Appendix E

### Additional supporting information

In this section, we provide some additional characterization and observation not discussed on the main text. They were separate from the main text because they do not support the discussion made during the chapters. However, they might constitute some useful information for further study.

#### X-ray diffraction (XRD) spectra

X-ray diffraction (XRD) spectra from grinded sample (<100  $\mu\text{m}$ ) were collected on a D8 Advance XRD (Bruker) equipped with a fixe copper anode (Cu  $K\alpha$  radiation) with a rotating sample holder in  $\theta/\theta$  mode with an incident X-ray energy of 40 kV and 25 mA. Scans were taken for  $2\theta$  ranges from  $3^\circ$  to  $65^\circ$  with  $0.01^\circ \text{ s}^{-1}$  steps. The XRD patterns were calibrated with high purity corundum platelet ( $\text{Al}_2\text{O}_3$ , NIST 1976b). Semi-quantitative peak assignments were performed on DIFFRAC.EVA v4.3 (Brucker) using the powder diffraction file data based (PDF-2, 2004, International Center for Diffraction Data).

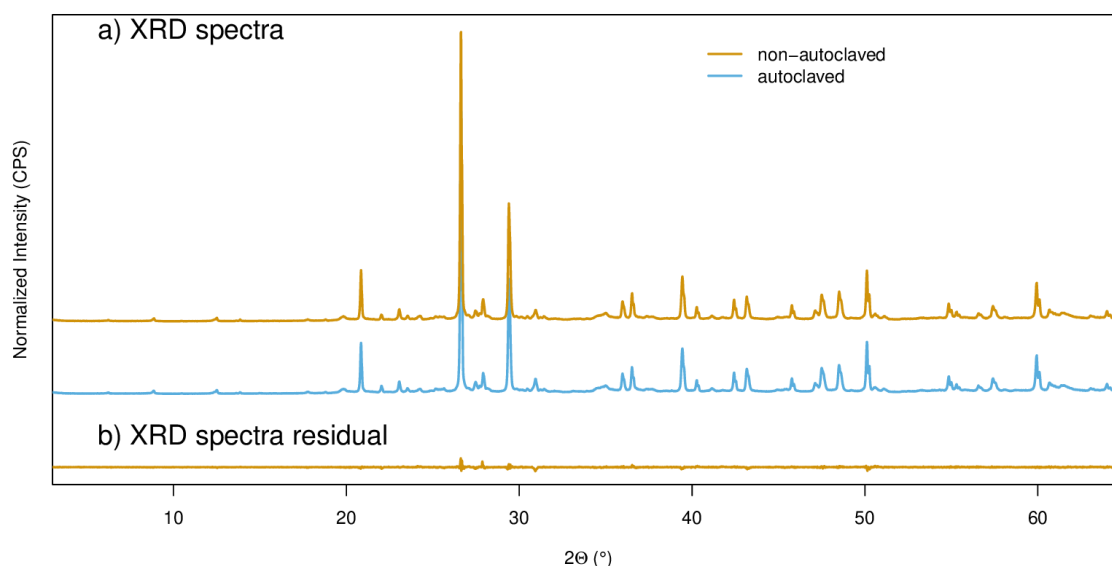


Figure E1. X-ray diffraction (XRD) of the wetland sediment a) spectrum and b) residual between non-autoclaved and autoclaved sediment spectrum. Overall differences of the measurement were inside the error of the measurement which are 0.07% in average and 3% in maximal. Intensities count were normalized by the intensity of the highest peak intensity to allow comparison.

Table E1. Mineralogy semi-quantitative pattern assignment.

pattern number	mineral	formula	prop. of pattern (%) <sup>a</sup>	
			non-autoclaved	autoclaved
PDF 46-1045	Quartz, syn	SiO <sub>2</sub>	33.1	34
PDF 05-0586	Calcite, syn	CaCO <sub>3</sub>	28.4	28
PDF 76-0929	Muscovite 2M#1	KAl <sub>2</sub> Si <sub>3</sub> AlO <sub>10</sub> (OH) <sub>2</sub>	11	10.8
PDF 70-3752	Albite	(Na <sub>0.98</sub> Ca <sub>0.02</sub> )(Al <sub>1.02</sub> Si <sub>2.98</sub> O <sub>8</sub> )	10.8	9.8
PDF 76-0824	Orthoclase	(K <sub>0.931</sub> Na <sub>0.055</sub> Ca <sub>0.009</sub> Ba <sub>0.005</sub> )(Al <sub>0.97</sub> Si <sub>3.03</sub> O <sub>8</sub> )	5.7	6.1
PDF 70-3754	Illite	K(Al <sub>4</sub> Si <sub>2</sub> O <sub>9</sub> (OH) <sub>3</sub> )	3.9	3.6
PDF 89-5862	Dolomite	CaMg(CO <sub>3</sub> ) <sub>2</sub>	2.3	2.7
PDF 12-0242	Clinocllore-1M#I#b	(Mg,Al) <sub>6</sub> (Si,Al) <sub>4</sub> O <sub>10</sub> (OH) <sub>8</sub>	2.1	2.4
PDF 07-0051	Montmorillonite	(Na,Ca) <sub>0.3</sub> (Al,Mg) <sub>2</sub> Si <sub>2</sub> O <sub>10</sub> (OH) <sub>2</sub> ·nH <sub>2</sub> O	1.1	1
PDF 74-1784	Kaolinite 1A	Al <sub>2</sub> Si <sub>2</sub> O <sub>5</sub> (OH) <sub>4</sub>	1.1	1.1
PDF 07-0027	Montmorillonite-chlorite	Na-Ca-Al-Si <sub>4</sub> O <sub>10</sub> -O	0.3	0.2
PDF 85-1432	Arfvedsonite	Na <sub>3</sub> (Fe,Mg) <sub>4</sub> FeSi <sub>8</sub> O <sub>22</sub> (F,OH) <sub>2</sub>	0.2	0.3

<sup>a</sup> estimate accuracy of 1%.

## Importance of dissolved organic carbon during autoclaving

Organic carbon content ( $f_{oc}$ ; Appendix B, Table B1) and texture did not differ between autoclaved and non-autoclaved sediments. However, under oxic conditions, DOC was massively released in the autoclaved experiment ( $\Delta\text{DOC}_{0 \rightarrow 300 \text{ days}} = 300 \text{ ppm}$ ) compared to non-autoclaved one ( $\Delta\text{DOC}_{0 \rightarrow 300 \text{ days}} = 10 \text{ ppm}$ ; Figure E2). A similar trend was observed under anoxic conditions, with  $\Delta\text{DOC}_{0 \rightarrow 300 \text{ days}} = 200 \text{ ppm}$  in the autoclaved experiment, and  $\Delta\text{DOC}_{0 \rightarrow 300 \text{ days}} = 19 \text{ ppm}$  in non-autoclaved experiment. The release of DOC under oxic condition due to autoclaving corresponded to 15% of the initial mass of organic carbon of the sediment. Assuming that sorption capacities was mainly drive by the organic content,<sup>35</sup> this reduces the  $K_d$  by a factor of 1.2 only. However, comparison between sorption capacity on autoclaved and non-autoclaved sediment (Appendix B, Table B4) indicated a  $K_d$  decrease by a factor of 1.8 to 2.9 for *S*-metolachlor and acetochlor, respectively. To conclude, autoclaving may not only change the DOC content but also the molecular structures of organic carbon, and thus its sorption properties. By consequence limiting the comparison between autoclaved and non-autoclaved degradation results.

SUVA may be a proxy of aromaticity in humic substances.<sup>68, 69</sup> Triplicate SUVA measurements after 300 days under oxic condition suggest less aromaticity and unsaturated polycondensated of humic substances in the autoclaved sample ( $\text{SUVA}_{254} = 0.42 \pm 1.18$  and  $\text{SUVA}_{280} = 0.09 \pm 0.00 \text{ L mg}^{-1} \text{ C m}^{-1}$ ) than in the non-autoclaved ( $\text{SUVA}_{254} = 6.34 \pm 0.00$  and  $\text{SUVA}_{280} = 11.97 \pm 1.63 \text{ L mg}^{-1} \text{ C m}^{-1}$ ; Appendix B, Table B2). This is agree with observations made by Berns, et al.<sup>70</sup> on the autoclaving effect in sediment organic carbon. Since no significant pesticide degradation was observed in the autoclaved control (Appendix B, Table B3), the autoclaved control may serve as abiotic control of degradation, although others

*Additional supporting information*

dissipation processes (e.g., sorption) may not be directly compared. In addition, the DOC released from the autoclaved sediment samples might create a too large background signals for an accurate isotopic ratio measurement by GC-IRMS, thereby hampering CSIA of pesticides from autoclaved experiments.

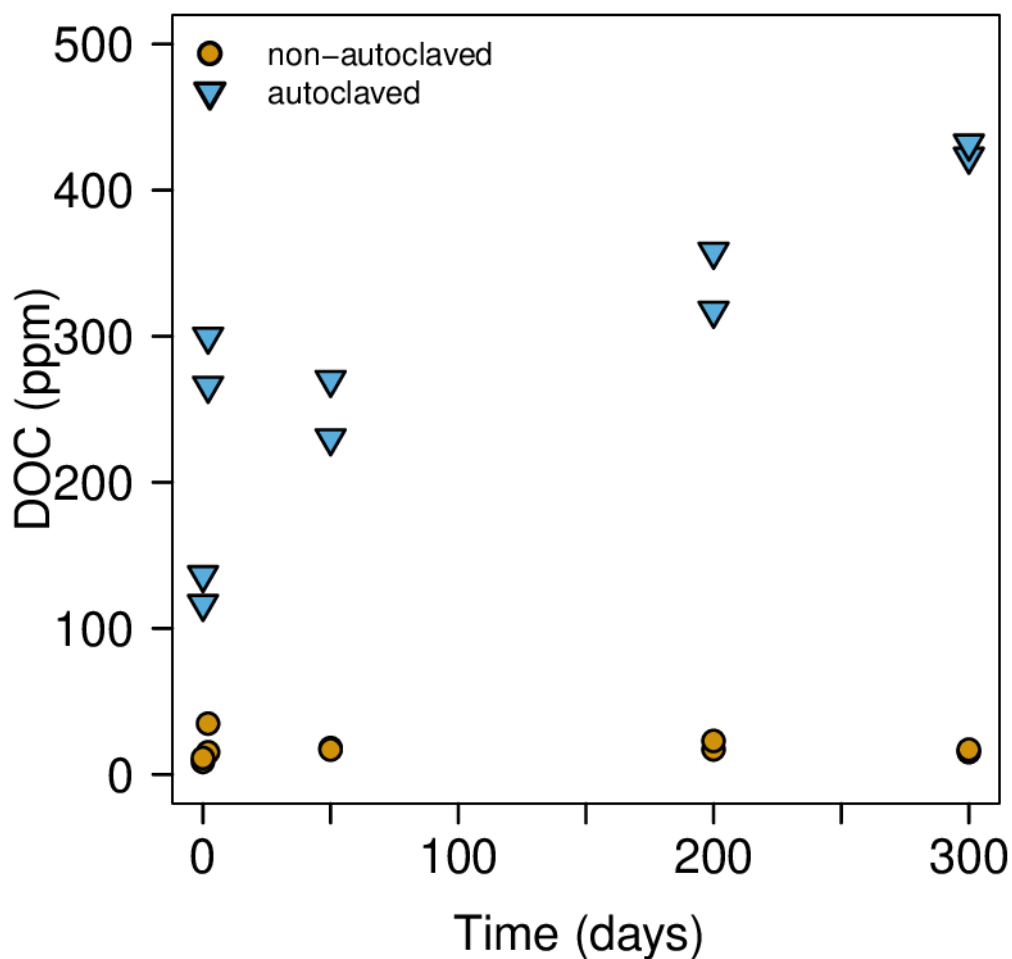


*Figure E2. Dissolved organic carbon (DOC) in non-autoclaved and autoclaved biodegradation experiments under oxic condition.*

## Isotopic bulk enrichment factor ( $\epsilon_{bulk,E}$ ) from previous studies

*Table E2. Isotopic bulk enrichment factor ( $\epsilon_{bulk,E}$ ) and apparent kinetic isotope effects for carbon, nitrogen and chlorine found in the literature.*

Experimental system	$\epsilon_{bulk,C}$ (‰)	$\epsilon_{bulk,N}$ (‰)	$\epsilon_{bulk,Cl}$ (‰)	AKIE <sub>C</sub>	AKIE <sub>N</sub>	Ref.
acetochlor - abiotic hydrolysis						
pH 12 (0.4 M 1:1 NaOH/KCl)	$-4.0 \pm 0.8$	n.s. <sup>a</sup>		$1.060 \pm 0.012$		A
biotic degradation						
lab-scale wetland column flow through experiment supply with ditch water	$-3.4 \pm 0.5$			$1.051 \pm 0.007$		B
<i>S</i> -metolachlor - abiotic hydrolysis						
pH 12 (0.4 M 1:1 NaOH/KCl)	$-2.8 \pm 0.6$	$-2.0 \pm 1.3$		$1.043 \pm 0.008$	$1.002 \pm 0.001$	A
pH 12 (0.05 M Na <sub>2</sub> HPO <sub>4</sub> with 0.1 M NaOH)	$-3.3 \pm 1.0$		$-9.7 \pm 2.9$	$1.052 \pm 0.001$		C
biotic degradation						
static oxic soil mesocosm with water content of 20% and 40%	$-1.5 \pm 0.5$			$1.023 \pm 0.001$		D
field data - open Raleigh system	$-1.4 \pm 0.4$			$1.0214 \pm 0.0004$		D
field data - best fit	$-1.1 \pm 0.5$			$1.017 \pm 0.001$		E

<sup>a</sup> n.s. not significant isotopic fractionation. <sup>c</sup> AKIE is calculated on eq. 4.3. Ref. A<sup>18</sup>, B<sup>71</sup>, C<sup>72</sup>, D<sup>30</sup>, E<sup>73</sup>

## Appendix F

### Supporting references

1. Laszakovits, J. R.; Berg, S. M.; Anderson, B. G.; O'Brien, J. E.; Wammer, K. H.; Sharpless, C. M., *p*-nitroanisole/pyridine and *p*-nitroacetophenone/pyridine actinometers revisited: Quantum yield in comparison to ferrioxalate. *Environ. Sci. Technol. Let.* **2017**, *4*, (1), 11–14.
2. Dulin, D.; Mill, T., Development and evaluation of sunlight actinometers. *Environ. Sci. Technol.* **1982**, *16*, (11), 815–820.
3. Schwarzenbach, R. P.; Gschwend, P. M.; Imboden, D. M., *Environmental organic chemistry*. third ed.; John Wiley & Sons: **2016**; p 1024.
4. Gaffney, J. S.; Marley, N. A.; Cunningham, M. M., Measurement of the absorption constants for nitrate in water between 270 and 335 nm. *Environ. Sci. Technol.* **1992**, *26*, (1), 207–209.
5. Zeng, T.; Arnold, W. A., Pesticide photolysis in prairie potholes: Probing photosensitized processes. *Environ. Sci. Technol.* **2013**, *47*, (13), 6735–6745.
6. Bodrato, M.; Vione, D., APEX (Aqueous Photochemistry of Environmentally occurring Xenobiotics): a free software tool to predict the kinetics of photochemical processes in surface waters. *Environ. Sci. Process. Impacts* **2014**, *16*, (4), 732–740.
7. Janssen, E. M. L.; Erickson, P. R.; McNeill, K., Dual roles of dissolved organic matter as sensitizer and quencher in the photooxidation of tryptophan. *Environ. Sci. Technol.* **2014**, *48*, (9), 4916–4924.
8. Vione, D.; Maurino, V.; Minero, C.; Carlotti, M. E.; Chiron, S.; Barbati, S., Modelling the occurrence and reactivity of the carbonate radical in surface freshwater. *Comptes Rendus Chimie* **2009**, *12*, (8), 865–871.
9. Remucal, C. K., The role of indirect photochemical degradation in the environmental fate of pesticides: A review. *Environ. Sci. Process. Impacts* **2014**, *16*, (4), 628–653.
10. Cory, R. M.; Cotner, J. B.; McNeill, K., Quantifying interactions between singlet oxygen and aquatic fulvic acids. *Environ. Sci. Technol.* **2009**, *43*, (3), 718–723.
11. Schmitt, M.; Erickson, P. R.; McNeill, K., Triplet-state dissolved organic matter quantum yields and lifetimes from direct observation of aromatic amine oxidation. *Environ. Sci. Technol.* **2017**, *51*, (22), 13151–13160.



## Supporting references

12. Westerhoff, P.; Mezyk, S. P.; Cooper, W. J.; Minakata, D., Electron pulse radiolysis determination of hydroxyl radical rate constants with Suwannee river fulvic acid and other dissolved organic matter isolates. *Environ. Sci. Technol.* **2007**, *41*, (13), 4640–4646.
13. Buxton, G. V.; Greenstock, C. L.; Helman, W. P.; Ross, A. B., Critical review of rate constants for reactions of hydrated electrons, hydrogen atoms and hydroxyl radicals ( $\cdot\text{OH}/\text{O}^-$ ) in Aqueous Solution. *J. Phys. Chem. Ref. Data* **1988**, *17*, (2), 513–886.
14. Appiani, E.; Ossola, R.; Latch, D. E.; Erickson, P. R.; McNeill, K., Aqueous singlet oxygen reaction kinetics of furfuryl alcohol: effect of temperature, pH, and salt content. *Environ. Sci. Process. Impacts* **2017**, *19*, (4), 507–516.
15. Cawley, K.; Korak, J.; Rosario-Ortiz, F., Quantum yields for the formation of reactive intermediates from dissolved organic matter samples from the Suwannee river. *Environ. Eng. Sci.* **2015**, *32*, 31–37.
16. Wenk, J.; von Gunten, U.; Canonica, S., Effect of dissolved organic matter on the transformation of contaminants induced by excited triplet states and the hydroxyl radical. *Environ. Sci. Technol.* **2011**, *45*, (4), 1334–1340.
17. Meyer, A. H.; Elsner, M.,  $^{13}\text{C}/^{12}\text{C}$  and  $^{15}\text{N}/^{14}\text{N}$  isotope analysis to characterize degradation of atrazine: Evidence from parent and daughter compound values. *Environ. Sci. Technol.* **2013**, *47*, (13), 6884–6891.
18. Masbou, J.; Drouin, G.; Payraudeau, S.; Imfeld, G., Carbon and nitrogen stable isotope fractionation during abiotic hydrolysis of pesticides. *Chemosphere* **2018**, *213*, 368–376.
19. Fenner, K.; Canonica, S.; Wackett, L. P.; Elsner, M., Evaluating pesticide degradation in the environment: Blind spots and emerging opportunities. *Science* **2013**, *341*, (6147), 752–758.
20. Smith, E. J.; Davison, W.; Hamilton-Taylor, J., Methods for preparing synthetic freshwaters. *Water Res.* **2002**, *36*, (5), 1286–1296.
21. Maillard, E.; Imfeld, G., Pesticide mass budget in a stormwater wetland. *Environ. Sci. Technol.* **2014**, *48*, (15), 8603–8611.
22. Ramnarine, R.; Voroney, R. P.; Wagner-Riddle, C.; Dunfield, K. E., Carbonate removal by acid fumigation for measuring the  $\delta^{13}\text{C}$  of soil organic carbon. *Can. J. Soil Sci.* **2011**, *91*, (2), 247–250.
23. IUSS working group WRB *World reference base for soil resources 2014, update 2015 international soil classification system for naming soils and creating legends for soil maps.*; FAO: Rome, Italie, **2015**; p 192.
24. Vogel, F.; Harf, J.; Hug, A.; von Rohr, P. R., The mean oxidation number of carbon (MOC)—a useful concept for describing oxidation processes. *Water Res.* **2000**, *34*, (10), 2689–2702.
25. Thomas, O.; Burgess, C., *UV-visible spectrophotometry of water and wastewater.* Elsevier: 2007; Vol. 27, p 360.

## Supporting references

26. OECD, Test No. 106: Adsorption – desorption using a batch equilibrium method. In *Guidelines for the Testing of Chemicals, Section 1*, OECD Publishing: Paris, France, **2000**; p 45.
27. Gulkowska, A.; Buerge, I. J.; Poiger, T.; Kasteel, R., Time-dependent sorption of two novel fungicides in soils within a regulatory framework. *Pest Manage. Sci.* **2016**, *72*, (12), 2218–2230.
28. Eichelberger, J. W.; Behymer, T. D.; Budde, W. L.; Munch, J. W. *EPA method 525.2: Determination of organic compounds in drinking water by liquid-solid extraction and capillary column gas chromatography/mass spectrometry*; U.S. Environmental Protection Agency (EPA): Cincinnati (US), **1995**; p 60.
29. Ivdra, N.; Herrero-Martin, S.; Fischer, A., Validation of user- and environmentally friendly extraction and clean-up methods for compound-specific stable carbon isotope analysis of organochlorine pesticides and their metabolites in soils. *J. Chromatogr. A* **2014**, *1355*, 36–45.
30. Alvarez-Zaldívar, P.; Payraudeau, S.; Meite, F.; Masbou, J.; Imfeld, G., Pesticide degradation and export losses at the catchment scale: Insights from compound-specific isotope analysis (CSIA). *Water Res.* **2018**, *139*, 198–207.
31. Van Breukelen, B. M., Quantifying the degradation and dilution contribution to natural attenuation of contaminants by means of an open system Rayleigh equation. *Environ. Sci. Technol.* **2007**, *41*, (14), 4980–4985.
32. Honti, M.; Fenner, K., Deriving persistence indicators from regulatory water–sediment studies - opportunities and limitations in OECD 308 data. *Environ. Sci. Technol.* **2015**, *49*, (10), 5879–5886.
33. Shrestha, P.; Junker, T.; Fenner, K.; Hahn, S.; Honti, M.; Bakkour, R.; Diaz, C.; Hennecke, D., Simulation studies to explore biodegradation in water–sediment systems: From OECD 308 to OECD 309. *Environ. Sci. Technol.* **2016**, *50*, (13), 6856–6864.
34. Honti, M.; Hahn, S.; Hennecke, D.; Junker, T.; Shrestha, P.; Fenner, K., Bridging across OECD 308 and 309 data in search of a robust biotransformation indicator. *Environ. Sci. Technol.* **2016**, *50*, (13), 6865–6872.
35. Bronner, G.; Goss, K. U., Sorption of organic chemicals to soil organic matter: Influence of soil variability and pH dependence. *Environ. Sci. Technol.* **2011**, *45*, (4), 1307–1312.
36. Gadd, G. M., Metals, minerals and microbes: geomicrobiology and bioremediation. *Microbiology* **2010**, *156*, (3), 609–643.
37. Konhauser, K., *Introduction to geomicrobiology*. Blackwell Science: **2007**; p 425.
38. Kendall, C.; Caldwell, A. E., Fundamental of isotope geochemistry. In *Isotope tracers in catchment hydrology*, Kendall, C.; McDonnell, J. J., Eds. Elsevier: 1998; pp 51–86.

39. Querin, O. M.; Victoria, M.; Alonso, C.; Ansola, R.; Martí, P., Chapter 3 - Discrete Method of Structural Optimization. In *Topology Design Methods for Structural Optimization*, Querin, O. M.; Victoria, M.; Alonso, C.; Ansola, R.; Martí, P., Eds. Academic Press: Oxford, **2017**; pp 27–46.
40. Ditzler, C.; Scheffe, K.; Monger, H. C., *Soil survey manual*. USDA - Soil Science Division Staff: Washington, D.C., **2017**.
41. OECD, Test No. 308: Aerobic and Anaerobic Transformation in Aquatic Sediment Systems. In OECD Publishing: Paris, France, **2002**.
42. Demoling, F.; Figueroa, D.; Bååth, E., Comparison of factors limiting bacterial growth in different soils. *Soil Biol. Biochem.* **2007**, *39*, (10), 2485–2495.
43. Hessen, D. O.; Ågren, G. I.; Anderson, T. R.; Elser, J. J.; de Ruiter, P. C., Carbon sequestration in ecosystems: The role of stoichiometry. *Ecology* **2004**, *85*, (5), 1179–1192.
44. Huntscha, S.; Singer, H. P.; McArdell, C. S.; Frank, C. E.; Hollender, J., Multiresidue analysis of 88 polar organic micropollutants in ground, surface and wastewater using online mixed-bed multilayer solid-phase extraction coupled to high performance liquid chromatography-tandem mass spectrometry. *J. Chromatogr. A* **2012**, *1268*, 74–83.
45. Jochmann, M. A.; Blessing, M.; Haderlein, S. B.; Schmidt, T. C., A new approach to determine method detection limits for compound-specific isotope analysis of volatile organic compounds. *Rapid Commun. Mass Spectrom.* **2006**, *20*, (24), 3639–3648.
46. Mazzafera, P., Catabolism of caffeine in plants and microorganisms. *Front. Biosci.* **2004**, *9*, 1348–1359.
47. Drouin, G. Micropollutant dissipation at the sediment-water interface by coupling modelling and compound-specific isotope analysis. Doctoral thesis, Laboratoire d'Hydrologie et de Géochimie de Strasbourg (LHyGeS), University of Strasbourg, Strasbourg, **2020**; p 294.
48. Price, W. E., Tracer caffeine diffusion in aqueous solutions at 298 K. The effect of caffeine self-association. *J. Chem. Soc., Faraday Trans. 1* **1989**, *85*, (2), 415–419.
49. Soetaert, K.; Herman, P. M. J.; Middelburg, J. J., A model of early diagenetic processes from the shelf to abyssal depths. *Geochim. Cosmochim. Acta* **1996**, *60*, (6), 1019–1040.
50. Shaw, S. B.; Beslity, J. O.; Colvin, M. E., Working toward a more holistic set of hydrologic principles to teach non-hydrologists: Five simple concepts within catchment hydrology. *Hydrol. Process.* **2019**, *33*, 2258–2262.
51. Alvarez-Zaldivar, P. Pesticide degradation and transport at catchment scale Compound-specific isotope analysis and numerical modelling. Doctoral thesis, Laboratoire d'Hydrologie et de Géochimie de Strasbourg (LHyGeS), University of Strasbourg, Strasbourg, **2018**; p 202.
52. Boesten, J.; Linden, A., Modeling the influence of sorption and transformation on pesticide leaching and persistence. *Journal of Environment Quality* **1991**, *20*, 425.

53. Walker, A., A simulation model for prediction of herbicide persistence. *J. Environ. Qual.* **1974**, *3*, (4), 396–401.
54. Jaikaew, P.; Malhat, F.; Boulange, J.; Watanabe, H., Aspect of the degradation and adsorption kinetics of atrazine and metolachlor in andisol soil. *Hellenic Plant Protection Journal* **2017**, *10*, 1–14.
55. Habets, F.; Boone, A.; Champeaux, J. L.; Etchevers, P.; Franchistéguy, L.; Leblois, E.; Ledoux, E.; Le Moigne, P.; Martin, E.; Morel, S.; Noilhan, J.; Quintana Seguí, P.; Rousset-Regimbeau, F.; Viennot, P., The SAFRAN-ISBA-MODCOU hydrometeorological model applied over France. *Journal of Geophysical Research: Atmospheres* **2008**, *113*, (D6).
56. Silva, V.; Mol, H. G. J.; Zomer, P.; Tienstra, M.; Ritsema, C. J.; Geissen, V., Pesticide residues in European agricultural soils – A hidden reality unfolded. *Sci. Total Environ.* **2019**, *653*, 1532–1545.
57. Hengl, T.; Mendes de Jesus, J.; Heuvelink, G. B. M.; Ruiperez Gonzalez, M.; Kilibarda, M.; Blagotić, A.; Shangguan, W.; Wright, M. N.; Geng, X.; Bauer-Marschallinger, B.; Guevara, M. A.; Vargas, R.; MacMillan, R. A.; Batjes, N. H.; Leenaars, J. G. B.; Ribeiro, E.; Wheeler, I.; Mantel, S.; Kempen, B., SoilGrids250m: Global gridded soil information based on machine learning. *PLoS One* **2017**, *12*, (2), e0169748.
58. Hippelein, M.; McLachlan, M. S., Soil/air partitioning of semivolatile organic compounds. 2. Influence of temperature and relative humidity. *Environ. Sci. Technol.* **2000**, *34*, (16), 3521–3526.
59. Davie-Martin, C. L.; Hageman, K. J.; Chin, Y.-P., An improved screening tool for predicting volatilization of pesticides applied to soils. *Environ. Sci. Technol.* **2013**, *47*, (2), 868–876.
60. Gish, T. J.; Prueger, J. H.; Daughtry, C. S. T.; Kustas, W. P.; McKee, L. G.; Russ, A. L.; Hatfield, J. L., Comparison of field-scale herbicide runoff and volatilization losses: An eight-year field investigation. *J. Environ. Qual.* **2011**, *40*, (5), 1432–1442.
61. Prueger, J. H.; Gish, T. J.; McConnell, L. L.; McKee, L. G.; Hatfield, J. L.; Kustas, W. P., Solar radiation, relative humidity, and soil water effects on metolachlor volatilization. *Environ. Sci. Technol.* **2005**, *39*, (14), 5219–5226.
62. Huang, L. Q.; Frink, C. R., Distribution of atrazine, simazine, alachlor, and metolachlor in soil profiles in Connecticut. *Bull. Environ. Contam. Toxicol.* **1989**, *43*, (1), 159–164.
63. Si, Y.; Takagi, K.; Iwasaki, A.; Zhou, D., Adsorption, desorption and dissipation of metolachlor in surface and subsurface soils. *Pest Manage. Sci.* **2009**, *65*, (9), 956–962.
64. Fox, G. A.; Pulijala, S. H.; Sabbagh, G. J., Influence of rainfall distribution on simulations of atrazine, metolachlor, and isoxaflutole/metabolite transport in subsurface drained fields. *J. Agric. Food. Chem.* **2007**, *55*, (14), 5399–5407.

65. Bauer-Marschallinger, B.; Paulik, C.; Hochstoger, S.; Mistelbauer, T.; Modanesi, S.; Ciabatta, L.; Massari, C.; Brocca, L.; Wagner, W., Soil moisture from fusion of scatterometer and SAR: Closing the scale gap with temporal filtering. *Remote Sensing* **2018**, *10*, (7), 1030.
66. Fono, L. J.; Kolodziej, E. P.; Sedlak, D. L., Attenuation of wastewater-derived contaminants in an effluent-dominated river. *Environ. Sci. Technol.* **2006**, *40*, (23), 7257–7262.
67. Leifer, A., *The kinetics of environmental aquatic photochemistry: Theory and practice*. American Chemical Society: **1988**; p 336.
68. Chin, Y.-P.; Aiken, G.; O'Loughlin, E., Molecular weight, polydispersity, and spectroscopic properties of aquatic humic substances. *Environ. Sci. Technol.* **1994**, *28*, (11), 1853–1858.
69. Wenk, J.; Aeschbacher, M.; Salhi, E.; Canonica, S.; von Gunten, U.; Sander, M., Chemical oxidation of dissolved organic matter by chlorine dioxide, chlorine, and ozone: Effects on Its optical and antioxidant properties. *Environ. Sci. Technol.* **2013**, *47*, (19), 11147–11156.
70. Berns, A. E.; Philipp, H.; Narres, H. D.; Burauel, P.; Vereecken, H.; Tappe, W., Effect of gamma-sterilization and autoclaving on soil organic matter structure as studied by solid state NMR, UV and fluorescence spectroscopy. *Eur. J. Soil Sci.* **2008**, *59*, (3), 540–550.
71. Elsayed, O. F.; Maillard, E.; Vuilleumier, S.; Nijenhuis, I.; Richnow, H. H.; Imfeld, G., Using compound-specific isotope analysis to assess the degradation of chloroacetanilide herbicides in lab-scale wetlands. *Chemosphere* **2014**, *99*, 89–95.
72. Ponsin, V.; Torrentó, C.; Lihl, C.; Elsner, M.; Hunkeler, D., Compound-specific chlorine isotope analysis of the herbicides atrazine, acetochlor and metolachlor. *Anal. Chem.* **2019**, *91*, (22), 14290–14298.
73. Lutz, S. R.; Velde, Y. V. D.; Elsayed, O. F.; Imfeld, G.; Lefrancq, M.; Payraudeau, S.; van Breukelen, B. M., Pesticide fate on catchment scale: conceptual modelling of stream CSIA data. *Hydrol. Earth Syst. Sci.* **2017**, *21*, (10), 5243–5261.



# Pesticides dissipation at the sediment-water interface: insight from compound-specific isotope analysis (CSIA)

## Résumé

La contamination des rivières par les pesticides à l'échelle de la planète impacte la biodiversité et la production d'eau potable. L'interface eau-sédiment des rivières joue un rôle clé dans la dissipation des pesticides mais son fonctionnement reste méconnu. Cette thèse a ciblé les processus de dégradation à cette interface en développant l'analyse isotopique composé-spécifique (AICS) d'un panel de pesticides, de l'échelle du laboratoire jusqu'aux rivières. Les résultats ont permis d'identifier les facteurs d'enrichissement isotopiques en carbone et azote spécifiques pour différents processus de dégradation (photolyse, biodégradation) pour interpréter des signatures isotopiques en rivière. Le rôle clé des écoulements en rivière sur la persistance et la dégradation des pesticides a été identifié. Des pistes d'amélioration de l'AICS sont proposées pour évaluer plus systématiquement la persistance des pesticides dans les rivières.

Mots-clés : transport réactif model, isotope stable, eau de surface, station d'épuration.

## Résumé en anglais

River contamination by pesticides on a global scale impacts biodiversity and the production of drinking water. The water – sediment interface in these environments plays a key role in the dissipation of pesticides, although its functioning remains poorly understood. This thesis targeted degradation processes at this interface by developing Compound-Specific Isotope Analysis (CSIA) for a panel of pesticides, from the laboratory scale to rivers. The results made it possible to identify the specific carbon and nitrogen isotopic enrichment factors for different degradation processes (photolysis, biodegradation) in order to interpret the isotope signatures in rivers. The key role of river runoff on the persistence and degradation of pesticides has been identified. Ways to improve the CSIA are proposed to more systematically assess the persistence of pesticides in rivers.

Keyword : Flow-Reactive transport model, stable isotope, surface water, wastewater treatment plants.